Univerzita Karlova v Praze

Přírodovědecká fakulta

Charles University in Prague

Faculty of Science

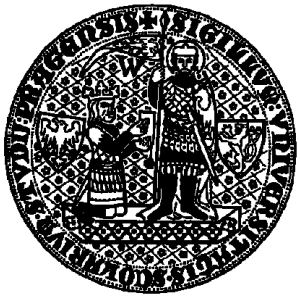

Czech Academy of Sciences

Institute of Physiology, v.v.i

Zvýšení lipidového katabolismu ve spojení s biogenezí mitochondrií v bílé tukové tkáni jako terapeutický cíl při prevenci a léčbě obezity a souvisejících metabolických poruch

Induction of lipid catabolism and mitochondrial biogenesis in white adipose tissue as therapeutic target for obesity and associated metabolic disorders

Disertační práce / Ph.D. thesis

Mgr. Kateřina Adamcová

Školitel / Supervisor: Ing. Petra Janovská, Ph.D. (RNDr. Pavel Flachs, Ph.D.)

Praha 2020

Prohlášení:

Prohlašuji, že jsem závěrečnou práci zpracovala samostatně a že jsem uvedla všechny použité informační zdroje a literaturu. Tato práce ani její podstatná část nebyla předložena k získání jiného nebo stejného akademického titulu.

Statement of authorship

I certify that the thesis represents valid work elaborated under the supervision of Ing. Petra Janovska, PhD and that neither this manuscript nor one with substantially similar content under my authorship has been submitted in support of an application for any other academical degree. My participation in the published papers is specified in the text and summarized in the list of Publications on page 127.

16.12.2020 in Prague

Mgr. Kateřina Adamcová

Statement of co-authors

I certify that Katerina Adamcova substantially contributed to the formation of the papers used as a basis of this thesis and that her participation specified in the text of the thesis is correct.

16.12.2020 in Prague

Ing.Petra Janovská, Ph.D.

Acknowledgment

I would like to my sincere thanks to both my supervisors RNDr. Pavel Flachs, Ph.D. and Ing. Petra Janovska, and to MUDr. Jan Kopecky, DrSc., the head of the department, for their scientific and financial support during my Ph.D. I also want to acknowledge all the co-authors of publications summarized in this thesis. I thank all my colleagues for creating a stimulating and friendly working environment, and my friends and family for being supportive and forcing me to finish this thesis.

Abstrakt

Funkcí tukové tkáně není jen ukládání tuků, ale také produkce a sekrece tzv. adipokinů, které ovlivňují metabolizmus na celotělové úrovni. Narušení funkčnosti tukové tkáně vede k rozvoji diabetu 2. typu, ukládání tuku v játrech, kardio-vaskulárním onemocněním a dalším poruchám. Mnoho vědeckého úsilí je věnováno tomu, jak obezitě a s ní spojeným komplikacím předejít, popř. je zvrátit. Uvažuje se např. o indukci mitochondriálního odřahujícího proteinu 1 (UCP1) v hnědé a bílé tukové tkáni a/nebo stimulaci metabolických drah v bílé tukové tkáni, které spotřebovávají energii bez účasti UCP1, jako jsou prázdné/jalové cykly. Tato dizerační práce je založena na výsledcích z experimentů s dvěma imbredními myšími kmeny lišícími se náchylností k obezitě, které byly vystaveny chladu, a z experimentů na myších krmených vysokotukou dietou, nebo vysokotukou dietou obohacenou n-3 polynenasycenými mastnými kyselinami.

Myši kmene A/J, které jsou rezistentní k obesitě indukované dietou, vykazovaly v chladu vyšší indukci jalového cyklu mastných kyselin a triacylglycerolu v epididymální tukové tkáni v porovnání s B6 myšmi, které jsou k obezitě náchylné.

Množství UCP1 proteinu a jeho mRNA, který je esenciální pro netřesovou termogenezi v hnědé tukové tkáni, byly po vystavení chladu zvýšeny u obou kmenů podobně, což znamená, že hnědá tuková tkáň nepřispívá k rozdílnému fenotypu A/J a B6 myší, jak bylo navrhnuto dříve. Dalším důležitým orgánem pro spotřebu glukózy a mastných kyselin jsou kosterní svaly. Z našich výsledků vyplývá, že cyklování Ca^{2+} iontů v kosterním svalu přispívá k zdravějšímu fenotypu A/J myší.

n-3 polynenasycené mastné kyseliny ovlivňují k remodelaci bílé tukové tkáně. Bioaktivní metabolity kyseliny eikosapentaenové a dokosahexaenové působí v prevenci hyperplasie tukové tkáně indukované vysokotukou dietou snížením počtu endoteliálních buněk a preadipocytů. Navíc přispívají k rovnovážnému stavu imunitního systému tkáně.

Experimenty obsažené v této dizertační práci ukázaly, že jalové metabolické cykly a kontrola obratu buněk tukové tkáně mohou významně zlepšit homeostázu volných mastných kyselin v plazmě a ostatních tkáních. I přesto že příspěvek jalových metabolických cyklů k celotělovému energetickému výdeji je pravděpodobně relativně málo významný.

Abstract

Adipose tissue is not only crucial in the storage of excessive fat and its release but also plays important role in the secretion of endo/para- and autocrine factors, thus influencing energy metabolism on the whole body level. The incapability of adipose tissue to meet its responsibilities leads to whole-body metabolic problems resulting in type 2 diabetes, storing of fat in the liver, coronary disease, and other diseases. How to prevent development of obesity and its consequences and/or completely reverse it, is a subject of great scientific interest. Activation of brown adipose tissue (**BAT**) and brite cells via induction of uncoupling protein 1 (**UCP1**) and/or stimulation of UCP1-independent energy-dissipating metabolic pathways such as futile cycles in white adipose tissue may be a promising path to fulfill this goal. This thesis is based on results from experiments with two cold-exposed inbred murine strains differing in the propensity to obesity and murine experiments with diet-induced obesity prevented by n-3 polyunsaturated fatty acids (**PUFA**).

Mice resistant to diet-induced obesity (A/J mice) showed higher induction of triacylglycerol (**TAG**)/fatty acid (**FA**) futile cycle in epididymal white adipose tissue by cold exposure in comparison to obesity-prone B6 mice.

Interestingly, the level of both Ucp1 mRNA and protein in BAT were induced similarly in both strains by cold exposure. Thus, BAT does not contribute to the lean phenotype of A/J mice as was proposed earlier. Besides BAT, skeletal muscles are also a large sink for glucose and fatty acids. Our results suggest that Ca^{2+} cycling in skeletal muscle contributes to a healthier phenotype of A/J mice.

n-3 PUFA were shown to be involved in the remodeling of epididymal white adipose tissue. Bioactive metabolites of eicosapentaenoic and docosahexaenoic acid prevented diet-induced hyperplasia by reducing the number of endothelial cells and preadipocytes and prevented disruption of immune balance.

To conclude, these experiments showed that the contribution of futile cycles, as well as control of fat cell turnover to buffer nonesterified fatty acids in plasma and to the prevention of fatty acids storing in extra-adipose tissues, leads to a healthy phenotype. Even though, the contribution of mentioned futile cycles probably would not influence whole-body energy expenditure.

Content

1 Introduction

The law of energy conservation, stating that energy can change the form, but cannot be created or destroyed, plays a crucial role in physiology. In other words, all accepted energy is either excreted, or stays in the body in the same or transformed form i.e. energy obtained from food is used for the performance of work (including basal metabolism), generation of heat, or is stored. Due to irregular and unpredictable energy intake, organisms evolved the ability to buffer these energy variances and started to store energy among others in the form of triacylglycerols (**TAG**). Both unicellular and multicellular organisms have a highly conserved mechanism of the storage of energy either as lipid droplets/bodies or specialized cells storing lipids, respectively [1]. These cells are called adipocytes and form adipose tissue (**AT**). AT metabolism represents an important component of whole-body metabolism. AT takes excessive fatty acids (**FA**) from plasma and builds TAG, and thereby stores metabolic energy. When the capacity of AT is exceeded, balance is disrupted, and lipids are ectopically stored in other tissues such as muscle, heart, and liver. This leads to impaired insulin sensitivity in these tissues. Insulin resistance, obesity, high levels of TAG, non-esterified fatty acids (**NEFA**), and glucose in blood then lead to the development of metabolic syndrome which results in an increased risk of heart disease, stroke, type 2 diabetes, and other diseases. Moreover, obesity leads to low-level, but chronic inflammation, which contributes to the development and/or amelioration of insulin resistance.

According to the World Health Organization, over the world in 2016 there were 1.9 billion adults overweight and of these 650 million were obese. Moreover, over the world there were 420 million adults having diabetes in 2014 [2, 3]. Treatment of obesity and related diseases has become a major challenge for medicine. Since the discovery of brown adipose tissue (**BAT**) in adult humans in the 1980s [4], significant attention is paid to the stimulation of non-shivering thermogenesis and thereby the energy expenditure of AT. Another approach is based on the concept of so called healthy adipocyte. 10-30% of obese people are metabolically healthy in terms of insulin sensitiveness, immune balance, maintenance of metabolic cycles, and storing TAG in adipocytes [5]. These topics will be discussed in the following chapters with the main focus on white adipose tissue (**WAT**).

1.1 Adipose tissue – general description

Adipose tissue consists of adipocytes, which are embedded in a connective tissue matrix and surrounded by capillaries and nerves. Also, fibroblasts, preadipocytes (see chapter 1.4), immune cells (see chapter 1.5) are present in AT. AT can be distinguished either by localization, morphology, or function. However, three main types of AT, white, brown, and beige/brite, are usually defined in the literature (**Fig.1.1**).

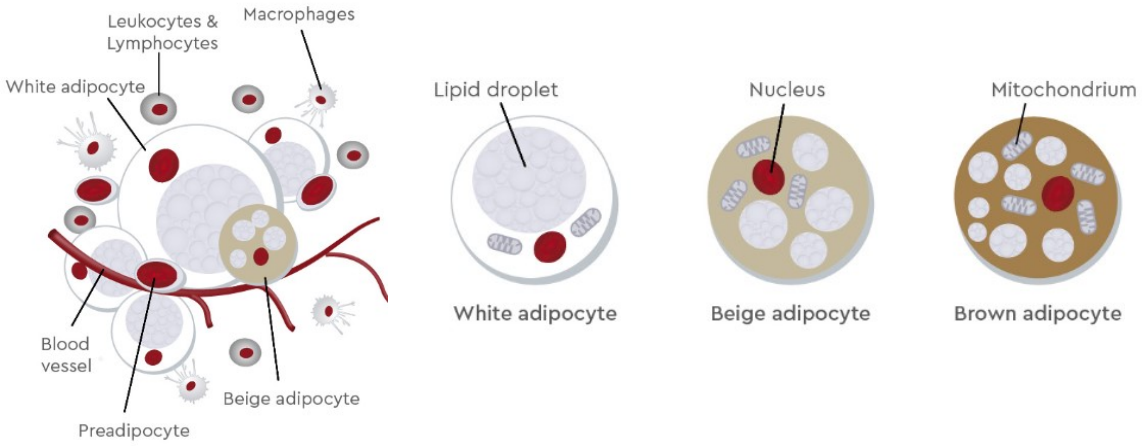

Fig.1.1 AT cells and morphology of different types of adipocytes taken from [6].

AT consists not only of adipocytes, but also of preadipocytes, immune cells, and blood vessels (collectively called stromal vascular fraction, SVF). The morphology of the three different types of adipocytes is shown. They differ mainly in the size and number of lipid droplets and the number and morphology of mitochondria.

WAT is characterized by unilocular adipocytes with one large lipid droplet and a relatively small amount of mitochondria. Adipocytes comprise of up to 90% lipid droplets, which mainly consist of TAG and are coated by perilipin protein. Mitochondria in WAT are smaller and fewer than in BAT. They are also not that well organized as in BAT and therefore have low oxidation ability [7]. For a long time, it had been thought that the only function of WAT is the storage of energy and, in case of emergency, the energy release. Nevertheless, this was disproved by a discovery of many bioactive molecules (adipokines), which AT can secrete and thereby influence the whole body homeostasis (**Fig.1.2**). The best known are leptin and adiponectin. The first discovered adipokine, leptin, suppresses food intake and its secretion is proportional to the body fat mass. Moreover, it reduces synthesis and increases oxidation of FA in AT and skeletal muscle [8, 9]. Adiponectin increases glucose uptake and promotes fatty acid oxidation (**FAox**) in skeletal muscle and suppresses gluconeogenesis in the liver [10]. Among other secreted molecules are also fibroblast growing factor 21 (**FGF21**), tumor necrosis factor alpha (**TNFα**), angiotensin, interleukin (**IL**) 6,

adipsin, resistin, etc. Other functions of WAT include thermic insulation, organ protection from mechanical damage, weight-bearing capacity, or use in echolocation in animals [1].

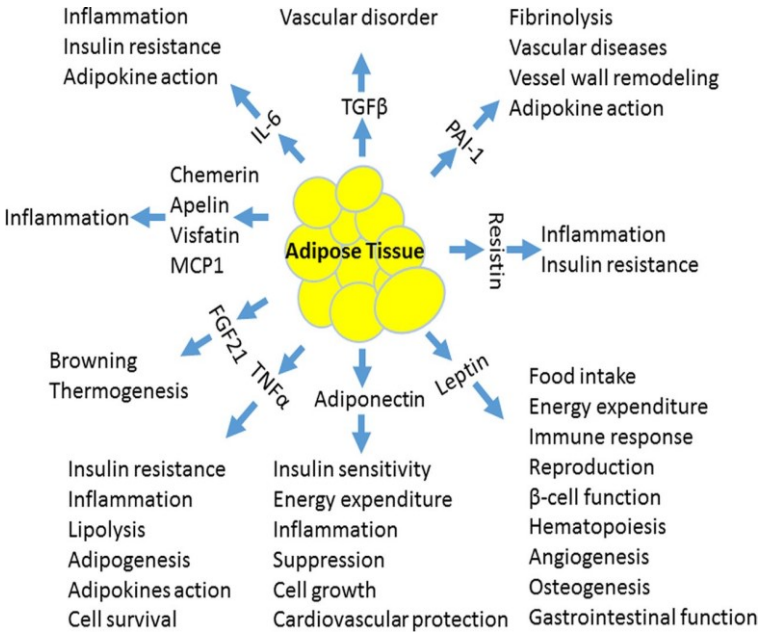

Fig.1.2 Endocrine function of adipose tissue taken from [11].

Adipokines regulate various pathways in the body such as insulin sensitivity, cardiovascular function, inflammation, and others.

FGF21, fibroblast growth factor 21; IL6, interleukin 6; MCP1, monocyte chemoattractant protein 1; PAI1, plasminogen activator inhibitor 1; TGFβ, transforming growth factor beta; TNFα, tumor necrosis factor alpha.

Age, sex, ethnicity, diet, physical activity, etc. influence the distribution and metabolism of WAT [12]. WAT is simplistically said localized either viscerally or subcutaneously. Visceral depots are surrounding body organs and in mice include omental, mesenteric, retroperitoneal, epi- and para- cardial, epigastric, perivascular, and gonadal (=epididymal/periovarial) depots. Subcutaneous depots in mice (dorsolumbar, inguinal, gluteal, etc.) are placed in the hypodermal layer of the skin [13]. However, the classification of individual depots is not unified and generally accepted. Also, some large depots like gonadal fat in rodents are hardly at all present in humans, and on the contrary, omental depot present in humans is neglected in rodents (**Fig.1.3**).

AT depots differ in their structural and functional properties and play different roles in pathology. Increased risk of insulin resistance, cardiovascular disease, and other metabolic consequences of metabolic syndrome are mainly connected to visceral obesity. This is thought to be caused by a straight connection of visceral fat with the liver via a portal vein in humans. Adipocytes from visceral depots also produce more pro-inflammatory cytokines (see chapter 1.5.1) in comparison to subcutaneous depots and were shown to express higher basal amounts of genes involved in lipogenesis, lipolysis, and FAox. On the other hand, subcutaneous adipocytes were shown to be the main source of leptin and adiponectin, and an increase in subcutaneous fat is associated with beneficial profiles of plasma lipids. The subcutaneous depot is characteristic by more rapid replication and differentiation of preadipocytes in comparison with preadipocytes of visceral adipose tissue [13, 14].

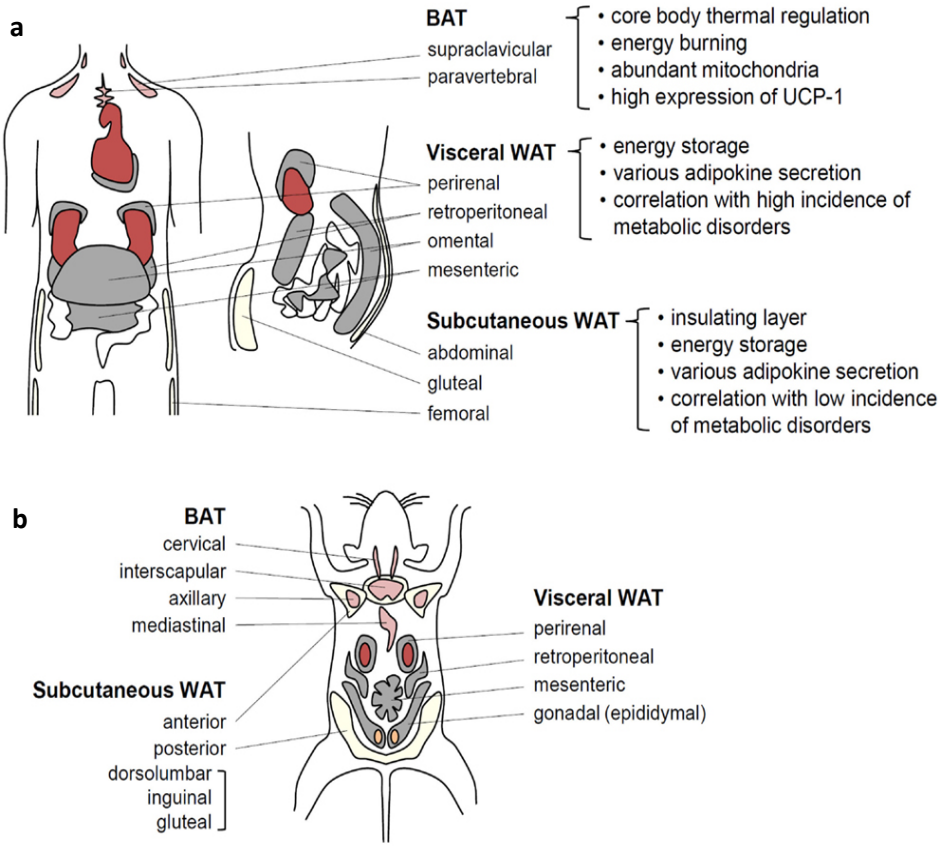

Fig.1.3 Comparison of human (a) and murine (b) various adipose tissue depots taken from [15].

Differences in localization of typical adipose tissue depots between humans and mice. Some of them are present just in humans (e.g. omental AT), some just in mice (e.g. gonadal AT).

BAT, brown adipose tissue; UCP1, uncoupling protein 1; WAT, white adipose tissue.

BAT was found in fetuses, newborns, small mammals, and also in adult humans [16]. Typically, it is localized between shoulder blades, ribs, and neck muscles and around blood vessels (**Fig.1.4b**). Brown adipocytes are in contrast to white adipocytes multilocular, meaning they have numerous small lipid droplets and contain a high amount of mitochondria. Cristae in mitochondria are well organized and present in large amounts, thereby mitochondria have a high oxidative capacity (**Fig.1.4a**). Adipocytes represent only half of BAT cells. They are densely innervated by the sympathetic adrenergic system and permeated by blood vessels [7]. The main function of BAT is to produce heat by non-shivering thermogenesis in cold stressed mammals, or in animals arousing from hibernation. FA within BAT or FA released from WAT to blood are used as a fuel for thermogenesis and for activation of proton conductance by uncoupling protein (**UCP**) 1. Due to the uncoupling of oxidative phosphorylation (**OXPHOS**) from mitochondrial respiration via UCP1, energy is not accumulated to adenosine triphosphate (**ATP**) synthesis but rather used for heat production (see chapter 1.2.5). Non-shivering thermogenesis in BAT is regulated by the hypothalamus via the sympathetic nervous system and β_3-adrenergic receptors of adipocytes [17]. Moreover, WAT lipolysis is activated via this type of receptors, which leads to the production of required FA.

Cold exposure (**CE**) also activates so called browning, i.e. presence of brown adipocytes in some white adipose depots. These depots, called “brite” or “beige”, contain UCP1 and can contribute to the production of heat [18]. On the other hand, brite [19] and brown adipocytes might whiten (**Fig.1.4c**) (become similar to WAT) under certain circumstances such as thermoneutrality, leptin receptor deficiency, high fat feeding, impairment of β-adrenergic signaling, and/or lipase deficiency. Whitened brown adipocytes have enlarged endoplasmic reticulum (**ER**), degenerating mitochondria, and are surrounded by an increased amount of macrophages and collagen fibrils [20].

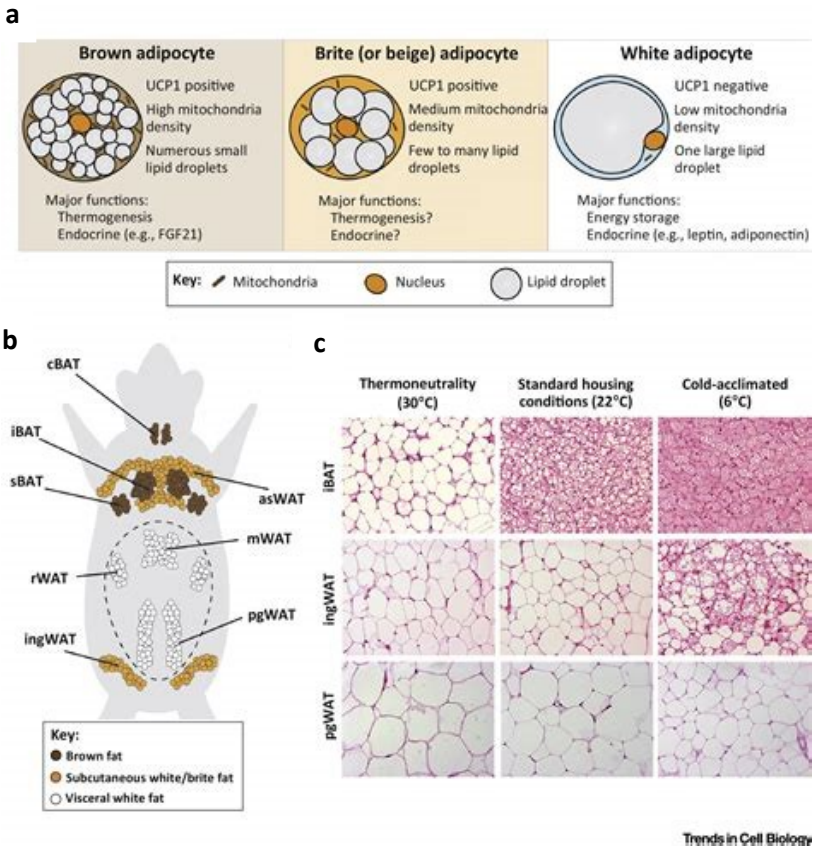

Fig. 1.4 The anatomy of adipose tissue and its plasticity in response to temperature taken from [18].

Various AT depots and their morphology and functions (a), their localization in mice (b), and morphology of various AT depots under different temperature conditions (c).

iBAT, interscapular BAT; sBAT, subscapular BAT; cBAT, cervical BAT; asWAT, anterior subcutaneous WAT; ingWAT, inguinal WAT; mWAT, mesenteric WAT; rWAT, retroperitoneal WAT; pgWAT, perigonadal WAT; UCP1, uncoupling protein 1; FGF21, fibroblast growing factor 21; the peritoneum is represented by a dotted line.

Low amounts of lipids are physiologically present in other organs such as the liver, skeletal muscle, pancreas, and blood vessel's wall and provide energy in the form of FA. However, when AT´s capacity is exceeded, FA are stored in relatively large amounts ectopically in these organs, and contribute to insulin resistance [13]. These adverse effects of FA in nonadipose cells are collectively termed lipotoxicity.

As was already mentioned in the introduction, many researchers focus on combating obesity via modulation/improving its metabolism. One direction is the induction of UCP1-mediated thermogenesis in BAT and/or WAT [21-24]. FA released from WAT or BAT in response to β-adrenergic stimulation by cold or various agents activate UCP1 energy-dissipating function which leads to full activation of mitochondrial oxidative capacity without ATP synthesis. Another option to

fight obesity and related diseases focuses on a phenomenon called healthy adipocyte. This is based on a healthy expansion of AT during weight gain, an increase of energy expenditure by futile cycling in WAT, and resolution of inflammation leading to metabolically flexible healthy adipocyte [25, 26]. In the following chapters, the role of metabolism, inflammation, and adipogenesis in achieving a healthy phenotype of AT and the contribution of CE and n-3 polyunsaturated fatty acids (PUFA) will be discussed.

1.2 Adipose tissue metabolism

The organism is an open thermodynamic system, which transforms energy from outside (food) to work and heat. Nutrients (carbohydrates, lipids, and proteins) are catabolysed to acetyl coenzyme A (**acetyl-CoA**), which is processed to CO_2 generating reduced forms of coenzymes nicotinamide adenine dinucleotide (**NAD**) NADH and flavin adenine dinucleotide (**FAD**) $FADH_2$. Energy from reduced coenzymes is then transformed into ATP in OXPHOS [27]. The amount of fat stores reflects the balance between AT energy intake and expenditure or basically between lipogenesis and breakdown of fat (TAG lipolysis and FAox). TAG are the main energetic reserve for animals including humans. In times of energy excess, TAG are formed by FA created by *de novo* lipogenesis (**DNL**) or FA uptaken from plasma, while in times of fasting/starvation or energy expenditure TAG are lipolysed to FA and glycerol, which are utilized in AT itself or released to the bloodstream for utilization in other organs. E.g. in lean fed rats around 50.1% of endogenous FA are released, around 49.7% are re-esterified and only 0.2% is oxidized in adipocytes *per se.* Fasting doubles FAox in association with a 1.4-times increase in lipolysis. Therefore, the metabolism of AT is a complex and finely tuned system of lipolysis, re-esterification, and DNL, and other pathways. A small shift in this balance could largely affect the WAT function [28, 29].

1.2.1 Fatty acid uptake

Ingested lipids are processed in the gastrointestinal tract to NEFA, monoacylglycerols (**MAG**), and diacylglycerols (**DAG**). These products diffuse to enterocytes, where TAG are synthesized and incorporated into chylomicrons (**Fig.1.5**). Chylomicrons consist of around 85 percent of TAG, 10 percent of phospholipids, and a small but necessary amount of proteins and cholesterol. Chylomicrons transport dietary lipids from intestines to other tissues in the body. NEFA are hydrolyzed from chylomicrons via lipoprotein lipase (**LPL**) and absorbed by AT, skeletal muscles, and heart. Remnants of chylomicrons are taken up by the liver, thereby transferring dietary fat to the liver. Very long-density lipoproteins (**VLDL**) particles are formed in the liver. VLDL transport endogenous products, and are the major source of circulating TAG. Tissues such as AT and skeletal muscles absorb NEFA from VLDL-TAG via LPL. It was shown that adipocyte-derived LPL

is required for FA uptake and storage so adipocytes can mediate the release of FA independently of vascular sources of LPL. Interestingly, adrenergic stimulation in BAT leads to the induction of Lpl mRNA resulting in a decrease of FA in plasma. In addition, adipocytes are able to express apolipoproteins (**apo**) CII and CIII which are needed for regulation of LPL activity [30].

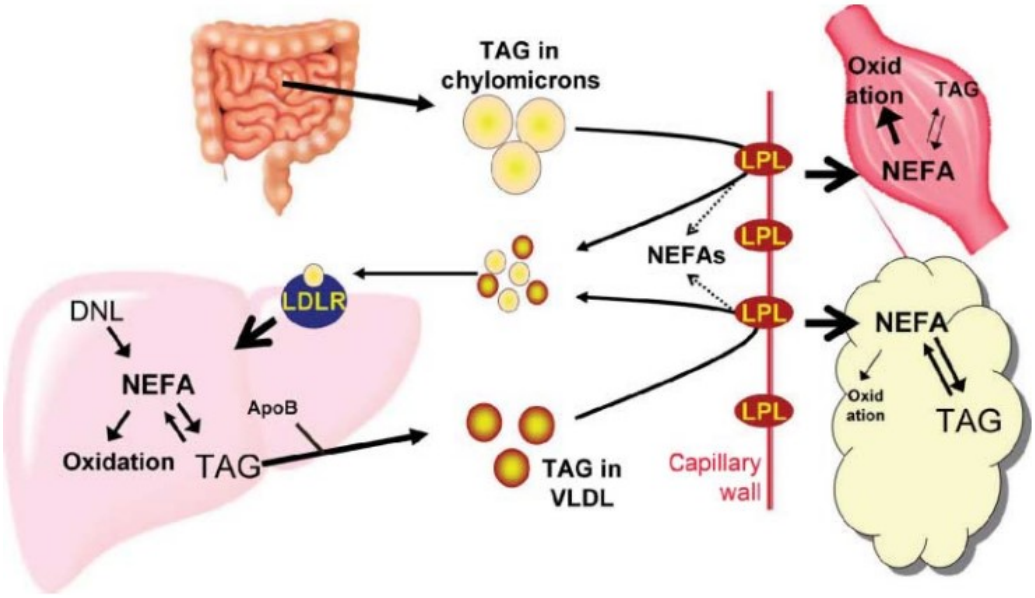

Fig.1.5 Fate of dietary fat in the body taken from [31].

Chylomicrons are formed in enterocytes from NEFA, DAG, MAG. TAG in chylomicrons are then processed by LPL to NEFA, which are used in muscles and adipose tissue, and the rest of chylomicrons (LDL) are processed in the liver, where VLDL are formed. VLDL are then released into the bloodstream.

ApoB, apolipoprotein B; DNL, *de novo* lipogenesis; LDLR, low-density lipoprotein receptor; LPL, lipoprotein lipase; NEFA, non-esterified fatty acids; TAG, triacylglycerol; VLDL, very low-density lipoprotein.

LPL-released NEFA are taken by target cells via fatty acid translocase/cluster of differentiation 36 (**CD36**) and fatty acid transport protein (**FATP**) 1 or in minority passively [32]. Intracellularly, FA are bound to FA binding proteins (**FABP**). FABP are thought to play an important role in the transport of lipids to specific compartments in the cell including lipid droplets, endoplasmic reticulum, mitochondria, peroxisome, cytosol, and nucleus for storage, signaling, trafficking and membrane synthesis, oxidation, and control of lipid-mediated transcriptional programs [31, 33].

1.2.2 Lipogenesis

TAG synthesis is a crucial pathway to store FA transported into adipocytes or FA synthesized *de novo*. TAG are created by esterification of FA and glycerol-3-phosphate (**G3P**; **Fig.1.6**). In order to start TAG synthesis, FA must be activated by acyl-coenzyme A synthetase

(**ACS**), which requires ATP, to acyl-Coenzyme A (**acyl-CoA**). There are at least five ACS isoforms, which differ in their substrate specificity depending on the FA´s length and saturation and their localization on tissue but also on cell organelles level [34]. G3P is then gradually esterified by three activated FA via acyltransferases.

The first step of lipogenesis is mediated by glycerol-3-phosphate acyltransferase (**GPAT**) and the product of this reaction is lysophosphatidic acid. GPAT is one of the key enzymes, inhibited by 5´adenosine monophosphate-activated protein kinase (**AMPK**) in energy-demanding conditions. It exists in two isoforms, mitochondrial and microsomal. Mitochondrial isoform has a higher affinity to short FA (with less than 16 carbons). Microsomal isoform exhibits no substrate preference and is in majority in most of the tissues. Generally, GPAT is sensitive to nutritional, hormonal, and developmental stimuli [35, 36]. Glucagon and cyclic adenosine monophosphate (**cAMP**) are probably involved in the reduction of Gpat mRNA during fasting [37].

The lysophosphatidic acid formation is followed by another acylation via acylglycerol-3-phosphate acyltransferase (**AGPAT**) to phosphatidic acid. AGPAT1 prefers short acyl-CoA (less than 16 carbons) and thereby can change the composition of the membrane. AGPAT2 favors longer acyl-CoA (more than 20 carbons). Phosphatidic acid is a basic building block for various products such as phosphatidyl-inositol, -glycerol, -serin, -choline, -ethanolamine, cardiolipin, and DAG [38]. DAG is formed from phosphatidic acid by phosphatidate phosphatases lipins. DAG can be also synthesized from MAG via MAG esterification by monoacylglycerol acyltransferase. MAG is made from DAG or TAG hydrolysis [39].

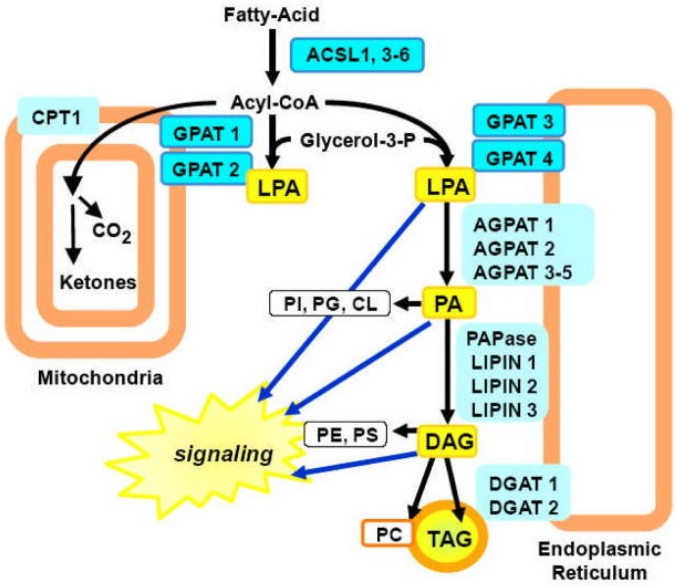

Fig.1.6 Lipogenesis taken from [40].

Fatty acid must be activated to acyl-CoA in order to be processed in lipogenesis. Acyl-CoA then gradually acylates the

glycerol backbone and form TAG. Multiple isoforms of involved enzymes catalyze each step in the glycerol-3-phosphate pathway of TAG synthesis. Both PA and DAG are also precursors for glycerophospholipids.
ACSL, long chain acyl-coenzyme A synthetase; AGPAT, acyl-glycerol-3-phosphate acyltransferase; CL, cardiolipin; CPT, carnitine palmitoyltransferase; DAG, diacylglycerol; GPAT, glycerol-3-phsphate acyltransferase; LPA, lysophosphatidic acid; PA, phosphatidic acid; PC, phosphatidylcholine; PE, phosphatidylethanolamine; PG, phosphatidylglycerol; PI, phosphatidylinositol; PS, phosphatidylserine.

Diacylglycerol acyltransferases (**DGAT**) then convert DAG to TAG. There are two mammalian forms DGAT1 and DGAT2. It is hypothesized that DGAT1 is mostly responsible for the incorporation of FA exogenously taken up from food or products of lipolysis and that protects cells from high concentrations of FA, while DGAT2 produces TAG from *de novo* synthesized FA (**Fig.1.7**; [39, 41]). The model shown by the study of Yen et al. [41] proposes that DGAT1 is activated the most in high FA concentration whereas DGAT2 works the most efficiently in low FA concentrations in animals. Interestingly, only Dgat2 transcription but both DGAT1 and DGAT2 activities are stimulated by glucose and insulin *in vitro*. Upregulation of both DGAT enzymes was observed during adipogenesis which indicates the role of adipogenic masters CCAAT-enhancer-binding protein (**CEBP**) α and peroxisome proliferator-activated receptor **(PPAR**) γ in their regulation. Obesity is associated with decreased Dgat1 and increased Dgat2 mRNA. Dgat2 mRNA is possibly regulated by leptin which is also upregulated in obesity. Lastly, n-3 PUFA as coenzyme A esters inhibits DGAT and thereby restricts lipogenesis in mice [42].

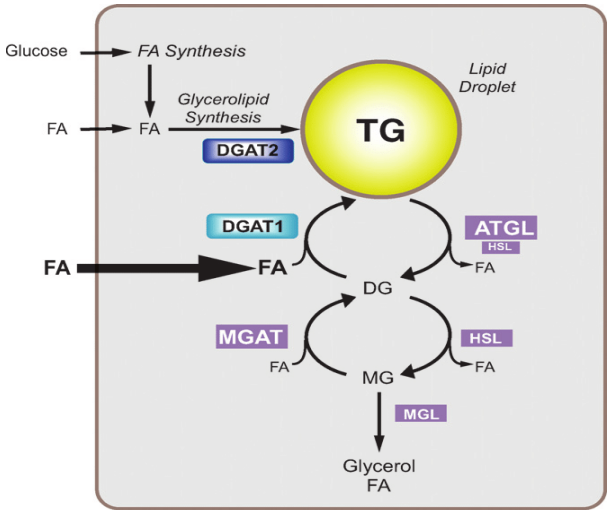

Fig.1.7 Model of different functions of DGAT1 and DGAT2 taken from [41].
DGAT1 incorporates exogenous FA, while DGAT2 is linked with endogenously produced FA by FA synthesis.
ATGL, adipose-tissue triglyceride lipase; DG, diacylglycerol; DGAT, diacylglycerol acyltransferase; FA, fatty acid; HSL, hormone-sensitive lipase; MG, monoacylglycerol; MGAT, monoacylglycerol acyltransferase; MGL, monoacylglycerol lipase; TG, triacylglycerol

1.2.2.1 Fatty acid synthesis

Although most of the FA used for TAG synthesis are transported to adipocytes from blood, adipocytes are also able to synthesize FA on their own. In humans treated with lipogenic diet, it may be as high as 40 percent of whole-body synthesis [43, 44]. FA synthesis is a very energy-consuming process, and even though it takes place in the cytoplasm of adipocytes and/or hepatocytes, it requires cooperation between mitochondrial and cytoplasmatic enzymes and involves fluxes of metabolites across the mitochondrial membrane (**Fig.1.8**). FA synthesis is mediated by multienzymatic complex – fatty acid synthase (**FASN**). The precursor for FA synthesis is acetyl-CoA, which is a product of catabolic processes in mitochondria. To get through the mitochondrial membrane to the cytoplasm, citrate synthesized from acetyl-CoA and oxaloacetate in mitochondria is transported via tricarboxylic carrier to the cytoplasm, where it is with coenzyme A converted via ATP citrate lyase (**ACLY**) to acetyl-CoA and oxaloacetate, consuming one ATP. Malonyl-coenzyme A synthesis catalyzed by acetyl-coenzyme A carboxylase (**ACC**) using acetyl-CoA as a substrate is the first step of FA synthesis. Next, FASN processes acetyl-CoA and malonyl-CoA with help of a reduced form of nicotinamide adenine dinucleotide phosphate (**NADP**) NADPH to form acyl-CoA, and the reaction is repeated until the primary product – palmitic acid is formed. $NADPH^{+}$ is supplied from the pentose phosphate pathway (**PPP**) or by malate oxidation via malic enzyme. Malate comes from the oxaloacetate created by ACLY. Palmitate can be further dehydrogenated or elongated.

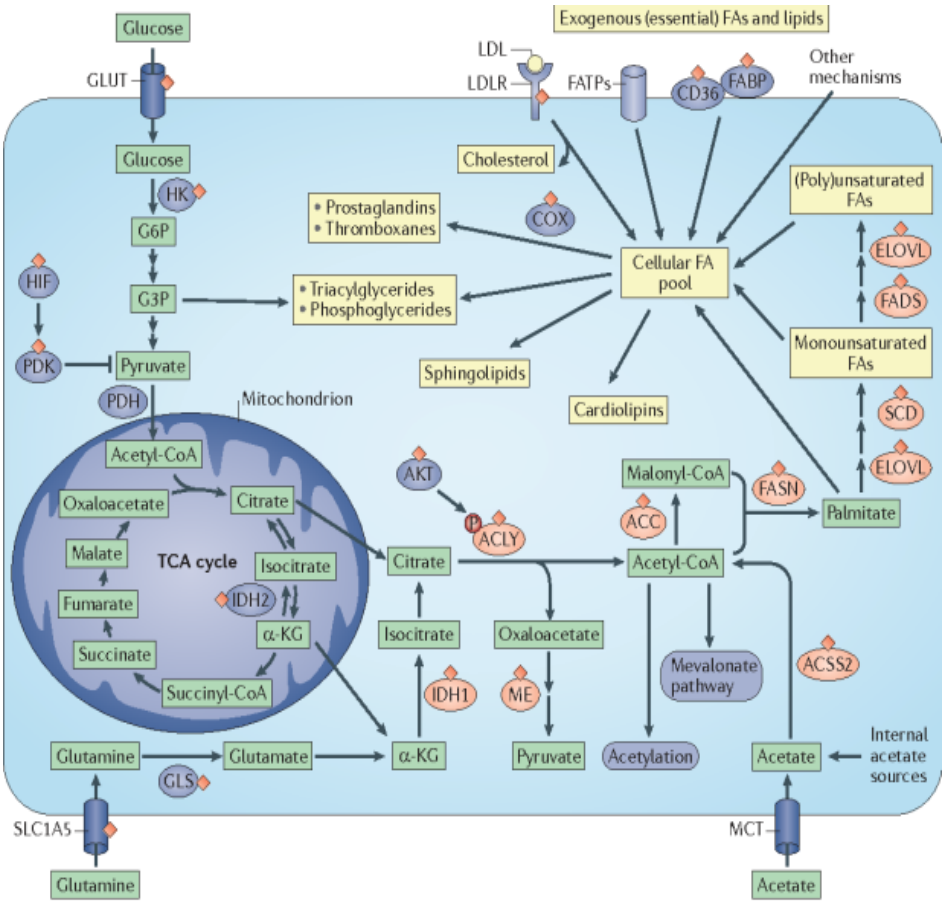

Fig.1.8 Fatty acid synthesis, uptake, and overview of fatty acid functions in the cell taken from [45].

Fatty acids can be synthesized *de novo*, uptaken, or lipolyzed from triacylglycerides. They also can be elongated and desaturated. Fatty acids are an important precursor for triacylglycerides, prostaglandins, phospholipids, and others.

α-KG, α-ketoglutarate; ACC, acetyl-CoA carboxylase; ACLY, ATP citrate lyase; ACSS2, cytoplasmic acetyl-CoA synthetase; COX, cyclooxygenase; ELOVL, very long-chain fatty acid elongase; FA, fatty acids; FABP, fatty acid binding protein; FADS, fatty acid desaturase; FASN, fatty acid synthase; FATP, fatty transporting protein; GLS, glutaminase; GLUT, glucose transporter; G3P, glyceraldehyde-3- phosphate; G6P, glucose-6-phosphate; HIF, hypoxia-inducible factor; HK, hexokinase; IDH, isocitrate dehydrogenase; LDL, low-density lipoprotein; LDLR, low-density lipoprotein receptor; MCT, monocarboxylate transporter; ME, malic enzyme; PDH, pyruvate dehydrogenase; PDK, pyruvate dehydrogenase (acetyl-transferring) kinase; SCD, stearoyl-CoA desaturase; SLC1A5, solute carrier family 1 member 5; TCA, tricarboxylic acid.

The major site of regulation of FA synthesis is ACC. It is inhibited by AMPK phosphorylation [46] and glucagon-stimulated-protein kinase A (**PKA**) phosphorylation. Next, ACC is inhibited by-product of FA synthesis – long chain-FA. On the other hand, ACC is partially activated by citrate, which enhances the polymerization of ACC. Also, sterol regulatory element binding protein (**SREBP**) -1c and carbohydrate-responsive element-binding protein (**ChREBP**),

key transcription factors of lipogenesis and DNL, induce ACC transcription [47]. In the fasting state, AMPK is activated, which inhibits FA synthesis and promotes FAox by phosphorylation of ACC, while in the postprandial state insulin activates phosphatases, which dephosphorylate ACC and activate it. Another crucial enzyme of FA synthesis, FASN, is sensitive to nutritional, hormonal, and developmental stimuli. In the fed state, in presence of insulin, Fasn mRNA is increased, while fasting leads to a reduction of Fasn mRNA, probably via glucagon and cAMP [37]. Also, PKA and AMPK attenuate the expression of lipogenic genes via phosphorylation of ChREBP [48]. Acly expression is regulated by nutrient availability in adipocytes. While its level increases upon carbohydrate consumption, it is suppressed by dietary fat. In addition, ACLY and ChREBP engage in a positive feedback regulatory loop to enable glucose uptake and DNL in 3T3-L1 adipocytes [49].

Stearoyl-CoA desaturase-1 (**SCD1**) is a key enzyme involved in TAG synthesis from FA. It converts saturated FA palmitate and stearate into monounsaturated fatty acids palmitoleate and oleate, respectively. SCD1 is not involved only in the desaturation of FA, it also has a broad impact on WAT lipid handling. SCD1 alters TAG composition in a depot-specific manner, reduces FA re-esterification, and regulates enzymes of lipolysis and glyceroneogenesis [50]. FA can be further elongated into very long-chain fatty acids (**VLCFA**) via at least six different elongases (**ELOVL1-6**) located in the endoplasmatic reticulum. They are thought to carry out substrate-specific elongation with FA of different lengths and degrees of unsaturation [51]. Elongases require malonyl-coenzyme A as a carbon source and NADPH to process the reaction [52]. Interestingly, ELOVL3 is an important regulator of endogenous synthesis of saturated VLCFA and TAG formation in BAT during the early phase of the tissue recruitment induced by CE [53]. Also, ELOVL6 is necessary for the full thermogenic recruitment of BAT. Loss of ELOVL6 causes reduced expression of mitochondrial electron transport chain components [54].

1.2.2.2 Glyceroneogenesis

G3P is the other substrate for lipogenesis. Glycerol can be phosphorylated directly by glycerol kinase (**GK**) to G3P. However, GK is in WAT, unlike BAT, present only negligibly. Therefore, G3P must be formed otherwise. It is generated either from glucose via glycolysis or by a more complex pathway called glyceroneogenesis. During fasting, when glycemia is low, another substrate must be used e.g. metabolites of amino acids, lactate, or pyruvate. Lactate is oxidized to pyruvate, which forms oxaloacetate via pyruvate carboxylase. Mitochondrial malate can be transported through dicarboxylate transporter and oxidized by malate dehydrogenase to oxaloacetate as well. Oxaloacetate is then processed by phosphoenolpyruvate carboxykinase (**PCK**) to phosphoenolpyruvate (**PEP**), from which G3P is created. Cytosolic PCK (**PCK1**) is the rate-

limiting enzyme of glyceroneogenesis. It was shown that overexpression of Pck1 leads to higher glyceroneogenesis and re-esterification in WAT, but also increased adipocyte size and fat mass. However, insulin sensitivity was not disrupted in mice with overexpression of Pck1, probably due to decreased circulating FA [55]. Glucocorticoids repress Pck1 gene transcription in WAT, while in BAT they have no effect. Interestingly, while fasting induces PCK1 activity in both WAT and BAT, CE decreases PCK1 activity in BAT and has no effect in WAT [56, 57].

1.2.3 Lipolysis

FA are stored in adipocytes in form of TAG, that must be firstly hydrolyzed to be able to provide NEFA as an energy source for other tissues (in white adipocytes) or as a substrate for non-shivering thermogenesis (in brown adipocytes) and glycerol as a carbon source for gluconeogenesis (**Fig.1.9**). During basal state, lipolysis is an ongoing process on a low scale. When a high amount of energy is required, lipolytic signals such as catecholamines trigger cascades leading to activation of enzymes involved in lipolysis.

In the basal state, various proteins are embedded in or adherent to the lipid droplet surface, e.g. perilipins, which protect lipid droplets from lipase action. These proteins are dissociated via adenylyl cyclase-cAMP-PKA-downstream kinases axis to enable lipolytic enzymes to hydrolyze TAG. Phosphorylation of perilipins, lipases, and lipases cofactors leads to assembly of the lipolytic complex on the perilipin scaffold and access of lipase to lipids in lipid droplets. Perilipin 1, highly expressed in WAT, plays a crucial role in restricting adipose lipolysis under basal conditions. Indeed, perilipin 1 null mice have an increased turnover of TAG. In BAT and generally oxidative tissues, perilipin 5 plays the main role in the coordination of lipolysis. While in oxidative tissues perilipin 2 is also found, in BAT perilipin 1 is present in addition to perilipin 5 [58].

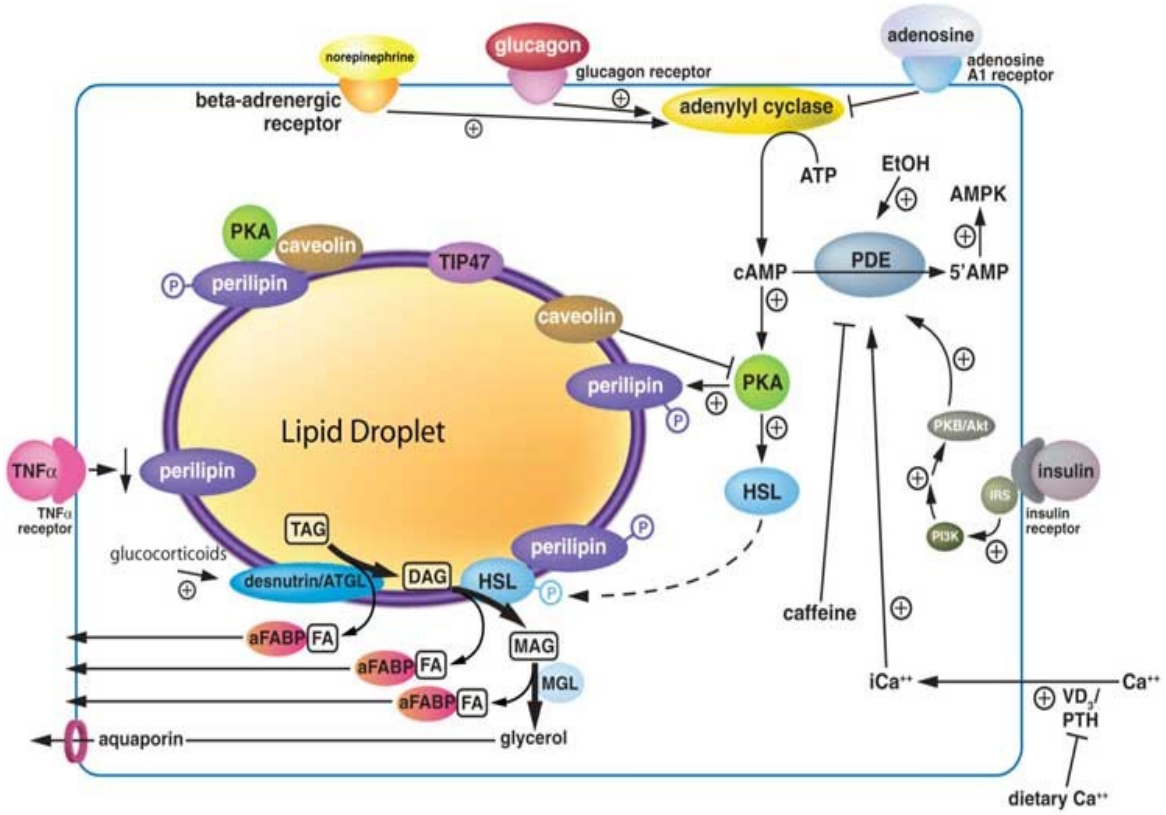

Fig.1.9 Scheme of lipolysis and its regulation taken from [59].

Overall, three fatty acids and glycerol are made in lipolysis via ATGL, HSL, and MGL. Regulation of lipolysis is based on protein phosphorylation, localization of enzymes, access of enzymes to lipid droplet, and hormonal influence. Also, other substances such as caffeine, Ca^{2+}, and others can affect lipolysis.

aFABP, adipose fatty acid binding protein; AMP, adenosine monophosphate; AMPK, adenosine monophosphate-activated protein kinase; ATGL, adipose triglyceride lipase; ATP, adenosine triphosphate; cAMP, cyclic adenosine monophosphate; DAG, diacylglycerol; EtOH, ethanol; FA, fatty acid; HSL, hormone sensitive lipase; IRS, insulin receptor substrate; MAG, monoacylglycerol; MGL, monoacylglycerol lipase; PDE, phosphodiesterase; PI3K, phosphoinositide 3-kinase; PKA, protein kinase A; PTH, parathyroid hormone; TNFα, tumor necrosis factor α

Adipose triglyceride lipase (**ATGL**) is mainly responsible for the first step of TAG hydrolysis (lipolysis) to DAG. The amount of ATGL is higher under basal conditions in BAT than in WAT. In addition, activation of PKA in BAT does not lead to an increase in ATGL recruitment to the lipid droplet, unlike in WAT [58]. The presence of ATGL on lipid droplets is similar in the basal state as well as in the activated state and the enzyme is not phosphorylated by PKA. Upon β-adrenergic stimulation, PKA phosphorylates perilipin, which results in comparative gene identification 58 (**CGI-58**, also known as ABHD5) dissociation from interaction with perilipin on lipid droplet. CGI-58 then binds and induces ATGL [60, 61].

Hormone sensitive lipase (**HSL**) hydrolyses DAG to MAG. It can also hydrolyze

cholesteryl esters, TAG, and other lipid species, however, HSL affinity to these substrates is much smaller. HSL can be phosphorylated on many sites by (and therefore, its activity can be modulated by) e.g. PKA, AMPK, and Ca2+/calmodulin-dependent kinase 2 (**CAMK2**). The phosphorylation by PKA induces HSL activity just moderately. However, when perilipin is also phosphorylated, the activity is increased as expected. Perilipin is upon stimulation of HSL needed for full HSL activation via its translocation from cytosol to lipid droplets. Thus, perilipin promotes stimulated lipolysis, while inhibiting basal lipolysis. Both AMPK and insulin inhibits HSL, AMPK via phosphorylation of HSL [62], insulin by the degradation of cAMP via phosphodiesterase, and by interfering with HSL translocation [63] (see more in Chapter 1.3).

The final step of lipolysis is enabled by monoacylglycerol lipase (**MGL**), which releases the third FA from the glycerol backbone [60]. MGL is abundant in many tissues and takes place in the cytoplasm, on lipid droplets, and in the plasma membrane.

The number of metabolic intermediates is released by each step. They can act in cell signaling and gene regulation and also as precursors for various metabolic pathways. In addition, FA are, besides energetic source, precursors for all lipid classes, ligands for nuclear receptors, and important factors for proper protein functions (acylation of proteins and their anchoring in lipid membrane). Therefore, organisms need to regulate lipolysis tightly.

1.2.4 Fatty acid oxidation

The fate of FA and glycerol obtained by lipolysis is different in WAT and BAT. Glycerol in BAT is used for glycolysis or recycled in lipogenesis. While FA are mostly burned in BAT by FAox, in WAT FAox is used in minor e.g. during fasting, and FA (as well as glycerol) are rather secreted to plasma and used in other tissues. Even though the net percentage of FAox in WAT is small, around 0.2% in the basal state, a small shift in this pathway can have a significant impact on energy handling on the whole body level [64]. FAox takes place mainly in mitochondria and peroxisomes, to a smaller extent also in the ER. The main function of oxidation in peroxisomes is to shorten VLCFA for easier and faster FAox in mitochondria. Before the oxidation itself, FA must be activated by ACS, which synthesizes acyl-CoA from coenzyme A, FA, and ATP. Long-chain ACS (ACSL) expression is regulated by the developmental stage of the animal and nutrient status of the cell [65].

Acyl-CoA is then transported into mitochondria by carnitine-palmitoyl transferase (**CPT**) 1. CPT1 in WAT is thought to be a rate-limiting enzyme, unlike in BAT. It is inhibited by malonyl-CoA, an intermediate in FA synthesis (see Chapter 1.2.2.1), and a product of ACC. Two isoforms of ACC have been identified and it seems that while ACC1-derived malonyl–coenzyme A is used for lipogenesis, malonyl-coenzyme A originated from ACC2 is directed to the proximity of

mitochondrial membrane, where inhibits CPT1 [66]. The AMPK-ACC-CPT1 axis tightly regulates mitochondrial long-chain FAox [47]. AMPK decreases malonyl-CoA level via inhibition of ACC activity, which results in increased CPT1-mediated transport of FA to mitochondria, where they are oxidized. AMPK also induces LPL leading to increased FA uptake to the cell, thereby increases substrate availability for FAox. In addition, AMPK is involved in the increase of mitochondrial biogenesis and oxidative capacity via activation of peroxisome proliferator-activated receptor gamma coactivator 1 (**PGC1**) [67, 68].

FAox itself consists of four repeating reactions, where FA is shortened by 2 carbons every turn while producing acetyl-CoA, $NADH_2$, and $FADH_2$, respectively. The first step of these four reactions is catalyzed by acyl-CoA dehydrogenases (**ACAD**), a rate-limiting enzyme in FAox. According to substrate specificity, ACADs can be distinguished on very long chain ACAD (**VLCAD**, 16-carbon fatty acyl substrate), long-chain ACAD (**LCAD**, 14-carbon), medium-chain ACAD (**MCAD**, 10-carbon), short-chain ACAD (**SCAD**, 4-carbon), and short/branched-chain ACAD (**SBACAD**) [69, 70]. The final product, acetyl-CoA is then metabolized in the tricarboxylic acid (**TCA**) cycle.

1.2.5 Oxidative phosphorylation and its uncoupling

OXPHOS is tightly connected to the transport of electrons, donated by the reduced electron carriers NADH and $FADH_2$ (originated from glycolysis, TCA cycle, or FAox). Mitochondrial electron transport chain complexes create electrochemical proton gradient which is used by ATP synthase to produce ATP (**Fig.1.10**). BAT has a relatively small amount of ATP synthase and high content of UCP1 proton transporter [71, 72], which uncouples the respiratory chain from ATP production to dissipate the proton motive force as heat. Therefore, in BAT metabolic energy is rather converted to heat via UCP1 than to ATP. Interestingly, protons can also, to some extent, channel through the membrane on its own (without any transporter). Leak through UCP1 and membrane leads to energy dissipation in form of heat, decrease in both reactive oxygen species (**ROS**), and ATP production. Reduced ATP results in attenuation of FA synthesis, and therefore the malonyl-CoA level, which blocks the transfer of FA to mitochondria via CPT1 [66]. Thus, uncoupling stimulates FAox and respiration and depresses DNL.

FA are not only a substrate or rather a source of reduced electron carriers for the respiratory chain, they are also necessary to activate UCP1 [17]. However, the mechanism of UCP1 activation is still not known. Currently, there are three models of UCP1 activation, i) FA may induce an allosteric change of UCP1 or ii) protonated FA could cross the membrane and deprotonate itself in the matrix of mitochondria (due to lower H^+ concentration) and return via UCP1 as FA anions (flip-flop model) or iii) it may serve as a site for protons inside the UCP1 to transport protons through the

membrane [17, 73, 74].

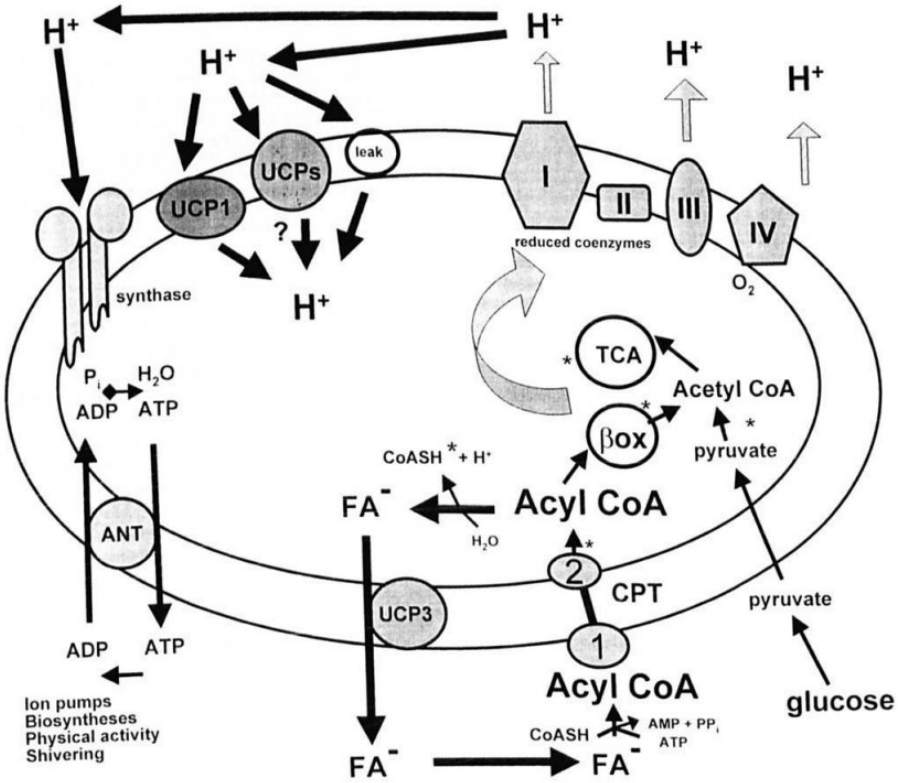

Fig.1.10 OXPHOS, ATP synthesis, and uncoupling of ATP synthesis taken from [75].

Activated fatty acids are oxidized and energy in form of ATP is produced by oxidative phosphorylation. UCP1 can uncouple this process and form heat instead of ATP via the reduction of membrane potential.

ADP, adenosine diphosphate; AMP, adenosine monophosphate; ATP, adenosine triphosphate; βox, β oxidation; CoASH, coenzyme A; CPT, carnitine palmitoyltransferase; FA, fatty acid; Pi, phosphate; PP, pyrophosphate; TCA, tricarboxylic acid cycle; UCP, uncoupling protein;

The supply of lipids is limited in activated BAT. BAT increases LPL activity, FA uptake [76], and glucose uptake to satisfy the demand for FA in activated BAT [77]. Glucose oxidation provides necessary ATP, which production is limited in uncoupled mitochondria, and byproduct lactate, which is transported to the blood. Part of the pyruvate pool is, however, used to produce oxaloacetate, which leads to an increase of TCA cycle capacity to proceed acetyl-CoA originated in FAox. Intermediates of glucose catabolism also replenish TAG by increased lipogenesis to sustain long-term thermogenesis [25]. A significant FA uptake into activated BAT results into decreased TAG in plasma. Interestingly, glucose uptake to stimulated BAT is regulated by both insulin and norepinephrine [77, 78].

1.2.6 Glucose metabolism

As was indicated above, the metabolism of glucose is important for both WAT and BAT providing necessary energy and intermediates for anaplerotic reactions (**Fig.1.11**). Both insulin-regulated (**GLUT4**) and non-insulin-regulated (**GLUT1**) glucose transporters are expressed in WAT and BAT in order to provide glucose for the cell. Glucose in WAT is converted to fat rather than oxidized for energy. Its utilization to FA in WAT was shown to be important in the regulation of whole-body metabolism on the GLUT4 knockout (KO) model in fat which resulted in impaired glucose tolerance. Glycolysis is also a supplier of reducing equivalents for the synthesis of FA *de novo* [79].

Another important pathway, parallel to glycolysis is PPP (**Fig.1.11**). The main function of PPP is to provide NADPH and metabolic intermediates for biosynthetic processes such as the synthesis of nucleotides, FA, aromatic amino acids, and others [80].

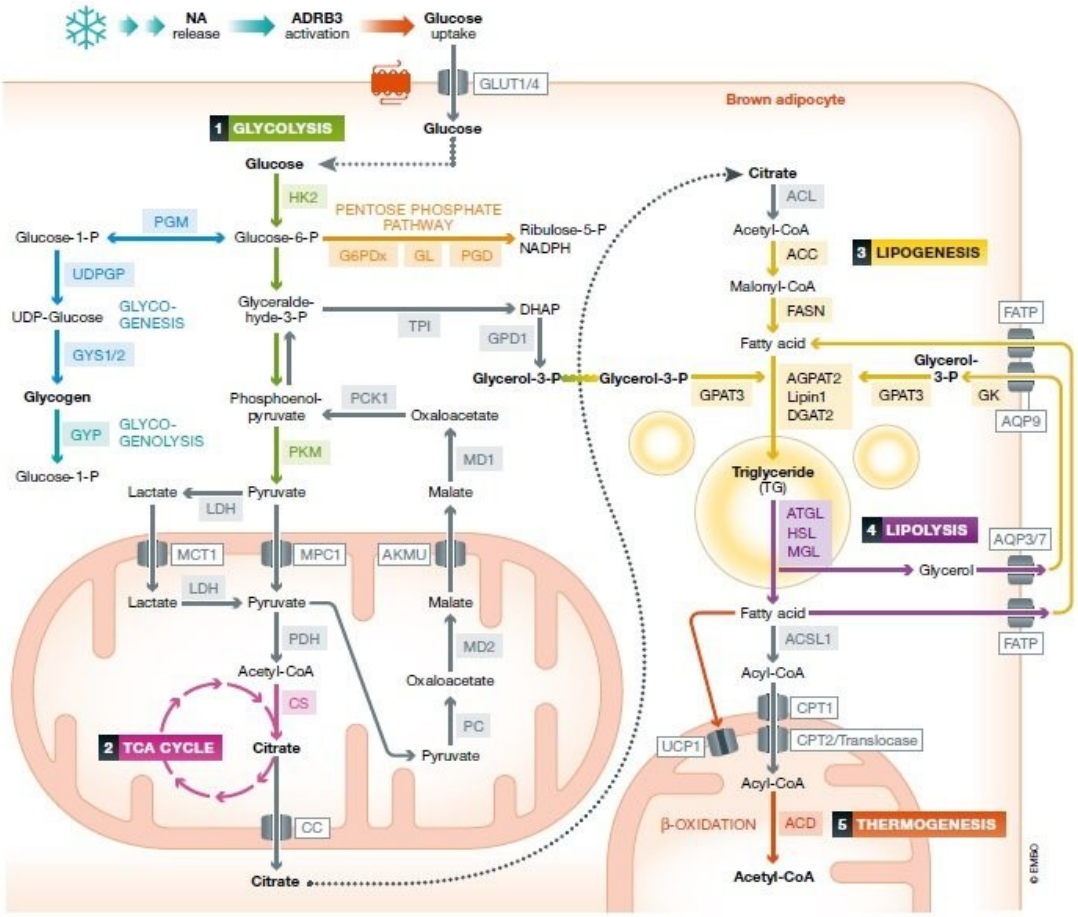

Fig.1.11 Glucose metabolism and its connection to other metabolic pathways taken from [79].

Glucose is uptaken to the cell via glucose transporters. It can be processed to pyruvate and then in TCA and provide

energy. However, glucose is in WAT mostly used for its conversion to fat. Glycolysis is an important supplier of reducing equivalents for the synthesis of FA *de novo*. Glycolysis also provides glycerol-3-phosphate for lipogenesis.
ACC, acetyl-CoA carboxylase; ACD, acyl-CoA dehydrogenases; ACL, ADRB3, β-3 adrenergic receptor; ATP citrate lyase; ACSL1, long chain acyl-CoA synthase; AKMU, alpha-ketoglutarate malate uniporter; AGPAT,1-acylglycerol-3-phosphate-O-acyltransferase; AQP 3/7/9, aquaporin 3/7/9; ATGl, adipose triglyceride lipase; CC, citrate carrier; CPT, carnitine palmitoyltransferase; CS, citrate synthase; DGAT2, diacylglycerol O-acyltransferase 2; DHATP, dihydroxyacetone phosphate; FASN, fatty acid synthase; FATP, fatty acid transport protein; G1P, glucose-1-phosphate; G6PDx, glucose-6-phosphate dehydrogenase X-type; GK, glycerol kinase; GL, gluconolactolase; glucose-6-P, glucose-6-phosphate; GLUT1/4, glucose transporters 1 and 4; GPAT3, glycerol-3-phosphat-O-acyltransferase 3; GPD1, glycerol-3-phosphate dehydrogenase 1; GYP, glycogen phosphorylase; GYS 1/2, glycogen synthase 1/2; HK2, hexokinase 2; HSL,hormone-sensitive lipase; LDH, lactate dehydrogenase; MA, malate; MD1/2, malate dehydrogenase 1/2; MCT1, monocarboxylate transporter 1; MGL, monoacylglycerol lipase; MPC, mitochondrial pyruvate carrier; NA, noradrenalin; NADPH, nicotinamide adenine dinucleotide phosphate; OA, ocaloacetate; PC, pyruvate carboxylase; PC1, pyruvate carrier 1; PCK1, phosphoenolpyruvate carboxykinase 1; PDH, pyruvate dehydrogenase; PGD, 6-phosphogluconate dehydrogenase; PGM, phosphoglucomutase; PKM, pyruvate kinase; TG, triglycerides; TPI, triosephosphate isomerase; UDP, uracil-diphosphate; UDPGP, UDP glucose pyrophosphorylase.

1.2.7 Futile cycling of fatty acids

FA needed for TAG synthesis do not necessarily have to be synthesized *de novo*. A certain amount of FA is released by lipolysis and re-esterified to TAG. This process is called the futile metabolic cycle of FA. In the basal state, 30-90 % of FA can be re-esterified [29, 81]. Fasting increases the lipolysis, but the portion of FA routed towards re-esterification is decreased to 10-20% due to energy request and also due to an increased amount of FA processed by oxidation [29]. Thus, the futile cycling of FA is also important for metabolism on the whole body level. The fate of FA hydrolyzed from TAG is to be oxidized or re-esterified in adipocytes or released to circulation and oxidized in muscles or re-esterified in the liver. Interestingly, Zhou et al. showed that all FA derived from lipolysis are first secreted and then part of them is taken back via CD36 and re-esterified [82]. Beneficial systemic effects of the futile cycle are reflected by fast and fine tuning of FA in plasma, due to the ability of futile substrate cycling to oscillate between two opposite metabolic pathways and to amplify the magnitude of small changes in the activity of the involved enzymes on the net amount of liberated FA. Thus, the redistribution of FA contributes to their physiological levels and prevents from their lipotoxicity in terms of fat accumulation in extra-adipose tissues and deterioration of insulin signaling. Moreover, FA re-esterification mediated by DGAT1 was shown to protect from stress in ER and related inflammatory response in the state of activated lipolysis in mice [83].

1.3 Regulation of adipose tissue metabolism

One of the main features of healthy adipocyte is the fine tuning of metabolic pathways in the basal conditions as well as in response to both acute and chronic demands of the organism. It is controlled by energy status, hormones, and neural system. In addition, AT metabolism is regulated on the level of the interaction with immune cells present in AT and vice versa.

1.3.1 General regulation of metabolism

While WAT is regulated by many stimuli (**Fig.1.12**) including catecholamines, insulin, glucocorticoids, and paracrine and endocrine factors in order to react fast and sensitively to constant changes (fasting, postprandial state, exercise, and/or stress), BAT is regulated primarily by the sympathetic nervous system [17, 84].

Generally, lipolysis is stimulated by catecholamines, glucagon, α-melanocyte-stimulating hormone, etc. through their binding to β-adrenergic receptors, which induces adenylate cyclase. Adenylate cyclase raises cAMP levels, which causes an increase in PKA activity. PKA, finally, phosphorylates target proteins. The inhibitory effect on lipolysis is mediated by catecholamines (via α-adrenergic receptors), adenosine, prostaglandin, nicotinic acid, and others involving inhibitory Gi protein-coupled receptors, which reduces adenylate cyclase activity and causes a decrease in cAMP levels. Another lipolysis-inhibitory pathway involves insulin and insulin-like growth factor, which act through insulin receptor, phosphoinositide 3-kinase (**PI3K**), and protein kinase B (**PKB**; also known as **AKT**). AKT then causes cAMP degradation via activation of phosphodiesterase 3B leading to deactivation of PKA.

Lipogenesis is stimulated by diet rich in carbohydrates, which leads to elevated plasmatic TAG. Glucose influences lipogenesis indirectly by its metabolic product acetyl-CoA, which promotes FA synthesis. Glucose also stimulates a release of insulin which leads to increased activity of lipogenic enzymes such as FASN and microsomal GPAT. Fasting has the opposite effect on lipogenesis. Glucagon decreases the activity of FASN and mitochondrial GPAT. Leptin is known to regulate food intake and downregulate the expression of genes involved in FA and TAG synthesis and thereby limit fat storage. Norepinephrine, adrenocorticotropic hormone, and glucagon decrease activation of FA via reduction of ACS activity in AT [85].

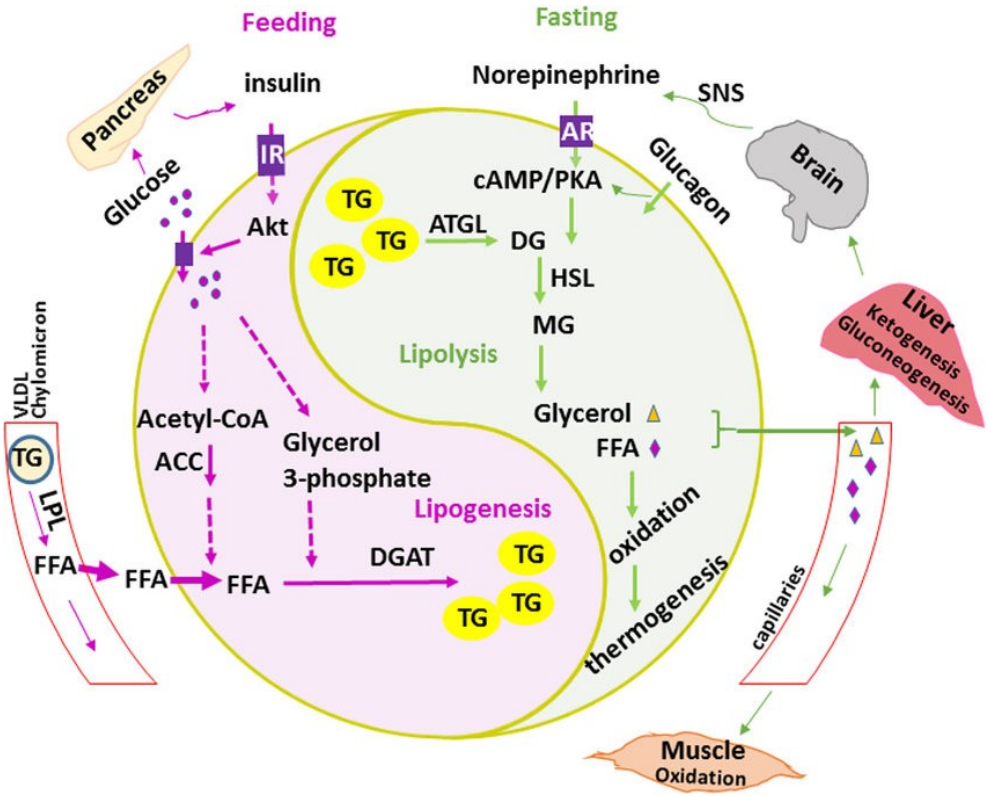

Fig.1.12 Contradictory hormone regulations of lipolysis and lipogenesis taken from [11].

Two main hormones insulin and norepinephrine influences the balance of lipogenesis and lipolysis. In the fed state, insulin prevails and glucose and fatty acid uptake is increased, which leads to the formation of triacylglycerols. On the other hand, in the fasted state, norepinephrine and glucagon activate lipolysis, and triacylglycerols are broken to fatty acids and glycerol, which are used by adipose tissue itself, muscle, and other tissues.

ACC, Acetyl-CoA carboxylase; AR, adrenergic receptor; ATGL, adipose triglyceride lipase; cAMP, cyclic adenosine monophosphate; DG, diacylglycerol; DGAT, diacylglycerol acyltransferase; FFA, free fatty acid; HSL, hormone sensitive lipase; IR, insulin receptor; LPL, lipoprotein lipase; MGL, monoacylglycerol lipase; PKA, protein kinase A; SNS, sympathetic nervous system; TG, triacylglycerol

1.3.2 Regulation of adipose tissue metabolism based on energy status

AMPK, a master sensor, and a regulator of energy state in cells, influences the activity of many enzymes and transcriptional factors. The key role of sensing the ATP/AMP ratio is provided by γ-subunit. Its domains are able to bind both AMP and ATP, which compete for the binding site. Upon exercise or fasting, AMP is increased. This leads to the activation of AMPK, i.e. to conformational changes of AMPK, which results in phosphorylation of α-subunit and induction of AMPK activity up to 100-fold. AMPK´s mission is to return the ATP/AMP ratio back to normal values both acutely by phosphorylation of many substrates and chronically by influencing gene expression. Thereby, ATP-producing pathways are stimulated and ATP-consuming pathways are inhibited (**Fig.1.13**) [67, 86].

AMPK was shown to inhibit FA synthesis by phosphorylation of ACC and SREBP1c, thereby reducing their activities. Inhibition of ACC leads to a decrease in malonyl coenzyme A enabling CPT1 to transport acyl-CoA to mitochondria for oxidation [86]. In addition, AMPK is involved in the increase of mitochondrial biogenesis and oxidative capacity via activation of PGC1. Lipolysis seemed to be the pathway that must be activated by AMPK. However, its regulation is very complex. Shortly after activation of lipolysis, HSL is regulated and phosphorylated by PKA which unblock inhibition of HSL by AMPK. In the long term, ATGL is activated and HSL is inhibited by AMPK leading to unfinished lipolysis with an increase in DAG [68].

Limiting lipolysis seems to be counterintuitive since oxidation of FA derived from lipolysis provides so much needed energy. However, the fate of FA is not only oxidation but also their reactivation and/or activation of mitochondrial uncoupling, both leading to decreased ATP [86, 87]. DAG re-esterification was shown to be higher with FA accumulation [88, 89]. Thus, AMPK likely play part in TAG/FA cycle regulation and regulate the balance between FA re-esterification and lipolysis [90]. The role of AMPK in activation of BAT and browning of WAT is still unclear, however, there are studies supporting induction of these processes [91, 92].

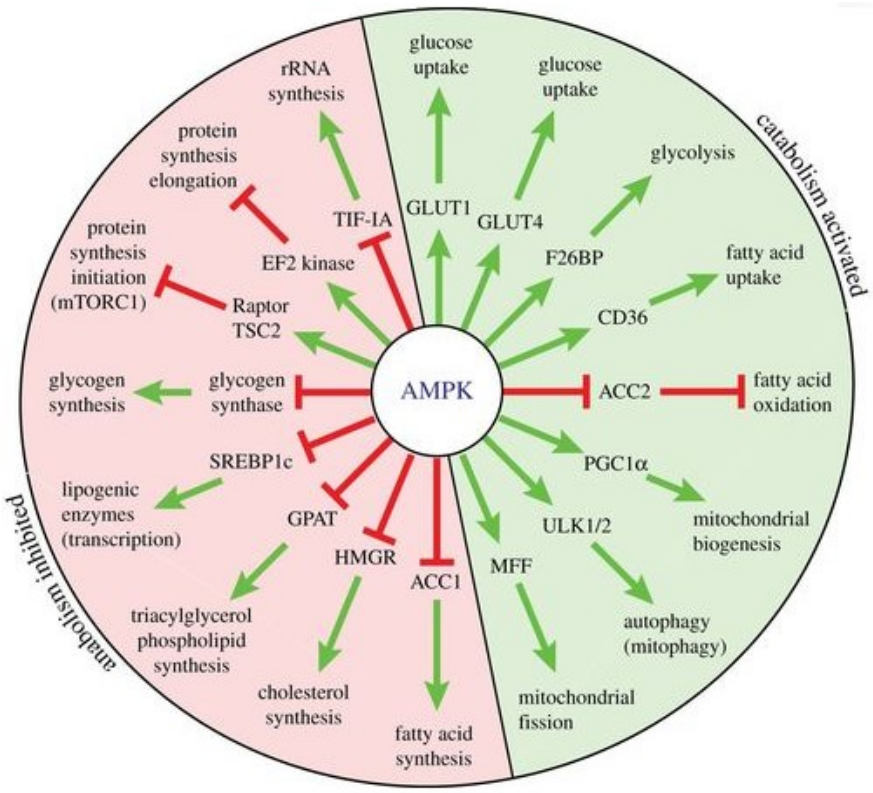

Fig.1.13 Metabolic pathways regulated by AMPK taken from [67].

AMPK aims to increase and preserve the energy state in the cell. It is done by activation of catabolic pathways such as glycolysis, glucose uptake, fatty acid oxidation, and uptake and inhibition of pathways requiring energy such as synthesis of fatty acids, triacylglycerols, cholesterol, glycogen, and proteins.

ACC, acetyl CoA carboxylase; CD36, cluster of differentiation 36; EF2 kinase, elongation factor 2 kinase; F26BP, fructose 2,6-biphosphate; GLUT, glucose transporter; GPAT, glycerol-3-phosphate acyltransferase; HMGCR, hydroxymethylglutaryl coenzyme A reductase; MFF, mitochondrial fission factor; mTORC1, mammalian target of rapamycin complex 1; PGC1α, peroxisome proliferator-activated receptor gamma coactivator 1-alpha ; SREBP1c, sterol regulatory element-binding protein 1c; TIF-1A, transcription intermediary factor 1-alpha; TSC2, tuberous sclerosis complex; ULK1/2, unc-51 like autophagy activating kinase

1.3.3 Regulation of adipose tissue metabolism on a transcriptional level

Metabolic pathways are regulated also on the level of gene expression by various transcription factors, co-activators, and nuclear receptors. Due to their important role in both glucose and lipid metabolism, this chapter will be mainly focused on the family of PPAR, PPARγ coactivators, and SREBP and ChREBP.

PPAR are nuclear receptors, which are activated by many endogenous ligands including phospholipids, endocannabinoids, PUFA, and oxylipins. PPAR function as a heterodimer in association with retinoid X receptor, forming co-activator complex, that binds to DNA sequence termed peroxisome proliferators response elements present in the promoter of target genes. This results in activation or repression of transcription of various genes. The family of PPAR consists of three members, PPARα, PPARβ/δ, and PPARγ. They are involved in energy metabolism regulation. However, they differ in the spectrum of their activity, tissue distribution, ligand specificity, and coactivator recruitment. PPARα is mainly expressed in the liver, and to a smaller extent in muscle, heart, and bone, while PPARβ/δ is expressed ubiquitously. Both of them are predominantly involved in whole-body regulation of energy expenditure, whereas PPARγ, present mainly in adipose tissue, macrophages, and colon, regulates energy storage, and cell differentiation [93].

PPARα plays a crucial role in intracellular lipid metabolism, especially FAox, and has a potential role in the oxidant/antioxidant pathway. PPARα is involved in all processes of FAox, predominantly in the liver, starting with uptake to the cell, through activation of FA and transport to the mitochondria, and ending with the oxidation itself. However, it is also expressed in WAT, where activation of PPARα induces genes involved in FAox such as Cpt1β, Ucp3, and acyl-CoA oxidase and in adipogenesis including Pparγ, adiponectin, and adipocyte protein 2 (**AP2**, also known as **FABP4**). In BAT, PPARα cooperates with PGC1α to control FAox and thermogenesis in response to CE [94, 95]. In summary, PPARα is a major regulator of FA metabolism and energy homeostasis and functions as a FA sensor [96].

PPARγ participates in various biological pathways such as adipocyte differentiation and

lipid and glucose metabolism (**Fig.1.14**), thus it becomes no wonder it is a target of antidiabetic drugs e.g. thiazolidinediones (**TZD**). PPARγ agonist pioglitazone, one of the TZD, decreases TNFα expression in AT and thereby contributes to improve insulin resistance. PPARγ induces the expression of genes involved in lipogenesis and FA storage. It stimulates FA uptake by inducing Lpl, Cd36, and Ap2. Also, activation of FA in the cell is increased via PPARγ stimulation of Acsl. Moreover, PPARγ induces Pck and pyruvate carboxylase, important enzymes for glyceroneogenesis, and Pdk4, a kinase that inhibits pyruvate dehydrogenase enzyme and thereby pyruvate is not used as a precursor for the TCA cycle but rather for glyceroneogenesis. In addition, PPARγ activation in fat induces mRNA levels of insulin-stimulated glucose transporter Glut4, which improves insulin sensitivity [97]. Overall, PPARγ not only promotes preadipocyte and adipocyte differentiation and the associated lipogenesis but also modulates angiogenesis, which is an important component of AT development and remodeling (see also 1.4)[98].

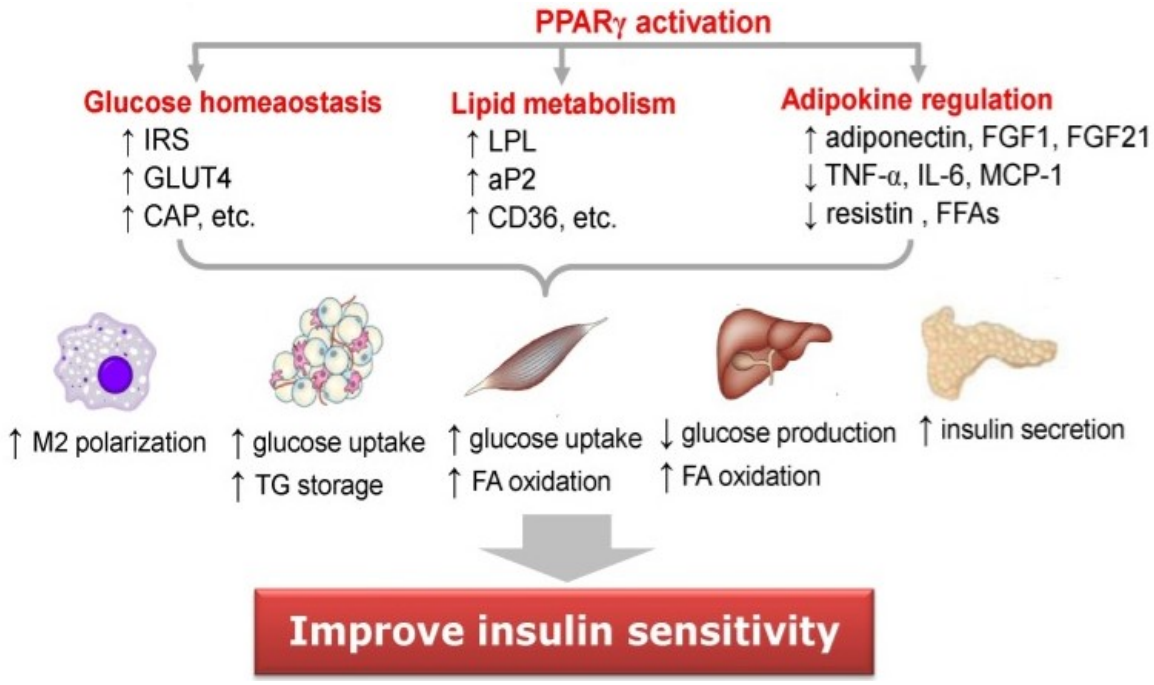

Fig.1.14 PPARγ downstream regulatory pathway taken from [99].

PPARγ influences transcription of many proteins involved in glucose and lipid homeostasis and adipokine regulation which affect glucose uptake in adipose tissue and skeletal muscle, fatty acid oxidation in skeletal muscle and liver, insulin secretion by the pancreas, and others. aP2, adipocyte protein 2; CD36, cluster of differentiation 36; FFA,free fatty acid; FGF, fibroblast growing factor; GLUT, glucose transporter; IL, interleukin; IRS, insulin receptor substrate; LPL,lipoprotein lipase; MCP,monocyte chemoattractant proteinPPAR,peroxisome proliferator-activated receptor; TNF, tumor necrosis factor.

Both PPARα and PPARγ agonists induce Ucp1 gene expression in BAT. However, PPARγ

is suppressed during thermogenic activation. Therefore, it was suggested that the main player in control of Ucp1 expression is PPARα and that PPARγ is rather involved in the differentiation of brown adipocytes [100].

PPARδ/β promotes FA metabolism via inducing Ucp1 mRNA in both WAT and BAT and activation of genes involved in oxidation and thermogenesis *in vitro* and suppresses inflammation induced by macrophages. It was also suggested that PPARβ/δ attenuates atherogenesis via the reduction of expression of inflammatory mediators and adhesion molecules [93].

Members of the PGC1 family interact with various transcription factors and chromatin-remodeling proteins. The outcome of these interactions is dependent on a tissue. Both PGC1α and PGC1β (**Fig.1.15**) play a significant role in the control of the energy metabolism of cells. They are involved in the regulation of adaptive thermogenesis, metabolism of glucose and FA, mitochondrial biogenesis, angiogenesis, immune response control, phospholipid synthesis, circadian clock, heart development and switch in skeletal muscle fiber type. [101, 102]. Both PGC1α and PGC1β are expressed mainly in tissues with high energy requirements and mitochondrial content, including BAT, heart, skeletal muscle, and kidney. Both PGC1α and PGC1β are able to partially compensate for each other functions. Double KO of PGC1α and β results in a severe reduction in mitochondria density and expression of genes involved in thermogenesis and mitochondrial respiration [101, 103]

In WAT, PGC1α expression is relatively low and it is stimulated during adipocyte differentiation, by TZD treatment or via β-adrenergic stimulation [101]. The main function of PGC1α in WAT seems to be the induction of Ucp1 expression associated with TZD-induced differentiation of brite adipocytes in WAT. In BAT, PGC1α induces mitochondrial biogenesis and thermogenic program, which involves activation of Ucp1 and deiodinase expression via coactivation of thyroid hormone receptor, PPARγ, and others. Overexpression of PGC1α activated thermogenesis also in WAT. Its unique function was demonstrated upon CE on mice with a whole-body deletion of all PGC1α isoforms. Mice were unable to regulate adaptive thermogenesis leading to cold intolerance. In thermoneutral conditions, the deletion of PGC1α did not influence the expression of genes involved in OXPHOS, Ucp1, iodothyronine deiodinase 2, and other gene expression in BAT.

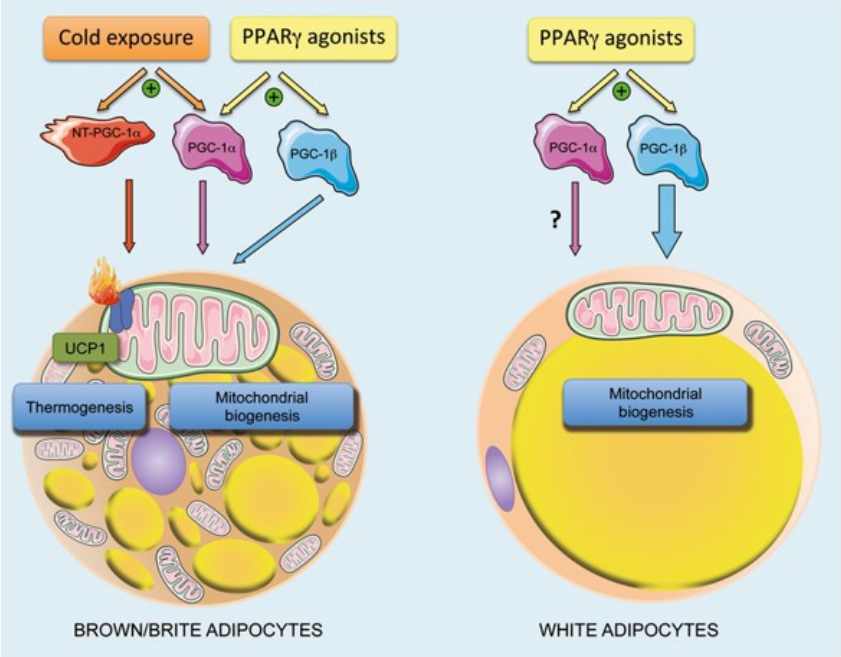

Fig.1.15 PGC functions in adipose tissue taken from [101].

PGC1α is in BAT activated not only by PPARγ agonist but also by cold exposure, unlike PGC1β. In WAT, both PGC1α and β are activated by PPARγ agonists. Downstream targets are genes involved in mitochondrial biogenesis.

NT-PGC, n-terminal peroxisome proliferator-activated receptor gamma coactivator; PGC, peroxisome proliferator-activated receptor gamma coactivator; PPAR, peroxisome proliferator-activated receptor; UCP, uncoupling protein.

Despite PGC1β low gene expression in WAT, it was shown to play a significant role in the regulation of mitochondrial gene expression in basal conditions. Also in BAT, PGC1β plays a major role in sustaining of basal mitochondrial function. Impairment of mitochondrial gene expression and oxidative capacity is the probable cause of cold intolerance in PGC1β whole-body KO mice even though, thermogenic program (i.e. expression of Ucp1 and iodothyronine deiodinase 2 genes) is not affected in mice with deletion of PGC1β [101]. To sum up, PGC1α function is important for the regulation of the thermogenic program after adrenergic stimulation which suggests the potential role of PGC1β in thermoneutral (basal) conditions and in compensation of lack of PGC1α [101].

Other key players in energy homeostasis regulation are transcription factors SREBP and ChREBP (**Fig.1.16**). SREBP induces the expression of genes involved in lipogenesis and cholesterogenesis such as Acc, Fasn, Elovl6, Scd1, hydroxymethylglutaryl-CoA synthase, and hydroxymethylglutaryl-CoA reductase [104, 105]. Moreover, it was shown that SREBP1 is required for adipogenesis probably via the production of endogenous PPARγ ligands [104]. However, the exact role of SREBP in adipogenesis is controversial. SREBP1c (also known as ADD1) acutely enhances TAG accumulation, but chronically its overexpression leads to lipodystrophy, while

SREBP1a overexpression results in enlarged (hypertrophic) white and brown adipocytes [104-106]. SREBP are activated upon energy intake by insulin action. On the other hand, fasting and starvation lead to activation of glucagon and AMPK, which both suppress SREBP transcription [104, 105].

ChREBP is involved in the regulation of lipogenic gene expression including Acc1, Fasn, and Elovl6, and hormones and hormone receptors influencing lipogenesis e.g. glucagon receptor [107]. Glucose activates canonical ChREBPα isoform which then induces the recently described isoform ChREBPβ [108]. Both isoforms are abundantly expressed in WAT and BAT. However, Chrebp mRNA is much more expressed in BAT and liver in comparison to WAT [107]. The expression of ChREBP is influenced by a state of satiety. Fasting results in phosphorylation of ChREBP by PKA and AMPK which prevents enter of ChREBP to the nucleus and initiation of the ChREBP target´s gene transcription. On the other hand, high glycemia leads to dephosphorylation/activation of ChREBP. Dephosphorylated ChREBP is then allowed to enter the nucleus where promotes target gene transcription [109]. ChREBP mRNA is also increased during the differentiation of adipocytes. In BAT, ChREBP and PPARα were shown to inhibit each other reciprocally, which suggests their role in the regulation of switch between lipogenesis and lipolysis [107, 109].

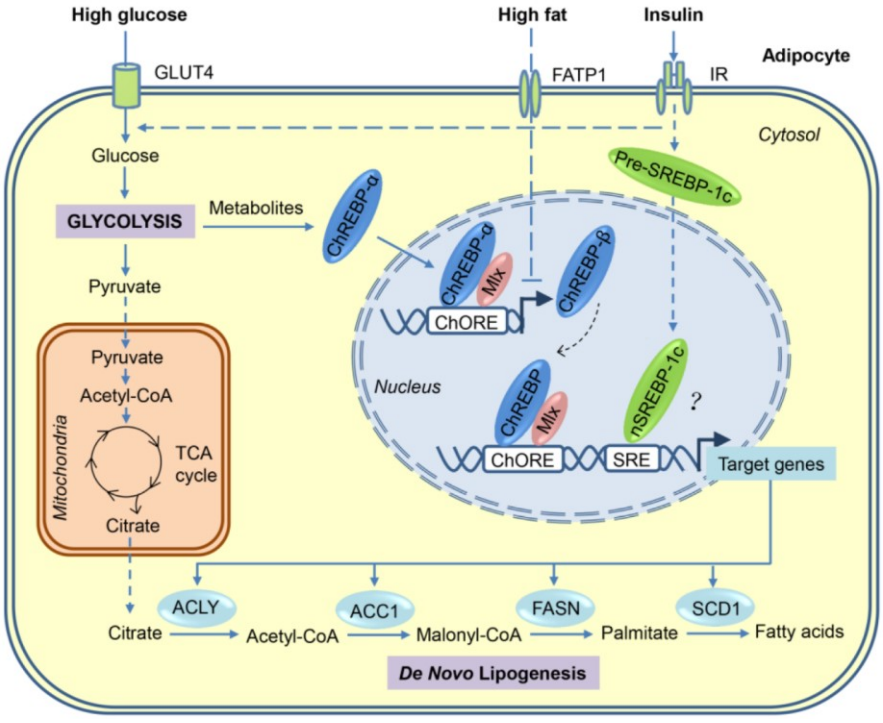

Fig.1.16 Regulation of SREBP and CHREBP action on the lipogenic program taken from [110].

Both Srebp and Chrebp activate transcription of genes involved in lipogenesis, such as ACLY, FASN, and others.

cAMP, cyclic adenosine monophosphate; ChRE, carbohydrate responsive element; ChREBP, carbohydrate responsive element binding protein; PUFA, polyunsaturated fatty acid; SRE, sterol responsive element; SREBP, sterol regulatory element binding protein.

1.4 Adipogenesis

The adipocyte number was assumed to be determined early in life, and through the time mostly stable. However, recent rodent studies demonstrated that new adipocytes can emerge and contribute to AT expansion [111]. In humans, approximately 10% of body fat cells are replaced per year [112]. Adipocytes are derived from pluripotent mesenchymal stem cells in a process called adipogenesis. Adipogenesis has two major steps: i) determination (initiation) and ii) differentiation (**Fig.1.17**) [112]. In determination, stem cells lose the ability to differentiate into specialized cell types and become committed to adipose lineage [113]. This step is done without any morphological changes and preadipocytes are formed [111]. Preadipocytes then undergo clonal mitotic expansion and differentiate into mature adipocytes, which are able to store TAG, respond to insulin, synthesize FA, etc. [114]. Mature adipocytes are not able to divide mitotically. However, some studies reported that adipocytes can de-differentiate and then re-differentiate [112].

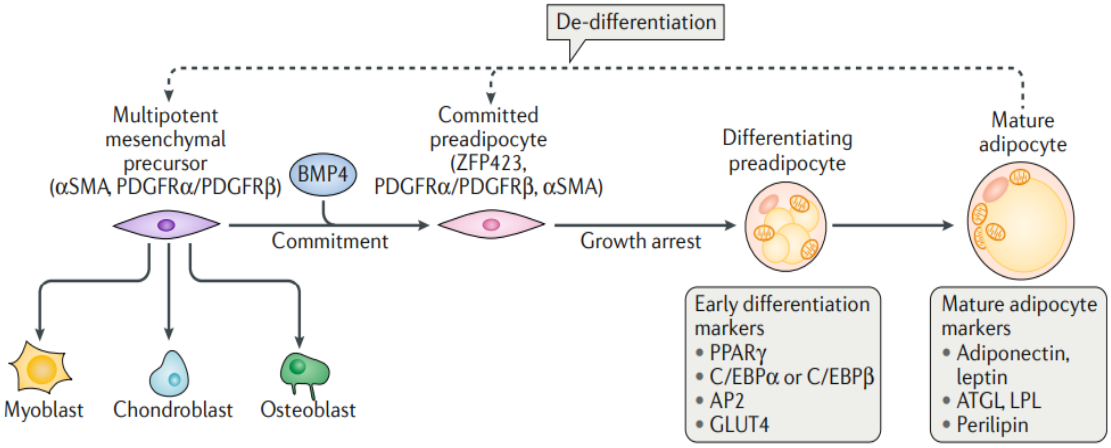

Fig.1.17 Scheme of adipogenesis taken from [111].

The multipotent mesenchymal precursor can differentiate into preadipocytes, myoblasts, chondroblasts, and osteoblasts. BMP plays important role in the commitment of multipotent precursors to adipogenesis. The second step is then differentiation to mature adipocyte. Many factors influence the differentiation of adipocytes such as PPARγ and CEBPα. Mature adipocyte express adiponectin, leptin, Atgl, and other markers.

AP2, adipocyte protein 2; αSMA, alpha smooth muscle actin; ATGL, adipose triglyceride lipase; BMP, bone morphogenetic protein; CEBP, CCAAT-enhancer-binding protein; GLUT, glucose transporter; LPL, lipoprotein lipase; PDGFR, platelet-derived growth factor receptor; PPAR, peroxisome proliferator-activated receptor; ZFP423, zinc finger protein 423.

All steps in adipogenesis are strictly regulated. In the early phase when the multipotent mesenchymal precursor is still not determined to adipocyte lineage, bone morphogenetic proteins (**BMP**), particularly, BMP2 and BMP4 drive adipocytes determination [111]. BMP4 promotes

adipogenesis and at the same time inhibits myogenesis [115]. Binding of BMP2 and BMP4 to BMP receptors leads to activation of transcription factor mother against-decapentaplegic homolog (**SMAD**) 4 [113], which moves adipogenesis to next step, differentiation, by stimulating of PPARγ. The transcription factor involved in both the early phase and differentiation phase is zinc finger protein (**ZFP**) 423. It sensitizes fibroblasts to BMP signaling, while suppressing osteogenesis, and enhances expression of another important regulator of adipogenesis CEBPα [111]. CEBPβ and CEBPδ play a significant role in the induction of PPARγ and CEBPα, which activate a positive feedback loop to further induce their expression [113]. PPARγ and CEBPα are by right called adipogenic masters. They are able to stimulate adipogenesis without any exogenous agent. While PPARγ induces expression of many genes i.e. Ap2 [111], Cd36, Lpl, Pdk4, Pck [98], CEBPα is required to extend adipocyte´s functions of insulin sensitivity [113]. Interestingly, while CEBPα is not necessary for embryonic adipogenesis (probably can be replaced by CEBPβ), in adult adipogenesis it is [111]. Also, other transcription factors such as GATA2/3, retinoic acid receptor α, or SMAD6/7 are involved in adipogenesis [113]. To sum up, at one moment there are plenty of signals that simultaneously activate one pathway while inhibiting another one and/or that activate and inhibit the same pathway. The ratio of these factors determines the fate of pluripotent mesenchymal stem cells [115]. Differentiation then results in a change of function and morphology of the cells. All transcription factors involved in differentiation are to some extent responsible for the production and storage of lipids in adipocyte, thus these factors enable the adipocyte to carry out its unique function [112]. The complexity of adipogenesis is shown in **Fig.1.18**.

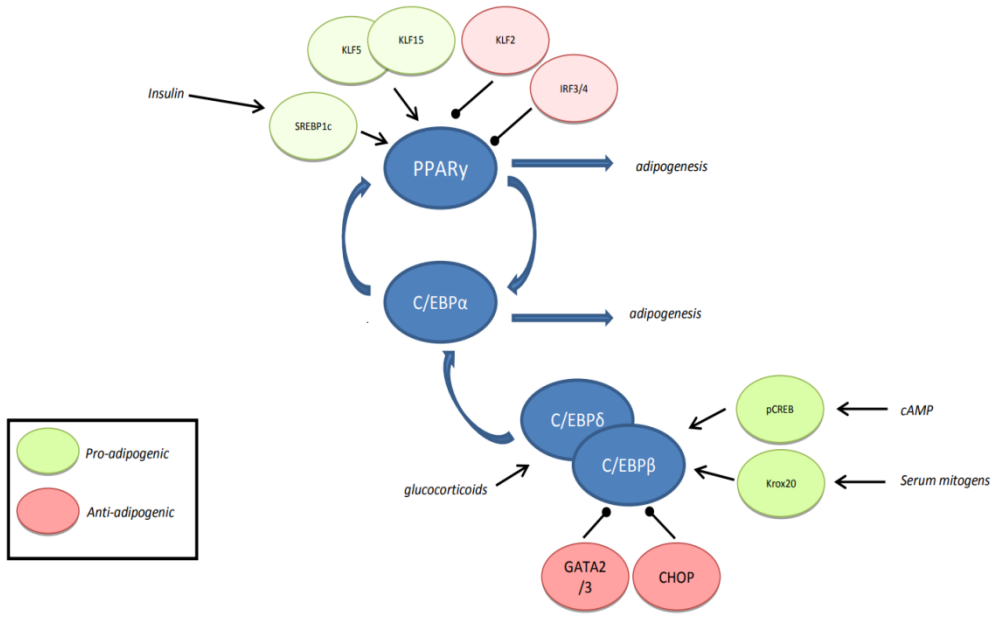

Fig.1.18 PPARγ and CEBP activation of adipogenesis taken from [112].

CEBP and PPARγ are essential factors in adipogenesis. CEBPα and PPARγ influence each other with a positive feedback loop, they are also activated by CEBPβ and δ. Moreover, other factors such as SREBP, KLF, GATA, and others positively or negatively regulate CEBP and PPARγ activation.

cAMP, cyclic AMP; CEBP, CCAAT-enhancer-binding proteins; CHOP, C/EBP homologous protein; CREB, cAMP response element-binding protein; IRF, interferon regulatory factor; KLF, Krüppel-like factor; PPAR, peroxisome proliferator-activated receptor; SREBP, sterol regulatory element binding protein.

Recently, it was shown, that WAT and BAT do not originate from the same progenitor cells. Brown adipocytes are more similar to myocytes derived from myogenic factor (**MYF**) 5 positive progenitor lineage, while white adipocytes are derived from MYF5 negative lineage. However, MYF5 positive cells were found even in WAT depots prone to browning [116]. Differentiation of brite cells is induced by PPARγ ligands, sympathetic stimulation, and others. PR domain containing 16 (**PRDM16**) plays a key role in brite and brown fat differentiation. It coactivates PGC1α and PPARγ and suppresses white fat cell markers expression [25, 117, 118]. Brite adipocytes can origin either from common progenitor residing within WAT via differentiation or from white adipocytes via transdifferentiation. Interestingly, platelet derived growth factor receptor (**PDGFR**) α^+ $CD4^+$ stem cells antigen (**Sca**) 1^+ early precursors, that were isolated from WAT, differentiated into both BAT and WAT depending on stimulating agents [19, 119]. It was also shown that brite adipocytes arise by *de novo* adipogenesis using AdipoChaser mouse (model tracking adipogenesis *in vivo*)[120].

Adipogenesis is positively regulated by insulin, glucocorticoids, and FA (e.g. from high fat diet, **HFD**). Insulin stimulates preadipocytes' conversion to additional adipocytes for nutrient

storage. Of note, it is unclear how preadipocytes discriminate between elevated insulin caused by overnutrition and physiologic increase postprandially. Glucocorticoids sensitize preadipocytes to insulin signaling, upregulate CEBP, are important for terminal differentiation, and enable preadipocytes growth arrest [111]. Saturated FA in HFD induced AT hypertrophy and hyperplasia. Obesity leads to chronic low-grade inflammation which is a result of insufficient adipogenesis and increased production of TNFα, IL6, and interferon γ (**IFNγ**) cytokines, which further impair adipocyte differentiation. Also transforming growth factor β (**TGFβ**) acts antiadipogenically via SMAD3, which inhibits PPARγ/CEBPα complex formation. However, acute (transient) inflammation is an important part of tissue remodeling, e.g. TGFβ promotes beneficial beige adipogenesis in WAT. TGFβ was also shown to promote the first part of adipogenesis by stimulating preadipocyte proliferation while inhibiting the second. Metabolites of PUFA, prostacyclin, and d-prostaglandin (**PG**) J2, stimulate adipogenesis. In contrast, PGF2a was shown to inhibit adipocyte differentiation *in vitro* [111, 114]. Also, docosahexaenoic acid (**DHA**) inhibited the differentiation of adipocytes in cell culture. Moreover, in post-confluent preadipocytes, DHA induced apoptosis [121].

1.4.1 Angiogenesis and adipogenesis

Angiogenesis and adipogenesis are during prenatal life spatially coupled processes. Postnatally, they interact via paracrine signals (**Fig.1.19**). Angiogenesis is required for efficient preadipocyte differentiation, while adipocyte differentiation is needed for neovascularization [122]. In developing tissue, angiogenesis precedes the formation of AT and is able to regulate AT growth. Vascular endothelial growth factor (**VEGF**) A, is expressed in AT and it is increased during adipocyte differentiation. VEGF is necessary to initiate the immature vessel formation both in the adult and during development [123]. PPARγ pathway seems to be involved in both adipogenesis and angiogenesis. PPARγ ligands induce Vegfa gene expression in adipocytes. Adipocytes produce many pro-angiogenic factors like angiopoietins, VEGF, TNFα, TGFβ, and leptin [124], and the ratio between these and angiostatic factors such as angiostatin, endostatin, and the thrombospondins influence the angiogenesis [125]. Moreover, the recruitment of inflammatory cells such as macrophages induces the production of angiogenic factors including TNFα, VEGF, IL1β, IL6, and IL8 [124].

Both hyperplasia and hypertrophy of adipocytes are behind the expansion of AT mass. These processes are linked to extensive neovascularization via the endothelial cells sprouting from preexisting blood vessels. Properly functional energy metabolism requires efficient blood perfusion to supply nutrients and oxygen and to export heat. E.g. BAT hyperplasia needs rapid activation of fat precursor cells and endothelial cells to develop capillaries, thus it is critically dependent on

angiogenesis [126].

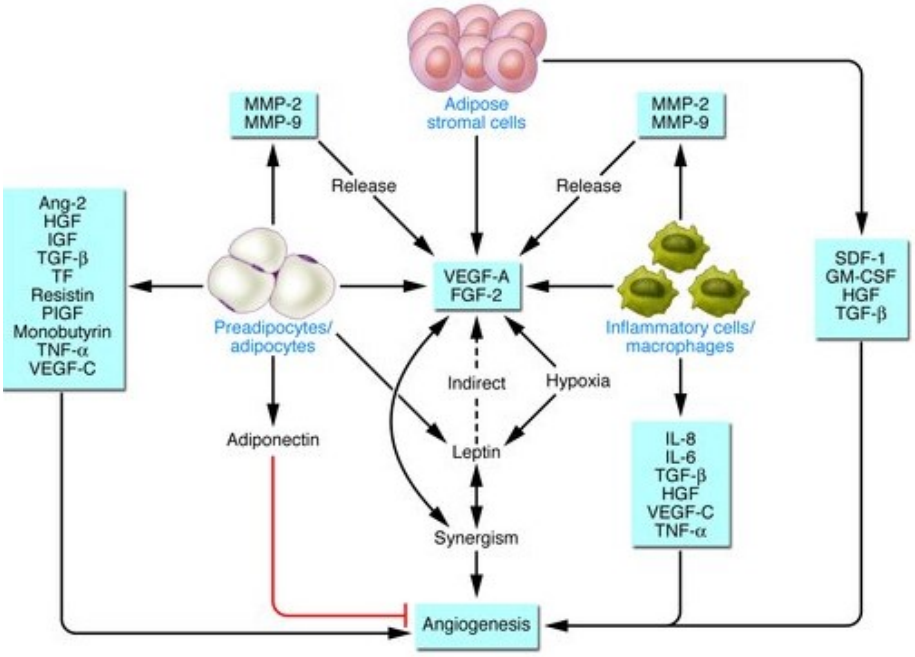

Fig.1.19 Adipogenesis and angiogenesis co-action taken from [124].

FGF, fibroblast growing factor; GM-CSF, granulocyte-macrophage colony-stimulating factor; HGF, hepatocyte growth factor; IGF, insulin-like growth factor; IL, interleukin; MMP, matrix metallopeptidase; PlGF, placenta growth factor; SDF, stromal cell-derived factor; TF, transcriptional factor; TGF, transforming growth factor; TNF, tumor necrosis factor; VEGF, vascular endothelial growth factor.

1.4.2 Remodeling of adipose tissue during hyperplasia and/or hypertrophy

The proper response of adipocytes to fluctuations of lipid stores is crucial due to AT ability to affect the whole-body metabolism [127]. There are two ways how AT can expand; hypertrophy and hyperplasia (**Fig.1.20**). In the case of hypertrophy, AT is expanded by enlarging existing adipocytes. Hyperplasia involves the formation of new cells - adipogenesis. In adults, hypertrophy seems to predominate. Adipose hypertrophy results in NEFA efflux, altered vascularization, increased leptin secretion, hypoxia, and adipocyte death, which induce extensive tissue remodeling of the extracellular matrix and deposition of collagen. Macrophages play a main role in the remodeling of AT [128]. They engulf dead adipocytes to help the cellular turnover of adipocytes and take up and process NEFA liberated by lysosomal enzymes. An increased number of proliferating macrophages was found in crown-like structures (**CLS**) in obesity probably due to macrophages´ proliferating factors including MCP1 secreted by dying adipocytes [129, 130]. CLS are microscopic foci of dying adipocytes, positively stained for markers for pro-inflammatory macrophages, namely F4/80, MAC2, TNFα, and IL6, [131]. The process of CLS formation and the removal of dead

adipocytes are considered to be beneficial for tissue homeostasis. Macrophages in CLS contain multiple lipid droplets and resemble foam cells. However, when the capacity of macrophages to buffer lipids is insufficient, they are unable to cope with the nutrient overload. Both obese and dying adipocytes secrete pro-inflammatory mediators including TNFα and monocyte chemoattractant protein (**MCP**) 1 to lure more macrophage to AT [129].

According to Surmi et al., during AT adaptation to HFD, there is a shift from mostly hypertrophy to mostly hyperplasia. Adipocytes in mouse AT after 20 weeks of HFD administration were smaller than at week 16. Also, collagen deposition and the number of dead adipocytes were strikingly decreased at week 20. However, these beneficial changes in AT were connected with toxic ectopic depositions of lipids in the liver [131]. Another study (using AdipoChaser mouse) showed, that adipogenesis/hyperplasia was initiated in epididymal fat after 4 weeks of HFD, while in subcutaneous fat, hyperplasia prevailed up to 12 weeks of HFD [120], which shows that various WAT depots have various responses (i.e. in preferation of hyperplasia or hypertrophy) to lipid overload.

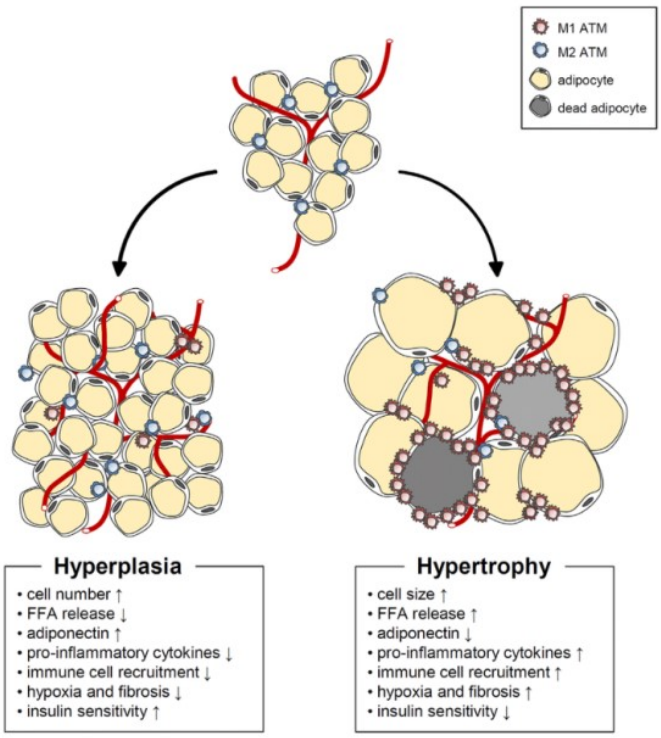

Fig.1.20 Hyperplasia vs hypertrophy taken from [15].

Changes in AT attributes in hyperplasia and hypertrophy.

ATM, adipose tissue macrophages; FFA, free fatty acid.

Macrophages regulate fibrinogenesis by secretion of matrix metallopeptidases which lead to altered angiogenesis and recruitment of fibroblasts. The expression of several metallopeptidases was increased in AT of diet- or genetically- induced obesity mice. Angiogenic factor platelet derived growth factor (**PDGF**) was induced in obesity as well. In lean mice, preadipocytes produce most PDGF, while in obesity macrophages become its significant contributor [131]. PDGFRα is able to directly activate PI3K/Akt2 pathway during hyperplasia, which is required for the proliferation of WAT progenitors [132].

The vasculature is unable to follow the rapid expansion of AT which contributes to increased inflammatory response via hypoxia-inducible factor (**HIF**) 1α [129, 133]. HIF1α was shown to regulate IL1β and other inflammatory genes in mice [129]. Hypoxia leads to increased expression of macrophage migration inhibitory factor, which inhibits macrophages emigration [134]. In preadipocytes, HIF1α produced by macrophages prevents angiogenesis. Inhibition of HIF1α in macrophages results in significant metabolic improvements [135].

In conclusion, AT remodeling involves many cellular responses such as modulation of angiogenesis, extracellular matrix remodeling, and recruitment of macrophages, which are changed dynamically. These processes contribute to the maintenance of healthy AT. However, chronic excessive energy supply in obesity initiates pathological remodeling. Pro-inflammatory responses and metabolic stress prevail over physiological changes leading to systemic inflammation and insulin resistance [15].

1.5 Adipose tissue imunometabolism

AT contains immune cells, fibroblasts, and endothelial cells on the top of adipocytes. All types of cells contribute to the secretory function of AT by producing cytokines, which influence metabolism and immune responses [136]. AT resident immune cells have a large range of functions from cell clearance to extracellular matrix remodeling and/or angiogenesis in lean subjects. In contrast, obesity induces signaling pathways which leads to chronic inflammation [137]. Recently, a new field, connecting metabolism and immunity, called immunometabolism raised. It can be described as the ability of both the immune system to coordinate systemic metabolic homeostasis and the tissue metabolism to affect activation, proliferation and polarization of immune cells including their own metabolism [137-139].

1.5.1 Cytokines

Cytokines are small signaling proteins produced by various cells including immune cells such as macrophages, B lymphocytes (**B cells**), T lymphocytes (**T cells**), mast cells, as well as endothelial cells, fibroblasts, and various stromal cells. In lean AT, interleukins connected with an

anti-inflammatory state and physiologic metabolic homeostasis prevail, namely IL4, IL5, IL13, IL10, and IL33 (**Fig.1.21**). On the contrary, obese individuals mainly produce and secrete pro-inflammatory cytokines such as TNFα, IL1β, and IL6 (**Fig.1.21**) [140].

T cells are the major source of cytokines, especially T cells with the presence of cell surface molecule CD4 known as helper T (**Th**) cells [141]. Based on the stimuli, Th cells are able to polarize into different phenotypes that express distinct cytokine profiles and exert different effector functions. Th2 cells produce type 2 cytokines such as IL4, IL5, and IL13 to promote the polarization of alternatively activated anti-inflammatory M2 macrophages. Th1 cells produce e.g. IFNγ, which promotes the polarization of classically activated pro-inflammatory M1 macrophages and participate in the elimination of intracellular microbes [142].

1.5.1.1 Type 2 immune response

Several cell types, including eosinophils and type 2 innate lymphoid cells (**ILC**) 2, have been identified to produce type 2 cytokines in lean AT. These immune cells may contribute to M2 polarization, inflammation resolution, and metabolic homeostasis in WAT [142].

IL4 exerts pleiotropic functions including involvement in the regulation of inflammation, adipogenesis, and lipolysis. IL4 inhibits production and secretion of IL1β and TNFα and secretion and activity of IL6 leading to reduced inflammation. Moreover, IL4 was shown to inhibit lipid accumulation via inhibition of adipogenesis and the promotion of lipolysis. Collectively, IL4 positively influences AT metabolism and inflammation leading to improvement in insulin sensitivity and glucose tolerance [143]. IL5 contributes to the cellular expansion of eosinophils and thereby to an increase in IL4 and IL13 production. IL5 is produced by ILC2, which are stimulated by IL33 [144]. IL33 induces M2 polarization via the upregulation of arginase (**Arg**) 1 and chemokines chemokine C-C motif ligand (**CCL**) 24 and CCL17 [145]. Moreover, IL33 elevates amounts of tissue eosinophils and enhances both serum and tissue IL13 levels, another member of so called type 2 immune response. IL13 together with IL4 and IL5 promote insulin sensitivity and glucose tolerance [146]. Another anti-inflammatory cytokine is IL10. IL10 is expressed by various immune cells including Th1, Th2, $CD8^+$ T cells, B cells, dendritic cells, macrophages, and eosinophils. It plays a central role in infection by limiting the response of immune cells leading to the prevention of damage to the host [147].

1.5.1.2 Type 1 immune response

Obesity increases the levels of class II major histocompatibility complex (**MHC II**) and costimulatory molecules on AT macrophages and/or dendritic cells (**DC**) and also on adipocytes, which function as antigen-presenting cells to promote $CD4^+$ T cell proliferation in AT and therefore

the production of IFNγ. This further activates adipocytes and macrophages and/or DC with elevated MHC II, thereby forming a positive loop to amplify Th1 cell-mediated inflammation in adipose tissue. Moreover, antigen-presenting cells residing in AT may secrete exosomes to promote activation and further Th1 polarization of $CD4^+$ T cells resulting in AT inflammation and insulin resistance [142].

IFNγ attenuates insulin action and lipid storage in adipocytes [133]. It is expressed by both T cells and natural killer (**NK**) cells upon activation. IFNγ was established to play role in mediating the immune response in type 1 diabetes and diet-induced obesity and in the regulation of AT inflammation and endothelial dysfunction in type 2 diabetes [148]. TNFα was believed to be produced by adipocytes. However, it was found that it is predominantly secreted by resident and infiltrating macrophages [133, 149]. TNFα disrupts metabolic homeostasis of adipocytes via downregulation of PPARγ expression, reducing adiponectin secretion by adipocytes and inducing expression of genes involved in lipolysis, ATGL, and HSL, thereby promoting the release of FA from adipocyte [133]. TNFα signaling is, however, not only detrimental for adipocytes but it contributes to normal expansion and remodeling during overfeeding. It was shown that TNFα is needed to properly adapt adipocytes to nutrient excess and prevent from systemic dyslipidemia [133]. IL1β worsens metabolic parameters either directly by inhibiting expression of genes coding GLUT4, PPARγ, and insulin receptor substrate 1 and 2 or indirectly via an increase in the secretion of TNFα and IL6 by macrophages [133]. IL6 is either pro-inflammatory or anti-inflammatory cytokine depending on whether it binds to its membrane receptor or to its soluble receptor [150]. Pro-inflammatory actions of IL6 include decreased insulin receptor gene expression, adipogenesis, and adiponectin secretion [151], while anti-inflammatory actions involve stimulation of M2 polarization and macrophages proliferation via upregulation IL4α receptor [150].

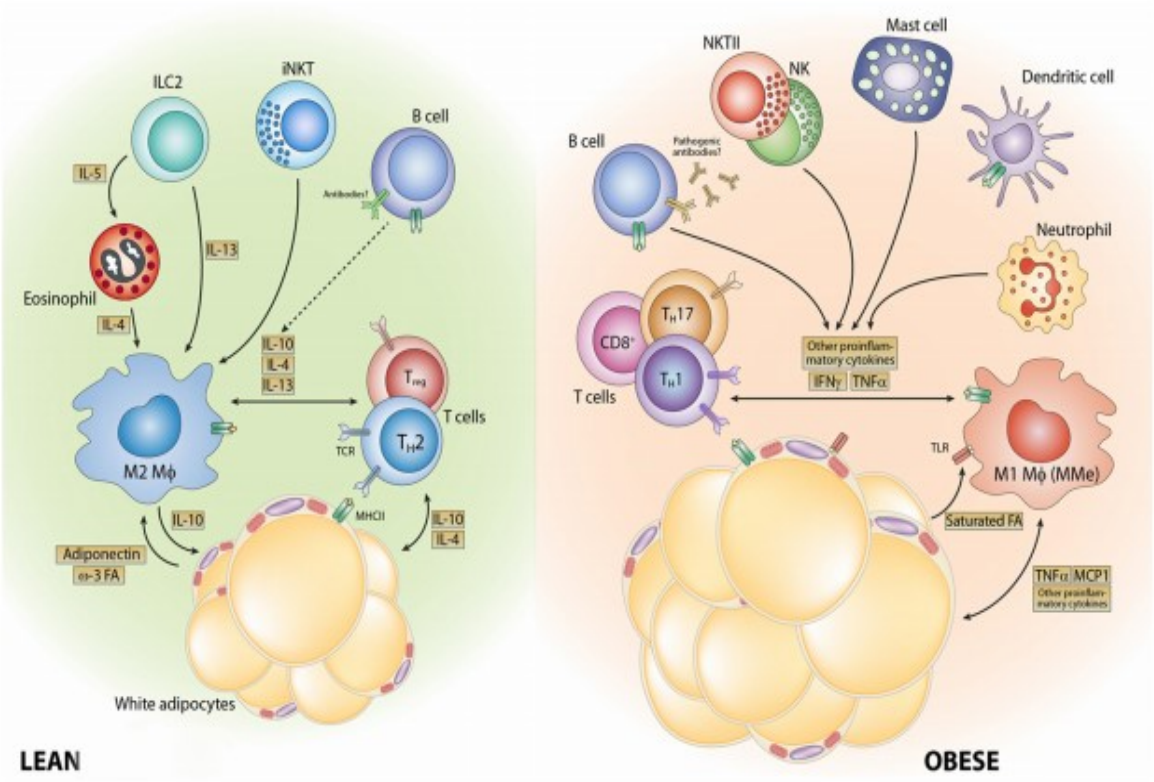

Fig.1.21 Adipose tissue immune cells and signaling via cytokines taken from [152].

CD, cluster of differentiation; FA, fatty acid; IL, interleukin; ILC, innate lymphoid cell; iNKT, invariant nature killer T-cell; MCP, Monocyte chemoattractant protein; MHC, major histocompatibility complex; NK, nature killer cell; NKT, nature killer T-cell; TCR, T-cell receptor; T_H, T helper cell; TNF, tumor necrosis factor; T_{reg}, regulatory Tcell

Chemokines are small chemotactic cytokines that play role in the recruitment of macrophages out of bone marrow and leukocyte chemotaxis into various tissues during inflammation, generally [131]. Based on their molecular structure are chemokines divided into 4 families: CXC, CC, C, and CX3C. While CXC group chemotaxes mainly neutrophils and are involved in early inflammation, most of the CC chemokines attract eosinophils, basophils, monocytes, and T-cells to contribute to chronic inflammation [153]. MCP1 (also known as CCL2) is the most studied chemokine in connection to regulation of migration and infiltration of monocytes/macrophages. In addition, expression of other cytokines such as MCP2, MCP3, macrophage inflammatory protein (**MIP**) 1, CCL5 (also known as **RANTES**) and chemokine C-X-C motif ligand (**CXCL**) 14 as well as C-C chemokine receptor (**CCR**) 2, CCR3, and CCR5 were found to be increased in dietary and/or genetically induced obesity murine models [131]. The inhibition of CCL2 diminishes the infiltration of macrophages but does not completely get rid of it. This suggests the involvement of other chemokines in the infiltration of leukocytes such as CCL5,

CXCL5, CXCL14, etc. [154].

1.5.2 Immune cells

Immune cells are classified as innate, adaptive, and so called bridging cells [137]. Immune cells are able to distinguished invaders from the body´s own cells. Innate immune cells are first to respond to an infection and their response serves to alert and trigger adaptive cells. Innate immune cells do not express antigen receptors or undergo clonal expansion. Neutrophils, macrophages, mast cells, and eosinophils belong to this group. Unlike innate immune responses, the adaptive responses are highly specific to the particular pathogen that induced them. However, these cells require training to learn not to attack their own cells. They provide long-lasting immune protection via specific memory cells. These responses involve T cells and B cells [155]. Innate and adaptive cells are bridged by immune cells e.g. invariant nature killer T (**iNKT**) cells, which are able to recognize antigens, however, only a limited set of them. Functionally, bridging immune cells resemble more innate immune cells as they act quickly and are not able to develop immunological memory [156]. Of note, the main focus in the practical part of the thesis is on macrophages, therefore, they were not included in the overview of innate immune cells but have a separate chapter.

1.5.2.1 Macrophages

The majority of leukocytes in AT are macrophages [133]. In a lean state, it is up to 75% of AT immune cells which corresponds to 10-15% of all cells in AT. Obese mice have up to 50% macrophages in AT [133, 137]. In humans, there are fewer macrophages from around 4% in lean to 12% in obese subjects [137]. Macrophages have been implicated in housekeeping functions like extracellular matrix remodeling, adipocyte precursors´ proliferation, and differentiation, angiogenesis, and keeping homeostasis during fasting and feeding [133, 137]. PPARγ was observed to be involved in some of these functions due to its ability to sensor FA. It is also thought to promote the secretion of IL4 and IL10 which activate anti-inflammatory macrophages. AT macrophages are also involved in the secretion of catecholamines during CE to promote WAT browning [133].

Macrophages progenitors are derived from the yolk sac, fetal liver, and bone marrow. Yolk sac produces progenitors populating all tissues. The fetal liver is initially seeded by progenitors from the yolk sac and is thought to be the source of circulating monocytes during the embryonic stage. As bone marrow grows after birth, hematopoiesis transfers from the liver to it [157]. Importantly, macrophages were shown to be able to reenter the cell cycle even if they were considered to be terminally differentiated [158]. Circulating monocytes are lured to AT, where they become macrophages and respond to the inflammation. Other factors influencing the number of

macrophages in AT are greater survival and proliferation of resident AT macrophages and inhibition of macrophages emigration via migration inhibitory factor [134].

AT murine macrophages are defined by expression of both F4/80 and CD11b markers [159]. Two groups of macrophages are mainly defined in the literature, namely pro-inflammatory M1 and anti-inflammatory M2. M1 macrophages are characterized by the expression of nitric oxide synthase 2 (**NOS2**), CD11c antigen, and TNFα secretion. M2 macrophages secrete IL10 and express CD206 antigen and Arg1 [137]. In a lean state, 90% of macrophages are M2 and only about 1% are M1 macrophages. In obesity both phenotypes are increased, however M1 induction is much larger, leading to more than 50% of the macrophages to be M1. This increase seems to be reversible as was shown in experiments with caloric restriction or TZD [157]. Many either subtypes or mixed phenotypes have been described in the literature [128, 138, 159]. Macrophages also differ in location, function and morphology, generally. They can be interspersed among adipocytes, aggregate around lipid droplets, or associate with vasculature [138]. Due to very complex classification and function of mixed phenotypes of macrophages, I will continue to talk mainly about M1 and M2 macrophages.

M1 and M2 macrophages differ in preference of metabolic pathways. M1 uses more glycolysis, while M2 prefers FAox for fulfilling energy requirements. However, this does not mean that M2 macrophages use only oxidative metabolism and vice versa (more in chapters about M1 and M2 macrophages) [157]. It was shown that an artificial increase of oxidative metabolism induces M2 polarization whereas its inhibition induces M1 polarization [157].

Multinucleated giant cells (**MGC**) are another type of macrophages. They are formed by the fusion of macrophages/monocytes [160]. Fusion is a mannose receptor-mediated phagocytic process with the participation of ER [161]. Two types of MGC were described, smaller Langhans with a limited number of nuclei and foreign body type giant cells highly variable in size [161]. The first type is induced by IFNγ, the latter by IL4, IL13, or α-tocopherol. Importantly, MGC are thought to contribute to the removal of debris from tissue [160].

1.5.2.1.1 M2 macrophages

In the lean state, M2 macrophages represent the majority of resident macrophages in AT. They are involved in anti-inflammatory reactions, helminth infections, wound healing, and tissue remodeling [157]. M2 polarization is driven by eosinophil-derived IL4 and IL13, which via STAT6 induce transcription factors PPARγ and PGC1β. These transcription factors then promote the expression of genes involved in oxidative metabolism, mitochondrial respiration, and biogenesis. Moreover, transcription factor PPARδ/β regulates Arg1 gene expression [128, 157].

M2 macrophages are described by high expression of non-opsonic pathogen receptors e.g.

CD206 (mannose receptor), and CD209 (dendritic cell-specific intercellular adhesion molecule 3-grabbing nonintegrin), which reflects M2 macrophages uptake of lipids, lipoproteins, glycoproteins, and apoptotic cells [145, 162]. Other markers of the M2 phenotype are low IL12 and IL23 and high IL10, IL1RA, and ARG1. ARG1, an enzyme of the urea cycle, metabolizes arginine to ornithine from which polyamines can subsequently be synthesized. This step decreases the production of nitric oxide by the competition of ARG1 with NOS2 for the arginine. Polyamines are necessary for collagen synthesis, and cell proliferation. They were also shown to drive M2 polarization [145, 162, 163]. Additionally, M2 macrophages express chemokines CCL17, CCL22, and CCL24, while chemokines CCL2 and CXCL4 drive macrophages to the M2 phenotype [145]. M2 macrophages also have upregulated ferroportin and downregulated ferritin and heme oxygenase in order to increase iron release which favors tissue repair and cell proliferation [145, 163].

Except for the metabolism of iron and altered amino acid metabolism, M1 and M2 macrophages differ in the metabolism of folate and glucose. M2 macrophages have been described to use aerobic metabolism. However, recently it has been published that glucose is utilized by both anti-inflammatory and pro-inflammatory macrophages. IL4 was shown to induce glucose metabolism via AKT and mammalian target of rapamycin complex 1 signaling. OXPHOS in M2 macrophages (also stimulated by IL4) is induced as well as glycolysis. Inhibition of glycolysis by 2-deoxyglucose and ATP synthase by oligomycin resulted in suppression of IL4 regulated genes and surface markers including Arg1 and CD206. IL4-induced polarization of macrophages was negatively influenced by etomoxir inhibition of CPT1α, however, in the case of inhibition CPT2, no effect on polarization was observed. FA are gained from TAG via CD36 and lysosomal lipase [157]. Lastly, the lack of FATP1 in macrophages induces a switch from FAox to glycolysis, which is accompanied by increased NOS2 and decreased ARG1 [164].

1.5.2.1.2 M1 macrophages

M1 macrophages play a crucial role in defense against bacterial and viral infection and their polarization is driven by Th1 cells via the production of IFNγ [157]. M1 macrophages, defined as $CD11c^{+}$, secrete TNFα, which downregulates Glut4 mRNA and insulin signaling. This leads to the disruption of insulin action in adipocytes. M1 macrophages recruit and activate other AT immune cells by secretion of chemokines like CXCL9 and CXCL10 and antigen presentation [137, 163]. They express low IL10 and high IL12, IL23, IL1β, and IL6. In addition, they produce reactive oxygen and nitrogen intermediates, express MHC II, and have the ability of efficient antigen-presenting [145]. M1 macrophages are also involved in collagen accumulation which leads to AT fibrosis, stress, and increased inflammation [137]. Since iron supports the growth of cells, M1 macrophages increase ferritin and repress ferroportin, which contributes to the bacteriostatic effect [145, 163]. All these changes are acutely beneficial and enable the proper function of immune cells. Impaired metabolism occurs with prolonged inflammation.

As it was described above, the metabolism of macrophages subsets does not rely exclusively on either glycolysis or FAox, both pathways are important. However, some differences can be found. First, glycolysis is the preferred pathway to produce energy to sustain induced secretory and phagocytic function. Unlike M2 macrophages in which PPP is inhibited by sedoheptulose kinase carbohydrate kinase-like protein, M1 macrophages use PPP to produce ribose, NADPH, and erythrose-4-phosphate, which are used for the generation of nucleotides, aromatic amino acids, and ROS. Secreted TNFα decreases LPL synthesis and activity [128]. TCA cycle is disrupted in M1 macrophages after synthesis of both citrate and succinate. Accumulated citrate, caused by suppression of isocitrate dehydrogenase 1, is used for the synthesis of FA and itaconate. Citrate is either converted to oxaloacetate and acetyl-CoA by ACLY or to cis-aconitate by aconitase. Oxaloacetate is used to replenish fumarate in the TCA cycle via arginine-succinate shunt and acetyl-CoA is used for FA synthesis. Induced synthesis of FA, lipids, and prostaglandins leads to the changed organization of plasma membrane and further stimulate inflammatory signaling. Itaconate, derived from cis-aconitate via immune-responsive gene 1, has antimicrobial features and inhibits succinate dehydrogenase, which results in the accumulation of succinate. The supply of succinate is completed via the conversion of glutamine. Succinate enhances HIF1α stabilization by inhibition of prolyl hydrolases, which leads to induced IL1β expression. M1 macrophages secrete succinate to extracellular space, where it is able to alert macrophages and other immune cells about the inflammation [158, 164, 165].

1.5.2.1.3 Obesity-induced transition to M1 macrophages

Upon high-fat feeding expression of genes such as Arg1 and Il10 is decreased while Tnfα and Nos2 are increased, indicating a rise of M1 macrophages. M1 macrophages highly express Il6, Nos2, and Ccr2, the characteristics of migratory phagocytic cells [131]. Interestingly, there was not any difference in Tnfα, Cd206, and Cd11c mRNA between recruited and resident macrophages [162]. The initiation of macrophages recruitment is thought to be promoted by endothelial cells and adipocytes. However, macrophages, themselves, contribute to the propagation of the signals for the further attraction of new macrophages [131]. Additionally, NEFA plasmatic levels are increased in obesity, which leads to activation of the toll-like receptor (**TLR**) 4 inflammatory signaling [129]. One of the main signals luring monocytes/macrophages to AT is MCP1. It is recognized by $Ly6C^{+}$ monocytes, which then migrate to AT and differentiate to M1 macrophages [157]. Another signaling pathway is via CCL5 and CCR1 receptor [137]. In obesity mainly M1 macrophages are recruited to AT/differentiate from monocytes, which is a central feature of the phenotypic switch. Nevertheless, some studies show that macrophages have mixed activation or at least do not belong strictly to the M1 or M2 phenotype, e.g. $CD11c^{+}Mgl^{mid}$ macrophages were observed in AT of mice, which had upregulated M2 genes involved in tissue remodeling and repair [159].

Unexpectedly, it was also shown, that macrophages are increased not only by recruitment but also by cell division in visceral AT. Moreover, depletion of blood monocytes had no impact on the amount of AT macrophages *in vivo* and MCP1 induced macrophages proliferation in AT explants [130]. M1 macrophages further support the increase of their numbers via contribution to the accumulation of collagen and thereby increase of AT fibrosis, stress, and inflammation. This also leads to the activation of other immune cells, which further promote M1 polarization [137]. Moreover, macrophages and adipocytes influence each other paracrinally. TNFα secreted by macrophages induce FA lipolysis and interfere with insulin signaling in adipocytes. Released FA then exacerbate the inflammatory polarization of macrophages via the TLR4 receptor [131, 157]. Overall, both increased M1/M2 ratio and altered cytokine balance contribute to pro-inflammatory crosstalk between adipocytes and AT immune cells and further propagation of inflammation [128].

1.5.2.2 Innate immune cells

The innate immune system is the dominant system of host defense in most organisms. Innate immune cells act non-specifically and quickly against pathogens. However, they are not able to remember pathogens and thus provide long-lasting immunity against a pathogen. The innate immune response involves neutrophils, macrophages, mast cells, and eosinophils [155].

Recruitment of neutrophils was observed at the very start of inflammation. It is mediated via cytosolic phospholipase A2a and precedes the recruitment of macrophages [166]. Neutrophils

secrete neutrophil elastase, which is able to induce M1 (pro-inflammatory) macrophages and also contributes to the origin of insulin resistance via degrading insulin receptor substrate 1 [129, 166]. Moreover, neutrophils produce myeloperoxidase, which uses H_2O_2 for oxidation reactions to produce hypochlorous acid, nitrogen dioxide, etc., which help with the pathogen killing during infection [167]. Blood monocytes reflect the accumulation of inflammatory $CD11c^+$ macrophages in WAT in mice [168].

Eosinophils are granulocytes mainly involved in parasitic infections and allergy reactions. They also regulate AT metabolic homeostasis, despite their low abundance [166]. They form around 5% of stromal vascular fraction (**SVF**) cells and their amount is decreased in obesity [129]. Eosinophils drive M2 (anti-inflammatory) polarization by secretion of IL4 and IL13 in lean AT, which was proved by a positive correlation between M2 macrophages and eosinophils [129, 137]. Eosinophils can be activated by IL33 either directly or via ILC-derived IL5 [167]. They also facilitate thermogenesis and brite adipogenesis via activation of β-adrenergic receptors by releasing IL4, thereby promoting insulin sensitivity [166].

ILC are other innate immune cells observed in AT. Three subtypes of ILC have been shown so far [167]. ILC1 are increased shortly after the onset of HFD feeding [129, 157]. They are activated by IL12, IL15, and IL18 and secrete IFNγ and TNFα [167]. In obesity, high amounts of INFγ are produced leading to the promotion of M1 polarization and insulin resistance [166]. ILC2 express IL4, IL5, and IL13, which promotes accumulation of eosinophils and M2 macrophages, that could be also activated via IL4 produced by eosinophils. They were also shown to produce methionine-enkephalin peptides by which regulate thermogenesis and browning in mice [129, 157, 166]. Moreover, they promote expansion and brite differentiation of $PDGFR\alpha^+$ progenitor cells via IL13. ILC2 are activated by IL25 and IL33. ILC3 are induced by IL1β and IL23 and release IL17 and IL22 [166].

NK cells are pro-inflammatory innate immune cells, which are also induced in AT by obesity. They are activated by IL12, IL15, and IL18 and secrete TNFα, IFNγ, granulocyte macrophage colony-stimulating factor, and CCL2 and thereby promote the recruitment of other immune cells during inflammation such as M1 macrophages. NK cells were also shown to act cytolytically on M2 macrophages. In obesity, macrophages positively regulate the amount of NK cells via the production of IL15 [129, 166].

1.5.2.3 Adaptive immune cells

The adaptive immune system is slower than the innate immune system, but it allows a stronger immune response as well as immunological memory. The adaptive immune cells recognize specific "non-self" antigens during a process called antigen presentation. Moreover, when a patho-

gen infects the body more than once, specific memory cells quickly eliminate it [169]. Among adaptive cells observed in AT belong B and T cells.

B cells in obesity increase production of TNFα and MIP2 which results in a rise of macrophages in AT. They also induce glucose intolerance, production of inflammatory cytokines, and a shift to M1 macrophages [128]. B cells promote pro-inflammatory T cell activation and cytokine production [128]. Th1 (pro-inflammatory) cells producing IFNγ are increased in obesity and contribute to M1 polarization [129]. Adipocytes themselves probably contribute to the recruitment of T cells by secretion of CCL5 [131]. On the other hand, regulatory T (**Treg**) cells help to maintain the anti-inflammatory environment by the production of IL10. SVF consists of around 10% of Treg cells in lean condition, upon obesity conditions their numbers decrease. *In vitro* was shown that M1 macrophages can inhibit Treg cells differentiation [129]. Natural killer T (**NKT**) cells stimulate Th2 response, which drives M2 polarization, via the production of IL4 and IL10. M2 macrophages then positively regulate NKT cells. Loss of M2 macrophages leads to a reduction of NKT cells and disruption of immune balance in AT in obesity. NKT cells are reduced with increased adiposity [129].

1.5.2.4 Bridging immune cells

Bridging immune cells are immune cells with features of both innate and adaptive immunity. They respond to pathogens quickly. They are able to recognize antigens, however only a limited set of them. Also, they are not able to develop immunological memory [156].

Three types of innate immune cells have been shown in the AT including γδT cells, invariant nature killer T, and B-1 cells. γδT cells are the main producer of IL17, which reduces AT expansion and is inducible by IL1β [137]. CD1d, a glycoprotein on macrophages and other antigen-presenting cells, involved in presenting lipid antigens, activates iNKT cells, which are, unlike other T cells, able to recognize it. This leads to the accumulation of iNKT in obese AT [138]. Due to the ability of dendritic cells to present antigens and link innate with adaptive immunity, they were added to bridging immune cells, even though they are classified as innate immune cells. DC are increased in obesity and lack of DC resulted in reduced macrophages in AT [167].

Innate and adaptive immune cells together with bridging cells orchestrate the immunological response of AT remodeling. The balance of pro-inflammatory and anti-inflammatory cells influences the resolution of inflammation in AT and therefore have an effect on whole-body metabolism.

1.6 Effect of n-3 PUFA and cold exposure on WAT metabolism

1.6.1 Polyunsaturated fatty acids

The immune and metabolic function of WAT is regulated by lipid mediators as well. Traditional eicosanoids (derived from n-6 PUFA) demonstrate pro-inflammatory effects, while n-3 PUFA derived mediators demonstrate mostly anti-inflammatory effects [170]. Both n-3 and n-6 PUFA are essential FA received from food or food supplements. Mammals are not able to produce these FA due to a lack of Δ12 and Δ15 desaturases. The main representatives are linoleic acid (**LA**; n-6 PUFA) and α-linolenic acid (**ALA**; n-3 PUFA). LA is a precursor for γ-linolenic acid (GLA), dihomo-γ-linolenic acid (**DGLA**), and arachidonic acid (**AA**). From ALA, eicosapentaenoic acid (**EPA**) and DHA are made. Both LA and ALA must undergo several reactions including desaturation, elongation, and FAox to produce these FA and compete for binding sites on specific enzymes (**Fig.1.22**). However, the conversion of ALA and LA is relatively ineffective, in the magnitude of percent, and dietary intake is thus the most effective way how to increase the composition of n-3 and n-6 PUFA in the body [171].

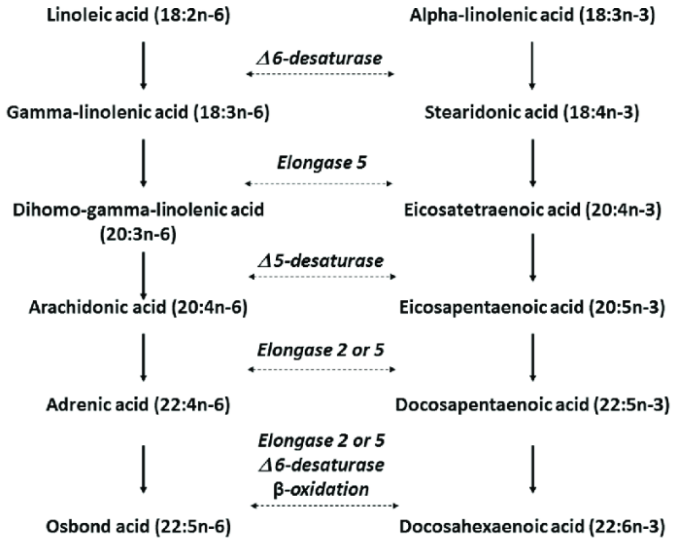

Fig.1.22 n-3 and n-6 PUFA pathway taken from [172].

Linoleic acid and α-linoleic acid are precursors for n-6 and n-3 series polyunsaturated fatty acids (PUFA). Among n-6 PUFA dihomo-γ-linoleic acid and arachidonic acid are formed. Among n-3 PUFA, eicosapentaenoic and docosahexaenoic acids are created.

Lipid mediators are produced from EPA, DHA, and AA, after their cleavage from membrane phospholipids via phospholipase A2. Three kinds of enzymes then metabolize EPA,

DHA, and AA cyclooxygenases (**COX**), lipoxygenases (**LOX**), and cytochrome P450 epoxygenase (**CYP450**) (**Fig.1.23**). COX 1 and 2 give rise to PG and thromboxanes (**TX**) from AA. 5-, 12- and 15- lipoxygenases metabolize AA to 5-hydroxyeicosatetraenoic acid (**HETE**), 12-HETE, and 15-HETE, respectively, and EPA to 5-hydroxyeicosapentaenoic acid (**HEPE**) and 12-HEPE, respectively. HETE are then precursors for leukotrienes, lipoxins, and hepoxilins. DHA is converted also by lipoxygenases, namely 12- and 15-LOX to 14-hydroxydocosahexaenoic acid (**HDoHE**), which is then metabolized to maresin 1 and 17-HDoHE. 17- HDoHE further serves as a precursor for D-series resolvins and protectins. Epoxygenase reaction is needed for metabolizing AA to epoxyeicosatrienoic acids (**EETs**) and dihydroxyeicosatrienoic acids (**DHETs**). Some of the products like 8-HETE from AA and 8- and 9-HEPE from EPA are created by non-enzymatic reactions [170].

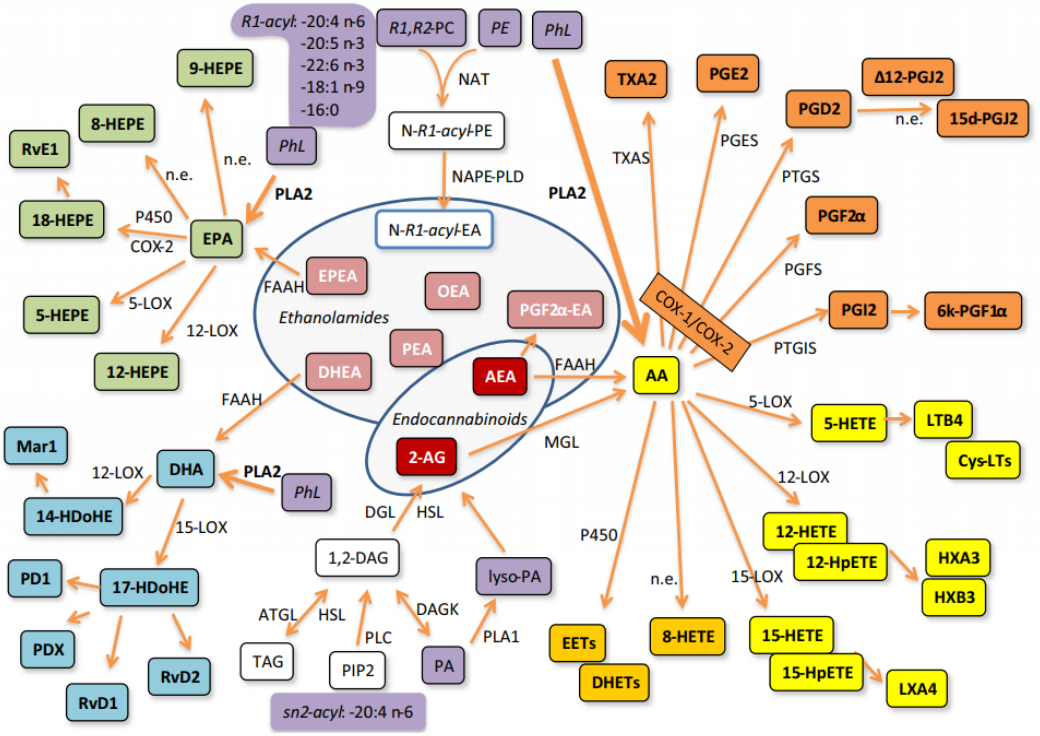

Fig.1.23 Overview of EPA, DHA, and AA-lipid mediators in WAT taken from [170].

As written in the text, arachidonic acid (AA), eicosapentaenoic acid (EPA), and docosahexaenoic acid (DHA) metabolites are formed via cyclooxygenases (COX), lipoxygenases (LOX), and cytochrome P450 epoxygenase (P450). Prostaglandins (PG), resolvins (Rv), protectins (P), leukotrienes (LT), thromboxanes (TX), and others are created. These metabolites influence the immune response of the cell/tissue.

AEA, arachidonoylethanolamide; AG, arachidonoyl glycerol; ATGL, adipose triglyceride lipase; DAG, diacylglycerol; DAGK, diacylglycerol kinase; DGL, diacylglycerol lipase; DHEA, docosahexaenoyl-ethanolamide; DHET, dihydroxyeicosatrienoic acid; EA, ethanolamide; EET, epoxide eicosatrienoic acid; EPEA, eicosapentaenoyl-ethanolamide; FAAH, fatty acid amide hydrolase; HDoHE, hydroxy-docosahexaenoic acid; HEPE, hydroxyeicosapentaenoic acid; HETE, hydroxyeicosatetraenoic acid; HpETE, hydroperoxy-eicosatetraenoic acid; HSL,

hormone-sensitive lipase; HX, hepoxilin; LX, lipoxin; MGL, monoacylglycerol lipase; NAT, N-acyl transferase; n.e., non-enzymatic oxidation; OEA, oleoylethanolamide; PA, phosphatidic acid; PE, phosphatidylethanolamine; PEA, palmitoylethanolamide; PGES, PGFS, and PTGS prostaglandin synthases; PhL, phospholipid; PIP2, phosphatidylinositol biphosphate; PL, phospholipase; PTGIS, prostacyclin synthase; TAG, triacylglycerol; TXAS, thromboxane synthase

.

n-3 PUFA exert anti-inflammatory effects in various tissues including WAT. Indeed, mice treated with n-3 PUFA drives polarization of AT macrophages toward M2 state (anti-inflammatory state). Moreover, DHA-derived lipid mediators resolvin D1 and protectin D1 were shown to decrease the accumulation of AT macrophages. Interestingly, $CD11b^-$ cells isolated from AT SVF were identified as the major producer of DHA-derived lipid mediators [173]. A human study, where patients with insulin resistance were treated with a diet supplemented with n3-PUFA-ethyl esters, showed reduced AT macrophages and MCP1 expression in AT with increased vascularity. Also, pro-inflammatory cytokines such as TNFα and MCP1 were decreased in human cocultures of macrophages and adipocytes exposed to DHA and EPA. EPA and DHA from fish oil exert both hypolipidemic and body weight-reducing effects as shown in a study with orally given fish oil, which reversed the negative effects of HFD-induced obesity. It improved glucose uptake, lipolysis, and DNL in WAT. In addition, fish oil decreased adipocyte volume as compared with the HFD group and increased the number of adipocytes on the level of the control group [174]. On the other hand, it was shown that n-3 PUFA reduced the number and differentiation of white adipocyte progenitors in mice. Transgenic fat-1 mice, which express desaturase converting n-6 PUFA to n-3 PUFA, further exhibited fewer and smaller adipocytes and downregulated genes involved in adipogenesis. Also Pdgfrα, the gene required for WAT progenitors´ proliferation, was less expressed in these mice [132]. Moreover, n-3 PUFA supplementation resulted in decreased cellularity of WAT (measured as the amount of DNA of adipocytes) in mice [175]. Another study using primary human adipocytes showed reduced size and number of lipid droplets and expression of lipogenic genes, but no change in adipogenic gene expression of adiponectin and PPARγ by DHA and EPA [176]. Different outcomes of these studies can be explained by differences in the model used (mice, humans, cells), doses and forms of n-3 supplements, and the ratio of n-3 to n-6 PUFA in the diet. The chemical form of n-3 PUFA affects both metabolic efficacy and bioavailability. n-3 PUFA are part of TAG, DAG, phospholipids, wax esters, ethyl esters, or they are free FA. In food, they are part of fish, meat, Krill, and Calanus, while in food supplements they are produced in form of oil or emulsion. After administration, they are stored in membrane phospholipids and as was described earlier, n-3, namely EPA and DHA, compete with n-6 PUFA, namely AA, for the same enzymes to be converted to other metabolically active products. Therefore, the ratio of pro-inflammatory n-6 to anti-inflammatory/pro-resolving n-3 PUFA in diet and consequently in a cell membrane is very

important for the inflammatory status of a cell. Regarding the metabolism of AT, n-3 PUFA was observed to increase FA oxidation and TAG/FA cycle in porcine adipocytes. Overall, n-3 PUFA were shown to improve the metabolic flexibility of adipocytes and phenotype of immune cells leading to healthy adipocyte [177, 178].

1.6.2 Cold exposure

Mammals belong to endotherms, meaning that they maintain their body temperature constant by several mechanisms to reduce heat loss and/or increase heat production, unlike ectotherms that rely on environmental heat sources. When endotherms are exposed to cold, they initially use inexpensive means to reduce heat loss including vasoconstriction, piloerection, and change of posture. However, if the challenge is stronger, they have to increase the production of heat endogenously engaging shivering thermogenesis [179]. During shivering, muscles involuntarily contract, which consumes ATP and produces heat. After a certain time of CE, shivering is being gradually replaced by non-shivering thermogenesis. Long-term shivering would lead to muscle damage, loss of body temperature control, and death. Non-shivering thermogenesis takes place in BAT [180]. The contribution of other organs such as skeletal muscle, liver, and WAT is still questioned. During CE, cell proliferation and differentiation as well as mitochondriogenesis and UCP1 protein amount are increased in BAT. In the basal state, purine nucleotides inhibit the UCP1 activity. In an activated state, norepinephrine triggers the lipolytic cascade, NEFA are released and UCP1 is activated. The exact mechanism of its activation is still unknown. However, the release of NEFA by lipolysis in BAT is probably switching on the uncoupling of mitochondria in BAT. FA are also used as a substrate for the non-shivering thermogenesis. Evidence that only BAT is involved in non-shivering thermogenesis was shown using UCP1 KO mice. When UCP1 KO mice acclimatized to 23°C are transferred straight to 5°C they start to shiver. They do not have any UCP1 so they are not able to develop any heat by non-shivering thermogenesis. Moreover, their endurance for shivering is not adequate, so eventually (within hours) they start to drop their body temperature [181, 182].

Acute cold stress stimulates sympathoadrenal secretion with an emphasis on energy use. Catecholamines stimulate lipolysis, glycogenolysis, and gluconeogenesis. Moreover, glucagon secretion is also increased. Glucagon contributes to elevated glycogenolysis and gluconeogenesis as well as lipolysis and production of ketone bodies. Stimulation of adrenergic receptors leads to inhibition of insulin release. Thus, glucose uptake into peripheral tissues decreases. However, acute CE increases glucose uptake to both white and red skeletal muscles 2-5-times, 8-times in the heart, up to 20-times in WAT, and more than 100-times in BAT. After prolong time in cold, uptake in heart, skeletal muscle, and WAT is further increased as opposite to BAT, where it decreased 36-

times. This phenomenon can be explained by increased insulin responsiveness in these tissues and/or elevated blood flow. During shivering both lipid and glucose catabolism are promoted [183, 184]. FA turnover in plasma is increased by CE. They are released from WAT in significant amounts and distributed to other tissues for oxidation. Indeed, an increase in the carnitine pool and their turnover were shown in cold-acclimated rats. The store of TAG in WAT and TAG and DAG in skeletal muscles decreases. In addition, TAG are also decreased in plasma. The activity of LPL is increased by CE in BAT and heart but decreased in WAT. Increased oxidation and turnover of body glucose by CE was shown in rats. Glucose is derived either from liver glycogen or from amino acid catabolism. Also, increased incorporation of glucose into TAG was shown in cold-acclimated rats. Interestingly, the proportion of CO_2 created by glucose oxidation is the same in the basal state as in cold exposed rats. Moreover, glucose and FA metabolism do not differ between rats using non-shivering thermogenesis and rats using shivering thermogenesis [185]. Thus, cold exposed animals rely on both main energy sources (glucose and FA) and it cannot be distinguished if glucose and FA are used for shivering or non-shivering thermogenesis.

Skeletal muscles represent 40% of body mass and thus have a capacity to generate large amounts of heat. It is still discussed whether skeletal muscles are able to contribute to non-shivering thermogenesis besides to their proven role in shivering. Studies with use of UCP1 KO mice provide abundant evidence against the involvement of muscle in non-shivering thermogenesis. UCP1 KO mice habituated to thermoneutral temperature are not able to produce enough heat in a long-lasting CE. In addition, soleus muscle from cold-acclimated UCP1 KO mice was shown to have severe hyperphosphorylation of ryanodine receptor 1 (**RyR1**) via PKA, depleted calstabin1, and decreased Ca^{2+} release from the sarcoplasmic reticulum (**SR**), markers of developmental dysfunction in shivering muscle [186]. In addition, Golozoubova et al. claim that muscle tissue cannot recruit UCP1 either via any hormones or neurotransmitters in order to meet the demand for heat. Moreover, only UCP1 and no other proteins (not even UCP2 or UCP3) were shown to be able to mediate non-shivering thermogenesis [187]. On the other hand, older studies by Jansky on cold-acclimated or norepinephrine-infused rats, which were curarized to inhibit shivering, suggested an important contribution of skeletal muscle to non-shivering thermogenesis. The oxygen consumption in leg muscle was doubled in both cold-acclimated and norepinephrine-infused rats [188]. Another argument for the involvement of skeletal muscle in non-shivering thermogenesis is the size of BAT. In mice weight of interscapular BAT is around 0.4% of body mass [189]. In addition, UCP1 KO can be gradually adapted to cold which means that either endurance of muscles for shivering is somehow increased or UCP1 independent non-shivering thermogenesis must exist. This could involve futile metabolic cycles such as phosphocreatine cycle in fat, futile protein turnover, and

futile sarcoendoplasmatic reticulum Ca^{2+} ATPase (**SERCA**) cycle in muscle [182].

Shivering is a repetitive process of contraction-relaxation, which leads to increased Ca^{2+} concentration in cytosol resulting in activation of ATP hydrolysis and production of heat. Na^{+}/K^{+} ATPase, myosin ATPase, and SERCA are involved in ATP utilization [182, 190]. During muscle contraction membrane depolarization leads to activation of dihydropyridine receptor (**DHPR**) that activates the release of Ca^{2+} from SR via RYR1. Ca^{2+} binds to myofilaments and muscle contracts. Additionally, cytosolic Ca^{2+} activates mitochondrial respiration and triggers other signaling pathways [182]. Once Ca^{2+} concentration exceeds a threshold, SERCA is activated and transport Ca^{2+} back to SR, ATP is consumed and muscle can relax. It was proposed that the sarcolipin uncoupling of SERCA activity could be the mechanism of non-shivering thermogenesis in the muscle (**Fig.1.24**). Sarcolipin binds to SERCA in the presence of high Ca^{2+} in the cytosol, allows ATP hydrolysis, but decreases Ca^{2+} transport to SR. That means that more ATP needs to be utilized in order to transport Ca^{2+} back to SR in the presence of sarcolipin [191]. Since the transport of Ca^{2+} is slowed down, high Ca^{2+} is present in the cytosol which leads to activation of mitochondrial metabolism and Ca^{2+} dependent signaling pathways important for changing the muscle phenotype to oxidative via PGC1 and PPAR. Indeed, overexpression of sarcolipin (which is more abundant in oxidative fibers) in glycolytic muscle promoted mitochondrial biogenesis and oxidative metabolism [182]. Moreover, myristoyl-, palmitoyl- and stearoyl- carnitine and esterified long-chain FA were able to trigger Ca^{2+} release from SR. This provides an important link between cold-induced lipolysis, Ca^{2+} cycling, FAox, and heat generation [192].

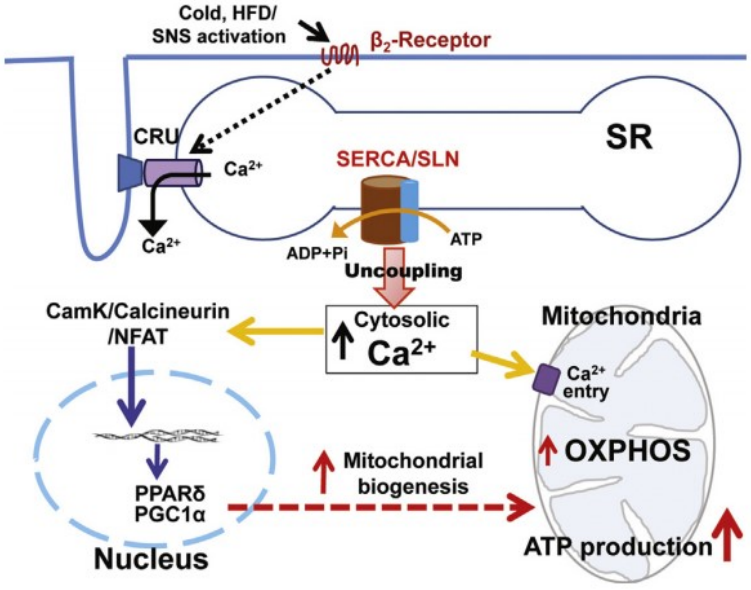

Fig.1.24 Noshivering thermogenesis mechanism in muscle by sarcolipin uncoupling of SERCA taken from [193].

Ca^{2+} is actively transported from cytosol to SR via SERCA using ATP. When sarcolipin is binded to SERCA, Ca^{2+} transport is uncoupled from ATP hydrolysis, which results in the futile cycling of the pump and increased ATP hydrolysis/heat production. This also leads to increased cytosolic Ca^{2+} levels, which activate the mitochondrial oxidative metabolism and ATP synthesis and Ca^{2+}-dependent signaling pathways promoting mitochondrial biogenesis.
ADP, adenosine diphosphate; ATP, adenosine triphosphate CamK, Ca^{2+}/calmodulin-dependent protein kinase; CRU, Ca^{2+} release unit; HFD, high-fat diet; NFAT, nuclear factor of activated T-cells; OXPHOS, oxidative phosphorylation; PGC, peroxisome proliferator-activated receptor gamma coactivator; Pi, phosphate; PPAR, peroxisome proliferator-activated receptor; SNS, sympathetic nervous system; SR, sarcoplasmic reticulum.

In addition, another indirect evidence of the existence of non-shivering thermogenesis in muscle was shown on mice with ablation of iBAT and UCP1 KO. Both models have upregulated sarcolipin in muscles when exposed to cold [194, 195]. Also in birds (which do not have UCP1) SERCA and RYR1 were upregulated after cold adaption [196]. Lastly, newborn mammals due to the high body surface to volume ratio need to produce a significant amount of heat. High sarcolipin expression was demonstrated two weeks after birth, indicating its importance for the generation of heat in neonates lacking the ability to shiver. While the significance of BAT in newborns was proven 50 years ago, the role of muscle contribution to non-shivering thermogenesis is still being discussed [197, 198].

2 Hypothesis and specific aims

The general goal of this thesis was to investigate the composition and functionality of AT with a focus on the modulation of lipid metabolism and adiposity under energy-demanding and energy-surplus conditions concerning attributes of healthy adipocyte.

The following specific aims were addressed:

- To characterize TAG/NEFA futile cycling in WAT and its involvement in resistance to obesity in two inbred murine strains C57BL/6JBomTac (**B6**) and A/JOlaHsd (**A/J**) differing in the propensity to obesity. This characterization was performed under the conditions of CE, i.e. in an energy-demanding situation leading to a maximal stimulation of WAT metabolism.

- To evaluate the contribution of non-shivering thermogenesis in BAT and/or other tissues to resistance to obesity in A/J and B6 mice. This characterization was performed under the conditions of CE (energy-demanding situation).
- To characterize the effect of n-3 PUFA on hyperplasia of WAT in mice fed HFD with a focus on the contribution of immunometabolism.

3 Methods

3.1 General description of conducted experiments

Murine strains B6 from Taconic, Denmark; A/J from Harlan, UK (publications A and B) and C57BL/6N (**B6/N**) obtained from Charles River Laboratories (publication C) were used to perform experiments presented in the thesis. Male mice were maintained at 30°C (publications A and B) or 20°C (publication C) in the Animal house of the Institute of Physiology on a 12:12 hour light-dark cycle with free access to water and food. Mice were three in a cage (pub. A and B) or single-caged (pub. C). Body weight and food consumption were monitored every second day (pub. A and B) or daily during the first week of the experiment and then once a week (pub. C). Mice were fed a standard laboratory chow diet (**STD**; energy density 13.0 $kJ.g^{-1}$, ~35.2% $wt.wt^{-1}$ of lipids, extruded R/M-H diet, SsniffSpezialdiäten, Soest, Germany), if not specified otherwise. All animal procedures were conducted following all appropriate regulatory standards under protocols 172/2009 or 81/2016 approved by the Animal Care and Use Committee of the Czech Academy of Sciences and followed the guidelines for the use and care of laboratory animals of the Institute of Physiology.

3.1.1 Design of animal study in publication A and B

Six-weeks old male B6 and A/J mice fed STD maintained at 30°C for at least one week and then were subgrouped into 3 groups: mice that stayed at 30°C for another week (30°C) and mice that were exposed to 6°C cold for 2 (6°C-2d) or 7 days (6°C- 7d) before killing; in publication B mice acclimated to thermoneutrality and exposed to cold for 7 days were used. In experiments where nuclear magnetic resonance (**NMR**) analysis of AT was done, mice were injected approximately 48 hours before dissection with 0,9% saline solution dissolved in 99,8% ^2H_2O (in order to obtain 5% ^2H_2O in the blood) and were given 5% ^2H_2O in H_2O to drink. Animals were dissected under ether anesthesia in a randomly fed state at the age of 9 weeks between 8-10 a.m.

3.1.2 Design of animal study in publication C

Six- weeks old male B6/N mice fed STD were maintained at 20°C for 7 weeks. At 13 weeks of age, mice were randomly divided into groups with various diets: control group fed STD; a corn oil-based HFD (~35% wt/wt as lipids) and HFD-based diet, in which 15% (wt/wt) of dietary lipids was replaced with EPAX 1050TG concentrate (**HFF**; Epax 1050 TG contained ~14% EPA and ~46% DHA, wt/wt; total EPA + DHA concentration of ~30 g/kg diet; EPAX AS, Aalesund, Norway). Two experiments differing in time-frame were performed; with feeding lasting either 1 or 8 weeks. Animals were dissected under ether anesthesia in a randomly fed state at the age of 14 or 21 weeks, respectively.

3.2 Plasma parameters and tissue lipid content

In plasma samples, collected in tubes with ethylenediaminetetraacetic acid (**EDTA)**, several parameters were measured (publication A). NEFA levels were evaluated using the NEFA C kit (Wako Chemicals, Germany). TAG levels were evaluated by Triacylglycerols Liquid kit (ErbaLachema Diagnostika, Brno, Czech Republic). Total cholesterol levels were evaluated by Cholesterol Liquid kit (ErbaLachema Diagnostika, Brno, Czech Republic). Insulin levels were evaluated using radio-immunoassay Sensitive Rat Insulin RIA Kit (LINCO Research, USA). β-hydroxybutyrate levels were evaluated using Autokit 3HB (Wako Chemicals, Germany). Adiponectin and leptin levels were measured by Mouse Serum Adipokine Multiplex Kit (Millipore Corporation, Billerica, MA, USA) and analyzed by BioPlex 200 system (BioRad, Veenendaal, Netherlands). FGF21 was quantified using enzyme-linked immunosorbent assay (Biovendor, Modrice, Czech Republic). *β-hydroxybutyrate, adiponectin, leptin, and FGF21 were measured by MSc. Jana Hansikova.* All measurements were performed according to the instructions in the kits.

TAG content in the liver was evaluated in ethanolic KOH tissue lysates which were 10-times diluted and then measured as TAG levels in plasma.

3.3 DNA measurement

DNA in WAT and white adipocytes that were digested with proteinase K was evaluated fluorometrically by *Dr. Petra Janovska* using Hoechst 3328. Adipocytes were isolated using collagenase for 30 min in a 37°C bath (see 3.7 flow cytometry).

3.4 *In vivo* evaluation of TAG synthesis and DNL-derived FA in epididymal WAT

Two days before dissection, mice were injected i.p. with a saline solution of ^2H_2O. Injected volume was calculated by multiplying body weight (**BW**) by 0.05 (in order to obtain 5% ^2H_2O in the blood) and 0.7 (70% of BW is water). To maintain 5% ^2H_2O in blood, 5% of drinking water was replaced by ^2H_2O for the last 2 days of the experiment.

Total lipids from eWAT were extracted by Folch extraction. Approximately 80 mg of eWAT was homogenized in 750µl 0.9% KCl and 2 ml methanol. 1 ml of dichloromethane was added to homogenate, which was vortexed and sonicated for 10 minutes in closed tubes. After 20 minutes of shaking 0.7ml of 0.9% KCl and 3 ml of dichloromethane were added and tubes were again shaken and then sonicated for 10 minutes. After centrifugation (room temperature, 2500g, 10 minutes) lower phase was taken and evaporated. TAG were purified by column chromatography (Discovery DSC-Si SPE Tubes, 500mg/3ml, Sigma-Aldrich) using hexane and methyl tert-butyl ether with a ratio of 96:4. Purification was checked by thin-layer chromatography using petrol ether: diethyl ether: acetic acid (70:10:1) as mobile phase and iodine vapors for visualization. The fraction with TAG was collected and evaporated to dryness.

Samples were analyzed by NMR in the lab of Dr. John Jones in Portugal or later by Dr.

Radek Pohl at the Institute of Organic Chemistry and Biochemistry of the CAS in the Czech Republic. The spectra were evaluated using NUTS software (ACORN NMR, Fremont, CA, USA). Using $^{1}H/^{2}H$ pyrazine standard relative areas of glycerol and a fatty-acyl moiety of TAG were calculated. TAG synthesis and DNL was estimated by ^{2}H enrichment of glycerol and FA methyls, respectively.

3.5 Light microscopy and immunohistochemical analysis of adipose tissue

Immunohistology analyses were performed by Dr. Kristina Bardova. AT samples were fixed in 10% neutral buffered formalin (Sigma-Aldrich, USA) for 24 hours and embedded in paraffin. Sections (5μm) were stained with hematoxylin-eosin for morphometry or processed to detect proteins using specific antibodies (see Table 3.1). Digital images were captured using an AX70 light microscope and DP 70 camera (both Olympus, Tokyo, Japan). Morphometry was performed using thresholding in Imaging Software NIS-Elements AR3.0 (Laboratory Imaging, Prague, Czech Republic). For further details and references see section Methods of respective papers.

Table 3.1 Antibodies used for immunohistochemistry

Primary antibody	Company	Catalog number	Secondary antibody	Company	Catalog number
anti-Atgl	Cell Signaling	2138	anti-rabbit IgG biotinylated secondary antibody	Vector Labs	Ba1000
anti-Dgat1	Abcam	ab189994	anti-goat IgG biotinylated secondary antibody	Vector Lab	Ba9500
anti-Ucp1	IPHYS*	----	anti-rabbit IgG biotinylated secondary antibody	Vector Labs	Ba1000
anti-Mac2	Cedarlane	CL8942AP	anti-mouse IgG biotinylated secondary antibody	Vector Labs	Ba2000
anti-F4/80	Santa Cruz	sc-377009	anti-mouse IgG, Alexa Fluor 488 conjugate	Invitrogen	A10680
anti-Ki-67	Abcam	ab15580	anti-rabbit IgG, Alexa Fluor 555 conjugate	Invitrogen	A21428
anti-Perilipin 1	Abcam	ab61682	anti-goat IgG, Alexa Fluor 633 conjugate	Invitrogen	A21082

* Made and provided by Dr. Jan Kopecky, Laboratory of Adipose Tissue, Institute of physiology (**IPHYS**).

3.6 RNA isolation and measurement of gene expression (qPCR)

Frozen tissues were homogenized in TRI Reagent using a mixer mill. In order to get rid of fat, membranes, and others, the homogenate was centrifuged (4°C, 12000g, 10 minutes) and interphase was taken and incubated 5 minutes at room temperature. 200ul of chloroform was added, mixed thoroughly, and incubated 10 minutes at room temperature. After centrifugation (4°C, 14000g, 15 minutes), the aqueous phase was removed and mixed with 0.5ml isopropanol. The solution was incubated 10 minutes at room temperature in order to precipitate RNA. After centrifugation (4°C, 12000g, 10 minutes) pellets were washed with 1ml 70% ethanol and centrifuged last time (4°C, 12000g, 5 minutes). Ethanol was removed and pellets were dried in a vac

uum for 5 minutes at 40°C and then dissolved in redistilled water.

Table 3.3 Sequences of used murine primers

Gene name	Gene ID	5´Sequence	3´Sequence
Acadl	11363	TGGCATCAACATCGCAGAGAAACA	ACCGATACACTTGCCCGCCGTCAT
Acadm	11364	TCGCCCCGGAATATGACAAAA	GCCAAGGCCACCGCAACT
Acadvl	11370	CAGGGGTGGAGCGTGTGC	CATTGCCCAGCCCAGTGAGTTCC
Actb	11461	GAACCCTAAGGCCAACCGTGAAAAGAT	ACCGCTCGTTGCCAATAGTGATG
Arg1	11846	TCCAACTGCCAGACTGTGGTC	ACGGGGACCTGGCCTTTGTT
Ccl2	20296	CATGCTTCTGGGCCTGCTGTT	CCTGCTGCTGGTGATCCTCTTGTA
Ccr2	12772	GTGGTTTGTGGTCTGTGGGCTT	GGAGTTCCCACTCACTCAAAGGACA
Cebpa	12606	ACGGGGACCATTAGCCTTGTGT	CTCCTTCCCCCAGTCGTTAGTG
Dgat1	13350	TGGCCAGGACAGGAGTATTTTTGA	CTCGGGCATCGTAGTTGAGCA
Dgat2	67800	CCAGCCCCCAGGTGTCAGAGGAG	GGGGCCGACGGGTCCAGAAGAAG
EF1a	13627	TGACAGCAAAAACGACCCACCAAT	GGGCCATCTTCCAGCTTCTTACCA
Elovl5	68801	CCTCTCGGGTGGCTGTTCTTCC	AGGCTTCGGCTCGGCTTGTC
Fasn	14104	CAAGGGGTGCGCTCTGTGGATGG	AGGCGGTAGAGATTGCGAAGGTTG
Fgf21	56636	AGCGCAGCCCTGATGGAATGGAT	CTGGAGGAGGGGGCTGGAGTC
Fgfr1	14182	ATGATGACGACGACGATGACTCCT	CCACTCGACGGGCACTTGAA
Fgfr2	14183	GAACCTTGGCGCCGGCTGCTACC	CTGCTGCTGCTGCTGCTGCTGTGG
Gk	14933	TCGTTCCAGCATTTTCAGGGTTAT	TCAGGCATGGAGGGTTTCACTACT
Hprt	15452	GCTGAGGCGGCGAGGGAGAG	GCTAATCACGACGCTGGGACTGC
IFNg	15978	GCCAAGTTTGAGGTCAACAACCCA	CCACCCCGAATCAGCAGCGA
IL1b	16176	TCCCCCACACGTTGACAGCTAGG	TCGGCCAAGACAGGTCGCTCA
Ki67	17345	ACTGGAGGTGAAAACCACACT	AGGGTAACTCGTGGAACCAA
Klb	83379	TGGCATGGGTTTGGCACAGGTAT	GGGCGGAAGTTTTTGTCGTAGTTA
5Lox	11689	TCAAACGATCACCCACCTTCTGC	TTCCCGGGCCTTAGTGTTGATAGC
12Lox	11685	GCAGGCCTGGTGTCGGGAGAT	GCTGGGCAGTGCATGTGAAAAC
15Lox	11687	ATCAGGGGGACACAATGAGC	CTTCCGTGCACCCTGTTTTT
Nos2	18126	CTTTGCCACGGACGAGACGGATAGG	CGGGCACATGCAAGGAAGGGAACT
Pck1	18534	GGCAGCATGGGGTGTTTGTAGGA	TTTGCCGAAGTTGTAGCCGAAGAAG
Pcna	18538	ACTCTACAACAAGGGGCACA	AGTGGAGAGCTTGGCAATGG
Pdgfra	18595	CAGGAAGGCGTAGGGAATCAGGT	TCTCACCTCACATCTGGTCGGC
Pdgfrb	18596	CCCCCAGCCTTGCCAGTTCCA	TGGGCAGCCTGAATCCTGTGG
15Pgdh	15446	TCCGGGACCTGCAAGCGAA	TGTCACTGGGACACAGCCACAC
Pnpla2	66853	CAAGGGGTGCGCTATGTGGATGG	AGGCGGTAGAGATTGCGAAGGTTG
Ppara	19013	TGCGCAGCTCGTACAGGTCATCAA	CCCCCATTTCGGTAGCAGGTAGTCTTA
Pparg	19016	GCCTTGCTGTGGGGATGTCTC	CTCGCCTTGGCTTTGGTCAG
Ppargc1a	19017	CCCAAAGGATGCGCTCTCGTT	TGCGGTGTCTGTAGTGGCTTGATT
Ppib	19035	ACTACGGGCCTGGCTGGGTGAC	TGCCGGAGTCGACAATGATGA
Pref1	13386	CCCCTGGCTGTGTCAATGGAGTCT	ATTGTTGGCGCAGGGGGTTGAGGT
18SRna	19791	GCCCGAGCCGCCTGGATAC	CCGGCGGGTCATGGGAATAAC
Sca1	110454	GGAACATTGCAGGACCCCAGA	ATGACCCTGGAGGCACACAGC
Scd1	20249	ACTGGGGCTGCTAATCTCTGGGTGTA	GGCTTTATCTCTGGGGTGGGTTTGTTA
Serca1	11937	GTGGGCGAGGTGGTCTGTATCTTC	AGTAGCCGGGAGCCCATCAGTCAC
Serca2a	11938	CACATGCACGCACCCGAACA	CGTGGAACCTTTGCCGCTCATT
Sln	66402	AAGCTAAGGCTCACTGGCTGGC	TCACAATGCCTGACACACCGCT

Tgfb	21803	GTGGCTGAACCAAGGAGACGGAA	CTCTCCGGTGCCGTGAGCTG
Tnfa	21926	AGCTGTCCCCACCTGGCCTCTC	CCCGTGGGGAGCAGAGGTTCAGT
Ucp1	22227	CACGGGGACCTACAATGCTTACAG	GGCCGTCGGTCCTTCCTT

RNA concentration and purity were measured by NanoDrop Instrument (Thermo Scientific, USA). 1 μg of RNA was transcribed using oligoT primers (GeneriBiotech, Czech Republic) and M-MLV reverse transcriptase (Invitrogen, USA). 20-times diluted cDNA was used for measurement of various transcripts by LightCycler480 (Roche, Germany) using SybrGreen I Master kit (Roche, Germany), see PCR conditions in table 3.2. The annealing temperature was set according to used primers. At the end of the measurement, a melting curve analysis was performed in order to verify the specificity of amplified PCR products. Data were normalized to the geometrical mean signal of reference genes (further details see in Methods of respective papers).

Table 3.2 qPCR conditions

95°C	95°C	55-60°C	72°C	95°C	65°C	97°C	40°C
6 minutes	10s	10s	20s	5s	60s	continuously	30s
		45x					
Preheating	Amplification			Melting curve			Cooling

Primers were designed using the NCBI database and Lasergene software (DNASTAR, USA), see primers´sequences in table 3.3.

3.7 Flow cytometry

3.7.1 Isolation of SVF and adipocytes

Enzymatic digestion in Krebs-Ringer Bicarbonate Buffer (**KRB**; pH=7.4) containing 0.1% collagenase type II (Sigma-Aldrich, Munich, Germany) and 4% bovine serum albumin (**BSA**, fraction V, FA free, Sigma-Aldrich) at 37°C for 30 minutes was used to release cells from eWAT. In order to separate SVF cells from floating adipocytes, a mixture of cells was centrifugated (4°C, 500g, 10 minutes). SVF cells were resuspended in KRB with 10mM EDTA and 4% BSA and passed through a 42 μm filter. Lysis Buffer (eBioscience, San Diego, CA, USA) was used to lyse red blood cells. If needed, adipocytes were taken by pipette with a cut tip for RNA isolation and qPCR analysis. Also, part of the SVF was taken for RNA isolation and qPCR analysis.

3.7.2 Staining of SVF for the flow cytometry measurement

SVF cells were then stained by antibodies conjugated with fluorescent markers (fluorophore). Fluorescent markers were excited by 4 different lasers of the BD LSR II flow cytometer and the emission was measured. Besides the chemical properties of stained cells, BD LSR II is able to measure also physical properties such as granularity and size of the cells.

To prevent nonspecific binding of specific antibodies, cells were incubated with Fc

block solution (AntiMouse CD16/CD32; eBioscience, San Diego, CA, USA) for 10 minutes on ice in dark. See antibodies used for extracellular staining (4°C, dark, 30 minutes) in Tables 3.4 and 3.5. Before intracellular staining, cells were fixed and permeabilized (Intracellular Fix and Perm Set, eBioScience, San Diego, CA, USA). Cells were then stained intracellularly by Ki67, a marker of cell proliferation (4°C, dark, 30 minutes). Stained cells were washed and analyzed using a BD LSR II flow cytometer (BD BioScience, San Jose, CA, USA). Data were analyzed using FlowJo 10.2 software (Tree Star, Ashland, OR, USA).

Table 3.4 Specific markers used to identify different populations

Cell type	Markers	Reference
Leukocytes	$CD45^+$	[199]
Macrophages	$CD45^+F4/80^+CD11b^+$	[159]
M1 macrophages	$CD45^+F4/80^+CD11b^+CD11c^+CD206^-$	[159]
M2 macrophages	$CD45^+F4/80^+CD11b^+CD11c^-CD206^+$	[159]
Double positive macrophages	$CD45^+F4/80^+CD11b^+CD11c^+CD206^+$	[159, 200, 201]
Double negative macrophages	$CD45^+F4/80^+CD11b^+CD11c^-CD206^-$	[159, 201-203]
Endothelial cells	$CD45^-CD31^+$	[204]
Progenitors	$CD45^-CD31^-CD34^+Sca1^+CD24^+$	[204, 205]
Preadipocytes	$CD45^-CD31^-CD34^+Sca1^+CD24^-$	[204, 205]

Table 3.5 Antibodies used in flow cytometry

Antigen	Fluorophore	Sources	Catalog Number	Dilution
CD45	PerCP	BD Biosciences	552991	1:160
CD31	APC	BD Biosciences	553932	1:100
CD34	BV421	BD Biosciences	562608	1:200
Sca1	BV510	BioLegend	108129	1:300
CD24	PE	BD Biosciences	553262	1:600
CD11b	APC-Cy7	BD Biosciences	552773	1:300
F4/80	Biotin	eBioscience	13-4801-81	1:40
CD206	FITC	GeneTex	GTX43682	1:40
CD11c	PE	Affymetrix,eBioscience	12-0114	1:200
Ki67	BV605	BioLegend	652413	1:100
Streptavidin	eFluor710	Affymetrix,eBioscience	49-4317	1:160

3.8 Western blotting

*Western blotting (**WB**) analysis was performed either by Dr. Petr Zouhar or Dr. Petra Janovska.* The amount of UCP1 protein was determined in the homogenate of BAT. Frozen samples of fat were crushed by UltraTurrax in the STE medium. Centrifuged infranatant was used for further analysis. The amount of protein was assessed using the bicinchoninic acid (**BCA**) assay. Mouse anti-human UCP1 (MAB6158; R&D system) was used for the detection of UCP1 protein in iBAT homogenate. Quantification was established using the detection of infra-red dye-labeled secondary antibodies the Odyssey IR Imaging Systems (Li-Cor Biosciences,

Lincoln, NE) [26]. Results are expressed in arbitrary units (**AU**).

For the quantification of AMPK, frozen samples of AT were crushed and mixed with a lysis buffer and Phosphatase Inhibitor-Mix I under the nitrogen. Tissue lysates were sonicated and centrifuged. The total amount of the α1 and α2 catalytic subunits of AMPK and the phosphorylated form of AMPK (**pAMPK**) were determined using sheep antibodies against α1 AMPK and α2 AMPK (gift from the University of Dundee, UK), and phosphospecific rabbit antibodies against the Thr172 of the α subunits of AMPK (Cell Signaling Technology, Danvers, MA). As secondary antibodies, a mixture of infrared dye-labeled antibodies was used (Rockland, USA). Band intensities were analyzed by AIDA software (Raytest, Straubenhardt, Germany).

3.9 Lipolysis measurement in adipocytes ex *vivo*

Lipolysis was measured by Dr. Petra Janovska. Adipocytes were isolated from eWAT using collagenase and KRB medium with 5 mM glucose and 4% BSA (fraction V, FA free, Sigma Aldrich) as described earlier [206], except that adenosine was included in the medium only during cell isolation, to suppress lipolysis [207]. Collagenase-digested samples were passed through a sterile 250 μm nylon mesh and the suspension was centrifuged at 4g for 1 min. Glycerol and NEFA released from adipocytes were measured at the end of a 1-hour-incubation at 37 °C either in the absence or presence of 10 μM isoproterenol (**ISO**; basal vs. ISO-stimulated lipolysis) [207] using Glycerol reagent (Sigma-Aldrich, Prague, Czech Republic) and WAKO-C kit (Wako Chemicals, Neuss, Germany), respectively. Results were adjusted to adipocyte DNA content (see chapter 3.3)[208].

3.10 Mass spectroscopy with labeled free quantification (MS-LFQ)

Preparation of samples was done by Dr. Marek Vrbacky from Bioenergetics Laboratory of IPHYS and samples were then measured in proteomics facility at Biocev in Vestec. Briefly, samples of BAT were solubilized using sodium deoxycholate reduced with tris(2-carboxyethyl)phosphine, alkylated with S-methyl methanethiosulfonate, digested sequentially with Lys-C and trypsin, and extracted with ethyl acetate saturated with water. Thereafter the samples were desalted on Empore C18 columns, dried in Speedvac, and dissolved in 0.1% trifluoroacetic acid + 2% acetonitrile. About 1 mg of peptide digests were separated on a 50 cm C18 column using 2.5 h elution gradient and analyzed in a DDA mode on Orbitrap Fusion Tribrid (Thermo Scientific) mass spectrometer. The resulting raw files were processed in MaxQuant with the LFQ algorithm MaxLFQ [209].

3.11 Lipidomics (Publication C; PUFA derivates)

Dr. Petra Janovska took care of the preparation of samples which were measured and evaluated by MSc. Marie Brezinova and Dr. Ondrej Kuda.

100mg of flash-frozen (stored in liquid nitrogen) eWAT samples were taken for lipid mediators isolation using solid-phase extraction procedure as before [210]. The analysis was performed using a UPLC-MS/MS platform (Ultimate 3000 RSLC, Dionex/Thermo and QTRAP 5500, AB SCIEX, Framingham, MA, USA) equipped with a C18 column 150 cm×2.1 cm, 1.9 μm with a precolumn. Analytes were ionized in negative ion mode and detected with multiple reaction monitoring methods as before [210, 211].

3.12 LC-MS based lipidomics and metabolomics (Publication B)

Both lipidomics and metabolomics were performed by a group of Assoc. Prof. Tomas Cajka in IPHYS. BAT and muscle samples (20 mg) were homogenized with methanol containing internal standards using a grinder (MM400, Retsch, Germany). Then, 1 mL of methyl tert-butyl ether with other internal standard was added, the tubes were shaken for 1 min and centrifuge at 16,000 rpm for 5 min.

3.12.1 LC-MS-based lipidomics

The LC-MS system consisted of a Vanquish UHPLC System (Thermo Fisher Scientific, Bremen, Germany) coupled to a Q Exactive Plus mass spectrometer (Thermo Fisher Scientific, Bremen, Germany). The upper organic phase was collected, evaporated, and resuspended in methanol with internal standard (CUDA), shaken for 30 s, centrifuged at 16000 rpm for 5 min, and used for LC-MS analysis. Lipids were separated on an Acquity UPLC BEH C18 column (50 × 2.1 mm; 1.7 μm) coupled to an Acquity UPLC BEH C18 VanGuard pre-column (5 × 2.1 mm; 1.7 μm) (Waters, Milford, MA, USA) using 7.5 min gradient elution and flow rate 0.6 mL/min.

3.12.2 LC-MS-based metabolomics

The bottom aqueous phase was collected, evaporated, resuspended in an acetonitrile/water (4:1, v/v) mixture with internal standards (CUDA and Val-Tyr-Val), shaken for 30 s, centrifuged at 16 000 rpm for 5 min, and used for LC-MS analysis. Polar metabolites were separated on an Acquity UPLC BEH Amide column (50 × 2.1 mm; 1.7 μm) coupled to an Acquity UPLC BEH Amide VanGuard pre-column (5 × 2.1 mm; 1.7 μm) (Waters, Milford, MA, USA) using 8 min gradient elution and flow rate 0.4 mL/min.

LC-MS data from lipidomic and metabolomic profiling were processed through MS-DIAL v.3.80 software. Internal standards spiked during the extraction were used to calculate the concentration of carnitine, acylcarnitines, and amino acids (pmol/mg) in analyzed samples.

3.13 INCA

Indirect calorimetry was performed by Dr. Kristina Bardova. The maximal heat production (**HPmax**), maximal norepinephrine stimulated heat production (**NEmax**) and resting heat production (**HPrest**) were evaluated using the 8-chamber system of indirect calorimetry (**INCA**, Somedic, Horby, Sweden) [212]. Mice were 1 week prior to the start of the experiment implanted by E-mitters (used for detection of body core temperature and activity) into the abdominal cavity. For the determination of cold-induced HPmax at rest, single-caged animals were placed in INCA with 5°C of ambient temperature without access to food. A mouse was removed from the measurement when its temperature dropped below 28°C. HP was calculated from metabolic rate (**MR**; i.e. oxygen consumption) according to the equation: HP [mW] = (4.44+1.43*RQ)*MR [ml/h], where RQ is respiratory quotient (i.e. the ratio between produced CO_2 and consumed O_2). HPmax was calculated from the maximal oxygen consumption of mice with no physical activity. NEmax was calculated from maximal oxygen consumption after injection of 1µg/g BW norepinephrine (mice in thermoneutrality, no physical activity). HPrest was calculated from oxygen consumption measured in thermoneutrality at the moment of no physical activity of mice. This protocol is partially modified from Meyer et.al. [213].

3.14 Positron emission tomography/computed tomography (PET/CT)

3.14.1 Adrenergic stimulation setup

4-5 hours-fasted mice were subcutaneously injected by ß$_3$-adrenergic receptor agonist CL 346 243 (1 µg/g of BW). After 40 minutes, pentobarbital (80 and 100 µg/g of BW in B6 and A/J mice, respectively) was injected intraperitoneally. Subsequently, 10 MBq of ^{18}F-fluorodeoxyglucose (**18FDG**; 170 µl) was applied to a lateral tail vein. After 1 hour of keeping anesthetized mice at thermoneutral temperature, mice were placed to µPET/CT Albira (Bruker Corp., Belgium; see Fig 3.1).

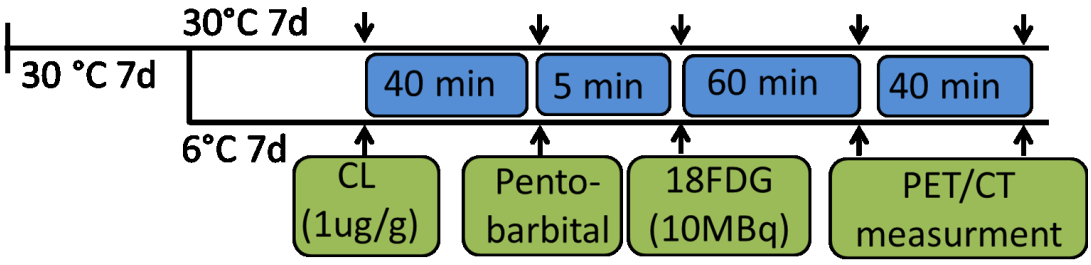

Figure 3.1 PET/CT setup

3.14.2 Acute cold setup

After 4-5 hours of fasting, mice were anesthetized using 2% isoflurane and 10 MBq of 18FDG (170µl) was applied to a lateral tail vein. Mice were placed at 4°C for 1 hour and then anesthetized by pentobarbital (80 and 100 µg/g of BW in B6 and A/J mice, respectively) and placed to µPET/CT Albira.

All animals had a CT (45 kV 0.4A) scan after a static PET scan for anatomical delineation of PET image. PET images were reconstituted using Albira Reconstructor software and evaluation of 18FDG uptake was performed in PMOD v.3.403 (PMOD Technologies, Ltd., Switzerland). BAT volume was determined by thresholding CT image and the resulting mask was applied on PET data. The resulting quantitative data were expressed as SUV [(g/ml)*(ccm)].

Mr. Liska from the Laboratory of Radiology, Dr. Bardova, Dr. Zouhar, Dr. Svobodova, MSc. Funda and I were involved in PET/CT measurement. Evaluation of PET/CT results was done by Dr. Kristina Bardova.

3.15 Oxygraph measurement and preparation of samples

In both BAT and skeletal muscle, respiration (consumption of oxygen by mitochondria) of cells after adding substrates and inhibitors was measured. The use of a hermetically closed metabolic chamber enabled to record of the change of oxygen concentration by an oxygen sensor in the chamber. Since the mitochondria consumed oxygen, the oxygen concentration dropped. From the rate of the oxygen decline, the respiratory rate of the mitochondria was calculated.

3.15.1 Brown adipose tissue

Mitochondria were prepared by Dr. Petra Janovska. Briefly, minced BAT was homogenized with Teflon-glass homogenizer (400 rpm) in the STE medium with BSA and centrifuged 13000g, 10 min, 4°C. Pellet was resuspended in STE medium with BSA (fraction V, FA free, Sigma-Aldrich), homogenized (Teflon-glass, 400 rpm), and centrifuged 800g, 10min, 4°C. The supernatant was centrifuged 13000g, 10 min, 4°C. Finally, the resuspended pellet in the STE medium without BSA was centrifuged 13000g, 10 min, 4°C. Protein concentration was measured using the BCA method.

Oxidation of pyruvate was measured by Oroboros oxygraph (Austria) as the rate of oxygen consumption (pmol O_2 /(s.mg protein)). To the 2ml of medium containing 80mM KCl, 10mM Tris-HCl, 5mM KH_2PO_4, 1mM EDTA, pH=7.4, 30°C 0.5-1 mg of protein was added. For the measurement of 10uM cytochrome c, 2.5mM malate, 10mM pyruvate, and 5-10-times 0.5mM GDP were gradually added. Ucp1 dependent fraction was then calculated as a maximum of rate after pyruvate addition minus minimum rate after GDP addition. Malate is used to replenish citric acid cycle intermediates, which had been lost during the isolation.

3.15.2 Skeletal muscle

Homogenate was prepared by Dr. Petra Janovska, COX measurement was done by Dr. Drahota and Dr. Ruslan, I together with *Dr. Ruslan* performed palmitoyl carnitine (**PC**) oxidation measurement.

10% muscle homogenate was prepared by Teflon-glass homogenizer in the medium containing 0.25M sucrose, 10mM Tris-HCl, pH=7.2 at 4°C.

COX activity was measured by OroborosOxygraph (Austria) as the rate of oxygen consumption (pmole oxygen/sec/mg protein). To the 2ml of medium containing 80mM KCl, 10mM Tris-HCl, 5mM KH_2PO_4, 1mM EDTA, pH=7.4, 30°C were gradually added muscle homogenate - 0.3mg protein, 2mM cytochrome c, 5mM Na-ascorbate, 1mM tetramethyl p-phenylenediamine dihydrochloride (TMPD) and 0.25mM KCN. From the rate of oxygen uptake after TMPD addition, KCN insensitive oxygen uptake was subtracted and divided by added protein (COX activity as pmol O_2 /(s.mg protein)).

The rate of PC oxidation was determined in the same medium after the addition of 2.5mg protein of muscle homogenate, 10uM cytochrome c, 2.5mM malate, 1.5mM ADP, and 3.12μM PC (pmol O_2 /(s.mg protein)).

3.16 Statistical analysis

All values in publication A and B are presented as means ± s.e.m., in publication C values are means ± s.d. Comparisons were judged to be significant at $p < 0.05$ or when indicated p value treated with FDR < 0.05. Data were analyzed by analysis of variance (one-way or two-way ANOVA). For statistical evaluation, SigmaStat 3.5 software (Systat Software, San Jose, CA, USA) was used. Logarithmic or square root transformations were used to stabilize variance or normality of samples when necessary and so data met the assumption of the tests (equal variance and normal distribution).

A multivariate statistical analysis, principal component analysis (**PCA**), was used for the lipidomic data evaluation in publication C. Analysis was performed using the statistical software SIMCA-P+12 (Umetrics AB, Malmo, Sweden). A multivariate statistical analysis, partial least squares-discriminant analysis (**PLSDA**) was used for evaluation of metabolomics/lipidomic data in publication B using Metaboanalyst.ca. Corresponding variable importance in projection (**VIP**) was evaluated.

3.17 My contribution

In summary, I was mainly involved in scheduling and preparing experiments, taking care of the animals, measurement of plasmatic parameters, TAG synthesis and DNL preparation of samples and data evaluation, preparation of samples, measurement and data evaluation of flow cytometry, PET/CT measurement, Oxygraph measurement, and data evaluation, qPCR and statistics.

4 Results

4.1 Publication A

In this and following study, two murine strains, obesity-prone B6 and obesity-resistant A/J mice were used. Rezistance of A/J mice to obesity was proven by Kopecky et al., where A/J mice fed HFD were shown to gain less weight in comparison to B6 mice fed HFD [212]. Moreover, B6 mice had significantly more increased insulin and glucose levels in plasma by HFD than A/J mice [214]. The aim of the study was to characterize CE-induced changes in eWAT metabolism and reveal whether these changes may contribute to whole-body thermogenesis and control of energy balance.

Pre-acclimatization to the thermoneutral temperature of A/J and B6 mice was followed by exposure to cold (6°C) for 2 or 7 days or not. To sustain body temperature in cold environment mice increased their food intake twice regardless of strain. Both murine strains also burnt lots of their body fat (**Table 4.1.1**) to defeat their body temperature. The weight of both epididymal and subcutaneous WAT decreased by more than 50% and 45% in A/J mice and 25% and 10% in B6 mice, respectively, after 7 days of CE (**Table 4.1.1**). A dramatic decrease after 2 days was observed in the weight of BAT due to the loss of stored lipids. BAT weight returned to the original value after 7 days in both murine strains (**Table 4.1.1**). Also, the body weight of mice was transiently decreased after 2 days of CE. Weight of liver increased by cold in both A/J and B6 mice with a transient decrease in day 2 in A/J mice. Under all studied conditions, the liver of A/J mice was smaller than the liver of B6 mice (**Table 4.1.1**). Interestingly, TAG in the liver changed only in A/J mice with a transient increase in day 2 of CE (**Table 4.1.1**).

Table 4.1.1 General characteristics of A/J and B6 mice in thermoneutrality and cold

	B6			A/J		
	30°C	6°C – 2d	6°C – 7d	30°C	6°C – 2d	6°C – 7d
Food consumption (g per day)	3.1 ± 0.1	5.2 ± 0.3[a]	6.6 ± 0.3[a,b]	3.1 ± 0.1	4.5 ± 0.1[a]	6.7 ± 0.2[a,b]
Body weight (g)	26.2 ± 0.4	24.3 ± 0.4[a]	25.9± 0.4[b]	23.0± 0.6[c]	20.3 ± 0.4[a,c]	21.6 ± 0.3[a,b,c]
Weight of AT depots						
eWAT (mg)	383 ± 28	350 ± 16	286 ± 11[a,b]	401 ± 30	260 ± 18[a,c]	179 ± 11[a,b,c]
scWAT (mg)	300 ± 24	231 ± 10[a]	267 ± 12	448 ± 31[c]	286 ± 20[a,c]	233 ± 11[a,b,c]
iBAT (mg)	101 ± 5	55 ± 2[a]	105 ± 3[b]	69 ± 4	47 ± 2	72 ± 2[b,c]
Liver						
Weight (mg)	1371 ± 3	1301 ± 2[a]	1517 ± 2[a,b]	1097 ± 4[c]	920 ± 3[a,c]	1136 ± 2[a,b,c]
TAG (mg/g tissue)	28.9 ± 1.6	29.4 ± 1.7	28.1 ± 1.3	26.7 ± 1.2	38.1 ± 3.6[a,c]	28.4 ± 0.9[b]
Plasma levels						
TAG (mmol l^{-1})	1.21 ± 0.11	0.49 ± 0.03[a]	1.05 ± 0.07[b]	1.90 ± 0.15[c]	0.62 ± 0.06[a,c]	2.17 ± 0.17[b,c]
NEFA (mmol l^{-1})	0.83 ± 0.07	0.39 ± 0.03[a]	0.56 ± 0.07[a]	0.95 ± 0.08	0.38 ± 0.04[a]	1.20 ± 0.18[b,c]
β-hydroxybutyrate (nmol μl^{-1})	0.28 ± 0.04	0.49 ± 0.06[a]	0.56 ± 0.10[a]	0.45 ± 0.04[c]	0.59 ± 0.08[a]	0.83 ± 0.28[a,b,c]
Cholesterol (mmol l^{-1})	2.6 ± 0.1	2.6 ± 0.1	2.0 ± 0.1[a,b]	2.3 ± 0.1[c]	1.6 ± 0.2[a,c]	1.7 ± 0.1[a,c]
Glucose (mg dl^{-1})	366 ± 14	296 ± 11[a]	273 ± 14[a]	337 ± 23	262 ± 15[a]	271 ± 14[a]
Insulin (ng ml^{-1})	0.93 ± 0.09	0.72 ± 0.11	0.90 ± 0.10	0.59 ± 0.07[c]	0.68 ± 0.11	0.61 ± 0.11[c]
Adiponectin (µg ml^{-1})	5.90 ± 0.31	5.19 ± 0.26[a]	6.18 ± 0.24[b]	5.56 ± 0.23	4.72 ± 0.26[a]	5.07 ± 0.31[b,c]
Leptin (ng ml^{-1})	1.68 ± 0.40	1.76 ± 0.19	2.43 ± 0.25[a]	3.39 ± 0.58[c]	1.57 ± 0.19[a]	1.53 ± 0.15[a,c]
FGF21 (pg ml^{-1})	351 ± 84	101 ± 10[a]	94 ± 11[a]	577 ± 121[c]	437 ±117[a,c]	246 ± 30[a,b,c]
Fgf21 expression						
Liver	0.074 ± 0.013	0.038 ± 0.006[a,]	0.023 ± 0.003[a,b,]	0.159 ± 0.024[c]	0.103 ± 0.022[a,c]	0.054 ± 0.006[a,b,c]
iBAT	0.004 ± 0.001	0.027 ± 0.004[a]	0.021 ± 0.003[a]	0.005 ± 0.001	0.020 ± 0.002[a]	0.039 ± 0.006[a,b,c]

Abbreviations: AT, adipose tissue; eWAT, epididymal white adipose tissue; FGF21 fibroblast growth factor 21; iBAT, interscapular brown adipose tissue; NEFA, non-esterified fatty acid; scWAT, subcutaneous white adipose tissue; TAG, triacylglycerol. Mice were maintained at 30°C or exposed to cold for either 2 days (6°C–2d) or 7 days (6°C–7d). Food consumption was measured 1 day before dissection. Data are means ± s.e.m.; *n*=12–15. [a]Significant difference as compared with 30°C within the strain. [b]Significant difference as compared with 6°C–2d within the strain. [c]Significant difference between strains within the treatment (ANOVA).

Plasmatic levels of NEFA were decreased after 2 days of CE despite massively activated lipolysis documented by a drastic decrease of WAT mass (**Table 4.1.1**). A decrease in NEFA levels was caused by elevated NEFA clearance by other tissues. NEFA levels were normalized after 7 days of CE. The plasma concentration of TAG was also transiently decreased due to CE. The change of plasmatic NEFA and TAG was more pronounced in A/J mice (**Table 4.1.1**). β-hydroxybutyrate level, a marker of hepatic ketogenesis, gradually increased by CE and was higher in A/J mice in all experimental conditions (**Table 4.1.1**). Total cholesterol and glucose levels were reduced in both strains by CE. While total cholesterol levels were higher in B6 mice independently of temperature, glucose levels were more or less the same in comparison of these two murine strains (**Table 4.1.1**). Insulin levels in plasma did not significantly change by exposure to cold and were significantly lower in A/J mice as compared to B6 mice in 30°C and 6°C-7d subgroups (**Table 4.1.1**). Leptin and adiponectin are important adipokines influencing insulin sensitivity. Adiponectin levels transiently decreased in both strains after two days of CE. After 7 days in cold conditions, B6 mice restored original levels. Although A/J mice also increased adiponectin level between day 2 and day 7 of CE, they achieved lower levels as compared to B6 mice exposed to 7-days cold (**Table 4.1.1**). Leptin plasmatic levels changed in B6 mice after 7 days in the cold and were elevated in comparison to thermoneutrality. On the other hand, A/J leptin plasma levels decreased after 2 days in the cold with no further change on the 7th day of CE. Leptin was significantly higher at thermoneutrality and lower after 7 days of CE in A/J mice than in B6 mice (**Table 4.1.1**). In addition, FGF21, a cytokine secreted mainly by the liver, but also by AT, was decreased in plasma by CE in both strains. The reduction corresponded with a cold-induced decrease in Fgf21 mRNA expression in the liver (**Table 4.1.1**). In all temperature conditions, FGF21 was higher in A/J mice in both plasma and liver. In BAT Fgf21gene expression was increased by cold 5-times and 8-times in B6 and A/J mice, respectively, resulting in almost 2 times higher mRNA expression in A/J mice than B6 after 7 days of CE (**Table 4.1.1**).

CE leads to activation of the body defending temperature mechanisms, i.e. shivering and non-shivering thermogenesis. To fulfill requirements of increased energy expenditure, food intake is increased and energy reserves in adipose tissues are being released. Significant amounts of FA are released from WAT after adrenergically activated-lipolysis. An excessive amount of NEFA in plasma could lead to lipotoxicity. Therefore, FA are, to some extent, re-uptaken and re-esterified in WAT. For detection of re-esterification and DNL, measurement of ^{2}H incorporation into a molecule of glycerol moiety and last methyl of FA from TAG by NMR was used (**Fig.4.1.1**). Since the incorporation of ^{2}H into glycerol can take place only before FA esterifies to glycerol, enrichment of glycerol reflects TAG synthesis. Enrichment of FA methyls in TAG corresponds to *de novo* FA synthesis. TAG synthesis increased after two days of CE in both strains to a similar extent. After 7 days of CE, the increase of TAG synthesis was much more pronounced in A/J mice (**Fig. 4.1.1a**). FA *de novo* synthesis was reduced in both strains by

2 days of CE (**Fig. 4.1.1b**). Longer exposure led to an increase of FA *de novo* synthesis which was higher in A/J mice. These results indicate higher activity of FA synthesis and re-esterification in A/J mice in comparison to B6 mice.

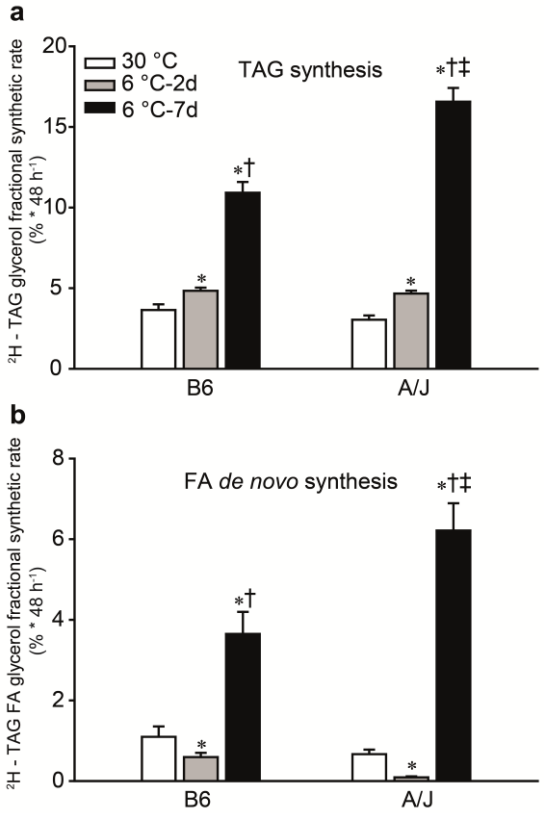

Figure 4.1.1 TAG and FA *de novo* synthesis in eWAT *in vivo*.
TAG synthesis (**a**) and DNL (FA *de novo* synthesis; (**b**)) in eWAT were measured using *in vivo* ^2H_2O incorporation by NMR in mice maintained at 30°C or exposed to cold for either 2 days (6°C–2d) or 7 days (6°C–7d). Data are means ± s.e.m.; *n*=8–10. *Significant difference compared with 30°C within the strain; †significant difference compared with 6°C–2d within the strain; ‡significant difference between strains within the treatment (ANOVA).

Lipolysis was measured *ex vivo* in adipocytes isolated from eWAT with and without β-adrenergic agonist ISO stimulating lipolysis. The amount of NEFA released into medium in basal conditions (without ISO) declined with CE conditions, unlike glycerol, which did not change. (**Fig.4.1.2**). However, when lipolysis was stimulated by ISO, no changes depending on ambient temperature or strain were observed. These results suggest an increased turnover of FA in CE mice as the ratio of NEFA to glycerol was decreased under basal conditions (**Fig. 4.1.2c**). Theoretically, 1 molecule of glycerol binds 3 FA. The ratio of NEFA to glycerol was 2.8 and 2.1 in thermoneutral maintained B6 respectively A/J mice and was lowered to 1 meaning that at least 1FA per TAG was re-esterified. Considering the strong induction of lipolysis by ISO, physiological differences were faded away under stimulated conditions (**Fig. 4.1.2d-f**).

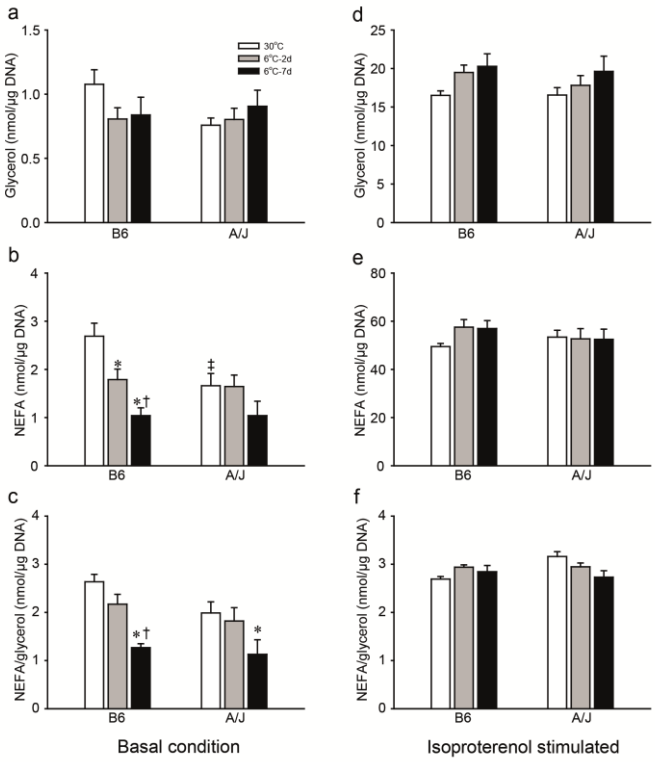

Figure 4.1.2 *Ex vivo* evaluation of lipolytic activity in adipocytes.
Release of glycerol (**a,d**) and NEFA(**b,e**) were measured using collagenase-liberated adipocytes from eWAT of mice maintained at 30°C or exposed to cold for 2 and 7 days (6°C-2d; 6°C-7d) in the basal (**a-c**) or isoproterenol-stimulated (**d-f**) state. The rate of re-esterification was calculated as ratio NEFA to glycerol release (**c, f**). Data are means ± s.e.m.; *n*=3-4 from three experiments. *Significantly different from 30°C within the strain; †significantly different from 6°C-2d within the strain; ‡significant difference between strains within the treatment (ANOVA).

To confirm data obtained by NMR measurement, immunohistochemistry (**Fig. 4.1.3**) and gene expression (**Fig. 4.1.4**) were evaluated in eWAT. As expected, the re-modeling of eWAT by CE was observed. However, only some adipocytes became paucilocular (cells with morphological appearance between white and brown adipocytes) and were surrounded by adipocytes which reduced their size but stayed unilocular (**Fig. 4.1.3a**). The emergence of the paucilocular cells was increased by CE and tended to be higher in A/J mice as compared with B6. To further characterize these cells, UCP1 immunostaining was performed. UCP1 is a classical marker of the browning of white adipocytes. However, UCP1 positivity was not detected in any of the paucilocular cells (**Fig. 4.1.3b**). Next, immunohistochemistry for ATGL and DGAT1 (**Fig. 4.1.3c,d**), markers of lipolysis, and re-esterification, respectively, were evaluated. Both markers increased in eWAT of cold exposed mice and the increase was higher in A/J mice. Interestingly, both ATGL and DGAT1 staining were localized mainly to smaller adipocytes.

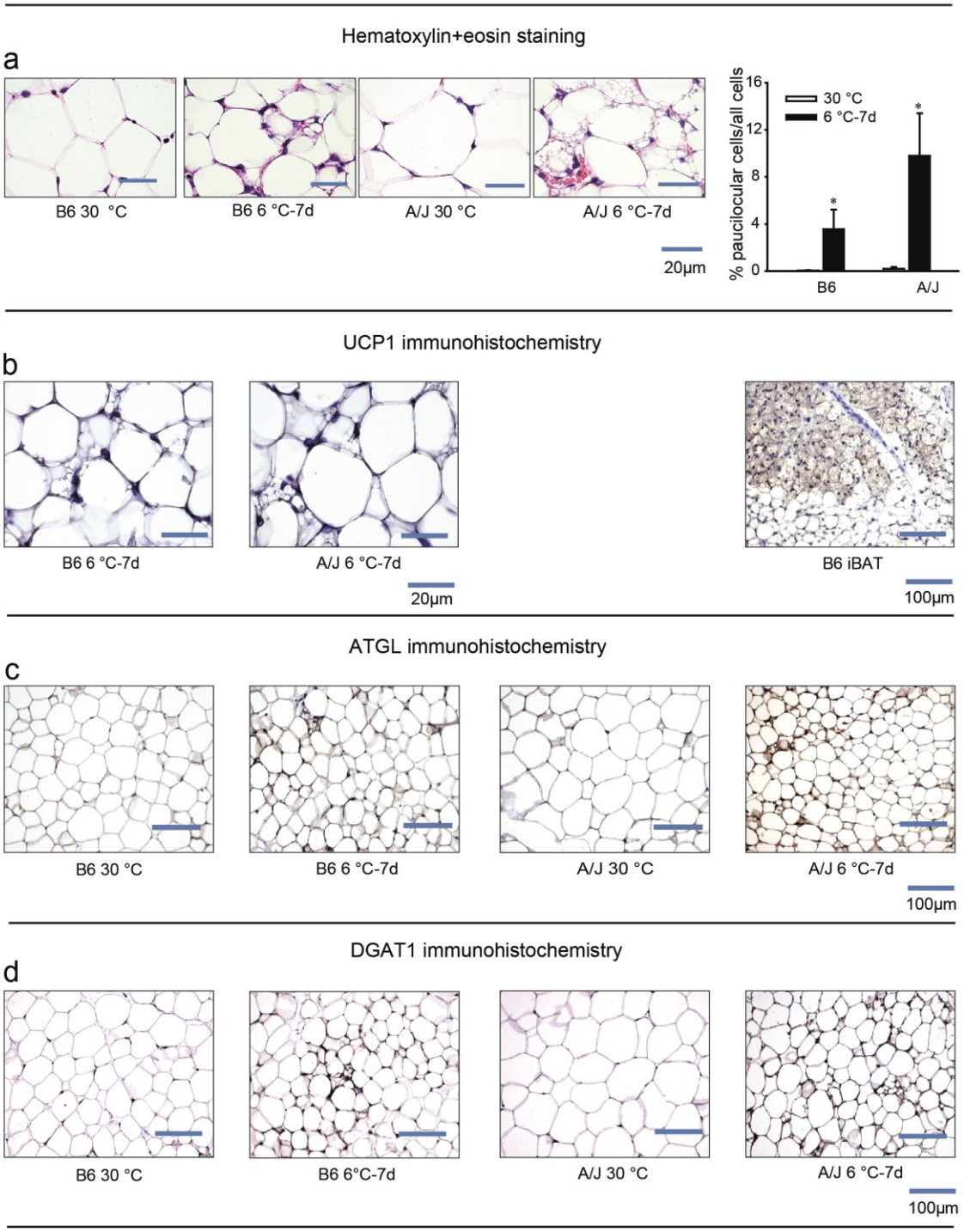

Figure 4.1.3 Morphology and immunohistochemistry of eWAT.
Mice were maintained at 30°C or exposed to cold for 7 days (6°C–7d). (**a**) Hematoxylin+eosin stained sections of eWAT. Mean adipocyte size was 1854 ± 98 µm^2 in A/J 30°C, 1314 ± 70 µm^2 in A/J 6°C–7d, 1407 ±99 µm^2 in B6 30°C, and 1126 ±64 µm^2 in B6 6°C–7d; with significant differences between A/J 30°C and all the other groups). The percentage of paucilocular/multilocular adipocytes relative to all adipocytes is based on the measurements of ~ 800 cells taken randomly from 2 to 3 sections per animal (**a**). Immunostaining for UCP1 (**b**); iBAT was used as a positive control, ATGL (**c**), and DGAT1 (**d**) in eWAT. Dark violet (**a, b**) or brown (**c, d**) color corresponds to a positive signal. Data are means ± s.e.m; *n*=9. *Significant difference compared with 30°C group within the strain (ANOVA).

Genes involved in lipolysis, DNL, re-esterification, FA oxidation were measured in eWAT by qPCR (**Fig. 4.1.4**). Atgl (also known as **Pnpla2**) and Dgat1 were, similarly to histo-

logical data, increased by cold, whereas, Pck1, gene coding main enzyme of glyceroneogenesis PCK1 in WAT, was not affected by CE (**Fig. 4.1.4a**). However, all of these genes were or tended to be higher in eWAT of A/J mice, especially in cold. Also, GK was evaluated in eWAT. Gk mRNA was not different either between strains or cold exposed groups. Relatively little of Gk mRNA in eWAT (**Fig. 4.1.4a**) was in agreement with the higher significance of GK in glyceroneogenesis of BAT than of WAT [57]. Dgat2 and Fasn gene expression (**Fig. 4.1.4a**) supported data from the NMR measurement of FA synthesis (**Fig. 4.1.1a**). Dgat2 is responsible for TAG synthesis from *de novo* synthesized FA [41]. Elovl5, a protein involved in FA synthesis, was increased by cold and both in thermoneutrality and after 2 days of CE was higher in A/J mice than in B6 (**Fig. 4.1.4a**). Therefore, gene expression data confirmed results from NMR. To find out if higher requirements for energy are covered, mRNA of transcription factors regulating mitochondrial biogenesis and oxidative lipid metabolism Pparα and Pgc1α and mRNA of genes involved in FAox Mcad (**Acadm**), Lcad (**Acadl**) and Vlcad (**Acadvl**) were measured (**Fig. 4.1.4b**). Pparα and Pgc1α were augmented by cold only in A/J mice with higher intensity after short-term CE. All of FAox genes were increased by CE with peak after 7 days of CE. Only Vlcad mRNA differs between strains, being higher in eWAT of A/J mice.

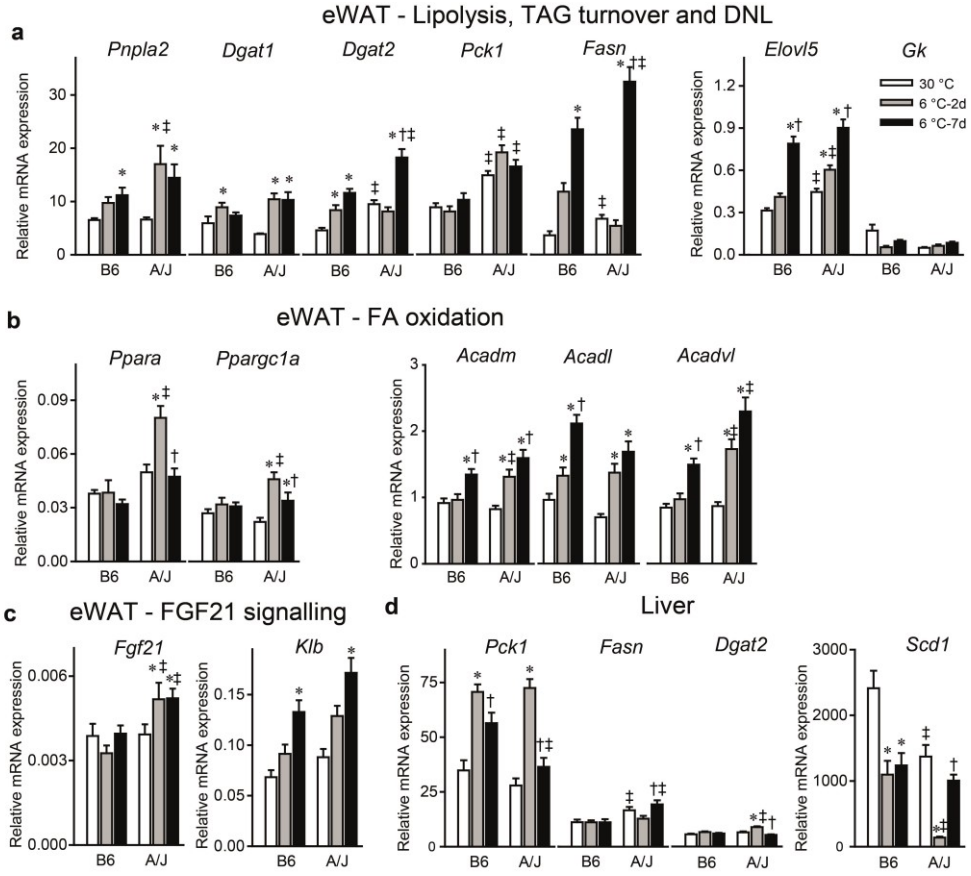

Figure 4.1.4 Gene expression in the eWAT and liver.
Expression of genes was analyzed in mice maintained at 30 °C or exposed to cold for 2 days (6°C–2d) or 7 days (6°C–7d). Gene expression in the eWAT (**a–c**) and liver (**d**) was normalized to the mean signal of three reference genes (actin, beta—Actb; eukaryotic translation elongation factor 1 alpha 1-Eef1a1; and peptidylprolyl isomerase B-Ppib); the delta-delta CT method [215] was used for calculating relative changes in gene expression. Data are means ± s.e.m.; *n*=8–10; pooled from two experiments. *Significant difference compared with 30°C within the strain; †significant difference compared with 6°C–2d within the strain; ‡significant difference between strains within the treatment (ANOVA).

Abbreviations: Acadm, acyl-CoA dehydrogenase medium-chain; Acadl, acyl-CoA dehydrogenase long chain; Acadvl, acyl-CoA dehydrogenase very long chain; Dgat1, diacylglycerol acyltransferase 1; Dgat2, diacylglycerol acyltransferase 2; Elovl5, fatty acid elongase 5; Fasn, fatty acid synthase; Fgf21, fibroblast growth factor 21; Gk, glycerol kinase; Klb, klotho beta; Pck1, phosphoenolpyruvate carboxykinase 1, cytosolic; Pnpla2, patatin-like phospholipase domain containing 2 also known as Atgl; Ppara, peroxisome proliferator-activated receptor alpha; Ppargc1a, peroxisome proliferative activated receptor, gamma, coactivator 1 alpha; Scd1, stearoyl-Coenzyme A desaturase 1.

In addition, since AMPK is a master regulator of energy handling, we measured protein expression of its phosphorylated form and total of α1 and α2 AMPK subunits (**Fig.4.1.5**). There was no effect of either cold or strain to total/unphosphorylated form. However, the activity of AMPK expressed as a ratio of phosphorylated to total AMPK tended to be increased by cold with a higher tendency in A/J in all temperature conditions. Next, we analyzed Fgf21, gene coding a protein influencing energy expenditure, fat and glucose utilization, and its cofactor Klotho beta (**Klb**) mRNA in eWAT. Fgf21 mRNA was elevated by CE only in A/J mice, while Klβ was increased in both strains by CE and tended to be higher in A/J mice (**Fig. 4.1.4c**).

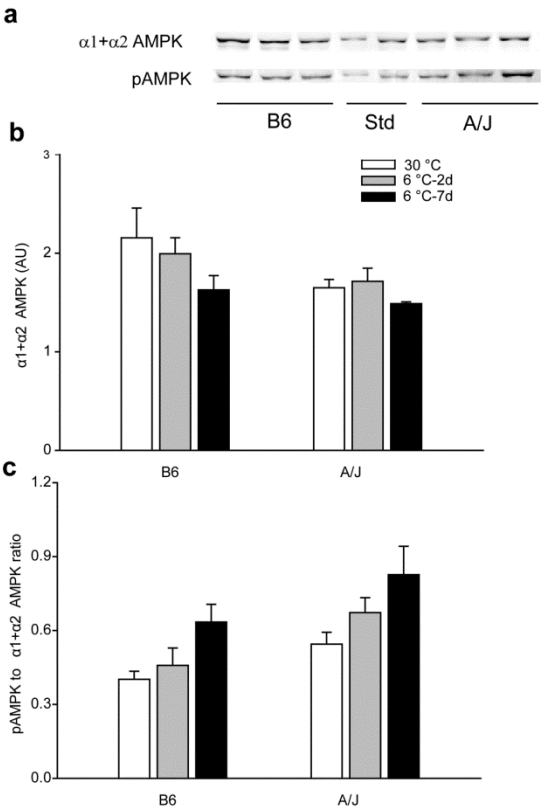

Figure 4.1.5 Content and phosphorylation of AMPK protein in eWAT.
The total content of α1+α2subunits of AMPK (α1+α2 AMPK) and phosphorylated form of AMPK (pAMPK) were evaluated by Western blotting in extracts of eWAT using mice maintained at 30°C or exposed to cold for 2 days (6°C-2d) or 7 days (6°C-7d). Signals on different blots were compared using a standard (Std) prepared from eWAT of 2-month-old B6 mice exposed to 6°C for 7 days and expressed in arbitrary units (AU). (**a**) image of a typical blot, the order of samples is for both B6 and A/J mice: 30°C, 6°C-2d, 6°C-7d, (**b**) content of α1+α2 AMPK, (**c**) ratio of pAMPK to α1+α2 AMPK; there was a difference between A/J and B6 mice (two-way ANOVA; p=0.013). In (**b**) and (**c**), data are means ± s.e.m.; n=6-8.

As mentioned above CE can activate browning, i.e. also Ucp1 gene expression, in WAT. To see if any strain-dependent changes would be observed in WAT prone to browning, we analyzed the expression of appropriate genes in subcutaneous WAT (**Fig.4.1.6**). Atgl, Dgat2, Fasn, and Vlcad (**Acadvl**) were upregulated by CE similarly to eWAT. In contrast to eWAT,

Ucp1 mRNA was upregulated by CE, however, it was independent on strains. Also, other measured genes did not differ between A/J and B6 mice.

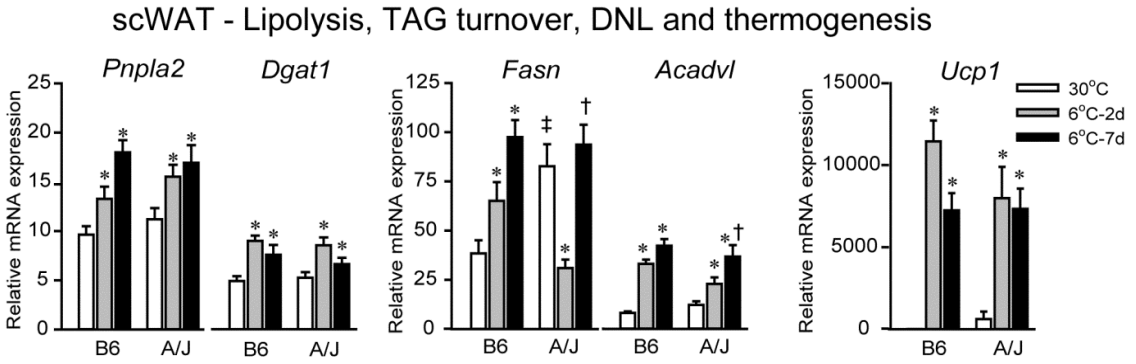

Figure 4.1.6 Gene expression in the subcutaneous WAT.
Expression of genes was analyzed in mice maintained at 30°C or exposed to cold for 2 days (6°C–2d) or 7 days (6°C–7d). Gene expression in the subcutaneous WAT was normalized to the mean signal of 2 reference genes (*actin, beta – Actb,* and eukaryotic translation elongation factor1 alpha 1 - *Eef1a1*) and for calculation of relative changes in gene expression, the delta-delta CT method was used [215]. Data are means ± s.e.m.; *n*=8–10; pooled from two experiments. *Significant difference compared with 30°C within the strain; †significant difference compared with 6°C–2d within the strain; ‡significant difference between strains within the treatment (ANOVA).
Abbreviations: Acadvl, acyl-CoA dehydrogenase very long chain; Dgat1, diacylglycerol acyltransferase 1; Fasn, fatty acid synthase; Pnpla2, patatin-like phospholipase domain containing 2 also known as Atgl; Ucp1, uncoupling protein 1.

Since the major site of lipogenesis except AT is the liver, we measured Dgat2, Fasn, Scd1, and Pck gene expression in this organ (**Fig.4.1.4d**). Dgat2 was transiently increased after 2 days and Fasn after 7 days of CE in A/J mice unlike B6 mice, where no response of these genes to cold was observed. In terms of strain differences, both Dgat2 and Fasn were higher in A/J mice, Dgat2 after 2 days of CE, Fasn in thermoneutrality, and after 7 days of CE. Scd1 was decreased by CE in B6 mice, while in A/J mice a transient decrease was observed on day 2 of CE. Pck1, in the liver representing not just glyceroneogenesis but also gluconeogenesis, was lower in A/J in comparison to B6 mice after 7 days of CE and was augmented by cold in both strains. An important link between hepatic DNL and AT re-esterification was observed by the negative correlation of hepatic Fasn and WAT Pck1 by day 7 of CE (**Table 4.1.2**).

Table 4.1.2 Correlation between Liver Fasn and eWAT Pck1 mRNA in B6 and A/J mice

	Liver Fasn	
eWAT Pck1	R	*P*
B6 mice	-0.720	0.0071
A/J mice	-0.687	0.0087

Abbreviations: eWAT, epididymal white adipose tissue; Fasn, fatty acid synthase; Pck1, cytosolic phosphoenolpyruvate kinase.

To conclude, cold-induced lipolysis led to the induction of contradictory pathways of re-esterification and DNL in order to avoid lipotoxicity. A/J mice responded with higher flexi-

bility, particularly in eWAT, to cold-induced stress than B6 mice. Moreover, the futile cycle contributed to the lean phenotype of A/J mice little but not negligibly by increased energy consumption by the above mentioned pathways.

4.2 Publication B

Experiments in publication B followed-up the results of publication A. Publication B aimed to investigate the contribution of non-shivering thermogenesis to the difference in the propensity to obesity, especially in BAT and maybe also in other tissues such as skeletal muscle in two murine strains. Previous studies using these two mouse strains showed that higher sensitivity to β-3 agonist and higher capacity to Ucp1mRNA induction in WAT can be connected to relative resistance of A/J mice to obesity [214].

During CE, an enormous amount of heat must be produced to defend body temperature. As was described in chapter 1.6.2, BAT is still considered to be a key player in non-shivering thermogenesis activated by cold. First, glucose uptake to BAT was assessed by PET/CT measurement using mice adapted to cold or not, stimulated by CL316,243, specific β3-adrenergic agonist, and injected with 18FDG (**Fig.4.2.1a**). CE increased the capacity of glucose uptake in the BAT region in both strains, but to our surprise, more in the obesity-prone B6 strain (**Fig.4.2.1a,b**). Thus, cold exposed B6 mice are able to recruit a higher capacity for glucose uptake after adrenergic stimulation than A/J strain.

UCP1 is a key player involved in non-shivering thermogenesis. Therefore, its gene expression level was measured by qPCR, and the protein level was assessed by WB. Gene expression of UCP1 was induced by cold in both strains to similar levels (**Fig.4.2.1c**). However, the rate of induction was much higher in B6 mice (10.2-times in B6, 5.9-times in A/J mice). CE increased UCP1 protein in both strains, while there were no significant differences between strains under both temperature conditions (**Fig.4.2.1d**). Also, the total capacity for non-shivering thermogenesis of iBAT, assessed by UCP1 protein expressed per the whole depot, did not differ between strains and was recruited by CE (**Fig.4.2.1e**). Even though the absolute levels of UCP1 were the same between strains, the fold change of UCP1 induction by cold was higher in B6 mice (7.8-times in B6 mice, 5.2-times in A/J mice; **Fig.4.2.1e**).

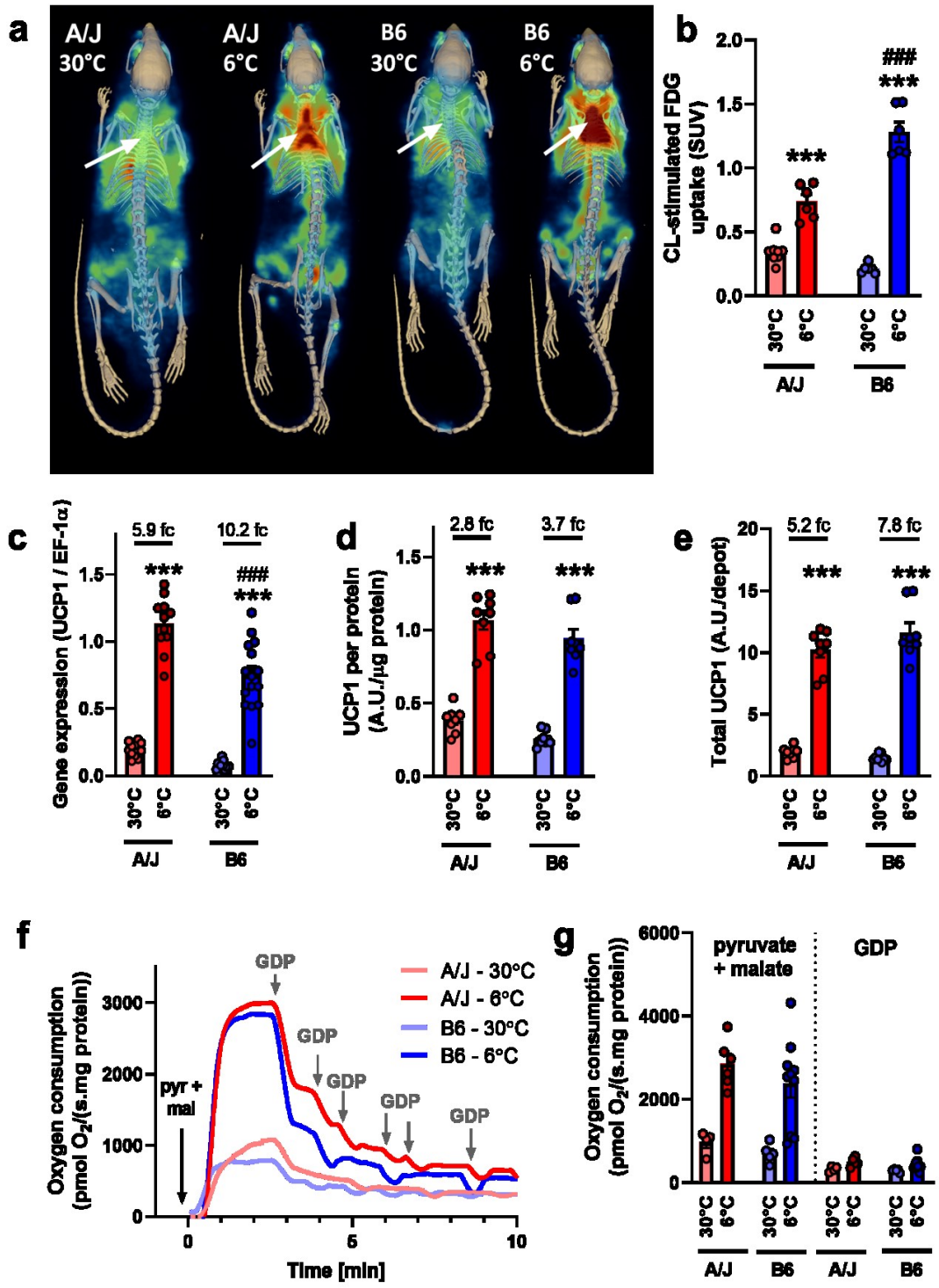

Fig 4.2.1 Higher recruitment of BAT thermogenic capacity in response to cold in B6 than in A/J mice.

A/J and B6 mice exposed to thermoneutral housing temperature (30°C) or cold (6°C) for 7 days, and subsequently treated as indicated in the text (*n*=6-8). Representative PET/CT scans showing FDG accumulation in tissues after stimulation of mice with CL316,243 (**a**). The arrows indicate the location of interscapular BAT. Quantification of FDG signal in BAT is in (**b**). Gene expression of UCP1 mRNA (**c**) and amount of UCP1 in interscapular BAT expressed per unit of total protein (**d**; Western blot quantification; antibody RD) were evaluated. The total amount of UCP1 in whole interscapular BAT depot (**e**); calculated as UCP1 per protein (**d**) multiplied by total protein in the depot (Fig. 4.2.2a). Oxygraph representative curves measured in mitochondria isolated from BAT are shown in (**f**) and quantified in (**g**) Statistics: *indicates a significant difference in comparison to the respective thermoneutral group, # indicates a significant difference in comparison to the A/J mice at the respective temperature (Two-way ANOVA). Data are means ± s.e.m.

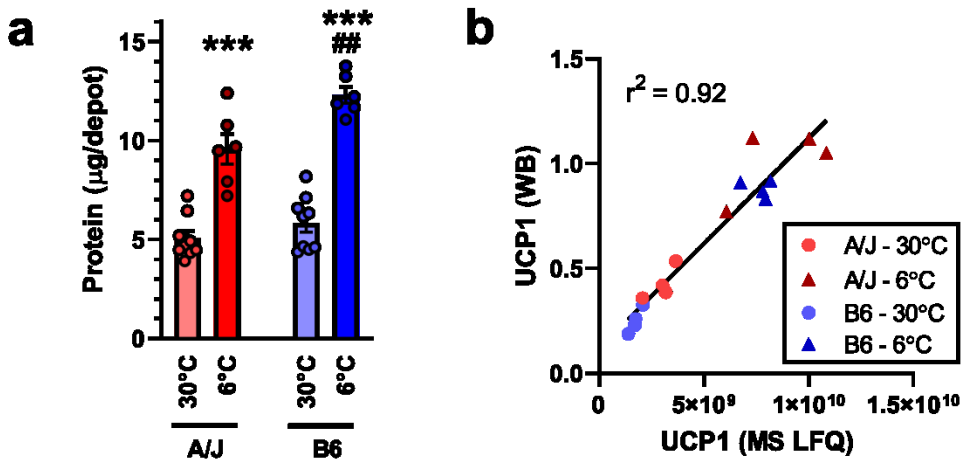

Fig.4.2.2 Ucp1 protein
A/J and B6 mice exposed to thermoneutral housing temperature (30°C) or cold (6°C) for 7 days (*n*=5-9) Total amount of protein in whole interscapular BAT depot (**a**). Comparison of two independent methods of assessment of UCP1 content (**b**): Western blot (WB; axis y; corresponds to Fig.4.2.1d) and label-free quantification using mass spectroscopy (MS LFQ; axis x) Statistics: *indicates a significant difference in comparison to the respective thermoneutral group, # indicates a significant difference in comparison to the A/J mice at the respective temperature (Two-way ANOVA and Tukey's multiple comparison test). Data are means ± s.e.m.

To validate the results of WB and to evaluate global changes in the proteome, MS-LFQ analysis (proteomics) of BAT was performed. Proteomics UCP1 data nicely correlated with data from WB (**Fig.4.2.2b**). In addition, functional measurement of isolated mitochondria using Oxygraph confirmed strain-independent UCP1 protein amount. The activity of UCP1 was measured as pyruvate-induced O_2 consumption inhibited by GDP (**Fig.4.2.1f,g**).

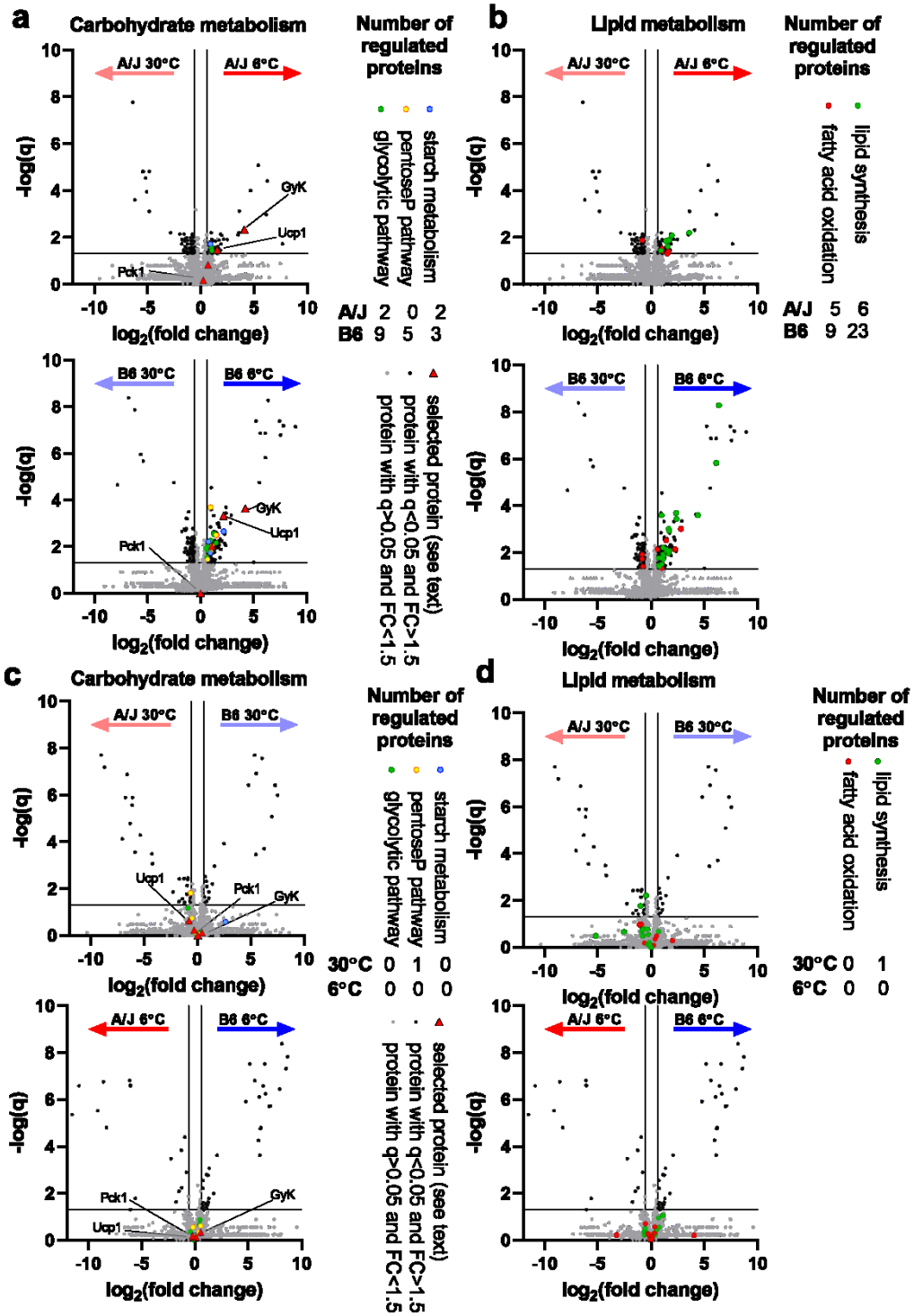

Fig.4.2.3 Proteomic analysis in BAT revealed more metabolic proteins regulated by cold in B6 mice
A/J and B6 mice were exposed to thermoneutral housing temperature (30°C) or cold (6°C) for 7 days (*n*=4-6). Temperature-dependent differences in the proteome of A/J and B6 mice (**a;b**). Proteins involved in carbohydrate metabolism (**a**); proteins involved in lipid metabolism (**b**); strain-dependent differences in the proteome of the thermoneutral and cold exposed mouse (**c;d**); proteins involved in carbohydrate metabolism (**c**); proteins involved in lipid metabolism (**d**); numbers of proteins significantly different between strains are indicated on right; q (on the y-axis) is the *p* value including false discovery rate.

Next, data from the BAT proteome analysis were evaluated. In accordance with previous results, more proteins significantly differed between thermoneutral and cold conditions than between strains in the corresponding temperature. From a total of 3501 proteins, that were evaluated, 170 and 360 proteins were regulated by CE in A/J and B6 mice, respectively, and only 54 and 58 proteins differed between strains in thermoneutrality and cold, respectively. Interestingly, differences in glucose metabolism were observed in the comparison of cold- and thermoneutrality- exposed mice, especially in B6 strain (**Fig.4.2.3a**). Key sources of glucose are blood glucose and glucose stored in form of glycogen in tissues such as the liver and skeletal muscle. However, not only glycogen catabolism was induced by cold but also anabolism, suggesting subtle regulation of glucose handling by storing it in glycogen and forming it by glycogenolysis. Thus, carbohydrates seem to be an important substrate for thermogenesis in BAT. Although there were no significant changes between strains in enzymes involved in glucose/glycogen metabolism (**Fig 4.2.3c** and **STable 4.2.2** in appendix), there were more significant differences in levels of proteins involved in carbohydrate metabolism induced by cold in B6 mice than in A/J mice (**Fig. 4.2.3a** and **STable 4.2.1** in appendix) which corresponded with PET/CT results of 18FDG uptake to BAT.

FA are another source of energy for thermogenesis. Indeed, several proteins involved in FAox were induced by CE (**Fig.4.2.3b** and **STable 4.2.1** in appendix). Interestingly, it seems that many of cold upregulated enzymes are involved in peroxisomal oxidation, where VLCFA (more than 22 carbons) are shortened to continue FAox in mitochondria. In contrast, mitochondrial FAox enzymes ACAD12 and ACADSB were downregulated by cold in both strains and other genes involved in FAox were not regulated by cold at all. ACAD12 substrate specificity is not known, but ACADSB is specialized to oxidize branch chained amino acids and short FA. There were no changes between strains in both temperatures in lipid metabolism (**Fig.4.2.3d** and **STable 4.2.2** in appendix). In addition, acylcarnitines, substrates for mitochondrial FAox were quantified by lipidomics and analyzed by PLSDA (**Fig.4.2.4** and **Dataset 4.2.1** in appendix). The separation of groups was better between temperature conditions than between strains. The acylcarnitine 15:2 was the most discriminating acylcarnitine between strains (**Table 4.2.1** and **Dataset 4.2.1** in appendix) in both temperature conditions. It was higher in A/J mice more than 520 times in thermoneutrality and 40 times in cold exposed mice than in B6 mice. Unfortunately, nothing is known about this acylcarnitine in literature. Interestingly, 3-OH isovalerylcarnitine, which is derived from leucine, belonged between the most discriminating acylcarnitines in both A/J and B6 mice between temperature conditions and was induced by cold in both studied strains.

Furthermore, lipid stores in BAT were decreased and needed to be replenished. FA are provided via blood from WAT or by a synthesis of FA *de novo* in BAT. In accordance, proteins involved in FA and lipid synthesis are increased by CE, especially in B6 mice (**Fig.4.2.3b** and **STable 4.2.1** in appendix). Interestingly, while ACOT1 was increased by CE 80-times in B6

mice, it was increased only 2-times in A/J mice. ACOT1 is cytosolic thioesterase, which hydrolyzes acyl-CoA to acyl and coenzyme A in order to restore coenzyme A levels. Also, ELOVL6 and ACSL5 were much more induced by cold in B6 mice. ACSL5 is a long-chain FA coenzyme A synthetase, which catalyzes the opposite pathway to ACOT enzymes and was induced by CE 20-times in B6 mice against 12-times in A/J mice. This enzyme forms acyl-CoA, which is used for FAox, lipid synthesis, or elongation of FA. Indeed, ELOVL6, which was induced by CE 70-times in B6 mice and 20-times in A/J mice, is responsible for elongation of long-chain FA with 16 carbons to 18 carbons. Loss of ELOVL6 is connected to lower BAT thermogenic capacity [54]. In addition, more enzymes involved in PPP, an important provider of NADPH for FA synthesis and/or elongation, were significantly upregulated by CE in B6 mice. GK, a crucial enzyme in BAT for TAG synthesis, was increased by cold in both A/J and B6 mice. Another enzyme involved in forming G3P, PCK1, was not regulated by cold in both strains (Fig.4.2.3a,c, and STable 4.2.1 in appendix), which was quite expected because PCK1 is more crucial for white fat, where GK is neglected. In conclusion, B6 mice regulated their metabolism more than A/J mice in response to cold. However, A/J mice had many genes involved in glycolysis, PPP, and lipid synthesis already upregulated in thermoneutrality in comparison to B6 mice, e.g. ACOT1, which was 80 times higher in B6 by CE, was almost 40 times higher in A/J mice than in B6 mice already in thermoneutrality. In addition, volcano plot analysis in BAT was set up to be significant with *p* value enriched by FDR less than 0.05. If only *p* value was used, more genes in A/J mice would be also upregulated by cold and the resulted fold change would be similar to B6 mice.

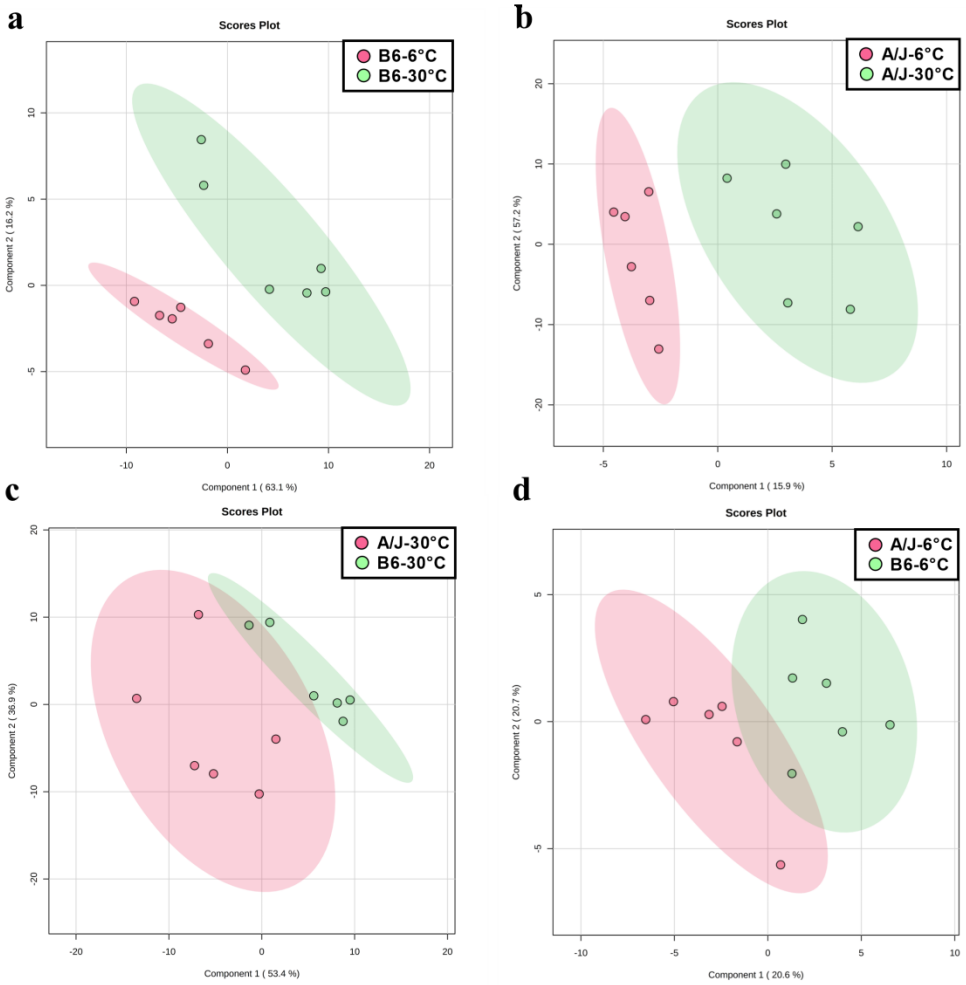

Fig.4.2.4 Partial least squares discriminant analysis of acylcarnitines data from BAT
A/J and B6 mice were exposed to thermoneutral housing temperature (30°C) or cold (6°C) for 7 days (*n*=4-6). Score plots of components 1 and 2 were generated using acylcarnitines profiles of B6 and A/J mice (**a**, **b**) and thermoneutral and cold exposed mice (**c**, **d**). See also dataset 4.2.1 in the appendix.

Table 4.2.1 The most contributing analytes to discrimination of acylcarnitines in BAT.

Compared groups	Acylcarnitine	Comp. 1	Comp. 2	*P*	FC
B6 CE x B6 TN	ACar 3:0-DC Malonyl-carnitine	2.27	2.07	1.5E-03	8.0
	ACar 2-M-4:0-OH 3-Hydroxyisovaleroylcarnitine	2.16	2.01	2.3E-06	6.1
	ACar 20:2 2	2.00	1.46	3.7E-02	0.2
	ACar 18:2 2	1.80	1.31	2.5E-02	0.2
	ACar 22:0	1.79	2.04	n.s.	n.s.
	ACar 16:2 2	1.69	1.23	1.6E-02	0.2
	ACar 20:1	1.48	1.21	n.s.	n.s.
	ACar 18:1-OH 3-Hydroxyoleylcarnitine	1.32	0.97	4.7E-02	0.3
A/J CE x A/J TN	ACar 2-M-4:0-OH 3-Hydroxyisovaleroylcarnitine	3.30	3.23	2.7E-05	10.1
	ACar 15:2	2.08	2.05	n.s.	n.s.
	ACar 20:5	1.75	1.72	n.s.	n.s.
	ACar 22:0	1.72	1.68	5.4E-03	3.6
	ACar 5:1	1.57	1.53	4.8E-03	3.0
	ACar 20:0	1.53	1.49	2.3E-02	2.5
	ACar 19:1 2	1.52	1.50	n.s.	n.s.
	ACar 3:0-DC Malonyl-carnitine	1.46	1.44	4.8E-02	3.4
	ACar 4:0-OH 3-Hydroxybutyrylcarnitine	1.39	1.36	n.s.	n.s.
A/J TN x B6 TN	ACar 15:2	4.93	4.65	3.9E-03	524.3
	ACar 20:2 2	1.41	1.37	n.s.	n.s.
A/J CE x B6 CE	ACar 15:2	5.74	5.32	7.0E-03	39.3
	ACar 22:1	1.83	1.71	1.3E-02	2.5
	ACar 22:2	1.64	1.61	1.8E-02	2.1
	ACar 13:0	1.54	1.45	n.s.	n.s.

VIP score of two largest components between strains or temperatures based on partial least squares discriminant analysis of acylcarnitines data from BAT in Fig.4.2.4. Cut off was set up at 1.3 for component 1. Statistical significance (*p*) is shown for the given analyte between compared groups, the same applies for fold change (FC). Values, which had $p>0.05$ and FC between 0.66 and 1.50 were not shown (n.s.).
Abbreviations: ACar, acylcarnitine; TN, thermoneutrality exposed mice; CE; cold exposed mice; Comp, component.

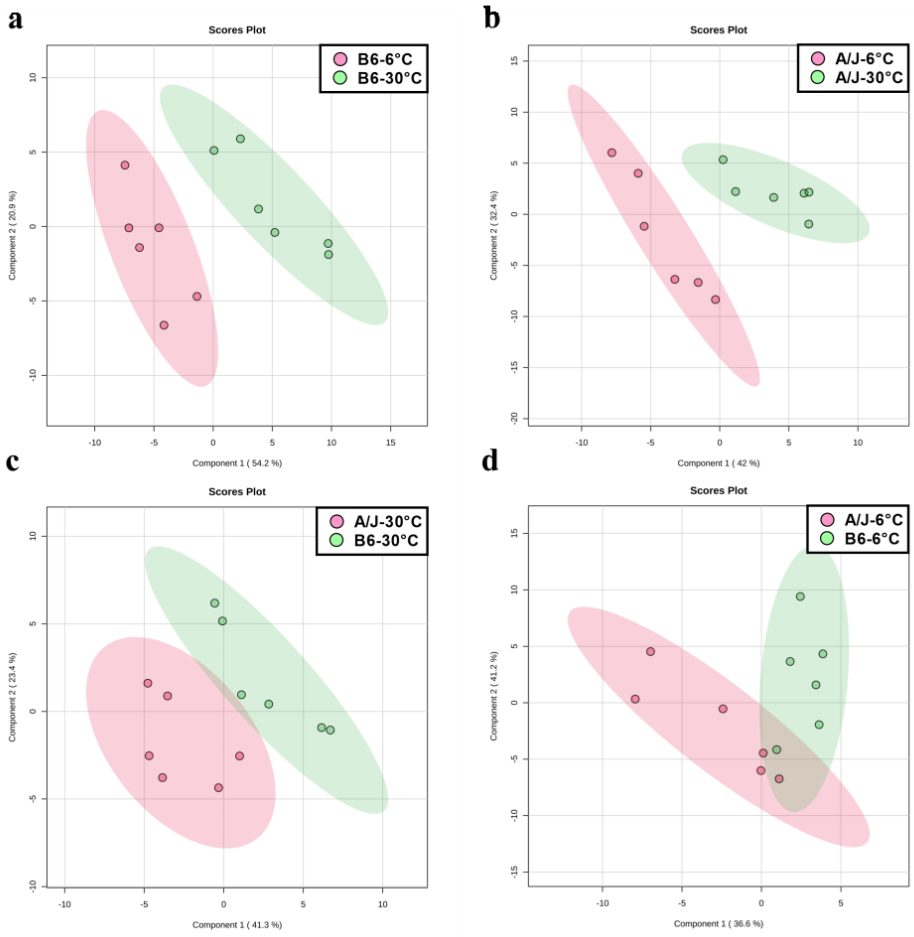

Fig.4.2.5 Partial least squares discriminant analysis of metabolome data from BAT
A/J and B6 mice were exposed to thermoneutral housing temperature (30°C) or cold (6°C) for 7 days (*n*=4-6). Score plots of components 1 and 2 were generated using metabolites profiles of B6 and A/J mice (**a**, **b**) and thermoneutral and cold exposed mice (**c**, **d**). See also dataset 4.2.2 in the appendix.

Table 4.2.2 The most contributing analytes to discrimination of metabolites in BAT

Compared groups	Metabolite	Comp. 1	Comp. 2	*p*	FC
B6 CE x B6 TN	Glycerol-2-phosphate	2.56	2.32	1.6E-02	5.8
	Glycero-3-phosphocholine	2.47	2.43	3.4E-06	0.1
	Anserine	2.04	2.42	n.s.	n.s.
	Carnosine	1.87	1.98	n.s.	n.s.
	Glutathione reduced	1.81	1.70	1.5E-05	4.5
	S-Lactoylglutathione	1.79	1.66	1.6E-02	3.6
	Val-Arg	1.69	2.14	n.s.	n.s.
	Trigonelline	1.50	1.38	8.3E-06	3.4
	Adenosine	1.48	1.52	n.s.	n.s.
A/J CE x A/J TN	Glycero-3-phosphocholine	3.01	2.69	1.5E-05	0.1
	β-Nicotinamide adenine dinucleotide, reduced	2.03	1.79	n.s.	n.s.
	Guanosine 5'-monophosphate	1.91	1.71	n.s.	n.s.
	Creatine phosphate	1.84	1.89	n.s.	n.s.
	S-Lactoylglutathione	1.75	1.70	n.s.	n.s.
	Glycerol-2-phosphate	1.69	1.50	5.1E-03	2.7
	Trigonelline	1.68	1.49	9.2E-05	2.90
	Anserine	1.53	1.92	n.s.	n.s.
	Adenosine 5'-monophosphate	1.51	1.78	n.s.	n.s.
A/J TN x B6 TN	Glycerol-2-phosphate	3.03	2.49	n.s.	n.s.
	Anserine	2.81	2.82	n.s.	n.s.
	N-Acetylhistamine	2.64	2.21	1.5E-03	2.7
	1-Methylnicotinamide	2.30	2.20	6.1E-05	0.4
	Glutathione reduced	2.05	1.68	4.5E-04	2.4
	β-Nicotinamide adenine dinucleotide	2.04	1.63	2.8E-02	0.5
	S-Lactoylglutathione	1.83	1.59	n.s.	n.s.
	Creatine phosphate	1.49	1.52	n.s.	n.s.
A/J CE x B6 CE	Creatine phosphate	3.02	2.87	n.s.	n.s.
	Guanosine 5'-monophosphate	2.59	2.23	n.s.	n.s.
	Adenosine 5'-monophosphate	2.52	2.43	n.s.	n.s.
	1-Methylnicotinamide	2.11	1.94	2.3E-03	0.4
	Ile-Gln	1.96	1.89	n.s.	n.s.
	Val-Arg	1.79	1.63	n.s.	n.s.
	β-Nicotinamide adenine dinucleotide	1.62	1.64	n.s.	n.s.
	N-6-Methyllysine	1.55	1.41	3.3E-02	0.5
	Adenosine	1.53	1.56	n.s.	n.s.
	Adenosine 5'-diphosphoribose	1.46	1.27	n.s.	n.s.

The VIP score of the two largest components between strains or temperatures is based on partial least squares discriminant analysis of metabolites data from BAT in Fig.4.2.5. Cut off was set up at 1.3 for component 1. Statistical significance (*p*) is shown for the given analyte between compared groups, the same applies for fold change (FC). Values, which had $p>0.05$ and FC between 0.66 and 1.50 were not shown (n.s.).
Abbreviations: TN, thermoneutrality exposed mice; CE; cold exposed mice; Comp, component.

Next, metabolome was analyzed by PLSDA, and VIP analytes were found (**Fig.4.2.5**, **Table 4.2.2**). Interestingly, the highest VIP score discriminating A/J and B6 cold-exposed mice had creatine-phosphate, an important molecule in energy metabolism. However, creatine-phosphate was not significant between these two groups. There were only two metabolites in cold-exposed mice that had a VIP score higher than 1.5 and were significant - methyl nicotinamide and N-6-methyllysine. Both were higher in B6 mice in comparison to A/J mice in cold. N-

6-methyllysine is part of methylated proteins/histones and it was found that methylation of lysine in proteins is important for brown adipocyte differentiation [216]. In addition, trimethyllysine is a precursor for L-carnitine [217]. Methylnicotinamide was shown to be a myokine signaling low muscle energy availability, leading to increased lipolysis [218]. However, it is also a methylated form of nicotinamide, which is a precursor for NAD. Methylation of nicotinamide is an irreversible reaction, therefore lower NAD is produced, which leads to lower FAox due to inhibition of NAD-dependent deacetylase Sirt3 [219]. In thermoneutrality, four significant metabolites separated A/J from B6 mice, methyl nicotinamide, and NAD, which were higher in B6 mice, while N-acetylhistamine and reduced form of glutathione were increased in A/J mice. N-acetylhistamine is one of the possible degradation products of histamine. Hypothalamic neuronal histamine was shown to regulate energy expenditure in BAT (by increased Ucp1 mRNA) through the activation of sympathetic nerves [220], which may be connected to lower Ucp1 induction in A/J mice by CE. Interestingly, reduced form of gluthatione was not the only one metabolite involved in protection against oxidative stress with high VIP score. Also anserine and lactoglutathione discriminated A/J from B6 mice in thermoneutrality. However, these two metabolites were not significantly different between A/J and B6 mice. CE induced glycerol-2-phosphate and trigonelline and decreased glycerol-3-phosphocholine in A/J mice. Trigonelline is methylated form of nicotinic acid, which is excreted by urine. It was suggested that it inhibits adipogenesis via downregulation of PPARγ and PPARγ-mediated pathways [221]. Glycerol-3-phosphocholine is involved in lipid metabolism. There was probably higher turnover of it by CE. Similar metabolites were increased, i.e. glycerol-2-phosphate, trigonelline and decreased i.e. glycerol-3-phosphocholine, in B6 mice by CE. Also oxidative stress protectors, reduced form of glutathione, lactoglutathione were upregulated. To sum up, many metabolites involved in energy metabolism and oxidative stress were cold-regulated in both A/J and B6 mice.

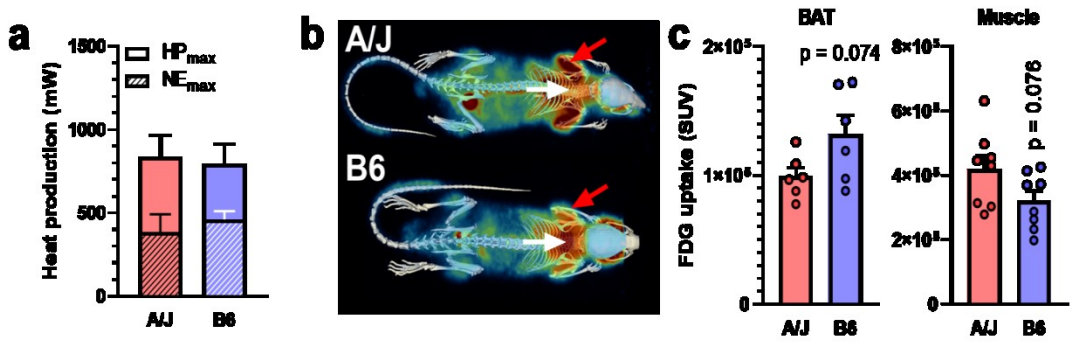

Fig.4.2.6 Gastrocnemius muscle contributes to heat production more in A/J mice than in B6 mice
A/J and B6 mice were exposed to thermoneutral housing temperature (30°C; *n*=4-6). Maximal and norepinephrine (NE)-stimulated heat production (HP) evaluated as in [213]. (**a**) Representative PET/CT scan of 18FDG uptake of A/J and B6 mice adapted to thermoneutrality and stimulated for 1h by cold (**b**); 18FDG uptake to BAT (white arrow in (**b**)) and skeletal muscle (red arrows in (**b**); **c**) Data are means ± s.e.m.

Both A/J and B6 mice are able to deal with CE as was proved by similar maximal heat production (**Fig. 4.2.6a**). Heat production was measured using INCA. The measurement was ended when body core temperature dropped below 28°C despite an increase in oxygen consumption/heat production. Due to the technical limitation of the system, in which minimal inner ambient temperature is restricted to 5°C, only mice kept in thermoneutrality were evaluated (CE animals did not reach the point, where animals started to fail to defend their body temperature). The portion of HPmax, which was not stimulated by norepinephrine, was higher in A/J than B6 mice (**Fig.4.2.6a**, counted as NEmax deducted from HPmax). Thus, another thermogenic organ and pathway which did not involve norepinephrine activation must had been involved in the production of heat in A/J mice. To identify which organ could be responsible for the production of heat in A/J mice, PET/CT measurement of 18FDG uptake was performed (**Fig.4.2.6b**). Both A/J and B6 mice were adapted to thermoneutrality and then acutely exposed to cold before measurement. While 18FDG uptake to BAT was higher in B6 mice in comparison to A/J mice, 18FDG was more accumulated in forelimb muscles of A/J mice (**Fig.4.2.6c**). Thus, skeletal muscle might be of high importance for thermogenesis in A/J mice.

To further explore the metabolism of skeletal muscle, proteomic and metabolomic/lipidomic analysis were performed. A lower number of proteins and significantly different proteins were detected in gastrocnemius muscle in comparison to BAT (**Fig. 4.2.7a,b** and **STables 4.2.3** and **4.2.4** in appendix). In addition, no or few proteins were significant with the use of FDR, therefore *p* value was used in the case of gastrocnemius muscle evaluation of proteomics. Proteins involved in the TCA cycle, OXPHOS, glycolysis, and starch metabolism were mostly induced by cold similarly in both strains. Only three proteins (one glycolytic and two involved in OXPHOS) were differentially regulated by the cold. Unfortunately, differences among the samples were so high and the number of samples quite low (n=4-6), that none of these proteins reached statistical significance. Also, differences between the strains in both thermoneutrality and cold were mostly below 1.5 fold change. Interestingly, some OXPHOS and TCA cycle proteins were down- and up-regulated in B6 mice as compared with A/J mice in respective temperature conditions. Subunits B1 and C2 of ATP synthase F_O complex and NADH dehydrogenase 1 and 3 were more than 1.5-times higher in B6 mice in thermoneutrality in comparison to A/J mice. B1 subunit of ATP synthase F_O complex was higher also in cold in B6 mice. Moreover, fructose-bisphosphate aldolase was almost 200-times higher in B6 mice than in A/J in thermoneutrality. NADH dehydrogenase NDUFAF6 was higher in the thermoneutrality of A/J mice more than 15-times in comparison to B6 mice. In addition, cytochrome c oxidase COX7A2L and isocitrate dehydrogenase were higher in A/J mice in comparison to B6 mice in both thermoneutrality and cold. To conclude, not many differences were observed in gastrocnemius muscle proteins involved in metabolism.

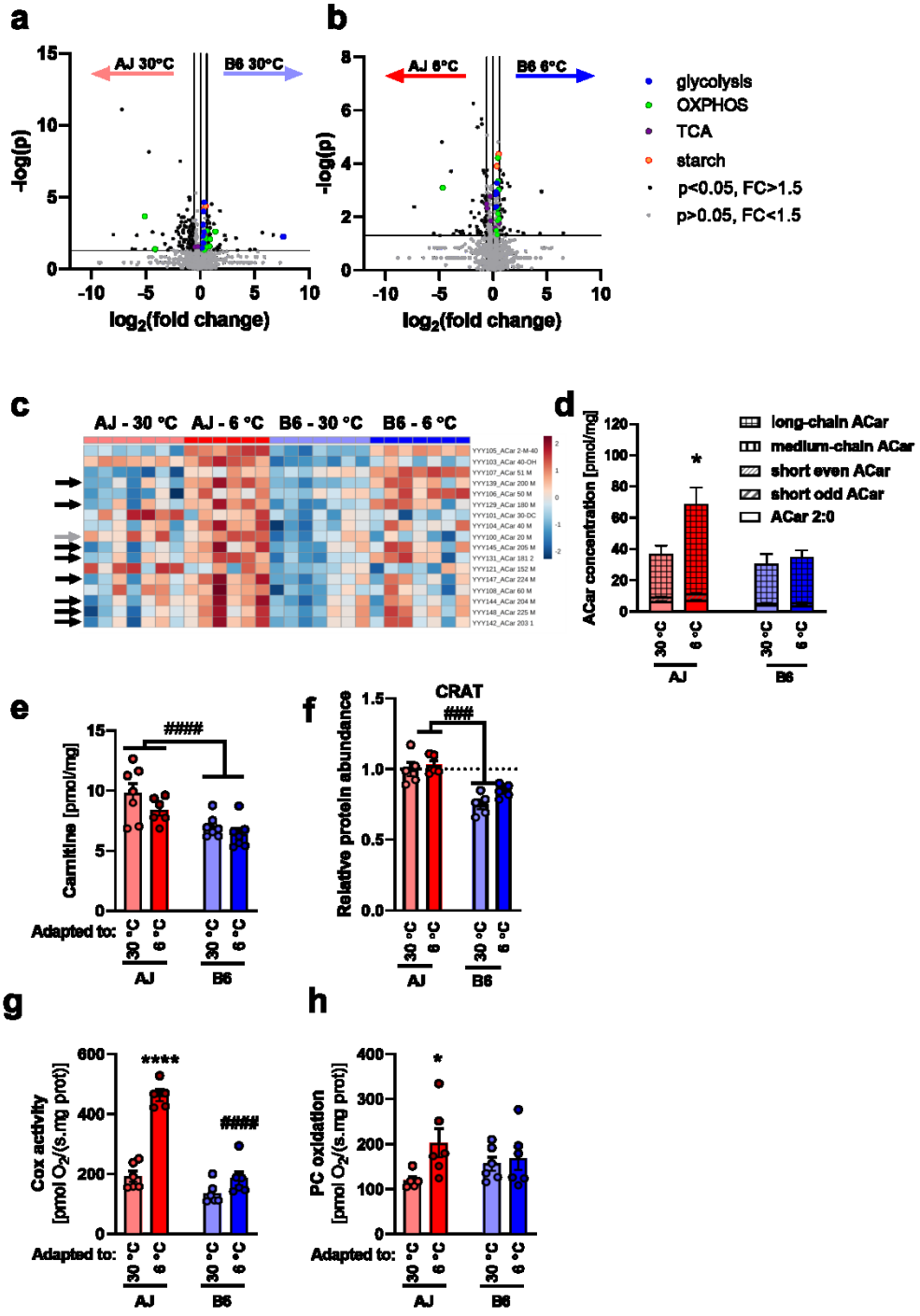

Fig 4.2.7 Adaptation of gastrocnemius muscle to cold.
A/J and B6 mice were exposed to thermoneutral housing temperature (30°C) or cold (6°C) for 7 days (*n*=4-6). Differences in the proteome in gastrocnemius muscle between A/J and B6 mice in thermoneutral (**a**) and cold exposed (**b**) mouse. Heat map showing the abundance of those acylcarnitines, which significantly differ among experimental groups (**c**; acylcarnitine species are ordered according to p value; black arrows highlight long-chain acylcarnitines, grey arrow points to acetylcarnitine); Cumulative concentrations of acylcarnitines, which significantly differ in their abundances among experimental groups (**d**): acetylcarnitine (ACar 2:0), short-chain odd-numbered acylcarnitines (3, 5, and 7 carbons), short-chain even-numbered acylcarnitines (4 and 6 carbons), medium-chain acylcarnitines (8-15 carbons), long-chain acylcarnitines (16 and more carbons); statistics performed on sum of all acylcarnitines. Carnitine levels in gastrocnemius muscle are shown in (**e**). Carnitine O-acetyltransferase (CRAT) protein levels evaluated in gastrocnemius muscle from protemic data (**f**). The activity of cytochrome oxidase (respiratory complex IV, Cox) in muscle homogenate (gastrocnemius and quadriceps muscle combined) was measured by Oroboros oxygraph as respiration after addition of N,N,N',N'-tetramethyl-p-phenylenediamine dihydrochloride (TMPD) and L-ascorbate (**g**). Maximal oxidation of palmitoyl carnitine in muscle homogenate (gastrocnemius and quadriceps muscle combined) measured by Oroboros oxygraph (**h**). Statistics: *indicates a significant difference in comparison to the respective thermoneutral group, #indicates a significant difference in

comparison to the A/J mice at the respective temperature (Two-way ANOVA and Tukey's multiple comparison test). Data are means ± s.e.m.

On the other hand, a higher carnitine level was revealed in A/J mice by metabolomic analysis (**Fig.4.2.7e**). Carnitine is needed for FA to enter the mitochondria. Thus, A/J mice have a higher capacity to transfer FA to mitochondria for FAox, suggesting they more rely on lipid oxidation as an energy source. Except for the role in FAox, acylcarnitines were also suggested to protect mitochondria from the overload of oxidative intermediates by their translocation to cytosol. Interestingly, the level of acetylcarnitine, a product of both glucose and FAox, was found to be higher in A/J mice (**Fig.4.2.7c,d**) as well as carnitine O-acetyltransferase (**CRAT**), an enzyme crucial for acetylcarnitine formation and an important player in fatigue resistance (**Fig.4.2.7f**). Therefore, a metabolic overload and fatigue of mitochondria are better prevented in A/J than B6 mice. To support these data the functional measurement of muscle homogenate was performed using the Oxygraph. Indeed, A/J mice responded to PC with malate with a higher increase in O_2 consumption in comparison to B6 mice (**Fig. 4.2.7h**). Also, the activity of COX was higher in cold exposed A/J mice than in B6 mice (**Fig. 4.2.7g**). In addition, a detailed analysis of metabolic data by PLSDA showed nice separation in all groups (**Fig. 4.2.8a-d**). Therefore, the VIP score was counted (**Table 4.2.3**). Panthothenic acid was one of the most contributing metabolites to the separation of A/J and B6 mice and it was increased in A/J mice in both thermoneutrality and cold. Panthothenic acid is a precursor for coenzyme A, which is an important activator of FA for FAox. Lysine, N-6 lysine, and N-6,N-6,N-6 trimethyllysine were increased in B6 mice in cold in comparison to A/J mice. Trimethyllysine is a precursor for the synthesis of L-carnitine, which is, however, increased in A/J mice (**Fig.4.2.7e**). This leads to two conclusions, either B6 mice had downregulated some enzyme in the L-carnitine biosynthesis pathway and therefore these metabolites accumulate, or B6 mice produced more carnitine and it was all used to produce acylcarnitines, but B6 mice were not able to recycle carnitine as well as A/J mice. In addition, B6 had upregulated Ucp3 mRNA in both thermoneutrality and cold in comparison to A/J mice (**Fig.4.2.8f**). UCP3 was proposed to transport FA out of the mitochondria and therefore, protect mitochondria from the toxicity of FA anions and peroxides [222].

It was more than 40 years ago when it was proposed that except for shivering, skeletal muscle is able to produce heat by non-shivering thermogenesis [188]. However, even nowadays, this proposition is still questioned. Calcium cycling is one of the most promising mechanisms of non-shivering thermogenesis in muscle. Sarcolipin uncouples SERCA and therefore decreases the transport of Ca^{2+} to sarcoplasmic reticulum which leads to an increase in Ca^{2+} in the cytosol and activates enzymes CAMK, NFAT, and others to trigger mitochondrial biogenesis gene expression. To explore, if Ca^{2+} cycling is involved in differences between A/J and B6 mice in skeletal muscle, SERCA1, SERCA2a, sarcolipin, and CAMK2D were evaluated from proteomic data. Indeed, both SERCA2a and CAMK2D proteins were higher in A/J mice in comparison to B6 mice (**Fig. 4.2.8e**). Unfortunately, sarcolipin protein is too small to be identified in our pro-

teomic analysis. However, we quantified sarcolipin mRNA levels and it was in agreement with results from proteomics, sarcolipin mRNA was induced by CE in A/J mice but not in B6 mice (**Fig.4.2.8f**). The same result was observed for Serca2a (**Fig. 4.2.8f**). Serca1 did not change either between strains or by CE. In addition, acylcarnitines levels, especially long chained-acylcarnitines, were increased by CE in A/J, but not in B6 mice (**Fig. 4.2.7d**). It was shown that long-chained carnitines and esterified LCFA are able to activate Ca^{2+} release from the sarcoplasmic reticulum.

Together, all three Ucp1 mRNA, protein, and activity were induced by CE similarly in BAT of A/J and B6 mice. B6 mice, in comparison to A/J mice, had a higher metabolic rate in BAT. These results did not correspond to the leaner phenotype of A/J mice. In contrast, A/J mice relied more on thermogenesis in the muscle, which could represent the link with the healthy phenotype of A/J mice and muscle Ca^{2+} cycling could be the hidden player in UCP-independent thermogenesis in A/J mice.

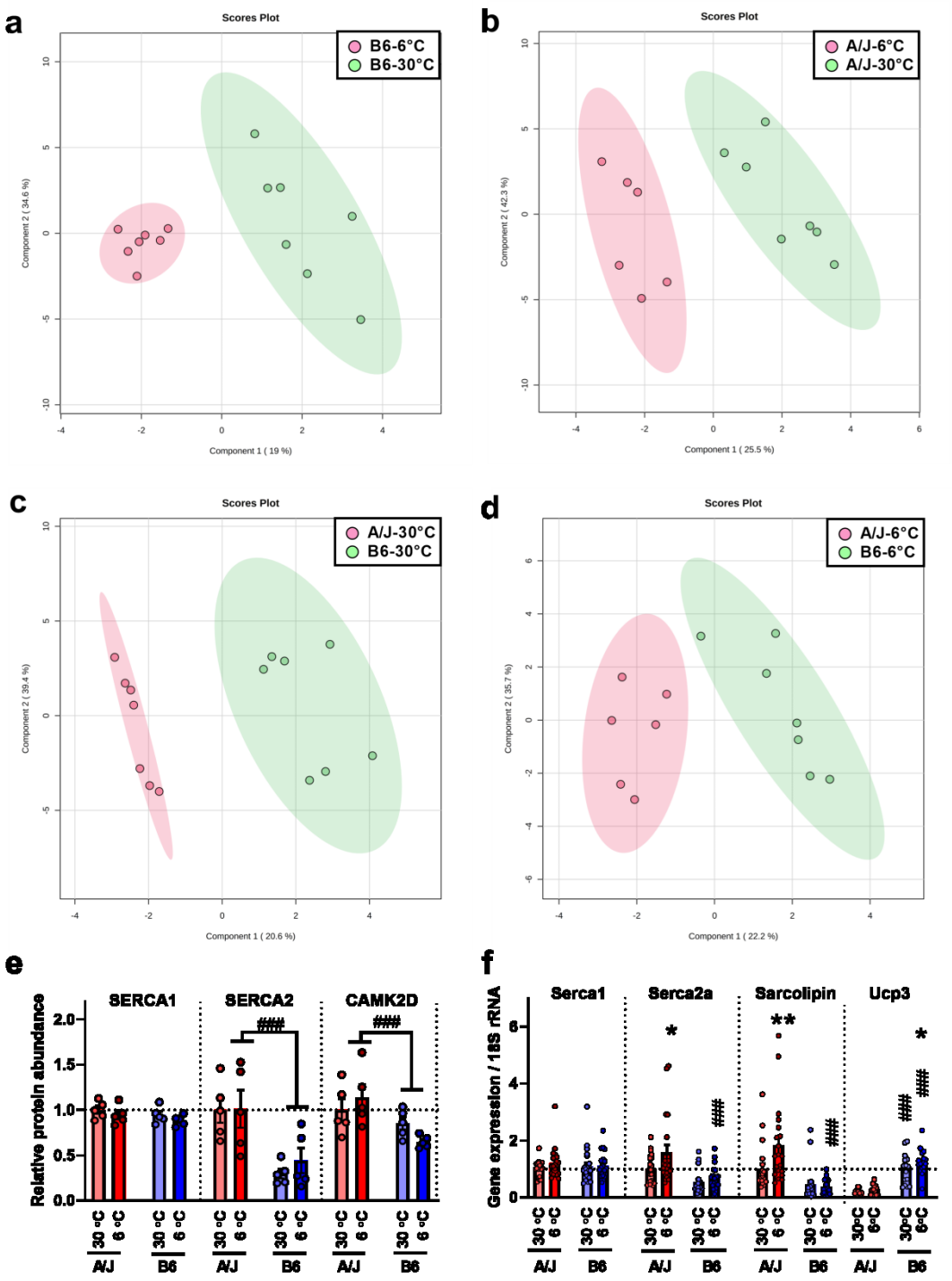

Fig 4.2.8 Adaptation of gastrocnemius muscle to cold.
A/J and B6 mice were exposed to thermoneutral housing temperature (30°C) or cold (6°C) for 7 days (*n*=5-7). Score plots of PLSDA components 1 and 2 were generated by using metabolites profiles of B6 and A/J mice (**a, b**) and thermoneutral and cold exposed mice (**c, d**) from gastrocnemius muscle (See also dataset 4.2.3 in appendix) by Metabolanalyst.ca. Quantification of the protein content of selected genes associated with calcium cycling by proteomics (**e**). Expression of genes associated with calcium cycling in musculus gastrocnemius (**f**; combined data from 3 independent experiments). Statistics:* indicates a significant difference in comparison to the respective thermoneutral group, # indicates a significant difference in comparison to the A/J mice at the respective temperature (2-way ANOVA and Tukey's multiple comparison test). Data are means ± s.e.m.

Table 4.2.3 The most contributing analytes to discrimination of metabolites in gastrocnemius muscle

Compared groups	Metabolite	Comp. 1	Comp. 2	*p*	FC
B6 CE x B6 TN	Glycine	2.67	2.60	2.7E-05	0.4
	Dimethylarginine	2.40	2.34	1.4E-04	0.5
	N-Acetylhistamine	2.25	2.19	1.8E-02	1.7
	1-Methylhistidine	2.12	2.08	2.8E-05	0.5
	Lysine	2.05	1.99	3.6E-03	0.5
	Guanine	2.01	2.01	n.s.	n.s.
	Disaccharide	1.79	2.09	n.s.	n.s.
	Serine	1.51	1.46	4.1E-05	0.6
A/J CE x A/J TN	Glycine	3.35	3.21	5.4E-06	0.3
	Inosine 5'-monophosphate	2.41	2.56	n.s.	n.s.
	Dimethylarginine	2.21	2.12	1.1E-04	0.5
	Glutathione oxidised	2.02	2.04	n.s.	n.s.
	Lysine	1.76	1.69	1.8E-04	0.5
	Serine	1.67	1.60	9.1E-05	0.5
	1-Methylhistidine	1.64	1.58	4.9E-04	0.5
	Asparagine	1.50	1.44	1.2E-04	0.6
A/J TN x B6 TN	N-Acetylhistamine	4.08	4.01	5.7E-04	4.1
	N6-Methyllysine	2.53	2.49	2.1E-06	0.4
	Ornithine	2.03	2.01	3.2E-03	0.4
	Guanine	2.01	1.97	n.s.	n.s.
	Arginine	1.90	1.87	1.1E-03	0.5
	Lysine	1.85	1.83	1.4E-03	0.5
	1-Methylhistidine	1.68	1.65	2.3E-04	0.5
	Pantothenic acid	1.55	1.52	3.4E-04	1.9
	Choline	1.53	1.50	7.1E-05	0.6
A/J CE x B6 CE	N6-Methyllysine	2.82	2.74	2.2E-06	n.s.
	Arginine	2.37	2.30	3.5E-05	0.5
	Lysine	2.18	2.11	2.4E-04	0.5
	Adenosine	1.92	1.87	n.s.	n.s.
	Histamine	1.92	1.86	1.0E-02	1.9
	Inosine 5'-monophosphate	1.77	1.82	n.s.	n.s.
	Glycine	1.77	1.71	5.3E-04	0.6
	1-Methylhistidine	1.75	1.70	2.9E-04	0.6
	Pantothenic acid	1.68	1.63	1.1E-04	1.7
	Ornithine	1.66	1.62	4.2E-03	0.6
	Dimethylarginine	1.53	1.48	1.5E-02	0.6
	N6,N6,N6-Trimethyllysine	1.52	1.47	3.3E-03	0.6

The VIP score of the two largest components between strains or temperatures based on partial least squares discriminant analysis of metabolites data from gastrocnemius muscle in Fig.4.2.8. Cut off was set up at 1.3 for component 1. Statistical significance (*p*) is shown for the given analyte between compared groups, the same applies for fold change (FC). Values, which had $p>0.05$ and FC between 0.66 and 1.50 were not shown (n.s.).
Abbreviations: TN, thermoneutrality exposed mice; CE; cold exposed mice; Comp, component.

4.3 Publication C

The study aimed to characterize the mechanism of WAT hyperplasia and its amelioration by dietary n-3 PUFA. In this study, B6 subtype N mice were used. Mice were for 1 or 8 weeks fed standard (STD), high fat (HFD), or n-3 PUFA-supplemented-high fat diet (HFF). As in the previous study (Chapter 4.1; Publication A), we focused on remodeling of eWAT affected by diet, and on inflammatory changes and their impact on WAT.

Body weights of mice fed both HFD and HFF were increased comparing to STD at both Week 1 and Week 8 with higher body weight gain after 8 weeks of feeding. No difference between HFD and HFF was observed (**Table 4.3.1**). Also, the weight of eWAT was augmented by HFD and HFF feeding. However, significant eWAT weight gain restriction was observed in the HFF compared to the HFD fed mice at Week 8 (**Table 4.3.1**). This difference was even more pronounced on the level of DNA content in eWAT, where the HFF group at both Week 1 and 8 had less DNA content than HFD. DNA content, a marker of cell number in the tissue, was increased in all groups at Week 8 compared to Week 1. Next, the DNA content of adipocytes was measured at Week 8 and it resembled the results from the whole tissue (**Table 4.3.1**).

Table 4.3.1 Effects of EPA/ DHA on body weight, eWAT weight, and DNA content.

	Week 1			Week 8		
	STD	HFD	HFF	STD	HFD	HFF
BW initial (g)	29.3 ± 1.9	29.6 ± 1.4	30.0 ± 2.4	28.1 ± 1.8[a]	28.1 ± 1.9[a]	28.2 ± 1.7[a]
BW dissection (g)	29.9 ± 1.9	33.9 ± 2.1[c]	33.9 ± 2.8[c]	34.0 ± 3.4[a]	48.8 ± 4.6[a,c]	47.0 ± 3.4[a,c]
BW gain (g)	0.7 ± 0.7	4.4 ± 0.8[c]	3.9 ± 1.1[c]	5.9 ± 2.9[a]	20.6 ± 3.8[a,c]	18.9 ± 3.1[a,c]
eWAT weight (mg)	509 ± 175	1084 ± 207[c]	1006 ± 284[c]	877 ± 365[a]	2310 ± 301[a,c]	1816 ± 254[a,b,c]
eWAT DNA (µg/depot)	194 ± 18	267 ± 47[c]	192 ± 30[b]	440 ± 98[a]	1313 ± 328[a,c]	1094 ± 183[a,b,c]
Adipocytes DNA (µg/depot)	n.d.	n.d.	n.d.	274 ± 67	541 ± 140[c]	445 ± 126

Mice were fed by standard (STD), high-fat diet (HFD), or a high-fat diet supplemented with n-3 PUFA (HFF) and sacrificed at Week 1 or Week 8. Initial body weight (BW), BW at dissection, BW gain, and weight of eWAT were evaluated. DNA was quantified in eWAT. Data are means ± s.d.; *n*=8 for Week 1, *n*=16–26 for Week 8. DNA content was also determined in collagenase-liberated adipocytes from eWAT at Week 8 (*n*=8). [a] Significantly different from Week 1 between mice given the same diet; [b] significantly different from the HFD group for the same period of dietary intervention; [c]significantly different from the STD group for the same period of dietary intervention; n.d., not determined.

Adipocyte size revealed an increase between Week 1 and Week 8 and partial rescue of adipocyte enlargement by HFF feeding at Week 8 (**Fig.4.3.1a-d**). As adipocytes grow, they reach their limit and die. Macrophages aggregate around dying adipocytes and form CLS. At week 1 no CLS were observed in any group. At Week 8 around 4% of CLS were in both HFD and HFF groups, almost none CLS were observed in the STD group (**Fig.4.3.1e-h**). There was no difference in the proliferation of macrophages within CLS between HFD and the HFF group at Week 8 (**Fig.4.3.1i,j**). Interestingly, only in the HFF group, MGC were detected, suggesting macrophages fusion in the HFF group (**Fig.4.3.1k**).

These results show the high remodeling of eWAT by HFD and HFF feeding. Both hypertrophy and hyperplasia were observed in both HFD and HFF groups. However, in the HFF group, n-3 supplementation partially counteracted these processes.

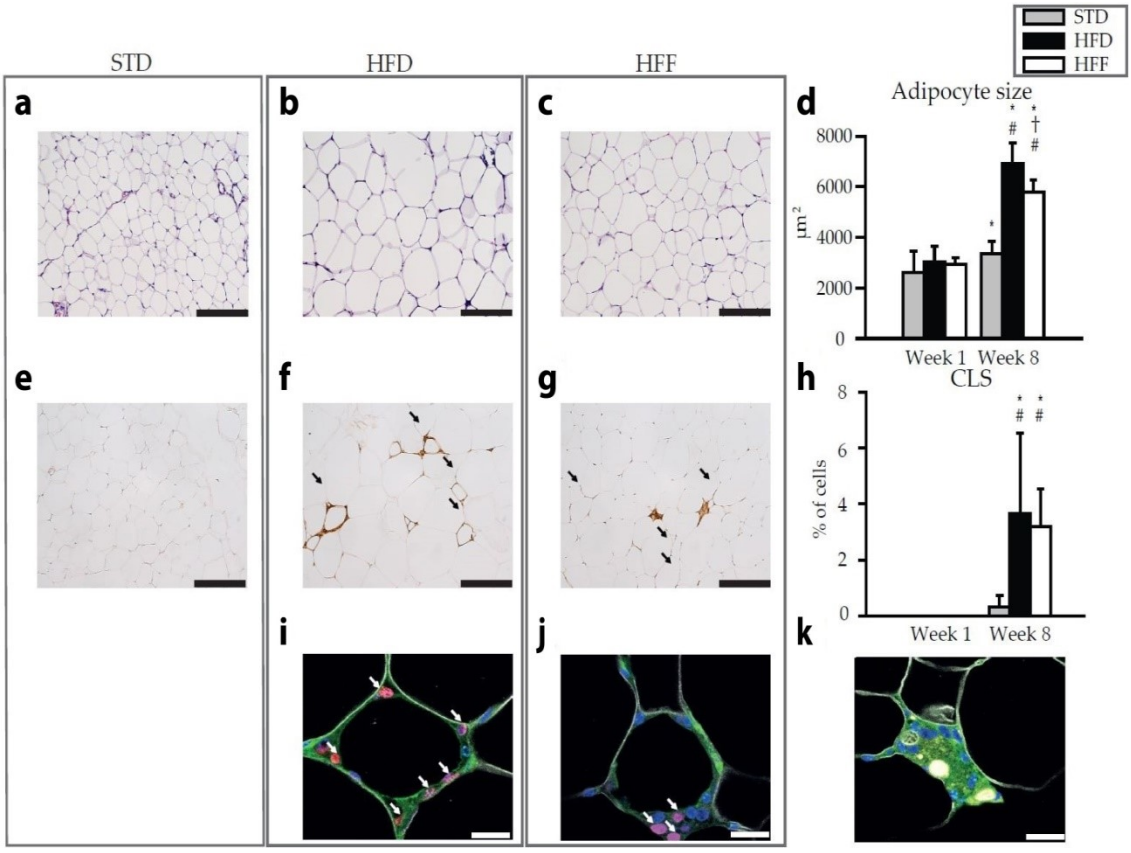

Fig. 4.3.1 Morphology and immunohistochemistry of eWAT.
Representative histological sections of eWAT from mice fed STD (**a,e**), HFD (**b,f,i**) or HFF (**c,g,j,k**) diet at Week 8. Hematoxylin and eosin staining for morphometry of adipocytes (**a,b,c**), as evaluated in (**d**). Immunohistochemical staining using macrophage marker MAC2 for quantification of CLS (**e,f,g;** arrows), as evaluated in (**h**). Representative sections showing the detection of macrophage proliferation within CLS based on immunofluorescence staining (**i**, **j**; nuclei by DAPI, blue; macrophages by anti-F4/80, green; the surface of lipid droplets by anti-perilipin 1, white; proliferating nuclei by anti-Ki67, red; proliferating macrophages are indicated with arrows). Representative section showing multinucleated giant cells (**k**). Data are means ± s.d.; *n*=6–8. *Significant difference from Week 1 between mice on the same diets; †significant difference from HFD for the same period of dietary intervention; # significant difference from STD for the same period of dietary intervention. Bar represents 200 µm (**a,b,c,e,f,g**) or 20µm (**i,j,k**).

Next, the anti-inflammatory effect of n-3 PUFA in eWAT was verified using lipidomics, and AA, ALA, DHA, EPA, LA, and DGLA metabolites were evaluated in the HFD and HFF groups at both weeks (**Tab.4.3.2**). Generally, AA-, ALA-, DGLA- and LA- metabolites were mostly increased in the HFD mice compared to HFF mice at both time points, whereas EPA-metabolites prevailed in the HFF mice at both weeks 1 and 8. To better understand these complex results PCA was performed (**Fig. 4.3.2a-c**). The more robust separation was observed at Week 8 comparing to Week 1 (**Fig. 4.3.2a,b**). Metabolites mostly explaining distribution by principal component 1 belonged to AA-hydroxyderivates, prostaglandins, thromboxane, and EPA-hydroxyderivates (**Fig. 4.3.1c**). Surprisingly, DHA metabolites did not differ between dietary groups at both time points.

Table 4.3.2 Effects of the omega-3 PUFA supplementation on lipid mediators evaluated in eWAT extracts.

		Week 1						Week 8					
		HFD			HFF			HFD			HFF		
AA-derived	11,12-DiHETrE	1.00	±	0.22	0.20	±	0.04^{b}	2.58	±	0.93	0.26	±	0.08^{b}
	14,15-DiHETrE	1.00	±	0.25	0.19	±	0.03^{b}	1.77	±	0.80	0.08	±	0.01^{b}
	5-HETE	1.00	±	0.15	0.84	±	0.09	1.48	±	0.10^{a}	0.45	±	$0.09^{a,b}$
	8-HETE	1.00	±	0.16	0.57	±	0.03^{b}	2.22	±	0.46^{a}	0.85	±	$0.14^{a,b}$
	11-HETE	1.00	±	0.18	0.56	±	0.09^{b}	2.44	±	0.47^{a}	0.93	±	$0.08^{a,b}$
	12-HETE	1.00	±	0.25	0.54	±	0.11^{b}	2.09	±	0.49	0.51	±	0.06^{b}
	15-HETE	1.00	±	0.24	0.48	±	0.09^{b}	1.58	±	0.28	0.70	±	0.14^{b}
	PGD2	1.00	±	0.17	0.70	±	0.12^{b}	5.06	±	1.20^{a}	2.69	±	$0.76^{a,b}$
	PGE2	1.00	±	0.23	0.55	±	0.08^{b}	1.53	±	0.25^{a}	1.06	±	$0.18^{a,b}$
	6-Keto-PGF1a	1.00	±	0.22	0.79	±	0.17	2.95	±	0.43^{a}	1.35	±	0.17^{b}
	11-Dh-TXB2	1.00	±	0.09	1.08	±	0.13	2.47	±	0.22^{a}	1.68	±	$0.08^{a,b}$
ALA-derived	9,10-DiHODE	1.00	±	0.19	0.50	±	0.08^{b}	0.12	±	0.02^{a}	0.08	±	$0.02^{a,b}$
	15,16-DiHODE	1.00	±	0.16	0.61	±	0.10^{b}	0.40	±	0.07^{a}	0.26	±	$0.04^{a,b}$
	9-HOTrE	1.00	±	0.16	0.70	±	0.10	0.88	±	0.12	0.95	±	0.27
	13-HOTrE	1.00	±	0.19	0.67	±	0.12^{b}	2.57	±	0.59^{a}	1.22	±	$0.42^{a,b}$
DGLA-derived	15-HETrE	1.00	±	0.22	0.65	±	0.12^{b}	2.37	±	0.51^{a}	0.78	±	$0.09^{a,b}$
DHA-derived	19,20-DiHDPA	1.00	±	0.20	1.11	±	0.17	1.28	±	0.58	0.60	±	0.07
	4-HDHA	1.00	±	0.08	1.00	±	0.12	2.57	±	0.14^{a}	2.02	±	0.23^{a}
	7-HDHA	1.00	±	0.07	0.97	±	0.11	2.18	±	0.21^{a}	1.95	±	0.20^{a}
	14-HDHA	1.00	±	0.15	1.21	±	0.30	1.01	±	0.19	1.99	±	0.49
	17-HDHA	1.00	±	0.13	1.13	±	0.26	1.14	±	0.14	1.84	±	0.38
EPA-derived	14,15-DiHETE	1.00	±	0.25	2.87	±	0.56^{b}	0.24	±	0.08^{a}	0.35	±	0.05^{a}
	17,18-DiHETE	1.00	±	0.26	2.23	±	0.45^{b}	0.16	±	0.03^{a}	0.48	±	$0.05^{a,b}$
	17,18-EpETE	1.00	±	0.26	2.80	±	0.46^{b}	0.73	±	0.18	1.20	±	0.33^{a}
	5-HEPE	1.00	±	0.21	2.13	±	0.45^{b}	0.32	±	0.08	2.01	±	0.27^{b}
	12-HEPE	1.00	±	0.18	1.78	±	0.44	0.68	±	0.20	3.44	±	0.93^{b}
	15-HEPE	1.00	±	0.15	1.62	±	0.41^{b}	1.14	±	0.49	2.63	±	0.76^{b}
	18-HEPE	1.00	±	0.22	1.96	±	0.42^{b}	0.74	±	0.15^{a}	0.92	±	$0.17^{a,b}$

LA-derived	9,10-DiHOME	1.00	±	0.22	0.56	±	0.10[b]	0.26	±	0.05[a]	0.15	±	0.02[a,b]
	12,13-DiHOME	1.00	±	0.21	0.57	±	0.09[b]	0.19	±	0.03[a]	0.13	±	0.02[a,b]
	9-HODE	1.00	±	0.17	0.60	±	0.06	1.81	±	0.18[a]	1.90	±	0.52[a]
	13-HODE	1.00	±	0.21	0.52	±	0.08[b]	1.43	±	0.30[a]	1.00	±	0.22[a,b]
	13-Oxo-ODE	1.00	±	0.20	0.51	±	0.05[b]	3.48	±	0.70[a]	2.49	±	0.55[a,b]

Abbreviations: AA, arachidonic acid; ALA, α-linolenic acid; DGLA, dihomo-γ-linolenic acid; DHA, docosahexaenoic acid; EPA, eicosapentaenoic acid; LA, linoleic acid; DiHETrE, dihydroxy-eicosatrienoic acid; HETE, hydroxy-eicosatetraenoic acid; HETrE, hydroxy-eicosatrienoic acid; PGD2, prostaglandin D2; PGE2, prostaglandin E2; PGF1a, prostaglandin 1α; Dh-TXB2, dehydro-thromboxane B2; DiHODE, dihydroxy-octadecadienoic acid; HOTrE, hydroxy-octadecatrienoic acid; DiHDPE, dihydroxy-docosapentaenoic acid; HDHA, hydroxy-docosahexaenoic acid; DiHETE, dihydroxy-eicosatetraenoic acid; EpETE, epoxy-eicosatetraenoic acid; HEPE, hydroxy-eicosapentaenoic acid; DiHOME, dihydroxy-octadecenoic acid; HODE, hydroxy-octadecadienoic acid; OxoODE, oxo-octadecadienoic acid. Data are expressed as relative values. Data are means ± s.e.m.; *n*=8-10. [a]Significant difference compared to Week 1 within the diets, [b]significant difference between the diets within the duration of the dietary intervention.

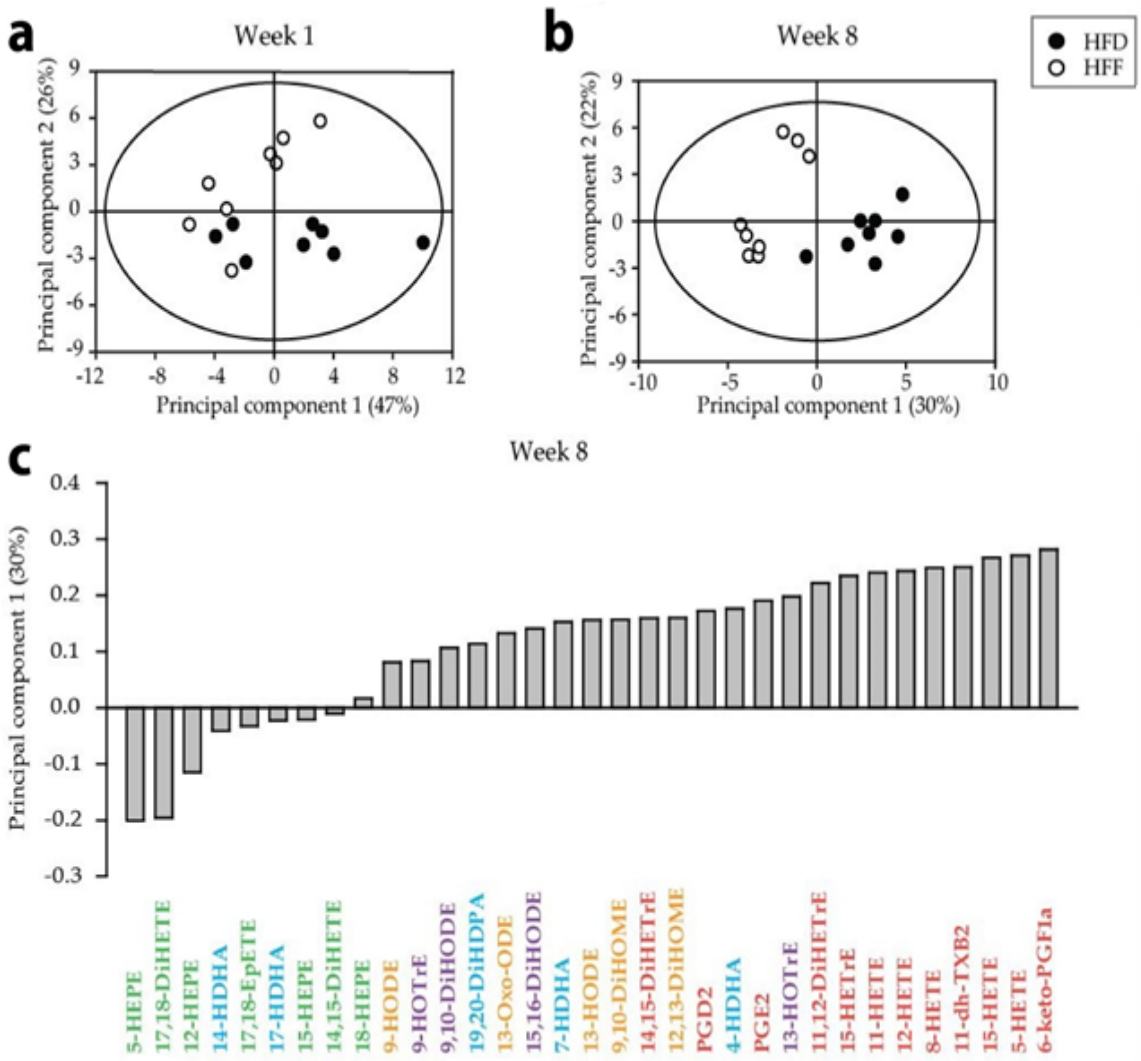

Figure 4.3.2.Principal component analysis of the lipidomic data from eWAT of the HFD and HFF mice.

Score plots of the principal components 1 and 2 were generated using the lipid mediator profiles at week 1 (**a**) and Week 8 (**b**). At Week 8 (**c**), results were expressed as a contribution score plot showing one bar per variable, indicating which species differ most between the groups and in which direction. Lipids derived from AA (red), LA (orange), ALA (purple), DHA (blue), and EPA (green) are discerned by colors. For the source data and the abbreviations, see Table 4.3.2.

As was described in Chapter 1.6.1, the main enzymes involved in the metabolism of PUFA are CYP450, COX, LOX. We focused on genes encoding LOX since mainly AA- and EPA- hydroxyderivates affected the PCA distribution. However, neither Alox5, Alox12 nor Alox15 gene expression differed between HFD and HFF mice at both Week 1 and Week 8 (**Table 4.3.3a**). Furthermore, these genes were evaluated in SVF and adipocytes fractions (see methods 3.7.1) isolated from eWAT at Week 8 and no differences were observed. Nonetheless, not only synthesis rate is important for tissue levels of lipid mediators, but also degradation rate. Gene expression of 15-hydroxyprostaglandin dehydrogenase (15-Pgdh), an enzyme responsible for the inactivation of selected prostaglandins, leukotrienes, and several hydroxy-eicosatetraenoic acid species, was decreased in both SVF and adipocytes (ADI) of HFF mice compared to HFD mice (**Table 4.3.3b**).

Table 4.3.3 Effect of the n-3 PUFA supplementation on relative mRNA levels of the genes for enzymes involved in their metabolism.

a

	Week 1		Week 8	
	HFD	**HFF**	**HFD**	**HFF**
Alox5	1.00 ± 0.21	0.90 ± 0.20	0.59 ± 0.15 [a]	0.60 ± 0.22 [a]
Alox12	1.00 ± 0.22	1.13 ± 0.52	1.82 ± 0.88 [a]	2.55 ± 0.85 [a]
Alox15	1.00 ± 0.81	0.69 ± 0.34	0.30 ± 0.16 [a]	0.45 ± 0.27 [a]
15Pgdh	1.00 ± 0.06	1.02 ± 0.06	1.34 ± 0.08 [a]	1.58 ± 0.07 [a]

B

	SVF		ADI	
	HFD	**HFF**	**HFD**	**HFF**
Alox5	1.00 ± 0.78	0.72 ± 0.27	0.11 ± 0.03	0.10 ± 0.03
Alox12	1.00 ± 0.53	1.24 ± 0.46	0.16 ± 0.08	0.26 ± 0.20
Alox15	1.00 ± 0.48	1.00 ± 0.53	0.19 ± 0.06	0.18 ± 0.03
15Pgdh	1.00 ± 0.56	0.65 ± 0.15 [b]	1.07 ± 0.23	0.80 ± 0.20 [b]

Abbreviations: *15Pgdh*, a gene for 15-hydroxyprostaglandin dehydrogenase; *Alox*, a gene for lipoxygenase. (**a**) eWAT of the HFD or HFF mice at Week 1 or Week 8. (**b**) SVF or adipocytes (ADI) isolated from eWAT of the HFD or HFF mice at Week 8. Data were normalized to the geometrical mean of two reference genes *Hprt*, *EF1a* for the whole eWAT mRNA, and *EF1a* and *Rn18s* for SVF and ADI mRNA. Data were expressed relative to those in eWAT of the HFD mice at Week 1 (**a**) or SVF of the HFD mice at Week 8 (**b**). Data are means ± s.d.; n = 8–10. [a] Significant difference compared to Week 1 for mice with the same diet, [b] significant difference between the diets for the same period of dietary intervention.
Abbreviations: Alox, arachidonate lipoxygenase; Pdgh, hydroxyprostaglandin dehydrogenase.

Based on lipidomics results, we focused on inflammatory changes in eWAT (**Fig. 4.3.3a,b**). Gene expression of Tnfα, Nos2, Ccl2, Ccr2, Arg1, and Tgfβ was compared between HFD and HFF mice. However, no changes were observed in the whole eWAT (**Fig. 4.3.3a**). Thus, all genes were evaluated also in SVF and adipocytes fractions of eWAT (**Fig. 4.3.3b**). As expected, expression of inflammatory genes Tnfα, Nos2, Tgfβ, and IL1β was decreased in SVF of HFF mice as compared to SVF of HFD mice. The expression of Ccl2 was decreased in adipocytes fraction of HFF mice. Anti-inflammatory gene Arg1 did not differ either in SVF or in adipocytes. Therefore, the higher pro-inflammatory profile of HFD mice compared to HFF mice was confirmed by qPCR.

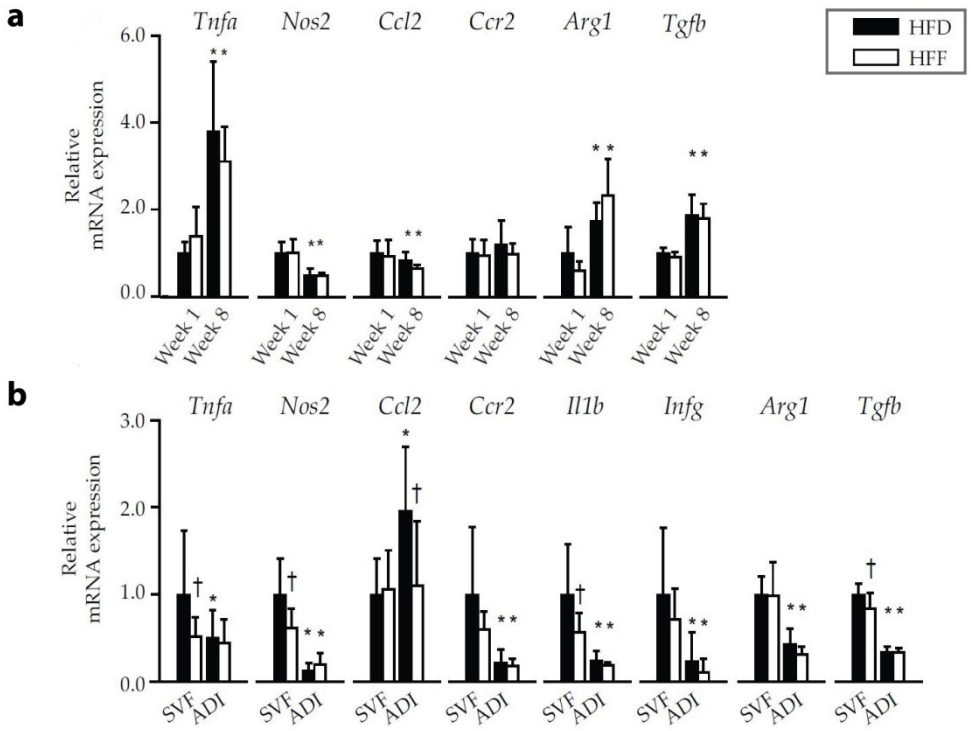

Figure 4.3.3 Gene expression of pro- and anti-inflammatory markers in eWAT or SVF and adipocytes (ADI) fractions.
Mice were fed HFD or HFF diet for 1 or 8 weeks. Gene expression in eWAT (**a**), or in SVF and ADI isolated from eWAT of mice fed the respective diets for 8 weeks (**b**) is shown. Data were normalized to the geometrical mean of two reference genes, *Hprt* and *EF1a* in (**a**), and EF1*a* and Rn18s in (**b**), and expressed relative to the HFD mice at Week 1 for whole eWAT depot (**a**) or to SVF of HFD group (Week 8) for SVF and ADI (**b**). Data are means ± s.d.; *n*=6–8. *Significant difference from Week 1 between mice with the same diet; †significant difference for the same period of dietary intervention.
Abbreviations: ADI, adipocytes; Arg1, arginase 1; Ccl2, C-C motif chemokine ligand 2; Ccr2, chemokine (C-C motif) receptor 2; Il1b, interleukin 1 beta; Infg, interferon gamma; Nos2, NO synthase 2; SVF, stromal vascular fraction; Tgfb, transforming growth factor beta; Tnfa, tumor necrosis factor a.

Consequently, we focused on the characterization of immune cells by flow cytometry in eWAT SVF (**Fig. 4.3.4g**), especially macrophages since changes in various populations of macrophages in mice fed HFD were documented. The number of leukocytes expressed per depot increased in time in the same manner in both dietary groups (**Fig. 4.3.4a**). Surprisingly, the number of macrophages did not differ between HFD and HFF mice (**Fig. 4.3.4b**). As expected it was higher in both dietary groups at Week 8 than Week 1. However, when individual subpopulations were evaluated using CD206 and CD11c markers (**Fig. 4.3.4 c-f**), a clear decrease of M1 ($CD11c^+/CD206^-$) and double-negative ($CD11c^-/CD206^-$) macrophages was observed in HFF mice as compared to HFD mice. On the other hand, double-positive macrophages ($CD11c^+/CD206^+$) were augmented in the HFF group as compared to the HFD group. M2 ($CD11c^-/CD206^+$) macrophages did not differ between dietary groups. All subtypes were increased at Week 8 in both dietary groups as compared to Week 1.

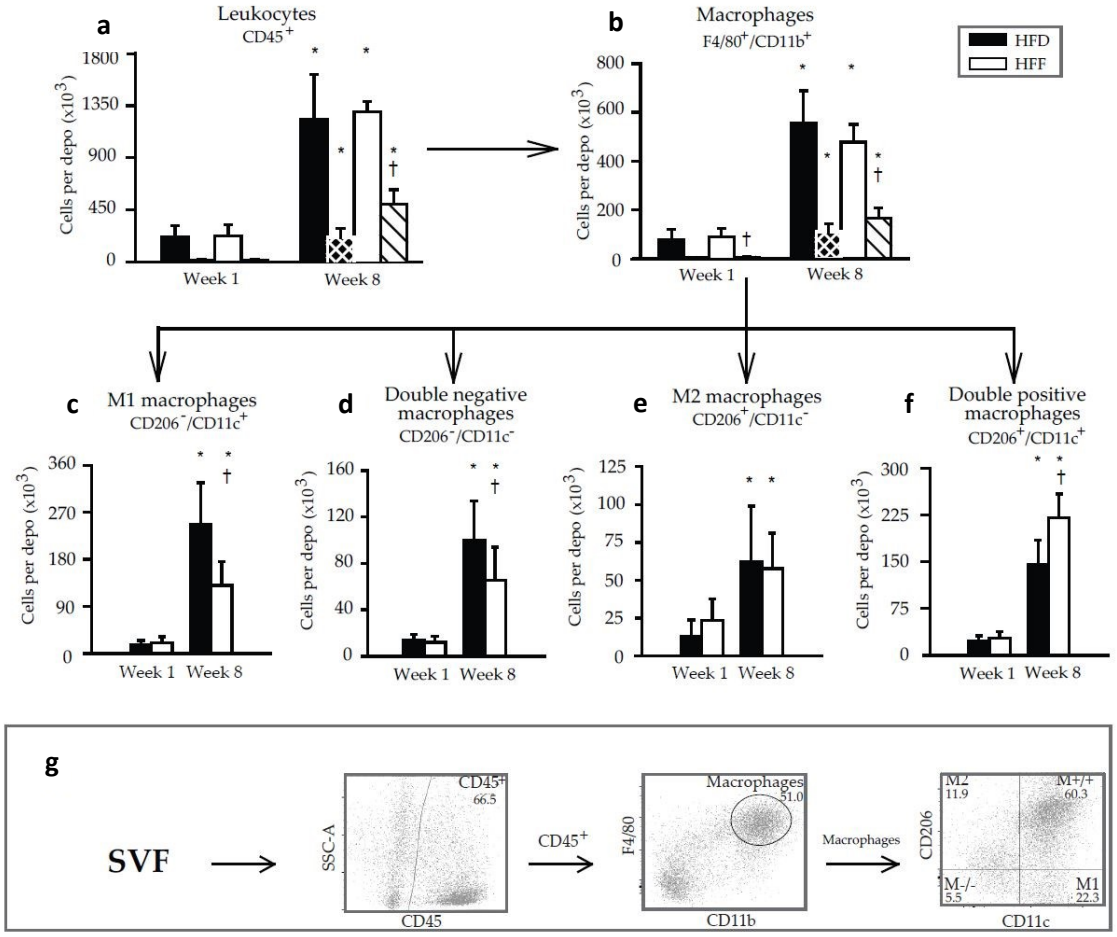

Figure 4.3.4 Flow cytometry analysis of immune cell subsets in SVF isolated from eWAT.
The numbers of cells are calculated per depot. Arrows indicate the gating strategy used. Cells were first gated on size and singularity for further analysis. Single cells were gated based on the expression of CD45 to identify leukocytes (**a**). Leukocytes were then gated on the co-expression of CD11b and F4/80 to identify macrophages (**b**). Finally, macrophages were further subdivided based on the expression of CD206 and CD11c into: M1 macrophages ($CD206^-/CD11c^+$; **c**), double-negative macrophages ($CD206^-/CD11c^-$; **d**), M2 macrophages ($CD206^+/CD11c^-$; **e**) and double-positive macrophages ($CD206^+/CD11c^+$; **f**). Striped columns (black with white stripes, HFD; white with black stripes, HFF) show the amount of proliferating cells per depot, which were detected using antibodies specific for the Ki67 proliferation marker. Illustrative flow cytometry plots and gating strategy are also shown (**g**). Data are means ± s.d.; n = 6–8. * Significant difference compared to Week 1 with the same diets; † significant difference between the diets for the same period of dietary intervention.

The ratio of M2 to M1 macrophages amount decreased in the HFD group and tended to be lower in the HFF group in Week 8 as compared to Week 1 (**Fig. 4.3.5**). Nevertheless, the M2/M1 ratio tended to be augmented in the HFF group at both Week 1 and Week 8 as compared to the HFD group and the difference between dietary groups tended to increase in time.

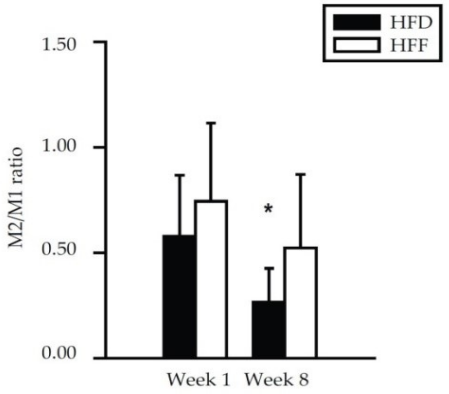

Figure 4.3.5 Ratio between M2 and M1 macrophages
M2/M1 ratio was counted from data from Fig.4.3.4 c, e. * Significant difference compared to Week 1 within the diets.

The proliferation of leukocytes and macrophages was also tested. At week 1 a very small amount of proliferating cells was found in both leukocyte (**Fig.4.3.4a**, striped bars) and macrophages (**Fig.4.3.4b**, striped bars) population in both dietary groups. On the contrary, at Week 8 around 25% of both leukocytes and macrophages were proliferating and an increase in proliferation of both populations was observed in the HFF group as compared to the HFD group.

Even though the changes in individual subsets of macrophages could be important in cellular remodeling, differences in both leukocytes and macrophages populations could not clarify the prevention of eWAT hyperplasia by n-3 PUFA quantitatively. Thus, the $CD45^-$ population was investigated in SVF of eWAT (**Fig. 4.3.6**). The amount of $CD45^-$ cells did not differ between dietary groups at Week 1, neither did their proliferation (**Fig. 4.3.6a**). Interestingly, there was a significant difference between dietary groups at Week 8. While the amount of $CD45^-$ cells in the HFD group increased almost 3 times between Week 1 and Week 8, there was no change in the number of $CD45^-$ cells in the HFF group in time, resulting in a substantially lower amount of $CD45^-$ cells in HFF group as compared to HFD group at Week 8. The percentage of proliferating cells increased in time and was higher in the HFF group comparing to the HFD group at Week 8 (**Fig.4.3.6a**, striped bars).

Furthermore, using CD45, CD31, CD34, Sca1 and CD24 markers, adipose progenitor cells ($CD45^-/CD31^-/CD34^+/Sca1^+/CD24^+$; **Fig. 4.3.6b**), preadipocytes ($CD45^-/CD31^-/CD34^+/Sca1^+/CD24^-$; **Fig.4.3.6c**), and endothelial cells ($CD45^-/CD31^+$; **Fig.4.3.6d**) were characterized. Progenitors did not change either between dietary groups or in time. The amount of proliferating cells increased between Week 1 and Week 8 and the fraction of proliferating progenitors was higher in the HFF group as compared to the HFD group in Week 8. Differences in preadipocytes and endothelial cells resembled changes in $CD45^-$ cells. There were no changes in Week 1. The amount of both preadipocytes and endtothelial cells increased in the HFD group between Week 1 and Week 8 with no changes in the HFF group in time, resulting in a larger amount of both types of cells in the HFD group as compared to the HFF group at Week 8. The

number of proliferating preadipocytes and endothelial cells increased between Week 1 and Week 8 in both dietary groups (**Fig. 4.3.6.c** and **d**, striped columns). The percentage of proliferating preadipocytes and endothelial cells was higher in the HFF group as compared to the HFD group in Week 8.

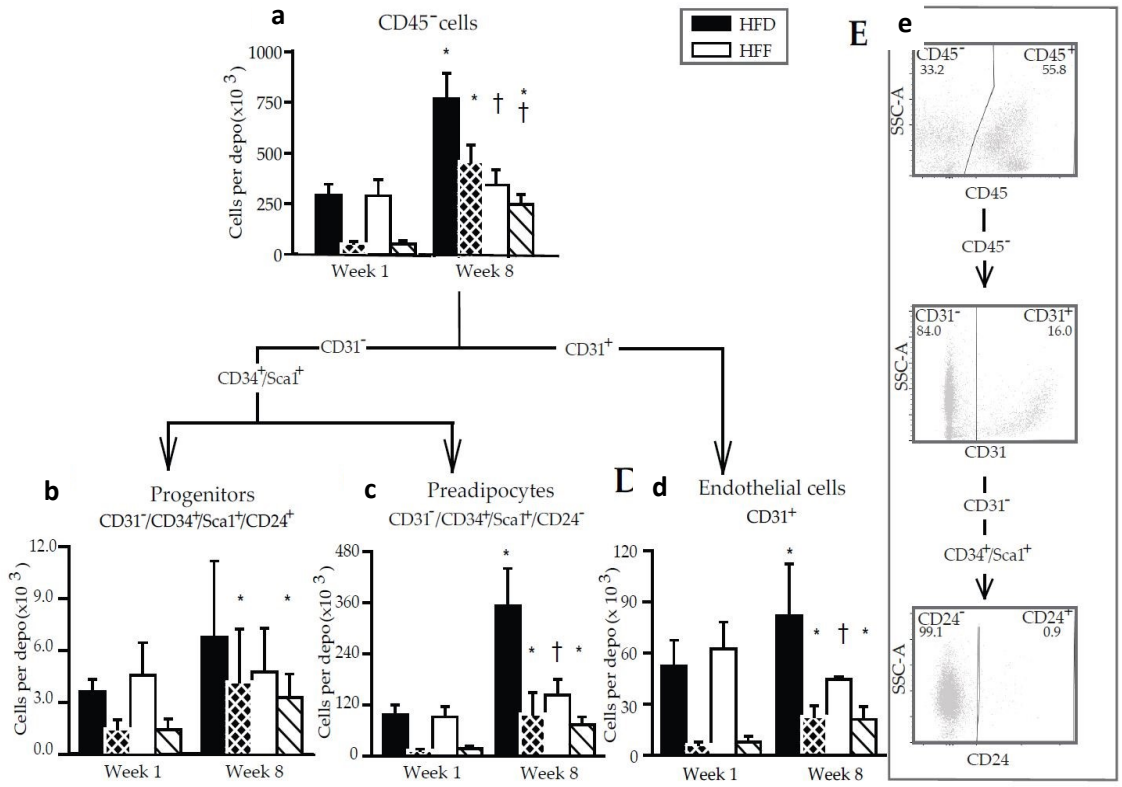

Figure 4.3.6 Flow cytometry analysis of non-immune cell subsets in SVF isolated from eWAT.
The numbers of cells are calculated per depot. Arrows indicate the gating strategy used. Cells were first gated on size and singularity for further analysis. Single cells were gated on the lack of CD45 expression to identify non-lymphoid cells (**a**). $CD45^-$cells were then gated on CD31 expression to identify endothelial cells (**d**). $CD31^-$cells were further subdivided based on the expression of Sca1, CD34 and CD24 into progenitors ($CD34^+/Sca1^+/CD24^+$; **b**) and preadipocytes ($CD34^+/Sca1^+/CD24^-$; **c**). Striped columns (black with white stripes, HFD; white with black stripes, HFF) show the amount of proliferating cells per depot, which were detected using antibodies specific for the Ki67 proliferation marker. Illustrative flow cytometry plots and gating strategy are shown in (**e**). Data are means ± s.d.; *n*=5–6. *Significant difference compared to Week 1 for mice fed the same diet; †significant difference between the diets for the same period of dietary intervention.

Pref1 gene expression (a marker of preadipocytes and adipocyte differentiation inhibitor [223]) was significantly decreased between dietary groups at Week 8 (**Table 4.3.4a**). A similar decrease in Pref1 gene expression was also observed in SVF at Week 8 ((**Table 4.3.4b**) corresponding to a drop in the number of preadipocytes in the HFF group. Moreover, Pparγ, and Cebpα gene expression were decreased in HFD and HFF in time, while gene expression of adipogenesis regulators Pdgfrα and Pdgfrβ was increased in both dietary groups between Week 1 and 8 (**Table 4.3.4a**). Gene expression of Pparγ and Pdgfrβ was decreased in SVF of HFF fed mice. There were no significant changes in expression of genes involved in adipogenesis in adipocytes (**Table 4.3.4b**).

Table 4.3.4 Effect of the omega-3 PUFA supplementation on relative gene expression enzymes involved in adipogenesis

a

	Week 1						Week 8					
	HFD			HFF			HFD			HFF		
Pparg	1.00	±	0.08	0.91	±	0.08	0.60	±	0.07[a]	0.62	±	0.05[a]
Pdgfra	1.00	±	0.08	1.20	±	0.07	1.61	±	0.23[a]	1.84	±	0.20[a]
Pdgfrb	1.00	±	0.11	1.03	±	0.15	1.95	±	0.21[a]	1.60	±	0.21[a]
Sca1	1.00	±	0.04	0.95	±	0.05	0.97	±	0.09	0.98	±	0.13
Pref1	1.00	±	0.16	0.98	±	0.17	0.65	±	0.12[a]	0.30	±	0.04[a,b]
Cebpa	1.00	±	0.06	1.04	±	0.06	0.68	±	0.06[a]	0.80	±	0.04[a]

b

	SVF						ADI					
	HFD			HFF			HFD			HFF		
Pparg	1.00	±	0.09	0.71	±	0.05[b]	2.97	±	0.24	2.32	±	0.23
Pdgfra	1.00	±	0.13	1.23	±	0.06	0.66	±	0.08	0.49	±	0.02
Pdgfrb	1.00	±	0.09	0.72	±	0.06[b]	0.06	±	0.01	0.08	±	0.02
Sca1	1.00	±	0.15	0.90	±	0.07	0.12	±	0.02	0.17	±	0.03
Pref1	1.00	±	0.19	0.41	±	0.08[b]	0.10	±	0.04	0.15	±	0.03
Cebpa	1.00	±	0.04	0.86	±	0.06	4.46	±	0.39	4.33	±	0.35

Abbreviations: Pparg, peroxisome proliferator-activated receptor γ; Pdgfra, platelet-derived growth factor receptor α; Pdgfrb, platelet-derived growth factor receptor β; Sca1, stem cells antigen-1; Pref1, preadipocyte factor 1; Cebpa, CCAAT/enhancer-binding protein α. (**a**) eWAT of mice fed HFD or HFF diet at Week 1 or Week 8. (**b**) SVF or adipocytes (ADI) isolated from eWAT of mice fed HFD or HFF diet at Week 8. Data were normalized to the geometrical mean of two reference genes *Hprt*, *EF1a* in the case of whole eWAT mRNA, and *EF1a* and *Rn18s* in the case of SVF and ADI mRNA, followed by normalization to HFD Week 1 in case of evaluation of the whole eWAT and to SVF of HFD Week 8 in SVF and ADI. Data are means ± s.d.; *n*=8-10. [a]Significant difference compared to Week 1 within the diets, [b]significant difference between the diets within the duration of the dietary intervention.

Altogether, dietary changes were observed only at Week 8, differences in time were in both dietary groups (**Fig. 4.3.7**). The immune cells, overall, did not contribute to observed changes in cell numbers by n-3 PUFA. However, individual populations of macrophages probably influenced the state of inflammation of eWAT. On the other hand, $CD45^-$ cells were more in accordance with the measurement of DNA amount, especially preadipocytes and endothelial cells. An increased percentage of proliferating $CD45^-$ cells suggests an elevated turnover of these cells. In conclusion, n-3 PUFA supplementation had an antiadipogenic effect during the development of obesity by limiting both hypertrophy and hyperplasia in eWAT.

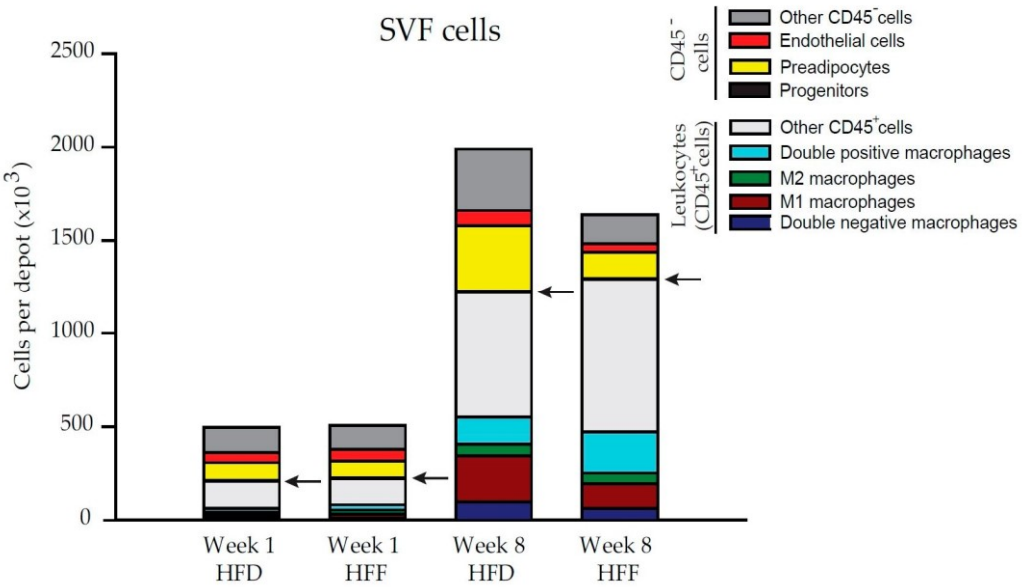

Figure 4.3.7 Flow cytometry analysis of cell subsets in SVF isolated from eWAT.
The numbers of cells are calculated per depot and re-plotted from Figures 4.3.4 and 4.3.6 data. Progenitors are indicated by arrows.

5 Discussion

5.1 Publication A

The principal finding of this publication was higher induction of futile TAG/FA cycle in eWAT of A/J mice than of B6 mice in response to CE. A/J mice were shown to differ from B6 mice in the ability to respond to HFD with i) higher FA oxidation in the liver [224, 225] and muscle [212] ii) induction of UCP1 in BAT and UCP2 in WAT [214] and iii) higher leptin levels in both plasma and WAT and prevention of glycemia and insulinemia induction [214]. We sought to find a mechanism that could contribute to explain this strain difference phenomenon via induction of stress response to CE in WAT. Activation of and/or properly functioning WAT could lead to the treatment of the metabolic syndrome.

The CE-induced decline in eWAT weight, which was more pronounced in A/J mice and was in accordance with increased requirements of energy supplies to defend body temperature in cold exposed mice. Indeed, food intake was more than doubled in cold when compared to thermoneutrality but did not differ between strains. The pronounced decrease in eWAT weight of A/J mice could be a result of higher FAox in eWAT itself and/or release of FA generated from TAG lipolysis to plasma. Indeed, CE led to the activation of ATGL, an enzyme essential for the first step of lipolysis [226] with a stronger effect in A/J mice. Interestingly, Zhou et al. showed that all FA derived from lipolysis are first secreted and then part of them is taken back via CD36 and re-esterified [82]. In addition, products of lipolysis mediated by ATGL were shown to increase oxidative capacity and FA *de novo* synthesis and re-esterification in WAT [227-229]. Another important player in energy homeostasis is AMPK. It is involved in the regulation of various metabolic pathways from lipolysis to FA synthesis [67]. The ratio of phosphorylated to AMPK protein was gradually elevated with time spent in the cold and the elevation tended to be higher in A/J mice. Thus, AMPK could contribute to more significant activation of ATGL and so lipolysis and FAox in eWAT. Indeed, genes involved in the FAox pathway were induced more in A/J mice by CE. In addition, CE-induced reduction of plasmatic FGF21 level, an upstream regulator of AMPK-SIRT1-PGC1α pathway, was smaller in A/J mice as compared to B6 mice. The reduction in plasma levels of FGF21 reflected mainly a reduction in gene expression of Fgf21 in the liver. Locally in both BAT and eWAT, Fgf21 mRNA was increased, which suggests an augmentation in the AMPK-SIRT1-PGC1α pathway in these tissues.

In accordance with Mottillo et al., CE-induced lipolysis was coupled with the induction of FA *de novo* synthesis and TAG synthesis [230] . FA synthesis started to augment on day 7 of CE. Interestingly, on day 2 of CE, a decrease in FA synthesis was observed probably due to some delay in reaction to cold-induced stress. The rate of re-esterification was increased a little after 2 days of CE and approx. 3- and 7-times after 7 days of CE in B6 and A/J mice, respectively. In addition, plasma TAG and NEFA transiently decreased on day 2 of CE but were

back to normal on day 7 of CE and the magnitude of change was more pronounced in A/J mice. This drop may be explained by cold induced-acceleration of plasma clearance of TAG as a result of increased uptake into BAT [231]. Circulating triglyceride-rich lipoproteins (TRLs) are the main source of FA for FAox in BAT and other tissues [232], see Fig.4.1.7. Increased FA and TAG synthesis in both WAT and the liver restore plasmatic levels of FA and TAG. Cold-induced lipolysis in WAT supplies the liver with NEFA, which are incorporated into VLDL-TAG in hepatocytes [233]. In addition, glycerol generated from TAG lipolysis is used for hepatic gluconeogenesis [57]. This cooperation between liver and WAT is further supported by i) our own observation of the strong negative correlation between expression of Pck1 mRNA in eWAT in cold exposed mice, ii) transient elevation of TAG content in the liver by day 2 of CE in A/J mice and Fasn gene expression in liver and iii) correlation of WAT mass and hepatic steatosis in PCK1 WAT specific KO mice [234].

In keeping with results from NMR, gene expression of Fasn and Dgat 1 and 2 was induced more in A/J mice by CE. Fasn, a multi-enzyme protein that catalyzes FA synthesis [235], was increased after 7 days of cold and it copied the course of the *de novo* FA synthesis measured by NMR. DGAT1 and DGAT2 are enzymes involved in re-esterification and each of them is thought to have a different role. DGAT1 is mostly responsible for the incorporation of FA exogenously taken up from food or products of lipolysis and protects cells from high concentrations of FA, whereas DGAT2 is believed to produce TAG from *de novo* synthesized FA [41, 236]. The model shown by Yen, et al. proposes that DGAT1 is activated the most in high FA concentration while DGAT2 works the most efficiently in low FA concentrations [41]. Indeed, Dgat1 mRNA was increased after 2 days of CE in both murine strains, while Dgat2 in A/J mice copied more Fasn gene expression and NMR outcomes with elevation after 7 days. Another important substrate for re-esterification is G3P. In most tissues, it is provided by simple phosphorylation of glycerol by GK. However, in WAT, the pathway to G3P is more complicated and the key player is enzyme PCK1 [57]. Gk mRNA was indeed present in neglected amounts in eWAT. Gene expression of Pck1 was present in amounts comparable with Dgat 1 and 2 gene expression. Surprisingly, it was not regulated by CE, only on the level of murine strain. However, it was already shown elsewhere that Pck1 activity in WAT does not respond to cold [56].

Since the liver is major site for DNL and our ^{2}H labeling method does not distinguish between eWAT and liver DNL and labeled FA in eWAT could be synthesized in the liver and then transported to eWAT, we measured essential enzymes for DNL in the liver. However, changes in gene expression of Fasn, and Dgat2 were insignificant in comparison to eWAT.

The induction of TAG synthesis in eWAT may be associated with the induction of adipogenesis by short CE. New adipocytes origin rather from increased differentiation of progenitors than from precursor proliferation. These eWAT adipocytes are UCP1-negative and small, therefore providing an additional place to store excessive lipids [120]. Indeed, we

observed small, UCP1 negative adipocytes in eWAT after cold induction. However, these small adipocytes could arise by shrinking of original large adipocytes which was supported by CE-induced ATGL and DGAT1 staining especially in areas of paucilocular cells.

Leptin is crucial for both UCP1- dependent [237, 238] and independent [239] thermogenesis in skeletal muscle and AT. Leptin plasma level corresponded to a decrease in WAT weight in A/J mice, but not in B6. Moreover, leptin is involved in a reduction of glyceroneogenesis and re-esterification via regulation of Pck1[240]. Thus, leptin may be an important metabolic signal involved in WAT metabolism, especially in A/J mice.

To summarize, we showed a link between the ability to induce TAG/NEFA cycle and lean phenotype on the model of cold exposed A/J and B6 mice, which differ in their propensity to obesity. Simultaneous activation of contradictory pathways of lipolysis and FA and TAG synthesis contributes to energy balance relatively little. However, even these small changes and proper regulation of NEFA could be important for metabolic flexibility and a healthy metabolism.

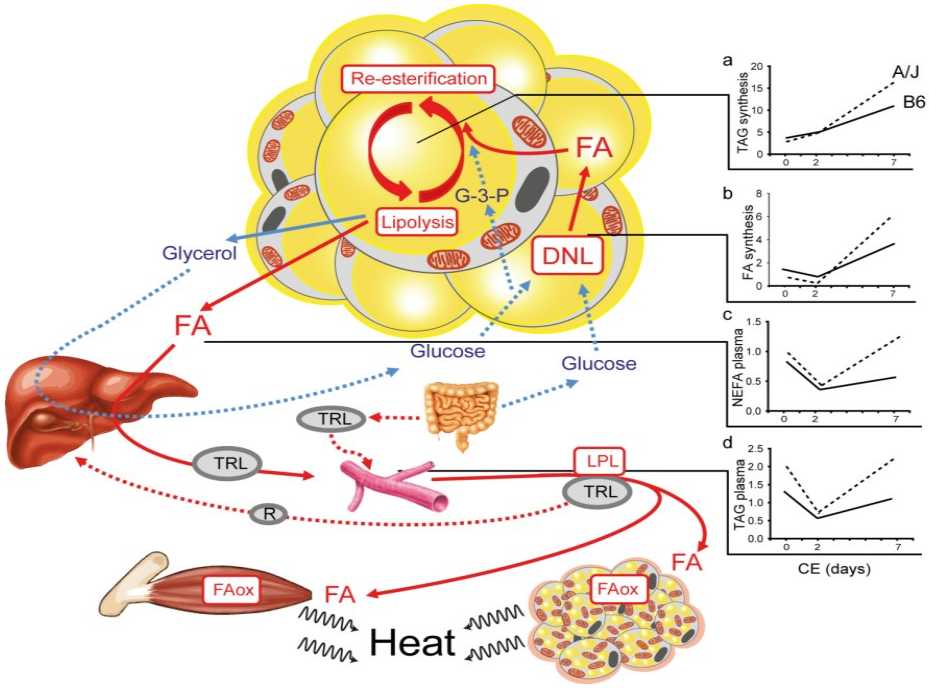

Fig.4.1.7 Interplay among the key organs involved in lipid metabolism during cold-induced thermogenesis.
The role of eWAT in the whole-body lipid metabolism is highlighted in this figure. It is based on data from Figure 4.1.1 and Table 4.1.1 (replotted in (**a-d**); continuous lines represent B6 mice, dotted lines represent A/J mice). Lipid fuels are essential for the induction of thermogenesis during cold exposure. Exogenous FA (in form of TAG) are incorporated into chylomicrons in enterocytes and released into the bloodstream. Chylomicrons from the bloodstream are captured by the liver, where are incorporated into VLDL-TAG. Endogenous FA released from WAT are also embedded into VLDL-TAG in the liver. TAG-rich lipoproteins (TRL) in circulation are then available for FAox in tissues such as BAT (fueling non-shivering thermogenesis) and skeletal muscle (fueling shivering and possibly also non-shivering thermogenesis). FA uptake in these tissues depends on the activity of LPL. Stimulation of FA release from WAT is coupled with increased FA re-esterification in WAT. Changes in WAT morphology and gene expression (see Fig. 4.1.3 and 4.1.4) as well as TAG synthesis (**a**) in eWAT were observed from the beginning of cold exposure, while endogenous FA synthesis (DNL) is initially suppressed and increases during adaptation to cold exposure (**b**). The initial drop in plasma lipid levels reflects the activation efflux of FA from WAT provided by the induction of DNL (**b**). This results in a biphasic response of NEFA levels (**c**) and TAG levels (**d**) to cold exposure in plasma. Of note, DNL is also induced by cold exposure in the liver and FA could be formed *de novo* from glucose and amino acids. For the units on the y-axis in the (**a-d**), see the source data in Figure 4.1.1 and Table 4.1.1. G-3-P, glycerol-3-phosphate; R, a remnant of TRL.

5.2 Publication B

Collectively, the results of this study indicate that i) UCP1-mediated thermogenesis in BAT cannot explain the different propensity to obesity in two mouse strains, and ii) skeletal muscle UCP1-independent thermogenesis contributes to the healthier phenotype of A/J mice. A/J mice were shown to have higher inducibility of UCP1 content when fed HFD in comparison to B6 mice, which protects them from obesity [241]. In the previous report, we identified the WAT UCP1-independent mechanism, TAG/FA cycling, contributing to a healthy phenotype. TAG/FA cycling is required for fine tuning of cold-induced lipolysis and consequent release of FA into the circulation. The aim of this study was to learn whether the strain-specific activation of WAT lipid metabolism is related to the differential induction of UCP1-mediated thermogenesis.

UCP1 was concluded as the only mediator of adrenergically induced thermogenesis in brown adipocytes. Not even high expression of its homologs, UCP2 and UCP3, were able to uncouple mitochondria in UCP1 absence. Moreover, FA were suggested to be a physiological activator of UCP1 [242]. Both Ucp1 mRNA and protein were activated by CE to similar levels in both mice strains. In agreement with these results, the measurement of BAT mitochondria function by the Oxygraph did not reveal any differences between strains in respiration using pyruvate and malate as substrates. Moreover, UCP1-dependent respiration was also similarly increased by cold in A/J and B6 mice.

The combustion capacity of glucose and lipids in activated BAT is huge comparing to other tissues [17, 243]. Although the amount of BAT is relatively small to other organs in the body, it has very high uptake of glucose per gram of tissue, leading to the conclusion of BAT being a significant glucose clearing organ. On the other hand, the quantitative role of BAT in the regulation of glycemia is probably minor [17]. Specific β3-adrenergic receptor agonist CL316,243 induced CE-activated uptake of glucose to BAT more in B6 mice than in A/J mice seemed to be UCP1-independent, which is in agreement with Olsen et al., where they showed no differences in glucose uptake to BAT after CL 316,243 stimulation between UCP1 KO and wild type mice [244]. On the other hand, Inokuma et al. observed norepinephrine stimulated induction of glucose uptake to BAT in UCP1 KO unlike in UCP1 wild type mice [245]. The essential difference in the conduction of these studies was the use of different anesthesia. In the case of Inokuma´s study pentobarbital was used, while in Olsen´s study they used isofluorane, which abolishes BAT-derived thermogenesis. Indeed, when Olsen et al. used pentobarbital, they also did not see any induction of glucose uptake to BAT in UCP1 KO mice. In our study, pentobarbital was used, and even if the UCP1 content and activity were in both strains similar, glucose uptake differed. Another explanation of this phenomenon could be higher insulinemia. Two opposite signaling pathways lead to stimulation of glucose uptake – via norepinephrine and GLUT1 during thermogenesis or via insulin and GLUT4 during anabolic processes. Indeed, B6 mice have higher insulin in plasma than A/J mice, but no induction by CE was observed [26]. In

addition, Olsen et al. described the mediation of glucose uptake via the mammalian target of rapamycin pathway [244], which could explain our differences. However, this pathway was not measured in our study.

In agreement with PET/CT results, proteomic analysis of BAT exposed more proteins involved in glycolysis, PPP, and starch metabolism induced by cold in B6 than in A/J mice. Glucose is used for replenishing the TCA cycle via pyruvate, for FA (and by extension TAG) and glycogen synthesis or processed by anaerobic glycolysis to lactate, which is transported to circulation [17, 79, 246]. Glucose may also be processed via PPP to provide nucleotides and amino acids for proliferation and differentiation of BAT induced by cold [79]. Transcriptome data from Hao et al. showed extensive regulation of glucose metabolism in B6 mice by CE [247]. Our and Hao data suggest not only induction of glucose uptake and oxidation by cold but also induced production of reducing equivalents for FA synthesis (by PPP) and glycerol synthesis from glucose for TAG synthesis/re-esterification. Even though the contribution of glucose to fuel BAT thermogenesis is only minor, it is still essential. Activation of the β3-adrenergic receptor leads to a rise in cAMP and consequently on one side activation of GLUT1 trafficking to membrane and glucose uptake and on the other hand activation of UCP1 non-shivering thermogenesis via FA release upon lipolysis [79]. Interestingly, BAT is not dependent on inner lipolysis as seen in ATGL specific KO in BAT. Thus, exogenous nutrients can fuel BAT [248]. External FA may be incorporated into TAG, activate UCP1, and/or be oxidized [246]. However, it was shown that increased oxidation of FA in BAT can consume a large number of FA and thereby inhibit uncoupled respiration in BAT [79].

Consistent data with glucose metabolism were observed when we focused on lipid metabolism in proteomics. Both FAox and lipid synthesis were induced much more in BAT of B6 mice as compared to A/J mice. Interestingly, enzymes involved in peroxisomal FAox were induced more than mitochondrial FAox enzymes by cold in both strains. Park et al. also showed increased peroxisomal oxidation in BAT by CE and that peroxisome-derived lipids regulate thermogenesis in AT via cold-induced mitochondrial fission [249]. Levels of coenzyme A, an important component of the FA activation pathway, seemed to be more regulated by cold in B6 mice. However, in A/J mice ACOT1 enzyme was already upregulated in thermogenesis. Acylcarnitines are another substrate from the plasma which can be transported to be oxidized in BAT [246]. Indeed, acylcarnitines were observed to be an essential source for BAT thermogenesis in newborn rats, which had increased CRAT as well as acylcarnitines and carnitine with a peak at day 10 after born [250]. Our proteomic analysis in BAT did not show any differences in CRAT, CPT1, or other important enzymes between strains or temperatures. However, we cannot exclude that acylcarnitines were transported to BAT via blood from other organs e.g. liver as seen in [251] where Simcox et al. showed that CE induced lipolysis in WAT activate liver HNF4α, which leads to an increased transcriptional program of Cpt1, Crat, Cpt2, and others in the liver. This results in increased production of acylcarnitines and their uptake from blood to BAT where

they fuel thermogenesis [251]. In our study, 3-OH-isovalerylcarnitine was the most upregulated acylcarnitine by cold in both strains. It origins from branched-chain amino acid leucine and the final product is acetyl-CoA, which fuels the TCA cycle. Metabolism of branched-chain amino acid was shown to be upregulated by cold in BAT. Moreover, inhibition of branched-chain amino acids metabolism led to cold intolerance in mice [252].

Interesting changes by CE were observed in the metabolism of nicotinic acid, nicotinamide, and NAD. Nicotinamide can be methylated to N-methylnicotinamide, converted to nicotinic acid, or to NAD, which can be formed also from nicotinic acid [253, 254]. It seems like both strains in cold try to prevent, via forming methylated nicotinic acid (trigonelline), high levels of nicotinic acid, which was shown to counteract β3-adrenergic signaling and thus inhibit activation of lipolysis. Nicotinamide also reduces glucose and FA uptake to BAT [79]. Moreover, B6 mice, as compared to A/J mice, had also increased methyl nicotinamide in both cold and thermoneutrality, and NAD in thermoneutrality. Increased methylnicotinamide may be a signal from skeletal muscle for BAT to induce substrate utilization [218], while increased NAD could be other prevention of forming nicotinamide and/or nicotinic acid [253, 254].

Heat production in mammals is represented by shivering and non-shivering thermogenesis. While during shivering thermogenesis, heat is produced by involuntary contractions of skeletal muscles, non-shivering thermogenesis is based on the uncoupling of ATP synthesis from OXPHOS by UCP1 in BAT [213]. Maximal heat production is thus composed of resting metabolic rate, shivering, adrenergic induced heat (mainly non-shivering thermogenesis in cold-adapted mammals), and possibly from other heat contributing pathways such as futile cycles, which include TAG/FA cycle [26], Ca^{2+} cycle [190, 255] and creatine cycle [256]. In addition, to preserve heat in non-thermoneutral conditions other mechanisms such as vasoconstriction, piloerection, and posture change serve [179]. Due to lower glucose uptake to BAT and overall poor induction of BAT metabolism in A/J mice, however, without any mark of A/J cold sensibility, we measured heat production of A/J and B6 mice. However, due to specific INCA settings of the lowest possible temperature 5°C, we could not measure cold exposed animals´ maximal heat production. Thus, only warm adapted animals were measured. Interestingly, a part of heat production, which was not induced by norepinephrine was higher in A/J mice. These results led us to search for another organ involved in thermogenesis in A/J mice by PET/CT scan of glucose uptake after cold stimulation. PET/CT showed higher glucose uptake into BAT in B6 mice as well as higher glucose uptake into skeletal muscle of A/J mice. Thus, there is a norepinephrine-independent mechanism of heat production in the skeletal muscle of A/J mice.

Interestingly, continuous Ca^{2+} recycling by the sarcoplasmic reticulum membrane that resulted in excessive muscle heat production was shown on example of a disease named malignant hyperthermia [190]. It led to the discovery of a small protein influencing metabolism in skeletal muscle, sarcolipin. Sarcolipin was shown to be a novel regulator of muscle metabolism and a potential target to modulate energy metabolism and to treat diet-induced obesity [193,

257]. Sarcolipin overexpression increases expression of mitochondrial biogenesis activators Pparδ and Pgc1α [193]. Moreover, sarcolipin induced cytosolic Ca^{2+} level leads to activation of CAMK2 and PGC1α thereby increasing mitochondrial biogenesis and oxidative metabolism [258]. Its contribution to muscle thermogenesis was shown in mice with specific deletion of sarcolipin in muscle, which after gradual exposition to cold increased Ucp1 mRNA in BAT and vice versa [195]. In addition, sarcolipin is induced in early neonatal stages and then gradually downregulated, which can be prevented by exposure to cold [197]. Indeed, our results supported sarcolipin as a protein important for muscle thermogenesis, especially in A/J mice. SERCA2, and CAMK2 protein levels and Serca2 and sarcolipin gene expression were observed to be higher in A/J mice. However, some authors doubt sarcolipin and SERCA role in meaningful thermogenesis [259]. Butler et al. shown that sarcolipin expression in skeletal muscle is very low and that its overexpression does not prevent diet-induced obesity [260]. Also, it was suggested that Ca^{2+} cycling in muscle is activated via norepinephrine, which does not correspond to our data. Thus, this topic has to be further studied. However, the role of sarcolipin in energy expenditure in the skeletal muscle of A/J mice seems to be crucial.

Regarding substrate support of muscle metabolism, A/J mice oxidized mainly FA as documented by higher carnitine as well as acetylcarnitine levels in gastrocnemius muscle. Also, PC oxidation was more induced in A/J than B6 mice by cold and COX activity and COX7A2L protein level were higher in A/J mice. The long isoform of COX protein was already shown to be upregulated in A/J mice in comparison to B6 [261]. In addition, pantothenic acid, a precursor for coenzyme A, was upregulated in A/J mice in both conditions, suggesting increased activation of FA in A/J mice. In contrast, B6 mice had higher levels of carnitine precursor in muscle in comparison to A/J mice. However, together with lower carnitine and acetylcarnitine levels, it seems that FAox in the muscle of B6 mice is not that sufficient and that acylcarnitines accumulate in mitochondria rather than being processed. It is consistent with higher Ucp3 mRNA content in B6 skeletal muscle and UCP3 role in skeletal muscle. UCP3 attenuates mitochondrial production of free radicals and protects against oxidative damage thanks to the activation of UCP3 by ROS and by-products of lipid peroxidation. In addition, UCP3 transports excessive FA out of mitochondria protecting it from the toxic effects of FA anions and peroxides [262, 263]. Thus, these results suggest, that B6 mice have a slower turnover of FA in skeletal muscle than A/J mice and rather protect themselves by increased UCP3 against oxidative damage.

Interestingly, the most upregulated enzyme in proteomic analysis of skeletal muscle was fructose bisphosphate aldolase. It was more than 200-times higher in B6 mice than in A/J mice in thermoneutrality. This enzyme is involved in glycolysis and/or gluconeogenesis. Also, other enzymes (STable 4.2.2 in appendix) such as UDP-glucose pyrophosphorylase, phosphorylase kinase subunit beta, phosphoglycerate kinase 1, phosphoglucomutase-1, etc. were increased in B6 mice in thermoneutrality and some of them also in cold more than in A/J mice. Shivering initially relies mainly on glycogen in muscles as a substrate for thermogenesis, but it was shown

that carbohydrate oxidation decreased and lipid oxidation was elevated after 12 hours of CE in humans [264]. So it seems that B6 mice are dependent on glucose/glycogen as substrate and already in thermoneutrality has upregulated carbohydrate metabolism, which leads to the suggestion that muscles of B6 mice are better prepared for shivering. Due to the difficulty of the measurement and its following evaluation, the shivering thermogenesis was not assessed in our experiments.

To conclude, B6 mice have a higher metabolic rate in BAT, however, it does not protect them against diet-induced obesity. In contrast, A/J mice rely more on thermogenesis in the muscle which could be connected to their healthier phenotype together with increased TAG/FA cycling in WAT [26] and some not yet discovered pathways.

5.3 Publication C

The principal finding of this study was that non-immune $CD45^-$ cells, mainly preadipocytes and endothelial cells are limited in the HFF group as compared to the HFD group after 8 weeks of feeding. This study confirmed previous results of Ruzickova et al. showing the contribution of n-3 PUFA in counteracting HFD-caused hyperplasia and hypertrophy [175]. The main goal of this study was to unravel how n-3 PUFA restrict the increase in fat caused by HFD and therefore contribute to healthy adipocyte.

The new concept documenting a close connection between tissue metabolism and immune cells activity, called immunometabolism has emerged last years [139, 265, 266]. The results of this study confirm this view. We showed that EPA- and DHA- derived lipid mediators and WAT cytokines influence the polarization of macrophages and are involved in diet-induced hypertrophy and hyperplasia prevention. Especially, induction of anti-inflammatory 5-, 12- and 15-HEPE and 17,18- diHETE and decrease in pro-inflammatory 5-,8- and 15- HETE were observed. Immune cells together with adipocytes contributed to setting balance on the pro-resolving side by reduced expression of pro-inflammatory Nos2, Tnfα, Tgfβ, IL1β, and Ccl2 genes. The expression of genes involved in lipid mediators formation did not differ between HFD and HFF groups either on the level of whole tissue or in separated SVF and adipocytes. However, EPA, DHA, and AA compete for these enzymes, so the regulation may be just on the level of the availability of the substrate. Degradation enzyme 15-Pgdh was lower in the HFF group as compared with the HFD group in both adipocytes and SVF.

Immune cells, adipocytes, and other cells in AT produce many active substances like adipokines, interleukins, and chemokines. Leukocytes per depot did not differ between HFD and HFF group, which can be explained by changed amounts of both pro-inflammatory and anti-inflammatory immune cells, leading to the same leukocytes levels in both dietary groups. Macrophages are the most discussed immune cells in AT when studying obesity [133]. Their numbers increased around 6 times after 8 weeks of both HFD and HFF diets. Macrophages were distinguished into four groups based on CD206 and CD11c antigens. M1 macrophages in-

creased in time in the HFD group and this increase was partly prevented in the HFF group which was in agreement with other results of this study. Double positive cells (mixed M1/M2 macrophages) that are involved in the resolution of inflammation [267], were increased in HFF as compared to the HFD group. It was shown that mixed M1/M2 macrophages have activated catabolism of lipids, which is associated with the anti-inflammatory phenotype of macrophages. MGC that are formed by the fusion of double-positive or M2 macrophages [268], were observed only in the HFF group at Week 8 by immunohistochemistry. MGC are involved in remodelation and repair [269] by an increased capacity to generate ROS [268]. To our surprise, anti-inflammatory M2 macrophages did not differ between HFF and HFD groups. However, the number of M2 macrophages is in a lean state extremely high and the change by HFD is more pronounced in M1 macrophages [157] and in the ratio of M2/M1 macrophages. The ratio of M2/M1 was decreased in time in HFD and at Week 8 tended to be higher in the HFF group.

Hyperplasia of WAT involves the proliferation of immune and adipocyte progenitor cells and the following differentiation into preadipocytes. Immune cells content was extremely increased in response to HFD feeding, showed by both immunohistochemistry of CLS and flow cytometry measurement of leukocytes/macrophages. One of the limitations of this study was that only macrophages were measured from various immune cells such as T cells, B cells, neutrophils, and others. The leukocyte population ($CD45^+$ cells) did not differ between HFD and HFF groups which means that overall $CD45^+$ cells did not contribute to the limitation of hyperplasia seen in the HFF group in terms of their quantity. However, they could qualitatively contribute to the reduction of inflammation or influence the proliferation of progenitors and other cells. In addition, both no change in macrophages content [206, 270-273] and the reduction of macrophages [206, 274-277] in response to n-3 PUFA was reported by others. This discrepancy is probably a result of different doses and/or forms of n-3 PUFA. The amount of non-immune $CD45^-$ cells was increased in response to HFD feeding as expected, and limited in the HFF group as compared to HFD. Mostly, preadipocytes and endothelial cells reflected the restriction in $CD45^-$ population by n-3 PUFA.

As was already suggested interaction/communication between immune and adipose lineage cells is crucial for healthy adipose tissue. Indeed, macrophages-derived products 15-Lox, 9- and 13- HODE are involved in the non-inflammatory removal of dying adipocytes. 15-Lox is required for efferocytosis of apoptotic adipocytes by macrophages and its KO leads to the impaired remodeling of AT [278]. Moreover, M2 macrophages contribute to the inhibition of growth and differentiation of adipocyte progenitors, which leads to controlled adiposity and systemic insulin sensitivity [135]. Furthermore, prostanoids regulating angiogenesis, e.g. prostaglandin E2, which augments angiogenesis [279], was reduced in the HFF group as compared to HFD and could contribute to a reduction in endothelial cells. In addition, 12- HETE, a product of 12/15 Lox, which is associated with interactions between monocytes and endothel, was reduced in the HFF group [280].

Interestingly, the proliferation of non-immune cells, measured by flow cytometry using the Ki67 marker, was increased in Week 8 as compared to Week 1 in both HFD and HFF groups. Moreover, a higher percentage of proliferating progenitors, preadipocytes, and endothelial cells was observed in the HFF group than in HFD in Week 8. This is in strong contrast with numbers of preadipocytes and endothelial cells and it leads to a theory about the involvement of apoptosis or necrosis. Indeed, n-3 PUFA supplementation was described as an inducer of apoptosis in WAT, previously [121, 281, 282]. Unfortunately, quantification of apoptosis in AT was in our study too challenging and no results were obtained so far. However, decreased levels of 5- and 12- HETE, negative mediators of apoptosis regulation, in the HFF group, indicate the involvement of n-3 PUFA in apoptosis. In addition, these two lipid mediators were one of the most discriminating analytes between HFF and HFD groups with a lower amount of both mediators in eWAT of the HFF group.

In conclusion, this study showed the involvement of n-3 PUFA in the remodeling of WAT in mice fed HFD. Even though immune cells numbers were not changed by n-3 PUFA supplementation, the polarization of macrophages, many bioactive compounds produced by immune cells influenced immune and adipose lineage cells balance and contributed to remodeling of AT. Adipose lineage cells, primarily preadipocytes and endothelial cells, are the key players in the prevention of diet-induced WAT hyperplasia by n-3 PUFA. These results promote the idea, that adiposity is linked with the control of fat cell turnover and that the turnover control could be independent of energy balance [283, 284].

6 Summary

In conclusion, this PhD thesis shows that:

1) CE-induced lipolysis led to the mobilization of lipid stores in all AT depots. This reduction was more pronounced in A/J mice. It was compensated by increased food intake, however, there was no difference between strains and no sign of cold intolerance in A/J mice. Consequently, CE induced re-esterification and DNL in order to avoid lipotoxicity of FA. A/J mice responded with higher flexibility to cold-induced stress than B6 mice. TAG/FA futile cycle contributes to energy expenditure relatively little. However, even these small changes and proper regulation of NEFA could be important for metabolic flexibility and a healthy metabolism.

2) A higher metabolic rate in BAT was not linked with the healthy phenotype of A/J mice, which rather relied on thermogenesis in muscle. Both Ucp1 mRNA and protein were induced by CE similarly in BAT of A/J and B6 mice, which corresponded to the functional test of BAT mitochondria by Oxygraph. However, both glucose uptake (measured by PET/CT) and proteomics in BAT revealed higher glucose utilization of B6 mice in comparison to A/J mice. On the contrary, glucose uptake was shown to be higher in muscle in A/J mice in comparison to B6 by PET/CT measurement. Also, lipid metabolism was induced in muscle more in A/J than in B6 mice. In addition, Ca^{2+} cycling, measured on mRNA and protein levels of involved enzymes was increased in A/J mice. These results support the idea, that muscle thermogenesis is the link with the healthy phenotype of A/J mice.

3) HFD supplemented by n-3 PUFA prevented WAT hyperplasia by reducing the number of preadipocytes and endothelial cells. Interestingly, a higher proliferation of these cells was shown suggesting increased turnover of preadipocytes and endothelial cells. Immune cells were not affected by n-3 PUFA quantitatively. However, the HFD-induced-decrease in M2/M1 macrophages ratio was prevented by n-3 PUFA. Moreover, the polarization of macrophages, many bioactive compounds produced by immune cells influenced immune and adipose lineage cells balance and contributed to the remodeling of AT. In conclusion, n-3 PUFA supplementation limits both hypertrophy and hyperplasia in eWAT during obesity development.

7 Abbreviations

AA	arachidonic acid
ACAD	acyl-CoA dehydrogenase
ACC	acetyl-CoA carboxylase
acetyl-CoA	acetyl-coenzyme A
ACLY	ATP citrate lyase
ACS	acyl-CoA synthase
acyl-CoA	acyl-coenzyme A
AGPAT	acylglycerol-3-phosphate acyltransferase phosphatidate phosphatase
A/J	A/JOlaHsd (murine strain)
ALA	α-linolenic acid
AMPK	AMP-activated kinase
ANG	angiopoietin
AP2	adipocyte protein 2, also known as FABP4
Apo	apolipoprotein
ARG	arginase
AT	adipose tissue
ATGL	adipose triglyceride lipase
ATP	adenosine triphosphate
B6	C57BL/6J (murine strain)
B6/N	C57BL/6N (murine strain)
BAT	brown adipose tissue
BCA	bicinchoninic acid assay
B cells	B lymphocytes
BMP	bone morphogenic protein
BSA	bovine serum albumin
CEBP	CCAAT-enhancer-binding protein
CAMK2	Ca^{2+} /calmodulin-dependent protein kinase 2
cAMP	cyclic adenosine monophosphate
CCL	CC chemokine ligand
CCR	CC chemokine receptor
CD36	fatty acid translocase
CE	cold exposure
CGI-58	comparative gene identification-58, also known as ABHD5
CLS	crown-like structure
COX	cyclooxygenase
CPT	carnitine palmitoyl transferase
CRAT	carnitine O-acetyltransferase
CREBP	cAMP response element-binding protein
CXCL	CXC chemokine ligand
CYP450	cytochrome P450 oxygenase
DAG	diacylglycerol
DC	dendritic cells
DGAT	diacylglycerol acyltransferase
DGLA	dihomo-γ-linolenic acid
DHA	docosahexaenoic acid

DHET	dihydroxyeicosatrienoic acid
DHPR	dihydropyridine receptor
DNA	deoxyribonucleic acid
DNL	*de novo* lipogenesis
EDTA	ethylenediaminetetraacetic acid
EET	epoxyeicosatrienoic acid
ELOVL	elongase
EPA	eicosapentaenoic acid
ER	endoplasmatic reticulum
eWAT	epididymal white adipose tissue
FA	fatty acid(s)
FABP	fatty acid binding protein
FAD	flavin adenine dinucleotide
FAox	fatty acid oxidation
FASN	fatty acid synthase
FATP	fatty acid transport protein
FDG	fluorodeoxyglucose
FGF21	fibroblast growing factor 21
G3P	glycerol-3-phosphate
GK	glycerol kinase
GLA	gamma-Linolenic acid
GLUT	glucose transporter
GPAT	glycerol-3-phosphate acyl transferase
HDOHE	hydroxydocosahexaenoic acid
HEPE	hydroxyeicosapentaenoic acid
HETE	hydroxyeicosatetraenoic acid
HFD	high-fat diet
HFF	high-fat diet supplemented with n-3 PUFA
HIF	hypoxia-inducible factor
HPmax	maximal heat production
HPrest	resting heat production
HSL	hormone sensitive lipase
ChREBP	carbohydrate responsive element-binding protein
IFNγ	interferon γ
IL	interleukin
ILC	innate lymphoid cells
INCA	indirect calorimetry
iNKT	invariant natur killer T cells
IPHYS	Institute of Physiology
IRE	insulin response element
ISO	isoproterenol
KLB	klotho beta
KRB	Krebs ringer buffer
LA	linoleic acid
LCAD	long-chain ACAD
LOX	lipooxygenase
LPL	lipoprotein lipase
LY6C	lymphocyte antigen 6 complex

MAG	monoacylglycerol
MCAD	medium-chain ACAD
MCP1	monocyte chemotactic protein 1
MGC	multinucleated giant cells
MGL	monoglyceride lipase
MHC II	class II major histocompatibility complex
MIP	macrophage inflammatory protein
MR	metabolic rate
MYF	myogenic factor
NAD	nicotinamide adenine dinucleotide
NADP	nicotinamide adenine dinucleotide phosphate
NEFA	non-esterified fatty acids
NK	natur killer cells
NKT	natur killer T-cells
NMR	nuclear magnetic resonance
NOS	nitric oxide synthase
OXPHOS	oxidative phosphorylation
pAMPK	phosphorylated form of AMPK
PC	palmitoyl carnitine
PCA	principal component analysis
PDGF	platelet derived growth factor
PDGFR	platelet-derived growth factor receptor
PEP	phosphoenolpyruvate
PCK	phosphoenolpyruvate carboxykinase
PCK1	phosphoenolpyruvate carboxykinase cytosolic form
PET/CT	positron emission tomography/computed tomography
PG	prostaglandin
PGC1	PPARγ coactivator 1
PI3K	phosphoinositide 3-kinase
PKA	protein kinase A
PKB	protein kinase B, Akt
PKC	protein kinase C
PLSDA	partial least squares-discriminant analysis
PPAR	peroxisome proliferator-activated receptor
PPP	pentosephosphate pathway
PRDM16	PR domain containing 16
PUFA	polyunsaturated fatty acids
qPCR	quantitative polymerase chain reaction
ROS	reactive oxygen species
RYR	ryanodine receptor
SBACAD	and short/branched-chain acyl-CoA dehydrogenase
SCA	stem cell antigen
SCAD	short-chain ACAD
SCD	stearoyl-CoA desaturase
SERCA	sarco/endoplasmic reticulum Ca^{2+} ATPase
SMAD	mother against-decapentaplegic homolog
SR	sarcoplasmic reticulum
SREBP	sterol regulatory element-binding protein

STD	standard chow diet
SVF	stromal vascular fraction
TAG	triacylglycerol(s)
T cells	T lymphocytes
TCA	tricarboxylic acid
TGF	transforming growth factor
TH	T helper cells
TLR	toll-like receptor
TNF	tumor necrosis factor
TREGS	T regulatory cells
TZD	thiazolidinediones
TX	thromboxanes
UCP1	uncoupling protein 1
VEGF	vascular endothelial growth factor
VIP	variable importance in projection
VLCAD	very long-chain ACAD
VLCFA	very long-chain fatty acid
VLDL	very low-density lipoprotein
WAT	white adipose tissue
ZFP	zinc finger protein chimera

8 List of publications used for thesis

Publication A:

Flachs P*, **Adamcova K***, Zouhar P, Janovska P, Bardova K, Svobodova M, Hansikova J, Kuda O, Rossmeisl M, Kopecky J. Induction of lipogenesis in white fat during cold exposure in mice: link to lean phenotype. *International Journal Obesity*. 2017; 41: 372–380. IF=4.36 (2020)

* These authors contributed equally to this work.

My personal contribution to this publication includes participation in the analysis of plasma markers, evaluation of NMR data, quantitative PCR analysis of gene expression, statistical analysis, and participation in writing a manuscript.

Publication B:

Publication under preparation

Janovska P, Bardova K, Vrbacky P, **Adamcova K**, Lenkova L, Funda J. Drahota Z, Rossmeisl M, Zouhar P, Kopecky J. Strain-specific involvement of brown fat and muscle in cold-induced thermogenesis in mice: link to lean phenotype.

My personal contribution to this publication includes supervision over animal experiments, quantitative PCR analysis of gene expression, analysis of plasma markers, Oxygraph measurement, and evaluation of both BAT and gastrocnemius muscle, statistical analysis, participation in both creations of figures, and writing a draft of a manuscript.

Publication C:

Adamcova K*, Horakova O*, Bardova K*, Janovska P, Brezinova M, Kuda O, Rossmeisl M, Kopecky J. Reduced Number of Adipose Lineage and Endothelial Cells in Epididymal fat in Response to Omega-3 PUFA in Mice Fed High-Fat Diet. *Marine Drugs.* 2018; 16 (12*)*: 515-534. IF=3.81 (2020)

* These authors contributed equally to this work.

My personal contribution to this publication includes supervision over the animal experiments, quantitative PCR analysis of gene expression, isolation of adipocytes and SVF, preparation of SVF cells for flow cytometry measurement, flow cytometry measurement and evaluation, principal component analysis of lipidomics data, statistical analysis, creation of figures and writing a draft of a manuscript.

9 References

1. Zwick, R.K., et al., *Anatomical, Physiological, and Functional Diversity of Adipose Tissue.* Cell Metab, 2018. **27**(1): p. 68-83.
2. obesity, W. 9.9.2020]; Available from: https://www.who.int/en/news-room/fact-sheets/detail/obesity-and-overweight.
3. diabetes, W. 9.9.2020]; Available from: https://www.who.int/news-room/fact-sheets/detail/diabetes.
4. Trayhurn, P., *Origins and early development of the concept that brown adipose tissue thermogenesis is linked to energy balance and obesity.* Biochimie, 2017. **134**: p. 62-70.
5. Bluher, M., *Metabolically Healthy Obesity.* Endocr Rev, 2020. **41**(3).
6. promocell. 9.9.2020]; Available from: https://www.promocell.com/f/2019/11/Adipose_Tissue.jpg.
7. Cinti, S., *The adipose organ*. 1999, Milano, Italy: Editrice Kurtis.
8. Zhang, Y., et al., *Positional cloning of the mouse obese gene and its human homologue.* Nature, 1994. **372**(6505): p. 425-432.
9. Zhou, Y.T., et al., *Induction by leptin of uncoupling protein-2 and enzymes of fatty acid oxidation.* Proceedings of the National Academy of Sciences U.S.A., 1997. **94**(12): p. 6386-6390.
10. Turer, A.T. and P.E. Scherer, *Adiponectin: mechanistic insights and clinical implications.* Diabetologia, 2012. **55**(9): p. 2319-2326.
11. Luo, L. and M. Liu, *Adipose tissue in control of metabolism.* J Endocrinol, 2016. **231**(3): p. R77-R99.
12. Wu, C.H., et al., *Truncal fat in relation to total body fat: influences of age, sex, ethnicity and fatness.* Int J Obes (Lond), 2007. **31**(9): p. 1384-91.
13. Wronska, A. and Z. Kmiec, *Structural and biochemical characteristics of various white adipose tissue depots.* Acta Physiol (Oxf), 2012. **205**(2): p. 194-208.
14. Chusyd, D.E., et al., *Relationships between Rodent White Adipose Fat Pads and Human White Adipose Fat Depots.* Front Nutr, 2016. **3**: p. 10.
15. Choe, S.S., et al., *Adipose Tissue Remodeling: its Role in energy Metabolism and Metabolic Disorders.* Frontiers in Endocrinology, 2016. **7**.
16. van der Lans, A.A., et al., *Cold acclimation recruits human brown fat and increases nonshivering thermogenesis.* J Clin Invest, 2013. **123**(8): p. 3395-403.
17. Cannon, B. and J. Nedergaard, *Brown adipose tissue: function and physiological significance.* Physiol Rev, 2004. **84**(1): p. 277-359.
18. Sanchez-Gurmaches, J., C.M. Hung, and D.A. Guertin, *Emerging Complexities in Adipocyte Origins and Identity.* Trends in Cell Biology, 2016. **26**(5): p. 313-326.
19. Carobbio, S., B. Rosen, and A. Vidal-Puig, *Adipogenesis: new insights into brown adipose tissue differentiation.* J Mol Endocrinol, 2013. **51**(3): p. T75-85.
20. Kotzbeck, P., et al., *Brown adipose tissue whitening leads to brown adipocyte death and adipose tissue inflammation.* J Lipid Res, 2018. **59**(5): p. 784-794.
21. Cypess, A.M. and C.R. Kahn, *Brown fat as a therapy for obesity and diabetes.* Current Opinion in Endocrinology Diabetes and Obesity, 2010. **17**(2): p. 143-149.
22. Trayhurn, P., *Brown Adipose Tissue-A Therapeutic Target in Obesity?* Front Physiol, 2018. **9**: p. 1672.
23. Trayhurn, P., *Recruiting Brown Adipose Tissue in Human Obesity.* Diabetes, 2016. **65**(5): p. 1158-60.
24. Carey, A.L. and B.A. Kingwell, *Brown adipose tissue in humans: therapeutic potential to combat obesity.* Pharmacol Ther, 2013. **140**(1): p. 26-33.
25. Flachs, P., et al., *Stimulation of mitochondrial oxidative capacity in white fat independent of UCP1: A key to lean phenotype.* Biochim.Biophys.Acta, 2013. **1831**(5): p. 986-1003.

26. Flachs, P., et al., *Induction of lipogenesis in white fat during cold exposure in mice: link to lean phenotype.* Int J Obes (Lond), 2017. **41**(3): p. 372-380.
27. Voet, D. and J.G. Voetova *Biochemie2*. 1994, Praha: Victoria Publishing.
28. Kopecky, J., *Mitochondrial uncoupling and lipid metabolism in adipocytes.* 674th Meeting of the Biochemical Society, Dublin, 2001. **29**(Pt 6): p. 791-7.
29. Wang, T., et al., *Metabolic partitioning of endogenous fatty acid in adipocytes.* Obes.Res., 2003. **11**(7): p. 880-887.
30. Gonzales, A.M. and R.A. Orlando, *Role of adipocyte-derived lipoprotein lipase in adipocyte hypertrophy.* Nutrition & Metabolism, 2007. **4**.
31. Frayn, K.N., P. Arner, and H. Yki-Jarvinen, *Fatty acid metabolism in adipose tissue, muscle and liver in health and disease.* Essays in Biochemistry, Vol 42, 2006. **42**: p. 89-103.
32. Wu, Q.W., et al., *FATP1 is an insulin-sensitive fatty acid transporter involved in diet-induced obesity.* Molecular and Cellular Biology, 2006. **26**(9): p. 3455-3467.
33. Furuhashi, M. and G.S. Hotamisligil, *Fatty acid-binding proteins: role in metabolic diseases and potential as drug targets.* Nature Reviews Drug Discovery, 2008. **7**(6): p. 489-503.
34. Coleman, R.A., T.M. Lewin, and D.M. Muoio, *Physiological and nutritional regulation of enzymes of triacylglycerol synthesis.* Annual Review of Nutrition, 2000. **20**: p. 77-103.
35. Bell, R.M. and R.A. Coleman, *Enzymes of Glycerolipid Synthesis in Eukaryotes.* Annual Review of Biochemistry, 1980. **49**: p. 459-487.
36. Coleman, R.A. and D.P. Lee, *Enzymes of triacylglycerol synthesis and their regulation.* Progress in Lipid Research, 2004. **43**(2): p. 134-176.
37. Su, H.S., et al., *Regulation of the fatty acid synthase promoter by insulin.* Journal of Nutrition, 2000. **130**(2): p. 315s-320s.
38. Eberhardt, C., P.W. Gray, and L.W. Tjoelker, *Human lysophosphatidic acid acyltransferase - cDNA cloning, expression, and localization to chromosome 9q34.3.* Journal of Biological Chemistry, 1997. **272**(32): p. 20299-20305.
39. Shi, Y.G. and D. Cheng, *Beyond triglyceride synthesis: the dynamic functional roles of MGAT and DGAT enzymes in energy metabolism.* American Journal of Physiology-Endocrinology and Metabolism, 2009. **297**(1): p. E10-E18.
40. Wendel, A.A., T.M. Lewin, and R.A. Coleman, *Glycerol-3-phosphate acyltransferases: rate limiting enzymes of triacylglycerol biosynthesis.* Biochim Biophys Acta, 2009. **1791**(6): p. 501-6.
41. Yen, C.L., et al., *Thematic review series: glycerolipids. DGAT enzymes and triacylglycerol biosynthesis.* J Lipid Res, 2008. **49**(11): p. 2283-301.
42. Chen, H.C., et al., *Increased insulin and leptin sensitivity in mice lacking acyl CoA : diacylglycerol acyltransferase 1.* Journal of Clinical Investigation, 2002. **109**(8): p. 1049-1055.
43. Chascione, C., et al., *Effect of carbohydrate intake on de novo lipogenesis in human adipose tissue.* American Journal of Physiology, 1987. **253**(6 Pt 1): p. E664-E669.
44. Swierczynski, J., et al., *Comparative study of the lipogenic potential of human and rat adipose tissue.* Metabolism, 2000. **49**(5): p. 594-599.
45. Rohrig, F. and A. Schulze, *The multifaceted roles of fatty acid synthesis in cancer.* Nat Rev Cancer, 2016. **16**(11): p. 732-749.
46. Park, H., et al., *Coordinate regulation of malonyl-CoA decarboxylase, sn-glycerol-3-phosphate acyltransferase, and acetyl-CoA carboxylase by AMP-activated protein kinase in rat tissues in response to exercise1.* J Biol.Chem., 2002. **277**(36): p. 32571-32577.
47. Schreurs, M., F. Kuipers, and F.R. van der Leij, *Regulatory enzymes of mitochondrial beta-oxidation as targets for treatment of the metabolic syndrome.* Obes Rev, 2010. **11**(5): p. 380-8.
48. Czech, M.P., et al., *Insulin signalling mechanisms for triacylglycerol storage.*

Diabetologia, 2013. **56**(5): p. 949-64.
49. Fernandez, S., et al., *Adipocyte ACLY Facilitates Dietary Carbohydrate Handling to Maintain Metabolic Homeostasis in Females.* Cell Rep, 2019. **27**(9): p. 2772-2784 e6.
50. Dragos, S.M., et al., *Reduced SCD1 activity alters markers of fatty acid reesterification, glyceroneogenesis, and lipolysis in murine white adipose tissue and 3T3-L1 adipocytes.* Am J Physiol Cell Physiol, 2017. **313**(3): p. C295-C304.
51. Jakobsson, A., R. Westerberg, and A. Jacobsson, *Fatty acid elongases in mammals: Their regulation and roles in metabolism.* Progress in Lipid Research, 2006. **45**(3): p. 237-249.
52. Nugteren, D.H., *Enzymic Chain Elongation of Fatty Acids by Rat-Liver Microsomes.* Biochimica Et Biophysica Acta, 1965. **106**(2): p. 280-&.
53. Westerberg, R., et al., *ELOVL3 is an important component for early onset of lipid recruitment in brown adipose tissue.* Journal of Biological Chemistry, 2006. **281**(8): p. 4958-4968.
54. Tan, C.Y., et al., *Brown Adipose Tissue Thermogenic Capacity Is Regulated by Elovl6.* Cell Reports, 2015. **13**(10): p. 2039-2047.
55. Franckhauser, S., et al., *Increased fatty acid re-esterification by PEPCK overexpression in adipose tissue leads to obesity without insulin resistance.* Diabetes, 2002. **51**(3): p. 624-630.
56. Feldman, D. and M. Hirst, *Glucocorticoids and regulation of phosphoenolpyruvate carboxykinase activity in rat brown adipose tissue.* Am J Physiol, 1978. **235**(2): p. E197-202.
57. Reshef, L., et al., *Glyceroneogenesis and the triglyceride/fatty acid cycle.* Journal of Biological Chemistry, 2003. **278**(33): p. 30413-30416.
58. Sztalryd, C. and D.L. Brasaemle, *The perilipin family of lipid droplet proteins: Gatekeepers of intracellular lipolysis.* Biochimica Et Biophysica Acta-Molecular and Cell Biology of Lipids, 2017. **1862**(10): p. 1221-1232.
59. Duncan, R.E., et al., *Regulation of lipolysis in adipocytes.* Annual Review of Nutrition, 2007. **27**: p. 79-101.
60. Zechner, R., et al., *Adipose triglyceride lipase and the lipolytic catabolism of cellular fat stores.* J Lipid Res, 2009. **50**(1): p. 3-21.
61. Zechner, R., et al., *FAT SIGNALS--lipases and lipolysis in lipid metabolism and signaling.* Cell Metab, 2012. **15**(3): p. 279-91.
62. Yeaman, S.J., *Hormone-sensitive lipase - New roles for an old enzyme.* Biochemical Journal, 2004. **379**: p. 11-22.
63. Carey, G.B., *Mechanisms regulating adipocyte lipolysis73.* Adv.Exp.Med.Biol., 1998. **441**: p. 157-170.
64. Shanske, S., et al., *Widespread tissue distribution of mitochondrial DNA deletions in Kearns-Sayre syndrome.* Neurology, 1990. **40**(1): p. 24-8.
65. Grevengoed, T.J., E.L. Klett, and R.A. Coleman, *Acyl-CoA Metabolism and Partitioning.* Annual Review of Nutrition, Vol 34, 2014. **34**: p. 1-30.
66. Wakil, S.J. and L.A. Abu-Elheiga, *Fatty acid metabolism: target for metabolic syndrome.* J Lipid Res, 2009. **50 Suppl**: p. S138-43.
67. Hardie, D.G., *Keeping the home fires burning: AMP-activated protein kinase.* J R Soc Interface, 2018. **15**(138).
68. Gaidhu, M.P., et al., *Prolonged AICAR-induced AMP-kinase activation promotes energy dissipation in white adipocytes: novel mechanisms integrating HSL and ATGL.* Journal of Lipid Research, 2009. **50**(4): p. 704-715.
69. Izai, K., et al., *Novel Fatty-Acid Beta-Oxidation Enzymes in Rat-Liver Mitochondria .1. Purification and Properties of Very-Long-Chain Acyl-Coenzyme-a Dehydrogenase.* Journal of Biological Chemistry, 1992. **267**(2): p. 1027-1033.
70. Ikeda, Y., K. Okamura-Ikeda, and K. Tanaka, *Purification and characterization of short-chain, medium-chain, and long-chain acyl-CoA dehydrogenases from rat liver*

mitochondria. Isolation of the holo- and apoenzymes and conversion of the apoenzyme to the holoenzyme. J Biol Chem, 1985. **260**(2): p. 1311-25.
71. Andersson, U., J. Houstek, and B. Cannon, *ATP synthase subunit c expression: physiological regulation of the P1 and P2 genes.* Biochemical Journal, 1997. **323**: p. 379-385.
72. Houstek, J., et al., *The expression of subnit c correlates with and thus may limit the boisynthesis of the mitochondrial F0 F1-ATPase in brown adipose tissue.* Journal of Biological Chemistry, 1995. **270**: p. 7689-7694.
73. Jezek, P., et al., *Fatty acid cycling mechanism and mitochondrial uncoupling proteins.* Biochim Biophys Acta, 1998. **1365**(1-2): p. 319-27.
74. Rothwell, N.J. and M.J. Stock, *A role for brown adipose tissue in diet-induced thermogenesis.* Nature, 1979. **281**(5726): p. 31-5.
75. Himms-Hagen, J. and M.E. Harper, *Physiological role of UCP3 may be export of fatty acids from mitochondria when fatty acid oxidation predominates: an hypothesis1*. Exp.Biol.Med.(Maywood.), 2001. **226**(2): p. 78-84.
76. Carneheim, C., J. Nedergaard, and B. Cannon, *Beta-adrenergic stimulation of lipoprotein lipase in rat brown adipose tissue during acclimation to cold.* American Journal of Physiology, 1984. **246**(4 Pt 1): p. E327-E333.
77. Shibata, H., et al., *Cold exposure reverses inhibitory effects of fasting on peripheral glucose uptake in rats.* American Journal of Physiology, 1989. **257**(1 Pt 2): p. R96-R101.
78. Stanford, K.I., et al., *Brown adipose tissue regulates glucose homeostasis and insulin sensitivity.* Journal of Clinical Investigation, 2013. **123**(1): p. 215-223.
79. Hankir, M.K. and M. Klingenspor, *Brown adipocyte glucose metabolism: a heated subject.* EMBO Rep, 2018. **19**(9).
80. Stincone, A., et al., *The return of metabolism: biochemistry and physiology of the pentose phosphate pathway.* Biol Rev Camb Philos Soc, 2015. **90**(3): p. 927-63.
81. Leibel, R.L., et al., *Alterations in adipocyte free fatty acid re-esterification associated with obesity and weight reduction in man.* Am J Clin Nutr, 1985. **42**(2): p. 198-206.
82. Zhou, D., et al., *CD36 level and trafficking are determinants of lipolysis in adipocytes.* FASEB Journal, 2012. **26**(11): p. 4733-4742.
83. Chitraju, C., et al., *Triglyceride Synthesis by DGAT1 Protects Adipocytes from Lipid-Induced ER Stress during Lipolysis.* Cell Metab, 2017. **26**(2): p. 407-418 e3.
84. Morrison, S.F. and C.J. Madden, *Central nervous system regulation of brown adipose tissue.* Compr Physiol, 2014. **4**(4): p. 1677-713.
85. Kersten, S., *Mechanisms of nutritional and hormonal regulation of lipogenesis4.* EMBO Rep., 2001. **21**(41): p. 282-286.
86. Daval, M., F. Foufelle, and P. Ferre, *Functions of AMP-activated protein kinase in adipose tissue.* J Physiol, 2006. **574**(Pt 1): p. 55-62.
87. Kadenbach, B., *Intrinsic and extrinsic uncoupling of oxidative phosphorylation.* Biochimica Et Biophysica Acta-Bioenergetics, 2003. **1604**(2): p. 77-94.
88. Daval, M., et al., *Anti-lipolytic action of AMP-activated protein kinase in rodent adipocytes.* J Biol.Chem., 2005. **280**(26): p. 25250-25257.
89. Djouder, N., et al., *PKA phosphorylates and inactivates AMPKalpha to promote efficient lipolysis.* EMBO Journal, 2010. **29**(2): p. 469-481.
90. Rossmeisl, M., et al., *Role of energy charge and AMP-activated protein kinase in adipocytes in the control of body fat stores.* Int J Obes Relat Metab Disord, 2004. **28 Suppl 4**: p. S38-44.
91. Wu, L., et al., *AMP-Activated Protein Kinase (AMPK) Regulates Energy Metabolism through Modulating Thermogenesis in Adipose Tissue.* Front Physiol, 2018. **9**: p. 122.
92. Desjardins, E.M. and G.R. Steinberg, *Emerging Role of AMPK in Brown and Beige Adipose Tissue (BAT): Implications for Obesity, Insulin Resistance, and Type 2 Diabetes.* Curr Diab Rep, 2018. **18**(10): p. 80.
93. Tyagi, S., et al., *The peroxisome proliferator-activated receptor: A family of nuclear*

receptors role in various diseases. J Adv Pharm Technol Res, 2011. **2**(4): p. 236-40.
94. Goto, T., et al., *Activation of peroxisome proliferator-activated receptor-alpha stimulates both differentiation and fatty acid oxidation in adipocytes.* J Lipid Res, 2011. **52**(5): p. 873-84.
95. Corrales, P., A. Vidal-Puig, and G. Medina-Gomez, *PPARs and Metabolic Disorders Associated with Challenged Adipose Tissue Plasticity.* Int J Mol Sci, 2018. **19**(7).
96. van Raalte, D.H., et al., *Peroxisome proliferator-activated receptor (PPAR)-alpha: a pharmacological target with a promising future.* Pharm Res, 2004. **21**(9): p. 1531-8.
97. Rosen, E.D. and B.M. Spiegelman, *PPARgamma : a nuclear regulator of metabolism, differentiation, and cell growth.* J Biol Chem, 2001. **276**(41): p. 37731-4.
98. Ferre, P., *The biology of peroxisome proliferator-activated receptors: relationship with lipid metabolism and insulin sensitivity.* Diabetes, 2004. **53 Suppl 1**: p. S43-50.
99. Choi, S.S., J. Park, and J.H. Choi, *Revisiting PPARgamma as a target for the treatment of metabolic disorders.* BMB Rep, 2014. **47**(11): p. 599-608.
100. Nedergaard, J., et al., *PPAR gamma in the control of brown adipocyte differentiation.* Biochimica Et Biophysica Acta-Molecular Basis of Disease, 2005. **1740**(2): p. 293-304.
101. Villena, J.A., *New insights into PGC-1 coactivators: redefining their role in the regulation of mitochondrial function and beyond.* FEBS J, 2015. **282**(4): p. 647-72.
102. Liu, C. and J.D.D. Lin, *PGC-1 coactivators in the control of energy metabolism.* Acta Biochimica Et Biophysica Sinica, 2011. **43**(4): p. 248-257.
103. Uldry, M., et al., *Complementary action of the PGC-1 coactivators in mitochondrial biogenesis and brown fat differentiation.* Cell Metabolism, 2006. **3**(5): p. 333-341.
104. Eberle, D., et al., *SREBP transcription factors: master regulators of lipid homeostasis.* Biochimie, 2004. **86**(11): p. 839-848.
105. Shimano, H., *SREBPs: physiology and pathophysiology of the SREBP family.* FEBS J, 2009. **276**(3): p. 616-21.
106. Horton, J.D., et al., *Overexpression of sterol regulatory element-binding protein-1a in mouse adipose tissue produces adipocyte hypertrophy, increased fatty acid secretion, and fatty liver.* Journal of Biological Chemistry, 2003. **278**(38): p. 36652-36660.
107. Iizuka, K., *Recent progress on the role of ChREBP in glucose and lipid metabolism.* Endocr J, 2013. **60**(5): p. 543-55.
108. Tang, Y., et al., *Adipose tissue mTORC2 regulates ChREBP-driven de novo lipogenesis and hepatic glucose metabolism.* Nat Commun, 2016. **7**: p. 11365.
109. Filhoulaud, G., et al., *Novel insights into ChREBP regulation and function.* Trends in Endocrinology and Metabolism, 2013. **24**(5): p. 257-268.
110. Song, Z., A.M. Xiaoli, and F. Yang, *Regulation and Metabolic Significance of De Novo Lipogenesis in Adipose Tissues.* Nutrients, 2018. **10**(10).
111. Ghaben, A.L. and P.E. Scherer, *Adipogenesis and metabolic health.* Nat Rev Mol Cell Biol, 2019.
112. Ali, A.T., et al., *Adipocyte and adipogenesis.* Eur J Cell Biol, 2013. **92**(6-7): p. 229-36.
113. MacDougald, O.A. and S. Mandrup, *Adipogenesis: forces that tip the scales.* Trends Endocrinol Metab, 2002. **13**(1): p. 5-11.
114. Feve, B., *Adipogenesis: cellular and molecular aspects.* Best Pract Res Clin Endocrinol Metab, 2005. **19**(4): p. 483-99.
115. Tang, Q.Q. and M.D. Lane, *Adipogenesis: from stem cell to adipocyte.* Annu Rev Biochem, 2012. **81**: p. 715-36.
116. Sanchez-Gurmaches, J., et al., *PTEN loss in the Myf5 lineage redistributes body fat and reveals subsets of white adipocytes that arise from Myf5 precursors.* Cell Metab, 2012. **16**(3): p. 348-62.
117. Wu, J., et al., *Beige adipocytes are a distinct type of thermogenic fat cell in mouse and human.* Cell, 2012. **150**(2): p. 366-376.
118. Langin, D., *Recruitment of brown fat and conversion of white into brown adipocytes: Strategies to fight the metabolic complications of obesity?* Biochimica et Biophysica

Acta, 2010. **1801**(3): p. 372-376.
119. Lee, Y.H., et al., *In vivo identification of bipotential adipocyte progenitors recruited by beta3-adrenoceptor activation and high-fat feeding.* Cell Metab, 2012. **15**(4): p. 480-491.
120. Wang, Q.A., et al., *Tracking adipogenesis during white adipose tissue development, expansion and regeneration.* Nat Med, 2013. **19**(10): p. 1338-44.
121. Kim, H.K., et al., *Docosahexaenoic acid inhibits adipocyte differentiation and induces apoptosis in 3T3-L1 preadipocytes.* J Nutr, 2006. **136**(12): p. 2965-9.
122. Fukumura, D., et al., *Paracrine regulation of angiogenesis and adipocyte differentiation during in vivo adipogenesis.* Circ Res, 2003. **93**(9): p. e88-97.
123. Hausman, G.J. and R.L. Richardson, *Adipose tissue angiogenesis.* J Anim Sci, 2004. **82**(3): p. 925-34.
124. Cao, Y., *Angiogenesis modulates adipogenesis and obesity.* J Clin Invest, 2007. **117**(9): p. 2362-8.
125. Jia, G., L.A. Martinez-Lemus, and J.R. Sowers, *Interaction of Adipogenesis and Angiogenesis in Dietary-Induced Obesity.* Diabetes, 2015. **64**(7): p. 2326-8.
126. Lijnen, H.R., *Angiogenesis and obesity.* Cardiovascular Research, 2008. **78**(2): p. 286-293.
127. Le Lay, S., N. Briand, and I. Dugail, *Adipocyte size fluctuation, mechano-active lipid droplets and caveolae.* Adipocyte, 2015. **4**(2): p. 158-60.
128. Thomas, D. and C. Apovian, *Macrophage functions in lean and obese adipose tissue.* Metabolism, 2017. **72**: p. 120-143.
129. Catrysse, L. and G. van Loo, *Adipose tissue macrophages and their polarization in health and obesity.* Cell Immunol, 2018. **330**: p. 114-119.
130. Amano, S.U., et al., *Local proliferation of macrophages contributes to obesity-associated adipose tissue inflammation.* Cell Metab, 2014. **19**(1): p. 162-71.
131. Surmi, B.K. and A.H. Hasty, *Macrophage infiltration into adipose tissue: initiation, propagation and remodeling.* Future Lipidology, 2008. **3**(5): p. 545-556.
132. Chen, C.Y., C.W. Su, and J.X. Kang, *Endogenous Omega-3 Polyunsaturated Fatty Acids Reduce the Number and Differentiation of White Adipocyte Progenitors in Mice.* Obesity (Silver Spring), 2020. **28**(2): p. 235-240.
133. Kohlgruber, A.C., N.M. LaMarche, and L. Lynch, *Adipose tissue at the nexus of systemic and cellular immunometabolism.* Semin Immunol, 2016. **28**(5): p. 431-440.
134. Lolmede, K., et al., *Immune cells in adipose tissue: key players in metabolic disorders.* Diabetes Metab, 2011. **37**(4): p. 283-90.
135. Nawaz, A., et al., *CD206(+) M2-like macrophages regulate systemic glucose metabolism by inhibiting proliferation of adipocyte progenitors.* Nat Commun, 2017. **8**(1): p. 286.
136. Waki, H. and P. Tontonoz, *Endocrine functions of adipose tissue.* Annu Rev Pathol, 2007. **2**: p. 31-56.
137. Schipper, H.S., et al., *Adipose tissue-resident immune cells: key players in immunometabolism.* Trends Endocrinol.Metab, 2012. **23**(8): p. 407-415.
138. Ferrante, A.W., Jr., *The immune cells in adipose tissue.* Diabetes Obes Metab, 2013. **15 Suppl 3**: p. 34-8.
139. Man, K., V.I. Kutyavin, and A. Chawla, *Tissue Immunometabolism: Development, Physiology, and Pathobiology.* Cell Metab, 2017. **25**(1): p. 11-26.
140. De Souza, C.T., et al., *Consumption of a fat-rich diet activates a proinflammatory response and induces insulin resistance in the hypothalamus.* Endocrinology, 2005. **146**(10): p. 4192-9.
141. Berger, A., *Th1 and Th2 responses: what are they?* BMJ, 2000. **321**(7258): p. 424.
142. Wang, Q. and H. Wu, *T Cells in Adipose Tissue: Critical Players in Immunometabolism.* Front Immunol, 2018. **9**: p. 2509.
143. Shiau, M.Y., et al., *Mechanism of Interleukin-4 Reducing Lipid Deposit by Regulating Hormone-Sensitive Lipase.* Sci Rep, 2019. **9**(1): p. 11974.

144. Rozenberg, P., et al., *CD300f:IL-5 cross-talk inhibits adipose tissue eosinophil homing and subsequent IL-4 production.* Sci Rep, 2017. **7**(1): p. 5922.
145. Mantovani, A., et al., *Macrophage plasticity and polarization in tissue repair and remodelling.* J Pathol, 2013. **229**(2): p. 176-85.
146. Duffen, J., et al., *Modulation of the IL-33/IL-13 Axis in Obesity by IL-13Ralpha2.* J Immunol, 2018. **200**(4): p. 1347-1359.
147. Saraiva, M. and A. O'Garra, *The regulation of IL-10 production by immune cells.* Nat Rev Immunol, 2010. **10**(3): p. 170-81.
148. Zhang, H., et al., *Interferon-gamma induced adipose tissue inflammation is linked to endothelial dysfunction in type 2 diabetic mice.* Basic Res Cardiol, 2011. **106**(6): p. 1135-45.
149. Chudek, J. and A. Wiecek, *Adipose tissue, inflammation and endothelial dysfunction.* Pharmacol Rep, 2006. **58 Suppl**: p. 81-8.
150. Braune, J., et al., *IL-6 Regulates M2 Polarization and Local Proliferation of Adipose Tissue Macrophages in Obesity.* J Immunol, 2017. **198**(7): p. 2927-2934.
151. Kuryszko, J., P. Slawuta, and G. Sapikowski, *Secretory function of adipose tissue.* Pol J Vet Sci, 2016. **19**(2): p. 441-6.
152. Villarroya, F., et al., *Inflammation of brown/beige adipose tissues in obesity and metabolic disease.* J Intern Med, 2018. **284**(5): p. 492-504.
153. Xu, L., et al., *Roles of Chemokines and Chemokine Receptors in Obesity-Associated Insulin Resistance and Nonalcoholic Fatty Liver Disease.* Biomolecules, 2015. **5**(3): p. 1563-79.
154. Zhou, H., et al., *In vivo simultaneous transcriptional activation of multiple genes in the brain using CRISPR-dCas9-activator transgenic mice.* Nat Neurosci, 2018. **21**(3): p. 440-446.
155. Alberts, B., et al., *Molecular Biology of the Cell, Sixth Edition.* Molecular Biology of the Cell, Sixth Edition, 2015: p. 1-1342.
156. Van Kaer, L., V.V. Parekh, and L. Wu, *Invariant natural killer T cells: bridging innate and adaptive immunity.* Cell Tissue Res, 2011. **343**(1): p. 43-55.
157. Fujisaka, S., et al., *M2 macrophages in metabolism.* Diabetol Int, 2016. **7**(4): p. 342-351.
158. Verdeguer, F. and M. Aouadi, *Macrophage heterogeneity and energy metabolism.* Exp Cell Res, 2017. **360**(1): p. 35-40.
159. Morris, D.L., K. Singer, and C.N. Lumeng, *Adipose tissue macrophages: phenotypic plasticity and diversity in lean and obese states.* Curr Opin Clin Nutr Metab Care, 2011. **14**(4): p. 341-6.
160. Milde, R., et al., *Multinucleated Giant Cells Are Specialized for Complement-Mediated Phagocytosis and Large Target Destruction.* Cell Rep, 2015. **13**(9): p. 1937-48.
161. Dittmar, T. and K.S. Zanker, *Cell fusion in health and disease. Volume II: cell fusion in disease. Introduction.* Adv Exp Med Biol, 2011. **714**: p. 1-3.
162. Zeyda, M. and T.M. Stulnig, *Adipose tissue macrophages.* Immunol.Lett., 2007. **112**(2): p. 61-67.
163. Biswas, S.K. and A. Mantovani, *Macrophage plasticity and interaction with lymphocyte subsets: cancer as a paradigm.* Nat Immunol, 2010. **11**(10): p. 889-96.
164. Van den Bossche, J., L.A. O'Neill, and D. Menon, *Macrophage Immunometabolism: Where Are We (Going)?* Trends Immunol, 2017. **38**(6): p. 395-406.
165. Diskin, C. and E.M. Palsson-McDermott, *Metabolic Modulation in Macrophage Effector Function.* Front Immunol, 2018. **9**: p. 270.
166. Kane, H. and L. Lynch, *Innate Immune Control of Adipose Tissue Homeostasis.* Trends Immunol, 2019. **40**(9): p. 857-872.
167. Chung, K.J., et al., *Innate immune cells in the adipose tissue.* Rev Endocr Metab Disord, 2018. **19**(4): p. 283-292.
168. Wouters, K., et al., *Circulating classical monocytes are associated with CD11c(+) macrophages in human visceral adipose tissue.* Sci Rep, 2017. **7**: p. 42665.

169. Pancer, Z. and M.D. Cooper, *The evolution of adaptive immunity.* Annu Rev Immunol, 2006. **24**: p. 497-518.
170. Masoodi, M., et al., *Lipid signaling in adipose tissue: Connecting inflammation & metabolism.* Biochim Biophys Acta, 2015. **1851**(4): p. 503-518.
171. Pahlavani, M., et al., *Adipose tissue inflammation in insulin resistance: review of mechanisms mediating anti-inflammatory effects of omega-3 polyunsaturated fatty acids.* J Investig Med, 2017. **65**(7): p. 1021-1027.
172. Bird, J.K., P.C. Calder, and M. Eggersdorfer, *The Role of n-3 Long Chain Polyunsaturated Fatty Acids in Cardiovascular Disease Prevention, and Interactions with Statins.* Nutrients, 2018. **10**(6).
173. Kuda, O., et al., *Cell type-specific modulation of lipid mediator's formation in murine adipose tissue by omega-3 fatty acids.* Biochem Biophys Res Commun, 2016. **469**(3): p. 731-6.
174. da Cunha de Sa, R.D.C., et al., *Fish oil reverses metabolic syndrome, adipocyte dysfunction, and altered adipokines secretion triggered by high-fat diet-induced obesity.* Physiol Rep, 2020. **8**(4): p. e14380.
175. Ruzickova, J., et al., *Omega-3 PUFA of marine origin limit diet-induced obesity in mice by reducing cellularity of adipose tissue.* Lipids, 2004. **39**(12): p. 1177-85.
176. Ferguson, J.F., et al., *Omega-3 polyunsaturated fatty acids attenuate inflammatory activation and alter differentiation in human adipocytes.* J Nutr Biochem, 2019. **64**: p. 45-49.
177. Masoodi, M., et al., *Lipid signaling in adipose tissue: Connecting inflammation & metabolism.* Biochim Biophys Acta, 2015. **1851**(4): p. 503-18.
178. Flachs, P., et al., *Stimulation of mitochondrial oxidative capacity in white fat independent of UCP1: a key to lean phenotype.* Biochim Biophys Acta, 2013. **1831**(5): p. 986-1003.
179. Terrien, J., M. Perret, and F. Aujard, *Behavioral thermoregulation in mammals: a review.* Front Biosci (Landmark Ed), 2011. **16**: p. 1428-44.
180. Cannon, B. and J. Nedergaard, *Brown adipose tissue: function and physiological significance.* Physiol Rev., 2004. **84**(1): p. 277-359.
181. Cannon, B. and J. Nedergaard, *Nonshivering thermogenesis and its adequate measurement in metabolic studies.* J Exp Biol, 2011. **214**(Pt 2): p. 242-53.
182. Pant, M., N.C. Bal, and M. Periasamy, *Sarcolipin: A Key Thermogenic and Metabolic Regulator in Skeletal Muscle.* Trends Endocrinol Metab, 2016. **27**(12): p. 881-892.
183. Vallerand, A.L., F. Perusse, and L.J. Bukowiecki, *Stimulatory effects of cold exposure and cold acclimation on glucose uptake in rar peripheral tissues.* American Journal of Physiology, 1990. **259**: p. R1043-R1049.
184. Castellani, J.W. and A.J. Young, *Human physiological responses to cold exposure: Acute responses and acclimatization to prolonged exposure.* Auton Neurosci, 2016. **196**: p. 63-74.
185. Himms-Hagen, J., *Lipid metabolism during cold-exposure and during cold-acclimation.* Lipids, 1972. **7**(5): p. 310-23.
186. Aydin, J., et al., *Nonshivering thermogenesis protects against defective calcium handling in muscle.* FASEB J, 2008. **22**(11): p. 3919-24.
187. Golozoubova, V., et al., *Only UCP1 can mediate adaptive nonshivering thermogenesis in the cold2.* FASEB Journal, 2001. **15**(11): p. 2048-2050.
188. Jansky, L., *Non-shivering thermogenesis and its thermoregulatory significance.* Biol Rev Camb Philos Soc, 1973. **48**(1): p. 85-132.
189. Block, B.A., *Thermogenesis in muscle.* Annu Rev Physiol, 1994. **56**: p. 535-77.
190. Periasamy, M., J.L. Herrera, and F.C.G. Reis, *Skeletal Muscle Thermogenesis and Its Role in Whole Body Energy Metabolism.* Diabetes Metab J, 2017. **41**(5): p. 327-336.
191. Bal, N.C., et al., *The Role of Sarcolipin in Muscle Non-shivering Thermogenesis.* Front Physiol, 2018. **9**: p. 1217.

192. el-Hayek, R., et al., *Activation of the Ca2+ release channel of skeletal muscle sarcoplasmic reticulum by palmitoyl carnitine.* Biophys J, 1993. **65**(2): p. 779-89.
193. Maurya, S.K., et al., *Sarcolipin Is a Key Determinant of the Basal Metabolic Rate, and Its Overexpression Enhances Energy Expenditure and Resistance against Diet-induced Obesity.* J Biol Chem, 2015. **290**(17): p. 10840-9.
194. Bal, N.C., et al., *Increased Reliance on Muscle-based Thermogenesis upon Acute Minimization of Brown Adipose Tissue Function.* J Biol Chem, 2016. **291**(33): p. 17247-57.
195. Bal, N.C., et al., *Both brown adipose tissue and skeletal muscle thermogenesis processes are activated during mild to severe cold adaptation in mice.* J Biol Chem, 2017. **292**(40): p. 16616-16625.
196. Dumonteil, E., H. Barre, and G. Meissner, *Sarcoplasmic reticulum Ca(2+)-ATPase and ryanodine receptor in cold-acclimated ducklings and thermogenesis.* Am J Physiol, 1993. **265**(2 Pt 1): p. C507-13.
197. Pant, M., N.C. Bal, and M. Periasamy, *Cold adaptation overrides developmental regulation of sarcolipin expression in mice skeletal muscle: SOS for muscle-based thermogenesis?* J Exp Biol, 2015. **218**(Pt 15): p. 2321-5.
198. Babu, G.J., et al., *Differential expression of sarcolipin protein during muscle development and cardiac pathophysiology.* J Mol Cell Cardiol, 2007. **43**(2): p. 215-22.
199. Baer, P.C., *Adipose-derived mesenchymal stromal/stem cells: An update on their phenotype in vivo and in vitro.* World J Stem Cells, 2014. **6**(3): p. 256-65.
200. Wentworth, J.M., et al., *Pro-inflammatory CD11c+CD206+ adipose tissue macrophages are associated with insulin resistance in human obesity.* Diabetes, 2010. **59**(7): p. 1648-56.
201. Garg, S.K., et al., *Changes in adipose tissue macrophages and T cells during aging.* Crit Rev Immunol, 2014. **34**(1): p. 1-14.
202. Zeyda, M., et al., *Newly identified adipose tissue macrophage populations in obesity with distinct chemokine and chemokine receptor expression.* Int J Obes (Lond), 2010. **34**(12): p. 1684-94.
203. Lumeng, C.N., et al., *Aging is associated with an increase in T cells and inflammatory macrophages in visceral adipose tissue.* J Immunol, 2011. **187**(12): p. 6208-16.
204. Berry, R. and M.S. Rodeheffer, *Characterization of the adipocyte cellular lineage in vivo.* Nat Cell Biol, 2013. **15**(3): p. 302-8.
205. Rodeheffer, M.S., K. Birsoy, and J.M. Friedman, *Identification of white adipocyte progenitor cells in vivo.* Cell, 2008. **135**(2): p. 240-9.
206. Flachs, P., et al., *Synergistic induction of lipid catabolism and anti-inflammatory lipids in white fat of dietary obese mice in response to calorie restriction and n-3 fatty acids.* Diabetologia, 2011. **54**(10): p. 2626-2638.
207. Viswanadha, S. and C. Londos, *Optimized conditions for measuring lipolysis in murine primary adipocytes.* J Lipid Res, 2006. **47**(8): p. 1859-64.
208. Medrikova, D., et al., *Sex differences during the course of diet-induced obesity in mice: adipose tissue expandability and glycemic control.* Int J Obes (Lond), 2012. **36**(2): p. 262-72.
209. Hartmannova, H., et al., *Acadian variant of Fanconi syndrome is caused by mitochondrial respiratory chain complex I deficiency due to a non-coding mutation in complex I assembly factor NDUFAF6.* Hum Mol Genet, 2016. **25**(18): p. 4062-4079.
210. Rossmeisl, M., et al., *Differential modulation of white adipose tissue endocannabinoid levels by n-3 fatty acids in obese mice and type 2 diabetic patients.* Biochim Biophys Acta, 2018. **1863**(7): p. 712-725.
211. Rombaldova, M., et al., *Omega-3 fatty acids promote fatty acid utilization and production of pro-resolving lipid mediators in alternatively activated adipose tissue macrophages.* Biochem Biophys Res Commun, 2017. **490**(3): p. 1080-1085.
212. Kus, V., et al., *Induction of muscle thermogenesis by high-fat diet in mice: association*

with obesity-resistance. Am J Physiol Endocrinol Metab, 2008. **295**(2): p. E356-67.
213. Meyer, C.W., et al., *Adaptive thermogenesis and thermal conductance in wild-type and UCP1-KO mice.* Am.J Physiol Regul.Integr.Comp Physiol, 2010. **299**(5): p. R1396-R1406.
214. Surwit, R.S., et al., *Diet-induced changes in uncoupling proteins in obesity-prone and obesity-resistant strains of mice.* Proc.Natl.Acad.Sci.U.S A., 1998. **95**(7): p. 4061-4065.
215. Livak, K.J. and T.D. Schmittgen, *Analysis of relative gene expression data using real-time quantitative PCR and the 2(-Delta Delta C(T)) Method.* Methods, 2001. **25**(4): p. 402-8.
216. Son, M.J., et al., *Methyltransferase and demethylase profiling studies during brown adipocyte differentiation.* BMB Rep, 2016. **49**(7): p. 388-93.
217. Schooneman, M.G., et al., *Acylcarnitines: reflecting or inflicting insulin resistance?* Diabetes, 2013. **62**(1): p. 1-8.
218. Strom, K., et al., *N(1)-methylnicotinamide is a signalling molecule produced in skeletal muscle coordinating energy metabolism.* Sci Rep, 2018. **8**(1): p. 3016.
219. Komatsu, M., et al., *NNMT activation can contribute to the development of fatty liver disease by modulating the NAD(+) metabolism.* Scientific Reports, 2018. **8**.
220. Yasuda, T., et al., *Hypothalamic neuronal histamine regulates sympathetic nerve activity and expression of uncoupling protein 1 mRNA in brown adipose tissue in rats.* Neuroscience, 2004. **125**(3): p. 535-40.
221. Ilavenil, S., et al., *Trigonelline attenuates the adipocyte differentiation and lipid accumulation in 3T3-L1 cells.* Phytomedicine, 2014. **21**(5): p. 758-65.
222. Rousset, S., et al., *The biology of mitochondrial uncoupling proteins.* Diabetes, 2004. **53 Suppl 1**: p. S130-5.
223. Wang, Y., et al., *Pref-1, a preadipocyte secreted factor that inhibits adipogenesis.* J Nutr, 2006. **136**(12): p. 2953-6.
224. Haramizu, S., et al., *Different contribution of muscle and liver lipid metabolism to endurance capacity and obesity susceptibility of mice.* J. Appl. Physiol. , 2009. **106**(3): p. 871-9.
225. Hall, D., et al., *Peroxisomal and microsomal lipid pathways associated with resistance to hepatic steatosis and reduced pro-inflammatory state.* J Biol Chem, 2010. **285**(40): p. 31011-23.
226. Zimmermann, R., et al., *Fat mobilization in adipose tissue is promoted by adipose triglyceride lipase.* Science, 2004. **306**(5700): p. 1383-1386.
227. Granneman, J.G., et al., *White adipose tissue contributes to UCP1-independent thermogenesis.* Am.J.Physiol Endocrinol.Metab, 2003. **285**(6): p. E1230-E1236.
228. Bezaire, V., et al., *Contribution of adipose triglyceride lipase and hormone-sensitive lipase to lipolysis in hMADS adipocytes.* J Biol.Chem., 2009. **284**(27): p. 18282-18291.
229. Mottillo, E.P., et al., *Lipolytic products activate peroxisome proliferator-activated receptor (PPAR) alpha and delta in brown adipocytes to match fatty acid oxidation with supply.* J Biol.Chem., 2012. **287**(30): p. 25038-25048.
230. Mottillo, E.P., et al., *Coupling of lipolysis and de novo lipogenesis in brown, beige, and white adipose tissues during chronic beta3-adrenergic receptor activation.* J Lipid Res, 2014. **55**(11): p. 2276-86.
231. Bartelt, A., et al., *Brown adipose tissue activity controls triglyceride clearance.* Nat.Med., 2011. **17**(2): p. 200-205.
232. Khedoe, P.P., et al., *Brown adipose tissue takes up plasma triglycerides mostly after lipolysis.* J Lipid Res, 2015. **56**(1): p. 51-9.
233. Mantha, L. and Y. Deshaies, *beta-Adrenergic modulation of triglyceridemia under increased energy expenditure.* Am J Physiol, 1998. **274**(6 Pt 2): p. R1769-76.
234. Olswang, Y., et al., *A mutation in the peroxisome proliferator-activated receptor gamma -binding site in the gene for the cytosolic form of phosphoenolpyruvate carboxykinase reduces adipose tissue size and fat content in mice.* Proceedings of the National Academy of Sciences, 2002. **99**(2): p. 625-630.
235. Wakil, S.J., J.K. Stoops, and V.C. Joshi, *Fatty acid synthesis and its regulation.* Annu Rev

Biochem, 1983. **52**: p. 537-79.
236. Shi, Y. and D. Cheng, *Beyond triglyceride synthesis: the dynamic functional roles of MGAT and DGAT enzymes in energy metabolism.* Am J Physiol Endocrinol Metab, 2009. **297**(1): p. E10-8.
237. Commins, S.P., et al., *Induction of uncoupling protein expression in brown and white adipose tissue by leptin.* Endocrinology, 1999. **140**(1): p. 292-300.
238. Watson, P.M., et al., *Differential regulation of leptin expression and function in A/J vs. C57BL/6J mice during diet-induced obesity.* Am.J.Physiol Endocrinol.Metab., 2000. **279**(2): p. E356-E365.
239. Ukropec, J., et al., *UCP1-independent thermogenesis in white adipose tissue of cold-acclimated Ucp1-/- mice.* J Biol.Chem., 2006. **281**(42): p. 31894-31908.
240. Niang, F., et al., *Leptin induces nitric oxide-mediated inhibition of lipolysis and glyceroneogenesis in rat white adipose tissue.* J Nutr, 2011. **141**(1): p. 4-9.
241. Collins, S., et al., *Strain-specific response to beta3-adrenergic receptor agonist treatment of diet-induced obesity in mice.* Endocrinology, 1997. **138**: p. 405-413.
242. Matthias, A., et al., *Thermogenic responses in brown fat cells are fully UCP1-dependent. UCP2 or UCP3 do not substitute for UCP1 in adrenergically or fatty scid-induced thermogenesis.* J Biol Chem, 2000. **275**(33): p. 25073-81.
243. Heeren, J. and L. Scheja, *Brown adipose tissue and lipid metabolism.* Curr Opin Lipidol, 2018. **29**(3): p. 180-185.
244. Olsen, J.M., et al., *β 3 -adrenergically induced glucose uptake in brown adipose tissue is independent of UCP1 presence or activity: Mediation through the mTOR pathway.* Molecular Metabolism, 2017.
245. Inokuma, K., et al., *Uncoupling protein 1 is necessary for norepinephrine-induced glucose utilization in brown adipose tissue.* Diabetes, 2005. **54**(5): p. 1385-1391.
246. Hankir, M.K., et al., *Dissociation Between Brown Adipose Tissue (18)F-FDG Uptake and Thermogenesis in Uncoupling Protein 1-Deficient Mice.* J Nucl Med, 2017. **58**(7): p. 1100-1103.
247. Hao, Q., et al., *Transcriptome profiling of brown adipose tissue during cold exposure reveals extensive regulation of glucose metabolism.* Am J Physiol Endocrinol Metab, 2015. **308**(5): p. E380-92.
248. Schreiber, R., et al., *Cold-Induced Thermogenesis Depends on ATGL-Mediated Lipolysis in Cardiac Muscle, but Not Brown Adipose Tissue.* Cell Metabolism, 2017. **26**(5): p. 753-+.
249. Park, H., et al., *Peroxisome-derived lipids regulate adipose thermogenesis by mediating cold-induced mitochondrial fission.* J Clin Invest, 2019. **129**(2): p. 694-711.
250. Hahn, P. and J. Skala, *Carnitine and brown adipose tissue metabolism in the rat during development.* Biochem J, 1972. **127**(1): p. 107-11.
251. Simcox, J., et al., *Global Analysis of Plasma Lipids Identifies Liver-Derived Acylcarnitines as a Fuel Source for Brown Fat Thermogenesis.* Cell Metab, 2017. **26**(3): p. 509-522 e6.
252. Carpentier, A.C., *Branched-chain Amino Acid Catabolism by Brown Adipose Tissue.* Endocrinology, 2020. **161**(7).
253. Pissios, P., *Nicotinamide N-Methyltransferase: More Than a Vitamin B3 Clearance Enzyme.* Trends in Endocrinology and Metabolism, 2017. **28**(5): p. 340-353.
254. Surjana, D., G.M. Halliday, and D.L. Damian, *Role of nicotinamide in DNA damage, mutagenesis, and DNA repair.* J Nucleic Acids, 2010. **2010**.
255. Ikeda, K., et al., *UCP1-independent signaling involving SERCA2b-mediated calcium cycling regulates beige fat thermogenesis and systemic glucose homeostasis.* Nat Med, 2017. **23**(12): p. 1454-1465.
256. Kazak, L., et al., *A Creatine-Driven Substrate Cycle Enhances Energy Expenditure and Thermogenesis in Beige Fat.* Cell, 2015. **163**(3): p. 643-655.
257. Bal, N.C., et al., *Sarcolipin is a newly identified regulator of muscle-based thermogenesis in mammals.* Nat Med, 2012. **18**(10): p. 1575-9.

258. Maurya, S.K., et al., *Sarcolipin Signaling Promotes Mitochondrial Biogenesis and Oxidative Metabolism in Skeletal Muscle.* Cell Rep, 2018. **24**(11): p. 2919-2931.
259. Campbell, K.L. and A.A. Dicke, *Sarcolipin Makes Heat, but Is It Adaptive Thermogenesis?* Front Physiol, 2018. **9**: p. 714.
260. Butler, J., et al., *The effects of sarcolipin over-expression in mouse skeletal muscle on metabolic activity.* Arch Biochem Biophys, 2015. **569**: p. 26-31.
261. Lapuente-Brun, E., et al., *Supercomplex assembly determines electron flux in the mitochondrial electron transport chain.* Science, 2013. **340**(6140): p. 1567-70.
262. Echtay, K.S., *Mitochondrial uncoupling proteins--what is their physiological role?* Free Radic Biol Med, 2007. **43**(10): p. 1351-71.
263. Schrauwen, P. and M. Hesselink, *UCP2 and UCP3 in muscle controlling body metabolism.* J Exp Biol, 2002. **205**(Pt 15): p. 2275-85.
264. Haman, F., et al., *Oxidative fuel selection and shivering thermogenesis during a 12- and 24-h cold-survival simulation.* J Appl Physiol (1985), 2016. **120**(6): p. 640-8.
265. Mathis, D. and S.E. Shoelson, *Immunometabolism: an emerging frontier.* Nat Rev Immunol, 2011. **11**(2): p. 81.
266. Mathis, D., *Organismal immunometabolism: advances in both directions.* Nat Rev Immunol, 2019. **19**(2): p. 83-84.
267. Bystrom, J., et al., *Resolution-phase macrophages possess a unique inflammatory phenotype that is controlled by cAMP.* Blood, 2008. **112**(10): p. 4117-27.
268. Quinn, M.T. and I.A. Schepetkin, *Role of NADPH oxidase in formation and function of multinucleated giant cells.* J Innate Immun, 2009. **1**(6): p. 509-26.
269. Hernandez-Pando, R., et al., *Inflammatory cytokine production by immunological and foreign body multinucleated giant cells.* Immunology, 2000. **100**(3): p. 352-8.
270. Bjursell, M., et al., *The beneficial effects of n-3 polyunsaturated fatty acids on diet induced obesity and impaired glucose control do not require Gpr120.* PLoS One, 2014. **9**(12): p. e114942.
271. Pavlisova, J., et al., *Corn oil versus lard: Metabolic effects of omega-3 fatty acids in mice fed obesogenic diets with different fatty acid composition.* Biochimie, 2016. **124**: p. 150-162.
272. Hames, K.C., et al., *Very-long-chain omega-3 fatty acid supplements and adipose tissue functions: a randomized controlled trial.* Am J Clin Nutr, 2017.
273. Holt, P.R., et al., *Docosahexaenoic Acid Supplementation is Not Anti-Inflammatory in Adipose Tissue of Healthy Obese Postmenopausal Women.* Int J Nutr, 2017. **1**(4): p. 31-49.
274. Kuda, O., et al., *n-3 fatty acids and rosiglitazone improve insulin sensitivity through additive stimulatory effects on muscle glycogen synthesis in mice fed a high-fat diet.* Diabetologia, 2009. **52**(5): p. 941-51.
275. Rossmeisl, M., et al., *Metabolic effects of n-3 PUFA as phospholipids are superior to triglycerides in mice fed a high-fat diet: possible role of endocannabinoids.* PLoS One, 2012. **7**(6): p. e38834.
276. Spencer, M., et al., *Omega-3 Fatty Acids Reduce Adipose Tissue Macrophages in Human Subjects With Insulin Resistance.* Diabetes, 2013.
277. Claria, J., et al., *Pro-resolving actions of SPM in adipose tissue biology.* Mol Aspects Med, 2017. **58**: p. 83-92.
278. Kwon, H.J., et al., *The contribution of arachidonate 15-lipoxygenase in tissue macrophages to adipose tissue remodeling.* Cell Death Dis, 2016. **7**(6): p. e2285.
279. Szymczak, M., M. Murray, and N. Petrovic, *Modulation of angiogenesis by omega-3 polyunsaturated fatty acids is mediated by cyclooxygenases.* Blood, 2008. **111**(7): p. 3514-21.
280. Wen, Y., et al., *Role of 12/15-lipoxygenase in the expression of MCP-1 in mouse macrophages.* Am J Physiol Heart Circ Physiol, 2008. **294**(4): p. H1933-8.
281. Todorcevic, M. and L. Hodson, *The Effect of Marine Derived n-3 Fatty Acids on Adipose*

Tissue Metabolism and Function. J Clin Med, 2015. **5**(1).
282. Yin, H., et al., *Role of mitochondria in programmed cell death mediated by arachidonic acid-derived eicosanoids.* Mitochondrion, 2013. **13**(3): p. 209-24.
283. Hensler, M., et al., *The inhibition of fat cell proliferation by n-3 fatty acids in dietary obese mice.* Lipids Health Dis., 2011. **10**: p. 128.
284. Spalding, K.L., et al., *Dynamics of fat cell turnover in humans.* Nature, 2008. **453**(7196): p. 783-787.

10 List of all author´s publications

Flachs P*, **Adamcova K***, Zouhar P, Janovska P, Bardova K, Svobodova M, Hansikova J, Kuda O, Rossmeisl M, Kopecky J. Induction of lipogenesis in white fat during cold exposure in mice: link to lean phenotype. *International Journal Obesity*. 2017; 41: 372–380. IF=4.36 (2020)
* These authors contributed equally

Adamcova K*, Horakova O*, Bardova K*, Janovska P, Brezinova M, Kuda O, Rossmeisl M, Kopecky J. Reduced Number of Adipose Lineage and Endothelial Cells in Epididymal fat in Response to Omega-3 PUFA in Mice Fed High-Fat Diet. *Marine Drugs.* 2018; 16 (12*)*: 515-534. IF=3.81 (2020)
* These authors contributed equally

Paluchova V, Oseeva M, Brezinova M, CA/Jka T, Bardova K, **Adamcova K**, Zacek P, Brejchova K, Balas L, Chodounska H, Kudova E, Schreiber R, Zechner R, Durand T, Rossmeisl M, Abumrad N, Kopecky J, Kuda O. Lipokine 5-PAHSA Is Regulated by Adipose Triglyceride Lipase and Primes Adipocytes for *De Novo* Lipogenesisin Mice. *Diabetes*.2020; 69: 300-312. IF=6.73 (2020)

Janovska P, Melenovsky V, Svobodova M, Havlenova T, Haluzik M. Hoskova E, Pelikanova T, Kautzner J, Monzo L, Jurcova I, **Adamcova K**, Lenkova L, Buresova J, Rossmeisl M, Kuda O, Cajka T. Kopecky J. Dysregulation of epicardial adipose tissue in cachexia due to heart failure: the role of natriuretic peptides and cardiolipin. *Journal of Cachexia, Sarcopenia and Muscle. 2020;* IF= 9.80 (2020)

Bardova K, Funda J, Pohl R, Cajka T, Hensler M, Kuda O, Janovska P, **Adamcova K**, Irodenko I, Lenkova L, Zouhar P, Horakova O, Flachs P, Rossmeisl M, Colca J, Kopecky J. Additive effects of omega-3 fatty acids and thiazolidinediones in mice fed a high-fat diet: triacylglycerol/fatty acid cycling in adipose tissue. *Nutrients.* 2020; IF 4.55 (2020)

Publication under preparation:
Janovska P, Bardova K, Vrbacky P, **Adamcova K**, Lenkova L, Funda J. Drahota Z, Rossmeisl M, Zouhar P, Kopecky J. Strain-specific involvement of brown fat and muscle in cold-induced thermogenesis in mice: link to lean phenotype.

11 Appendix

A. Supplementary Tables and Datasets

B. Publications enclosed in full
(Publication A, Publication C)

A. Supplementary Tables and Datasets

STable 4.2.1 Selected proteins from proteomic analysis of BAT in A/J and B6 mice

Protein name	Gene name	FC 30°C/6°C	p_raw	p_FDR	KEGG pathway
Acyl-Coenzyme A dehydrogenase family, member 12 (MCG142036)	Acad12 mCG_142036	1.6505	0.022602	0.15892	FAOX
Acyl-Coenzyme A dehydrogenase family, member 12 (MCG142036)	Acad12 mCG_142036	1.7083	0.0034029	0.039308	FAOX
ATP-binding cassette sub-family D member 3 (68 kDa peroxisomal membrane protein) (PMP68) (70 kDa peroxisomal membrane protein) (PMP70)	Abcd3 Pmp70 Pxmp1	0.49971	0.000964	0.03098	FAOX
ATP-binding cassette sub-family D member 3 (68 kDa peroxisomal membrane protein) (PMP68) (70 kDa peroxisomal membrane protein) (PMP70)	Abcd3 Pmp70 Pxmp1	0.50369	0.0025834	0.032636	FAOX
Extended synaptotagmin-1 (E-Syt1) (Membrane-bound C2 domain-containing protein)	Esyt1 Fam62a Mbc2	1.7627	0.0001842	0.013102	FAOX
Extended synaptotagmin-1 (E-Syt1) (Membrane-bound C2 domain-containing protein)	Esyt1 Fam62a Mbc2	1.789	0.001074	0.018673	FAOX
Monoglyceride lipase	Mgll	0.49101	0.0015207	0.038197	FAOX
Monoglyceride lipase	Mgll	0.37406	4.542E-05	0.0029459	FAOX
Non-specific lipid-transfer protein (NSL-TP) (EC 2.3.1.176) (Propanoyl-CoA C-acyltransferase) (SCP-chi) (SCPX) (Sterol carrier protein 2) (SCP-2) (Sterol carrier protein X) (SCP-X)	Scp2 Scp-2	0.34734	0.0027242	0.049015	FAOX
Non-specific lipid-transfer protein (NSL-TP) (EC 2.3.1.176) (Propanoyl-CoA C-acyltransferase) (SCP-chi) (SCPX) (Sterol carrier protein 2) (SCP-2) (Sterol carrier protein X) (SCP-X)	Scp2 Scp-2	0.49675	0.0049551	0.04727	FAOX
Peroxisomal acyl-coenzyme A oxidase 1 (AOX) (EC 1.3.3.6) (Palmitoyl-CoA oxidase)	Acox1 Acox Paox	0.82473	0.27021	0.56899	FAOX
Peroxisomal acyl-coenzyme A oxidase 1 (AOX) (EC 1.3.3.6) (Palmitoyl-CoA oxidase)	Acox1 Acox Paox	0.82699	0.016136	0.1025	FAOX

Peroxisomal bifunctional enzyme (PBE) (PBFE) [Includes: Enoyl-CoA hydratase/3,2-trans-enoyl-CoA isomerase (EC 4.2.1.17) (EC 5.3.3.8); 3-hydroxyacyl-CoA dehydrogenase (EC 1.1.1.35)]	Ehhadh	0.33571	0.0032183	0.051701	FAOX
Peroxisomal bifunctional enzyme (PBE) (PBFE) [Includes: Enoyl-CoA hydratase/3,2-trans-enoyl-CoA isomerase (EC 4.2.1.17) (EC 5.3.3.8); 3-hydroxyacyl-CoA dehydrogenase (EC 1.1.1.35)]	Ehhadh	0.20987	0.0001935	0.0073484	FAOX
Peroxisomal multifunctional enzyme type 2 (MFE-2) (17-beta-hydroxysteroid dehydrogenase 4) (17-beta-HSD 4) (D-bifunctional protein) (DBP) (Multifunctional protein 2) (MPF-2) [Cleaved into: (3R)-hydroxyacyl-CoA dehydrogenase (EC 1.1.1.n12); Enoyl-CoA hydratase 2 (EC 4.2.1.107) (EC 4.2.1.119) (3-alpha,7-alpha,12-alpha-trihydroxy-5-beta-cholest-24-enoyl-CoA hydratase)]	Hsd17b4 Edh17b4	0.53373	0.0029665	0.050364	FAOX
Peroxisomal multifunctional enzyme type 2 (MFE-2) (17-beta-hydroxysteroid dehydrogenase 4) (17-beta-HSD 4) (D-bifunctional protein) (DBP) (Multifunctional protein 2) (MPF-2) [Cleaved into: (3R)-hydroxyacyl-CoA dehydrogenase (EC 1.1.1.n12); Enoyl-CoA hydratase 2 (EC 4.2.1.107) (EC 4.2.1.119) (3-alpha,7-alpha,12-alpha-trihydroxy-5-beta-cholest-24-enoyl-CoA hydratase)]	Hsd17b4 Edh17b4	0.66232	0.0001948	0.0073484	FAOX
Short/branched chain specific acyl-CoA dehydrogenase, mitochondrial (SBCAD) (EC 1.3.8.5) (2-methyl branched chain acyl-CoA dehydrogenase) (2-MEBCAD) (2-methylbutyryl-coenzyme A dehydrogenase) (2-methylbutyryl-CoA dehydrogenase)	Acadsb	1.5597	0.018225	0.14522	FAOX
Short/branched chain specific acyl-CoA dehydrogenase, mitochondrial (SBCAD) (EC 1.3.8.5) (2-methyl branched chain acyl-CoA dehydrogenase) (2-MEBCAD) (2-methylbutyryl-coenzyme A dehydrogenase) (2-methylbutyryl-CoA dehydrogenase)	Acadsb	1.7933	0.0004982	0.011918	FAOX

Very long-chain acyl-CoA synthetase (VLACS) (VLCS) (EC 6.2.1.-) (Fatty acid transport protein 2) (FATP-2) (Fatty-acid-coenzyme A ligase, very long-chain 1) (Long-chain-fatty-acid--CoA ligase) (EC 6.2.1.3) (Solute carrier family 27 member 2) (THCA-CoA ligase) (Very long-chain-fatty-acid-CoA ligase)	Slc27a2 Acsvl1 Facvl1 Fatp2 Vlacs Vlcs	0.32454	0.0016295	0.039576	FAOX
Very long-chain acyl-CoA synthetase (VLACS) (VLCS) (EC 6.2.1.-) (Fatty acid transport protein 2) (FATP-2) (Fatty-acid-coenzyme A ligase, very long-chain 1) (Long-chain-fatty-acid--CoA ligase) (EC 6.2.1.3) (Solute carrier family 27 member 2) (THCA-CoA ligase) (Very long-chain-fatty-acid-CoA ligase)	Slc27a2 Acsvl1 Facvl1 Fatp2 Vlacs Vlcs	0.1428	8.868E-06	0.0009649	FAOX
Alpha-enolase (EC 4.2.1.11) (2-phospho-D-glycerate hydro-lyase) (Enolase 1) (Non-neural enolase) (NNE)	Eno1 Eno-1	0.71118	0.021713	0.15892	glycolysis
Alpha-enolase (EC 4.2.1.11) (2-phospho-D-glycerate hydro-lyase) (Enolase 1) (Non-neural enolase) (NNE)	Eno1 Eno-1	0.6163	0.0007513	0.014976	glycolysis
ATP-dependent 6-phosphofructokinase, platelet type (ATP-PFK) (PFK-P) (EC 2.7.1.11) (6-phosphofructokinase type C) (Phosphofructo-1-kinase isozyme C) (PFK-C) (Phosphohexokinase)	Pfkp Pfkc	0.49199	0.0014347	0.03664	glycolysis
ATP-dependent 6-phosphofructokinase, platelet type (ATP-PFK) (PFK-P) (EC 2.7.1.11) (6-phosphofructokinase type C) (Phosphofructo-1-kinase isozyme C) (PFK-C) (Phosphohexokinase)	Pfkp Pfkc	0.41499	4.357E-05	0.0029189	glycolysis
Bisphosphoglycerate mutase (BPGM) (EC 5.4.2.4) (2,3-bisphosphoglycerate mutase, erythrocyte) (2,3-bisphosphoglycerate synthase) (EC 5.4.2.11) (BPG-dependent PGAM)	Bpgm	0.7982	0.076148	0.30216	glycolysis
Bisphosphoglycerate mutase (BPGM) (EC 5.4.2.4) (2,3-bisphosphoglycerate mutase, erythrocyte) (2,3-bisphosphoglycerate synthase) (EC 5.4.2.11) (BPG-dependent PGAM)	Bpgm	0.64	0.0003475	0.0099329	glycolysis
Glucose-6-phosphate isomerase (GPI) (EC 5.3.1.9) (Autocrine motility factor) (AMF) (Neuroleukin) (NLK) (Phosphoglucose isomerase) (PGI) (Phosphohexose isomerase) (PHI)	Gpi Gpi1	0.50838	0.0007579	0.027947	glycolysis

Glucose-6-phosphate isomerase (GPI) (EC 5.3.1.9) (Autocrine motility factor) (AMF) (Neuroleukin) (NLK) (Phosphoglucose isomerase) (PGI) (Phosphohexose isomerase) (PHI)	Gpi Gpi1	0.42558	3.799E-05	0.0026695	glycolysis
Hexokinase-1 (EC 2.7.1.1) (Hexokinase type I) (HK I) (Hexokinase, tumor isozyme)	Hk1	0.72027	0.065399	0.27851	glycolysis
Hexokinase-1 (EC 2.7.1.1) (Hexokinase type I) (HK I) (Hexokinase, tumor isozyme)	Hk1	0.52684	0.0001096	0.0055985	glycolysis
Hexokinase-2 (EC 2.7.1.1) (Hexokinase type II) (HK II)	Hk2	0.59143	0.030128	0.1718	glycolysis
Hexokinase-2 (EC 2.7.1.1) (Hexokinase type II) (HK II)	Hk2	0.3672	0.0001528	0.0068908	glycolysis
Phosphoglycerate kinase 1 (EC 2.7.2.3)	Pgk1 Pgk-1	0.69638	0.023974	0.15892	glycolysis
Phosphoglycerate kinase 1 (EC 2.7.2.3)	Pgk1 Pgk-1	0.65549	0.0006454	0.013536	glycolysis
Glycerol-3-phosphate dehydrogenase [NAD(+)], cytoplasmic (GPD-C) (GPDH-C) (EC 1.1.1.8)	Gpd1 Gdc-1 Gdc1 Ki-aa4010	0.63095	0.018797	0.14615	Gpd1
Glycerol-3-phosphate dehydrogenase [NAD(+)], cytoplasmic (GPD-C) (GPDH-C) (EC 1.1.1.8)	Gpd1 Gdc-1 Gdc1 Ki-aa4010	0.47597	0.0003327	0.0095906	Gpd1
Glycerol kinase (GK) (Glycerokinase) (EC 2.7.1.30) (ATP:glycerol 3-phosphotransferase)	Gk Gyk	0.058757	2.341E-05	0.0046639	GyK
Glycerol kinase (GK) (Glycerokinase) (EC 2.7.1.30) (ATP:glycerol 3-phosphotransferase)	Gk Gyk	0.053983	1.396E-06	0.0002355	GyK
1-acyl-sn-glycerol-3-phosphate acyltransferase (EC 2.3.1.51)	Agpat1 mCG_5502	0.77218	0.03897	0.20091	lipid synthesis
1-acyl-sn-glycerol-3-phosphate acyltransferase (EC 2.3.1.51)	Agpat1 mCG_5502	0.61819	0.0029269	0.035385	lipid synthesis
1-acyl-sn-glycerol-3-phosphate acyltransferase beta (EC 2.3.1.51) (1-acylglycerol-3-phosphate O-acyltransferase 2) (1-AGP acyltransferase 2) (1-AGPAT 2) (Lysophosphatidic acid acyltransferase beta) (LPAAT-beta)	Agpat2	0.57539	0.0040586	0.060635	lipid synthesis

1-acyl-sn-glycerol-3-phosphate acyltransferase beta (EC 2.3.1.51) (1-acylglycerol-3-phosphate O-acyltransferase 2) (1-AGP acyltransferase 2) (1-AGPAT 2) (Lysophosphatidic acid acyltransferase beta) (LPAAT-beta)	Agpat2	0.31238	1.2E-05	0.0011904	lipid synthesis
1-acyl-sn-glycerol-3-phosphate acyltransferase gamma (EC 2.3.1.51) (1-acylglycerol-3-phosphate O-acyltransferase 3) (1-AGP acyltransferase 3) (1-AGPAT 3) (Lysophosphatidic acid acyltransferase gamma) (LPAAT-gamma)	Agpat3 Lpaat3	0.7008	0.040861	0.20799	lipid synthesis
1-acyl-sn-glycerol-3-phosphate acyltransferase gamma (EC 2.3.1.51) (1-acylglycerol-3-phosphate O-acyltransferase 3) (1-AGP acyltransferase 3) (1-AGPAT 3) (Lysophosphatidic acid acyltransferase gamma) (LPAAT-gamma)	Agpat3 Lpaat3	0.51201	1.734E-06	0.0002543	lipid synthesis
Acetoacetyl-CoA synthetase (EC 6.2.1.16)	Aacs	0.56018	0.0035363	0.055612	lipid synthesis
Acetoacetyl-CoA synthetase (EC 6.2.1.16)	Aacs	0.52778	0.0009134	0.016997	lipid synthesis
Acetyl-CoA carboxylase 1 (ACC1) (EC 6.4.1.2) (ACC-alpha) (Acetyl-CoA carboxylase 265) [Includes: Biotin carboxylase (EC 6.3.4.14)]	Acaca Acac Gm738	0.59456	0.012339	0.11621	lipid synthesis
Acetyl-CoA carboxylase 1 (ACC1) (EC 6.4.1.2) (ACC-alpha) (Acetyl-CoA carboxylase 265) [Includes: Biotin carboxylase (EC 6.3.4.14)]	Acaca Acac Gm738	0.36094	0.0002099	0.0076029	lipid synthesis
Acetyl-coenzyme A synthetase, cytoplasmic	Acss2	0.95443	0.75232	0.88258	lipid synthesis
Acetyl-coenzyme A synthetase, cytoplasmic	Acss2	0.50211	0.0024551	0.031486	lipid synthesis
Acyl-CoA desaturase 1 (EC 1.14.19.1) (Delta(9)-desaturase 1) (Delta-9 desaturase 1) (Fatty acid desaturase 1) (Stearoyl-CoA desaturase 1)	Scd1	0.5306	0.017458	0.14214	lipid synthesis
Acyl-CoA desaturase 1 (EC 1.14.19.1) (Delta(9)-desaturase 1) (Delta-9 desaturase 1) (Fatty acid desaturase 1) (Stearoyl-CoA desaturase 1)	Scd1	0.32038	0.0004084	0.010794	lipid synthesis
Acyl-CoA synthetase family member 2, mitochondrial (EC 6.2.1.-)	Acsf2	0.7023	0.070379	0.29126	lipid synthesis
Acyl-CoA synthetase family member 2, mitochondrial (EC 6.2.1.-)	Acsf2	0.58885	0.0034697	0.039807	lipid synthesis
Acyl-CoA synthetase short-chain family member 3, mitochondrial (EC 6.2.1.1)	Acss3	0.69175	0.061945	0.26972	lipid synthesis
Acyl-CoA synthetase short-chain family member 3, mitochondrial (EC 6.2.1.1)	Acss3	0.52343	0.0020929	0.028598	lipid synthesis

Acyl-coenzyme A thioesterase 1 (Acyl-CoA thioesterase 1) (EC 3.1.2.2) (CTE-I) (Inducible cytosolic acyl-coenzyme A thioester hydrolase) (Long chain acyl-CoA thioester hydrolase) (Long chain acyl-CoA hydrolase)	Acot1 Cte1	0.47046	0.17536	0.46288	lipid synthesis
Acyl-coenzyme A thioesterase 1 (Acyl-CoA thioesterase 1) (EC 3.1.2.2) (CTE-I) (Inducible cytosolic acyl-coenzyme A thioester hydrolase) (Long chain acyl-CoA thioester hydrolase) (Long chain acyl-CoA hydrolase)	Acot1 Cte1	0.012149	3.074E-12	5.185E-09	lipid synthesis
Acyl-coenzyme A thioesterase 11 (Acyl-CoA thioesterase 11) (EC 3.1.2.-) (Acyl-CoA thioester hydrolase 11) (Adipose-associated thioesterase) (Brown fat-inducible thioesterase) (BFIT)	Acot11 Bfit Thea	0.33998	0.0006017	0.024628	lipid synthesis
Acyl-coenzyme A thioesterase 11 (Acyl-CoA thioesterase 11) (EC 3.1.2.-) (Acyl-CoA thioester hydrolase 11) (Adipose-associated thioesterase) (Brown fat-inducible thioesterase) (BFIT)	Acot11 Bfit Thea	0.1919	2.691E-06	0.0003631	lipid synthesis
ATP-citrate synthase (EC 2.3.3.8) (ATP-citrate (pro-S-)-lyase) (Citrate cleavage enzyme)	Acly	0.56917	0.014159	0.12629	lipid synthesis
ATP-citrate synthase (EC 2.3.3.8) (ATP-citrate (pro-S-)-lyase) (Citrate cleavage enzyme)	Acly	0.37177	0.0002518	0.0083554	lipid synthesis
Elongation of very long chain fatty acids protein 6 (EC 2.3.1.199) (3-keto acyl-CoA synthase Elovl6) (ELOVL fatty acid elongase 6) (ELOVL FA elongase 6) (Fatty acyl-CoA elongase) (Long chain fatty acid elongase) (Myelin-associated SUR4 protein) (Very long chain 3-ketoacyl-CoA synthase 6) (Very long chain 3-oxoacyl-CoA synthase 6)	Elovl6 Face Lce Masr	0.047117	0.02411	0.15892	lipid synthesis
Elongation of very long chain fatty acids protein 6 (EC 2.3.1.199) (3-keto acyl-CoA synthase Elovl6) (ELOVL fatty acid elongase 6) (ELOVL FA elongase 6) (Fatty acyl-CoA elongase) (Long chain fatty acid elongase) (Myelin-associated SUR4 protein) (Very long chain 3-ketoacyl-CoA synthase 6) (Very long chain 3-oxoacyl-CoA synthase 6)	Elovl6 Face Lce Masr	0.014524	5.273E-09	1.482E-06	lipid synthesis
Ethanolamine-phosphate cytidylyltransferase (Phosphate cytidylyltransferase 2, ethanolamine, isoform CRA_b)	Pcyt2 mCG_2151	0.53378	0.019532	0.14866	lipid synthesis

Ethanolamine-phosphate cytidyl-yltransferase (Phosphate cytidyl-yltransferase 2, ethanolamine, isoform CRA_b)	Pcyt2 mCG_2151	0.46209	0.0011354	0.018959	lipid synthesis
Fat storage-inducing transmembrane protein 2 (Fat-inducing protein 2)	Fitm2 Fit2	0.52942	0.0013205	0.035869	lipid synthesis
Fat storage-inducing transmembrane protein 2 (Fat-inducing protein 2)	Fitm2 Fit2	0.45701	0.0006461	0.013536	lipid synthesis
Fatty acid synthase (EC 2.3.1.85) [Includes: [Acyl-carrier-protein] S-acetyltransferase (EC 2.3.1.38); [Acyl-carrier-protein] S-malonyltransferase (EC 2.3.1.39); 3-oxoacyl-[acyl-carrier-protein] syn-thase (EC 2.3.1.41); 3-oxoacyl-[acyl-carrier-protein] reductase (EC 1.1.1.100); 3-hydroxyacyl-[acyl-carrier-protein] dehydratase (EC 4.2.1.59); Enoyl-[acyl-carrier-protein] reductase (EC 1.3.1.39); Oleoyl-[acyl-carrier-protein] hydrolase (EC 3.1.2.14)]	Fasn	0.63499	0.018835	0.14615	lipid synthesis
Fatty acid synthase (EC 2.3.1.85) [Includes: [Acyl-carrier-protein] S-acetyltransferase (EC 2.3.1.38); [Acyl-carrier-protein] S-malonyltransferase (EC 2.3.1.39); 3-oxoacyl-[acyl-carrier-protein] syn-thase (EC 2.3.1.41); 3-oxoacyl-[acyl-carrier-protein] reductase (EC 1.1.1.100); 3-hydroxyacyl-[acyl-carrier-protein] dehydratase (EC 4.2.1.59); Enoyl-[acyl-carrier-protein] reductase (EC 1.3.1.39); Oleoyl-[acyl-carrier-protein] hydrolase (EC 3.1.2.14)]	Fasn	0.30424	0.0002536	0.0083554	lipid synthesis
Glycerol-3-phosphate acyltransferase 1, mitochondrial (GPAT-1) (EC 2.3.1.15) (P90)	Gpam Gpat1	0.3158	0.000174	0.012995	lipid synthesis
Glycerol-3-phosphate acyltransferase 1, mitochondrial (GPAT-1) (EC 2.3.1.15) (P90)	Gpam Gpat1	0.32486	0.000266	0.0086197	lipid synthesis
Long-chain-fatty-acid--CoA ligase 5 (EC 6.2.1.3) (Long-chain acyl-CoA synthetase 5) (LACS 5)	Acsl5 Facl5	0.083996	3.77E-05	0.0062577	lipid synthesis
Long-chain-fatty-acid--CoA ligase 5 (EC 6.2.1.3) (Long-chain acyl-CoA synthetase 5) (LACS 5)	Acsl5 Facl5	0.048192	1.576E-06	0.0002531	lipid synthesis
Phosphatidylserine decarboxylase proenzyme, mitochondrial (Fragment)	Pisd	0.5501	0.036283	0.19173	lipid synthesis
Phosphatidylserine decarboxylase proenzyme, mitochondrial (Fragment)	Pisd	0.46759	0.0004791	0.01171	lipid synthesis
Phosphoethanolamine/phosphocholine phosphatase (EC 3.1.3.75)	Phospho1	0.2613	6.785E-05	0.0081088	lipid synthesis
Phosphoethanolamine/phosphocholine phosphatase (EC 3.1.3.75)	Phospho1	0.19497	1.12E-06	0.0002042	lipid synthesis

Very-long-chain (3R)-3-hydroxyacyl-CoA dehydratase 2 (EC 4.2.1.134) (3-hydroxyacyl-CoA dehydratase 2) (HACD2) (Protein-tyrosine phosphatase-like member B)	Hacd2 Ptplb	0.48197	0.0068128	0.082083	lipid synthesis
Very-long-chain (3R)-3-hydroxyacyl-CoA dehydratase 2 (EC 4.2.1.134) (3-hydroxyacyl-CoA dehydratase 2) (HACD2) (Protein-tyrosine phosphatase-like member B)	Hacd2 Ptplb	0.45914	0.0001264	0.006126	lipid synthesis
Very-long-chain 3-oxoacyl-CoA reductase (EC 1.1.1.330) (17-beta-hydroxysteroid dehydrogenase 12) (17-beta-HSD 12) (3-ketoacyl-CoA reductase) (KAR) (Estradiol 17-beta-dehydrogenase 12) (EC 1.1.1.62) (KIK-I)	Hsd17b12 Kik1	0.38755	0.0002309	0.014349	lipid synthesis
Very-long-chain 3-oxoacyl-CoA reductase (EC 1.1.1.330) (17-beta-hydroxysteroid dehydrogenase 12) (17-beta-HSD 12) (3-ketoacyl-CoA reductase) (KAR) (Estradiol 17-beta-dehydrogenase 12) (EC 1.1.1.62) (KIK-I)	Hsd17b12 Kik1	0.31744	9.21E-06	0.0009708	lipid synthesis
Very-long-chain enoyl-CoA reductase (EC 1.3.1.93) (Synaptic glycoprotein SC2) (Trans-2,3-enoyl-CoA reductase) (TER)	Tecr Gpsn2	0.89646	0.35402	0.58223	lipid synthesis
Very-long-chain enoyl-CoA reductase (EC 1.3.1.93) (Synaptic glycoprotein SC2) (Trans-2,3-enoyl-CoA reductase) (TER)	Tecr Gpsn2	0.62906	0.0009351	0.01708	lipid synthesis
Phosphoenolpyruvate carboxykinase, cytosolic [GTP] (PEPCK-C) (EC 4.1.1.32)	Pck1 Pepck	0.85503	0.43791	0.65786	Pck1
Phosphoenolpyruvate carboxykinase, cytosolic [GTP] (PEPCK-C) (EC 4.1.1.32)	Pck1 Pepck	1.0133	0.96122	0.9888	Pck1
6-phosphogluconate dehydrogenase, decarboxylating (EC 1.1.1.44)	Pgd	0.47279	0.0031057	0.05126	pentose phosphate
6-phosphogluconate dehydrogenase, decarboxylating (EC 1.1.1.44)	Pgd	0.36493	4.895E-05	0.0031154	pentose phosphate
Glucose-6-phosphate 1-dehydrogenase X (G6PD) (EC 1.1.1.49)	G6pdx G6pd G6pd-1	0.68944	0.031102	0.17535	pentose phosphate
Glucose-6-phosphate 1-dehydrogenase X (G6PD) (EC 1.1.1.49)	G6pdx G6pd G6pd-1	0.51544	0.0008693	0.01638	pentose phosphate
Ribose-5-phosphate isomerase (EC 5.3.1.6) (Phosphoriboisomerase)	Rpia Rpi	0.72079	0.001339	0.035877	pentose phosphate
Ribose-5-phosphate isomerase (EC 5.3.1.6) (Phosphoriboisomerase)	Rpia Rpi	0.52814	1.15E-06	0.0002042	pentose phosphate

Transaldolase (EC 2.2.1.2)	Taldo1	1.0014	0.94509	0.99487	pentose phosphate
Transaldolase (EC 2.2.1.2)	Taldo1	0.62972	0.0028464	0.034912	pentose phosphate
Transketolase (TK) (EC 2.2.1.1) (P68)	Tkt	0.63234	0.0059723	0.076919	pentose phosphate
Transketolase (TK) (EC 2.2.1.1) (P68)	Tkt	0.46988	0.0003118	0.0091455	pentose phosphate
Glycogen [starch] synthase, liver (EC 2.4.1.11)	Gys2	0.054974	0.0034281	0.054485	starch
Glycogen [starch] synthase, liver (EC 2.4.1.11)	Gys2	0.22319	2.827E-05	0.0022177	starch
Glycogen phosphorylase, liver form (EC 2.4.1.1)	Pygl	0.96594	0.86759	0.96334	starch
Glycogen phosphorylase, liver form (EC 2.4.1.1)	Pygl	0.53418	0.0010554	0.018525	starch
UTP--glucose-1-phosphate uridylyltransferase (EC 2.7.7.9) (UDP-glucose pyrophosphorylase) (UDPGP) (UGPase)	Ugp2	0.54046	0.000352	0.019142	starch
UTP--glucose-1-phosphate uridylyltransferase (EC 2.7.7.9) (UDP-glucose pyrophosphorylase) (UDPGP) (UGPase)	Ugp2	0.60561	0.0001282	0.006126	starch
Mitochondrial brown fat uncoupling protein 1 (UCP 1) (Solute carrier family 25 member 7) (Thermogenin)	Ucp1 Slc25a7 Ucp	0.34863	0.0011684	0.033825	Ucp1
Mitochondrial brown fat uncoupling protein 1 (UCP 1) (Solute carrier family 25 member 7) (Thermogenin)	Ucp1 Slc25a7 Ucp	0.22562	3.949E-06	0.0004757	Ucp1

A/J and B6 mice were exposed to thermoneutral housing temperature (30°C) or cold (6°C) for 7 days (*n*=4-6). Proteomic data were analyzed and assigned to KEGG metabolic pathways. Fold change (FC) between thermoneutral and cold-exposed mice was counted, transparent background corresponds to A/J mice, yellow to B6 mice.

STable 4.2.2 Selected proteins from proteomic analysis of BAT in thermoneutral and cold exposed mice.

Protein name	Gene name	FC AJ/B6	p_raw	p_FDR	KEGG pathway
Acyl-Coenzyme A dehydrogenase family, member 12 (MCG142036)	Acad12 mCG_142036	1.15	0.44796	0.79998	FAOX
Acyl-Coenzyme A dehydrogenase family, member 12 (MCG142036)	Acad12 mCG_142036	1.19	0.23114	0.59788	FAOX
ATP-binding cassette sub-family D member 3 (68 kDa peroxisomal membrane protein) (PMP68) (70 kDa peroxisomal membrane protein) (PMP70)	Abcd3 Pmp70 Pxmp1	1.04	0.65298	0.89048	FAOX
ATP-binding cassette sub-family D member 3 (68 kDa peroxisomal membrane protein) (PMP68) (70 kDa peroxisomal membrane protein) (PMP70)	Abcd3 Pmp70 Pxmp1	1.05	0.78874	0.90904	FAOX
Extended synaptotagmin-1 (E-Syt1) (Membrane-bound C2 domain-containing protein)	Esyt1 Fam62a Mbc2	0.78	0.043253	0.43943	FAOX
Extended synaptotagmin-1 (E-Syt1) (Membrane-bound C2 domain-containing protein)	Esyt1 Fam62a Mbc2	0.79	0.0172	0.26922	FAOX

Monoglyceride lipase	Mgll	1.90	0.002574	0.10474	FAOX
Monoglyceride lipase	Mgll	1.45	0.0094806	0.19723	FAOX
Non-specific lipid-transfer protein (NSL-TP) (EC 2.3.1.176) (Propanoyl-CoA C-acyltransferase) (SCP-chi) (SCPX) (Sterol carrier protein 2) (SCP-2) (Sterol carrier protein X) (SCP-X)	Scp2 Scp-2	0.85	0.46986	0.81438	FAOX
Non-specific lipid-transfer protein (NSL-TP) (EC 2.3.1.176) (Propanoyl-CoA C-acyltransferase) (SCP-chi) (SCPX) (Sterol carrier protein 2) (SCP-2) (Sterol carrier protein X) (SCP-X)	Scp2 Scp-2	1.22	0.12055	0.53763	FAOX
Peroxisomal acyl-coenzyme A oxidase 1 (AOX) (EC 1.3.3.6) (Palmitoyl-CoA oxidase)	Acox1 Acox Paox	0.61	2.35E-05	0.0029891	FAOX
Peroxisomal acyl-coenzyme A oxidase 1 (AOX) (EC 1.3.3.6) (Palmitoyl-CoA oxidase)	Acox1 Acox Paox	0.61	0.011153	0.21952	FAOX
Peroxisomal bifunctional enzyme (PBE) (PBFE) [Includes: Enoyl-CoA hydratase/3,2-trans-enoyl-CoA isomerase (EC 4.2.1.17) (EC 5.3.3.8); 3-hydroxyacyl-CoA dehydrogenase (EC 1.1.1.35)]	Ehhadh	1.54	0.14986	0.65248	FAOX
Peroxisomal bifunctional enzyme (PBE) (PBFE) [Includes: Enoyl-CoA hydratase/3,2-trans-enoyl-CoA isomerase (EC 4.2.1.17) (EC 5.3.3.8); 3-hydroxyacyl-CoA dehydrogenase (EC 1.1.1.35)]	Ehhadh	0.96	0.81572	0.92267	FAOX
Peroxisomal multifunctional enzyme type 2 (MFE-2) (17-beta-hydroxysteroid dehydrogenase 4) (17-beta-HSD 4) (D-bifunctional protein) (DBP) (Multifunctional protein 2) (MPF-2) [Cleaved into: (3R)-hydroxyacyl-CoA dehydrogenase (EC 1.1.1.n12); Enoyl-CoA hydratase 2 (EC 4.2.1.107) (EC 4.2.1.119) (3-alpha,7-alpha,12-alpha-trihydroxy-5-beta-cholest-24-enoyl-CoA hydratase)]	Hsd17b4 Edh17b4	0.95	0.57729	0.85179	FAOX
Peroxisomal multifunctional enzyme type 2 (MFE-2) (17-beta-hydroxysteroid dehydrogenase 4) (17-beta-HSD 4) (D-bifunctional protein) (DBP) (Multifunctional protein 2) (MPF-2) [Cleaved into: (3R)-hydroxyacyl-CoA dehydrogenase (EC 1.1.1.n12); Enoyl-CoA hydratase 2 (EC 4.2.1.107) (EC 4.2.1.119) (3-alpha,7-alpha,12-alpha-trihydroxy-5-beta-cholest-24-enoyl-CoA hydratase)]	Hsd17b4 Edh17b4	1.18	0.11615	0.53763	FAOX
Short/branched chain specific acyl-CoA dehydrogenase, mitochondrial (SBCAD) (EC 1.3.8.5) (2-methyl branched chain acyl-CoA dehydrogenase) (2-MEBCAD) (2-methylbutyryl-coenzyme A dehydrogenase) (2-methylbutyryl-CoA dehydrogenase)	Acadsb	0.70	0.024062	0.32309	FAOX
Short/branched chain specific acyl-CoA dehydrogenase, mitochondrial (SBCAD) (EC 1.3.8.5) (2-methyl branched chain acyl-CoA dehydrogenase) (2-MEBCAD) (2-	Acadsb	0.81	0.082848	0.49612	FAOX

methylbutyryl-coenzyme A dehydrogenase) (2-methylbutyryl-CoA dehydrogenase)					
Very long-chain acyl-CoA synthetase (VLACS) (VLCS) (EC 6.2.1.-) (Fatty acid transport protein 2) (FATP-2) (Fatty-acid-coenzyme A ligase, very long-chain 1) (Long-chain-fatty-acid--CoA ligase) (EC 6.2.1.3) (Solute carrier family 27 member 2) (THCA-CoA ligase) (Very long-chain-fatty-acid-CoA ligase)	Slc27a2 Acsvl1 Facvl1 Fatp2 Vlacs Vlcs	2.12	0.00266	0.10682	FAOX
Very long-chain acyl-CoA synthetase (VLACS) (VLCS) (EC 6.2.1.-) (Fatty acid transport protein 2) (FATP-2) (Fatty-acid-coenzyme A ligase, very long-chain 1) (Long-chain-fatty-acid--CoA ligase) (EC 6.2.1.3) (Solute carrier family 27 member 2) (THCA-CoA ligase) (Very long-chain-fatty-acid-CoA ligase)	Slc27a2 Acsvl1 Facvl1 Fatp2 Vlacs Vlcs	0.93	0.56455	0.74097	FAOX
Alpha-enolase (EC 4.2.1.11) (2-phospho-D-glycerate hydro-lyase) (Enolase 1) (Non-neural enolase) (NNE)	Eno1 Eno-1	1.09	0.24068	0.74503	glycolysis
Alpha-enolase (EC 4.2.1.11) (2-phospho-D-glycerate hydro-lyase) (Enolase 1) (Non-neural enolase) (NNE)	Eno1 Eno-1	0.94	0.56123	0.73975	glycolysis
ATP-dependent 6-phosphofructokinase, platelet type (ATP-PFK) (PFK-P) (EC 2.7.1.11) (6-phosphofructokinase type C) (Phosphofructo-1-kinase isozyme C) (PFK-C) (Phosphohexokinase)	Pfkp Pfkc	1.04	0.59024	0.85851	glycolysis
ATP-dependent 6-phosphofructokinase, platelet type (ATP-PFK) (PFK-P) (EC 2.7.1.11) (6-phosphofructokinase type C) (Phosphofructo-1-kinase isozyme C) (PFK-C) (Phosphohexokinase)	Pfkp Pfkc	0.88	0.29358	0.59788	glycolysis
Bisphosphoglycerate mutase (BPGM) (EC 5.4.2.4) (2,3-bisphosphoglycerate mutase, erythrocyte) (2,3-bisphosphoglycerate synthase) (EC 5.4.2.11) (BPG-dependent PGAM)	Bpgm	0.94	0.45563	0.80283	glycolysis
Bisphosphoglycerate mutase (BPGM) (EC 5.4.2.4) (2,3-bisphosphoglycerate mutase, erythrocyte) (2,3-bisphosphoglycerate synthase) (EC 5.4.2.11) (BPG-dependent PGAM)	Bpgm	0.75	0.010837	0.21588	glycolysis
Glucose-6-phosphate isomerase (GPI) (EC 5.3.1.9) (Autocrine motility factor) (AMF) (Neuroleukin) (NLK) (Phosphoglucose isomerase) (PGI) (Phosphohexose isomerase) (PHI)	Gpi Gpi1	0.86	0.22446	0.74503	glycolysis
Glucose-6-phosphate isomerase (GPI) (EC 5.3.1.9) (Autocrine motility factor) (AMF) (Neuroleukin) (NLK) (Phosphoglucose isomerase) (PGI) (Phosphohexose isomerase) (PHI)	Gpi Gpi1	0.72	0.0045878	0.1346	glycolysis
Hexokinase-1 (EC 2.7.1.1) (Hexokinase type I) (HK I) (Hexokinase, tumor isozyme)	Hk1	1.84	0.0013169	0.06589	glycolysis
Hexokinase-1 (EC 2.7.1.1) (Hexokinase type I) (HK I) (Hexokinase, tumor isozyme)	Hk1	1.34	0.059533	0.43384	glycolysis
Hexokinase-2 (EC 2.7.1.1) (Hexokinase type II) (HK II)	Hk2	1.72	0.014057	0.26333	glycolysis

Hexokinase-2 (EC 2.7.1.1) (Hexokinase type II) (HK II)	Hk2	1.07	0.78958	0.90934	glycolysis
Phosphoglycerate kinase 1 (EC 2.7.2.3)	Pgk1 Pgk-1	1.11	0.56573	0.84867	glycolysis
Phosphoglycerate kinase 1 (EC 2.7.2.3)	Pgk1 Pgk-1	1.04	0.51901	0.72087	glycolysis
Glycerol-3-phosphate dehydrogenase [NAD(+)], cytoplasmic (GPD-C) (GPDH-C) (EC 1.1.1.8)	Gpd1 Gdc-1 Gdc1 Ki-aa4010	1.23	0.078985	0.57396	Gpd1
Glycerol-3-phosphate dehydrogenase [NAD(+)], cytoplasmic (GPD-C) (GPDH-C) (EC 1.1.1.8)	Gpd1 Gdc-1 Gdc1 Ki-aa4010	0.93	0.55081	0.73547	Gpd1
Glycerol kinase (GK) (Glycerokinase) (EC 2.7.1.30) (ATP:glycerol 3-phosphotransferase)	Gk Gyk	0.75	0.2293	0.74503	GyK
Glycerol kinase (GK) (Glycerokinase) (EC 2.7.1.30) (ATP:glycerol 3-phosphotransferase)	Gk Gyk	0.69	0.069464	0.4552	GyK
1-acyl-sn-glycerol-3-phosphate acyltransferase (EC 2.3.1.51)	Agpat1 mCG_5502	1.17	0.18928	0.73404	lipid synthesis
1-acyl-sn-glycerol-3-phosphate acyltransferase (EC 2.3.1.51)	Agpat1 mCG_5502	0.94	0.44048	0.65984	lipid synthesis
1-acyl-sn-glycerol-3-phosphate acyltransferase beta (EC 2.3.1.51) (1-acylglycerol-3-phosphate O-acyltransferase 2) (1-AGP acyltransferase 2) (1-AGPAT 2) (Lysophosphatidic acid acyltransferase beta) (LPAAT-beta)	Agpat2	1.40	6.03E-05	0.006099	lipid synthesis
1-acyl-sn-glycerol-3-phosphate acyltransferase beta (EC 2.3.1.51) (1-acylglycerol-3-phosphate O-acyltransferase 2) (1-AGP acyltransferase 2) (1-AGPAT 2) (Lysophosphatidic acid acyltransferase beta) (LPAAT-beta)	Agpat2	0.76	0.096178	0.52206	lipid synthesis
1-acyl-sn-glycerol-3-phosphate acyltransferase gamma (EC 2.3.1.51) (1-acylglycerol-3-phosphate O-acyltransferase 3) (1-AGP acyltransferase 3) (1-AGPAT 3) (Lysophosphatidic acid acyltransferase gamma) (LPAAT-gamma)	Agpat3 Lpaat3	1.29	0.0052913	0.16624	lipid synthesis
1-acyl-sn-glycerol-3-phosphate acyltransferase gamma (EC 2.3.1.51) (1-acylglycerol-3-phosphate O-acyltransferase 3) (1-AGP acyltransferase 3) (1-AGPAT 3) (Lysophosphatidic acid acyltransferase gamma) (LPAAT-gamma)	Agpat3 Lpaat3	0.95	0.56367	0.74082	lipid synthesis
Acetoacetyl-CoA synthetase (EC 6.2.1.16)	Aacs	1.18	0.25926	0.74503	lipid synthesis
Acetoacetyl-CoA synthetase (EC 6.2.1.16)	Aacs	1.11	0.37756	0.61235	lipid synthesis
Acetyl-CoA carboxylase 1 (ACC1) (EC 6.4.1.2) (ACC-alpha) (Acetyl-CoA carboxylase 265) [Includes: Biotin carboxylase (EC 6.3.4.14)]	Acaca Acac Gm738	1.17	0.25419	0.74503	lipid synthesis
Acetyl-CoA carboxylase 1 (ACC1) (EC 6.4.1.2) (ACC-alpha) (Acetyl-CoA carboxylase 265) [Includes: Biotin carboxylase (EC 6.3.4.14)]	Acaca Acac Gm738	0.71	0.041121	0.36563	lipid synthesis
Acetyl-coenzyme A synthetase, cytoplasmic	Acss2	1.17	0.4402	0.79483	lipid synthesis
Acetyl-coenzyme A synthetase, cytoplasmic	Acss2	0.62	0.0031885	0.1115	lipid synthesis
Acyl-CoA desaturase 1 (EC 1.14.19.1) (Delta(9)-desaturase 1) (Delta-9 desaturase 1) (Fatty acid	Scd1	1.00	0.91519	0.99987	lipid synthesis

desaturase 1) (Stearoyl-CoA desaturase 1)					
Acyl-CoA desaturase 1 (EC 1.14.19.1) (Delta(9)-desaturase 1) (Delta-9 desaturase 1) (Fatty acid desaturase 1) (Stearoyl-CoA desaturase 1)	Scd1	0.60	0.020808	0.2796	lipid synthesis
Acyl-CoA synthetase family member 2, mitochondrial (EC 6.2.1.-)	Acsf2	1.62	0.0045716	0.15677	lipid synthesis
Acyl-CoA synthetase family member 2, mitochondrial (EC 6.2.1.-)	Acsf2	1.36	0.10847	0.53763	lipid synthesis
Acyl-CoA synthetase short-chain family member 3, mitochondrial (EC 6.2.1.1)	Acss3	0.61	0.0093065	0.2104	lipid synthesis
Acyl-CoA synthetase short-chain family member 3, mitochondrial (EC 6.2.1.1)	Acss3	0.46	0.0023009	0.088979	lipid synthesis
Acyl-coenzyme A thioesterase 1 (Acyl-CoA thioesterase 1) (EC 3.1.2.2) (CTE-I) (Inducible cytosolic acyl-coenzyme A thioester hydrolase) (Long chain acyl-CoA thioester hydrolase) (Long chain acyl-CoA hydrolase)	Acot1 Cte1	36.70	0.024035	0.32309	lipid synthesis
Acyl-coenzyme A thioesterase 1 (Acyl-CoA thioesterase 1) (EC 3.1.2.2) (CTE-I) (Inducible cytosolic acyl-coenzyme A thioester hydrolase) (Long chain acyl-CoA thioester hydrolase) (Long chain acyl-CoA hydrolase)	Acot1 Cte1	1.35	0.073808	0.46655	lipid synthesis
Acyl-coenzyme A thioesterase 11 (Acyl-CoA thioesterase 11) (EC 3.1.2.-) (Acyl-CoA thioester hydrolase 11) (Adipose-associated thioesterase) (Brown fat-inducible thioesterase) (BFIT)	Acot11 Bfit Thea	1.71	0.0058895	0.17469	lipid synthesis
Acyl-coenzyme A thioesterase 11 (Acyl-CoA thioesterase 11) (EC 3.1.2.-) (Acyl-CoA thioester hydrolase 11) (Adipose-associated thioesterase) (Brown fat-inducible thioesterase) (BFIT)	Acot11 Bfit Thea	0.96	0.68931	0.83793	lipid synthesis
ATP-citrate synthase (EC 2.3.3.8) (ATP-citrate (pro-S-)-lyase) (Citrate cleavage enzyme)	Acly	1.21	0.2672	0.74503	lipid synthesis
ATP-citrate synthase (EC 2.3.3.8) (ATP-citrate (pro-S-)-lyase) (Citrate cleavage enzyme)	Acly	0.79	0.11003	0.53763	lipid synthesis
Elongation of very long chain fatty acids protein 6 (EC 2.3.1.199) (3-keto acyl-CoA synthase Elovl6) (ELOVL fatty acid elongase 6) (ELOVL FA elongase 6) (Fatty acyl-CoA elongase) (Long chain fatty acid elongase) (Myelin-associated SUR4 protein) (Very long chain 3-ketoacyl-CoA synthase 6) (Very long chain 3-oxoacyl-CoA synthase 6)	Elovl6 Face Lce Masr	0.78	0.37499	0.61078	lipid synthesis
Ethanolamine-phosphate cytidylyltransferase (Phosphate cytidylyltransferase 2, ethanolamine, isoform CRA_b)	Pcyt2 mCG_2151	1.25	0.25645	0.74503	lipid synthesis
Ethanolamine-phosphate cytidylyltransferase (Phosphate cytidylyltransferase 2, ethanolamine, isoform CRA_b)	Pcyt2 mCG_2151	1.08	0.72897	0.86549	lipid synthesis
Fat storage-inducing transmembrane protein 2 (Fat-inducing protein 2)	Fitm2 Fit2	1.21	0.016606	0.28634	lipid synthesis

Fat storage-inducing transmembrane protein 2 (Fat-inducing protein 2)	Fitm2 Fit2	1.05	0.76492	0.89413	lipid synthesis
Fatty acid synthase (EC 2.3.1.85) [Includes: [Acyl-carrier-protein] S-acetyltransferase (EC 2.3.1.38); [Acyl-carrier-protein] S-malonyltransferase (EC 2.3.1.39); 3-oxoacyl-[acyl-carrier-protein] synthase (EC 2.3.1.41); 3-oxoacyl-[acyl-carrier-protein] reductase (EC 1.1.1.100); 3-hydroxyacyl-[acyl-carrier-protein] dehydratase (EC 4.2.1.59); Enoyl-[acyl-carrier-protein] reductase (EC 1.3.1.39); Oleoyl-[acyl-carrier-protein] hydrolase (EC 3.1.2.14)]	Fasn	1.67	0.02149	0.32309	lipid synthesis
Fatty acid synthase (EC 2.3.1.85) [Includes: [Acyl-carrier-protein] S-acetyltransferase (EC 2.3.1.38); [Acyl-carrier-protein] S-malonyltransferase (EC 2.3.1.39); 3-oxoacyl-[acyl-carrier-protein] synthase (EC 2.3.1.41); 3-oxoacyl-[acyl-carrier-protein] reductase (EC 1.1.1.100); 3-hydroxyacyl-[acyl-carrier-protein] dehydratase (EC 4.2.1.59); Enoyl-[acyl-carrier-protein] reductase (EC 1.3.1.39); Oleoyl-[acyl-carrier-protein] hydrolase (EC 3.1.2.14)]	Fasn	0.80	0.10603	0.53763	lipid synthesis
Glycerol-3-phosphate acyltransferase 1, mitochondrial (GPAT-1) (EC 2.3.1.15) (P90)	Gpam Gpat1	1.22	0.25816	0.74503	lipid synthesis
Glycerol-3-phosphate acyltransferase 1, mitochondrial (GPAT-1) (EC 2.3.1.15) (P90)	Gpam Gpat1	1.26	0.11241	0.53763	lipid synthesis
Long-chain-fatty-acid--CoA ligase 5 (EC 6.2.1.3) (Long-chain acyl-CoA synthetase 5) (LACS 5)	Acsl5 Facl5	1.77	0.023602	0.32309	lipid synthesis
Long-chain-fatty-acid--CoA ligase 5 (EC 6.2.1.3) (Long-chain acyl-CoA synthetase 5) (LACS 5)	Acsl5 Facl5	1.02	0.93455	0.98774	lipid synthesis
Phosphatidylserine decarboxylase proenzyme, mitochondrial (Fragment)	Pisd	1.84	0.0092735	0.2104	lipid synthesis
Phosphatidylserine decarboxylase proenzyme, mitochondrial (Fragment)	Pisd	1.56	0.066509	0.45262	lipid synthesis
Phosphoethanolamine/phosphocholine phosphatase (EC 3.1.3.75)	Phospho1	1.99	0.0002225	0.016976	lipid synthesis
Phosphoethanolamine/phosphocholine phosphatase (EC 3.1.3.75)	Phospho1	1.48	0.031383	0.31165	lipid synthesis
Very-long-chain (3R)-3-hydroxyacyl-CoA dehydratase 2 (EC 4.2.1.134) (3-hydroxyacyl-CoA dehydratase 2) (HACD2) (Protein-tyrosine phosphatase-like member B)	Hacd2 Ptplb	1.08	0.41216	0.78012	lipid synthesis
Very-long-chain (3R)-3-hydroxyacyl-CoA dehydratase 2 (EC 4.2.1.134) (3-hydroxyacyl-CoA dehydratase 2) (HACD2) (Protein-tyrosine phosphatase-like member B)	Hacd2 Ptplb	1.02	0.96634	0.99699	lipid synthesis
Very-long-chain 3-oxoacyl-CoA reductase (EC 1.1.1.330) (17-beta-hydroxysteroid dehydrogenase 12) (17-beta-HSD 12) (3-ketoacyl-CoA reductase) (KAR) (Estradiol 17-beta-dehydrogenase 12) (EC 1.1.1.62) (KIK-I)	Hsd17b12 Kik1	1.13	0.097187	0.61407	lipid synthesis
Very-long-chain 3-oxoacyl-CoA reductase (EC 1.1.1.330) (17-beta-	Hsd17b12 Kik1	0.92	0.52104	0.72087	lipid synthesis

hydroxysteroid dehydrogenase 12) (17-beta-HSD 12) (3-ketoacyl-CoA reductase) (KAR) (Estradiol 17-beta-dehydrogenase 12) (EC 1.1.1.62) (KIK-I)					
Very-long-chain enoyl-CoA reductase (EC 1.3.1.93) (Synaptic glycoprotein SC2) (Trans-2,3-enoyl-CoA reductase) (TER)	Tecr Gpsn2	1.17	0.10945	0.62149	lipid synthesis
Very-long-chain enoyl-CoA reductase (EC 1.3.1.93) (Synaptic glycoprotein SC2) (Trans-2,3-enoyl-CoA reductase) (TER)	Tecr Gpsn2	0.82	0.084422	0.49719	lipid synthesis
Phosphoenolpyruvate carboxykinase, cytosolic [GTP] (PEPCK-C) (EC 4.1.1.32)	Pck1 Pepck	0.98	0.83336	0.99004	Pck1
Phosphoenolpyruvate carboxykinase, cytosolic [GTP] (PEPCK-C) (EC 4.1.1.32)	Pck1 Pepck	1.16	0.42279	0.64573	Pck1
6-phosphogluconate dehydrogenase, decarboxylating (EC 1.1.1.44)	Pgd	1.18	0.23996	0.74503	pentose phosphate
6-phosphogluconate dehydrogenase, decarboxylating (EC 1.1.1.44)	Pgd	0.91	0.41813	0.64325	pentose phosphate
Glucose-6-phosphate 1-dehydrogenase X (G6PD) (EC 1.1.1.49)	G6pdx G6pd G6pd-1	0.93	0.59961	0.86155	pentose phosphate
Glucose-6-phosphate 1-dehydrogenase X (G6PD) (EC 1.1.1.49)	G6pdx G6pd G6pd-1	0.69	0.015024	0.24603	pentose phosphate
Ribose-5-phosphate isomerase (EC 5.3.1.6) (Phosphoriboisomerase)	Rpia Rpi	1.55	0.0001829	0.01509	pentose phosphate
Ribose-5-phosphate isomerase (EC 5.3.1.6) (Phosphoriboisomerase)	Rpia Rpi	1.14	0.018201	0.27826	pentose phosphate
Transaldolase (EC 2.2.1.2)	Taldo1	1.23	0.13398	0.62149	pentose phosphate
Transaldolase (EC 2.2.1.2)	Taldo1	0.77	0.069522	0.4552	pentose phosphate
Transketolase (TK) (EC 2.2.1.1) (P68)	Tkt	1.45	0.0065062	0.18217	pentose phosphate
Transketolase (TK) (EC 2.2.1.1) (P68)	Tkt	1.08	0.58799	0.75764	pentose phosphate
Glycogen [starch] synthase, liver (EC 2.4.1.11)	Gys2	0.16	0.013628	0.26103	starch
Glycogen [starch] synthase, liver (EC 2.4.1.11)	Gys2	0.69	0.12628	0.53763	starch
Glycogen phosphorylase, liver form (EC 2.4.1.1)	Pygl	1.46	0.0084635	0.20525	starch
Glycogen phosphorylase, liver form (EC 2.4.1.1)	Pygl	0.81	0.14479	0.55406	starch
UTP--glucose-1-phosphate uridylyltransferase (EC 2.7.7.9) (UDP-glucose pyrophosphorylase) (UDPGP) (UGPase)	Ugp2	0.99	0.9321	0.99987	starch
UTP--glucose-1-phosphate uridylyltransferase (EC 2.7.7.9) (UDP-glucose pyrophosphorylase) (UDPGP) (UGPase)	Ugp2	1.11	0.18823	0.59788	starch
Mitochondrial brown fat uncoupling protein 1 (UCP 1) (Solute carrier family 25 member 7) (Thermogenin)	Ucp1 Slc25a7 Ucp	1.73	0.010701	0.22838	Ucp1
Mitochondrial brown fat uncoupling protein 1 (UCP 1) (Solute carrier family 25 member 7) (Thermogenin)	Ucp1 Slc25a7 Ucp	1.12	0.56239	0.74002	Ucp1

A/J and B6 mice were exposed to thermoneutral housing temperature (30°C) or to cold (6°C) for 7 days (n=4-6). Proteomic data were analyzed and assigned to KEGG metabolic pathways. Fold change (FC) between A/J and B6 mice was counted, transparent background corresponds to thermoneutral, blue to cold-exposed mice.

STable 4.2.3 Selected proteins from proteomic analysis of gastrocnemius muscle in A/J and B6 mice.

Protein name	Gene name	FC 30°C/6°C	p_raw	p_FDR	KEGG pathway
Beta-enolase (EC 4.2.1.11) (2-phospho-D-glycerate hydro-lyase) (Enolase 3) (Muscle-specific enolase) (MSE) (Skeletal muscle enolase)	Eno3 Eno-3	1.00	0.92691	0.99959	glycolysis
Beta-enolase (EC 4.2.1.11) (2-phospho-D-glycerate hydro-lyase) (Enolase 3) (Muscle-specific enolase) (MSE) (Skeletal muscle enolase)	Eno3 Eno-3	1.00	0.92896	0.99999	glycolysis
Fructose-bisphosphate aldolase (EC 4.1.2.13)	Aldoart1	0.03	0.14744	0.93301	glycolysis
Fructose-bisphosphate aldolase (EC 4.1.2.13)	Aldoart1	2.81	0.38855	0.95655	glycolysis
Fructose-bisphosphate aldolase A (EC 4.1.2.13) (Aldolase 1) (Muscle-type aldolase)	Aldoa Aldo1	0.95	0.26894	0.93301	glycolysis
Fructose-bisphosphate aldolase A (EC 4.1.2.13) (Aldolase 1) (Muscle-type aldolase)	Aldoa Aldo1	0.97	0.62759	0.96144	glycolysis
Glucose-6-phosphate isomerase (GPI) (EC 5.3.1.9) (Autocrine motility factor) (AMF) (Neuroleukin) (NLK) (Phosphoglucose isomerase) (PGI) (Phosphohexose isomerase) (PHI)	Gpi Gpi1	0.99	0.72315	0.99164	glycolysis
Glucose-6-phosphate isomerase (GPI) (EC 5.3.1.9) (Autocrine motility factor) (AMF) (Neuroleukin) (NLK) (Phosphoglucose isomerase) (PGI) (Phosphohexose isomerase) (PHI)	Gpi Gpi1	0.94	0.40399	0.95655	glycolysis
Hexokinase-2 (EC 2.7.1.1) (Hexokinase type II) (HK II)	Hk2	0.82	0.0038374	0.35284	glycolysis
Hexokinase-2 (EC 2.7.1.1) (Hexokinase type II) (HK II)	Hk2	0.89	0.024175	0.95655	glycolysis
Phosphoglucomutase-1 (PGM 1) (EC 5.4.2.2) (Glucose phosphomutase 1) (Phosphoglucomutase-2)	Pgm1 Pgm2	0.94	0.14788	0.93301	glycolysis
Phosphoglucomutase-1 (PGM 1) (EC 5.4.2.2) (Glucose phosphomutase 1) (Phosphoglucomutase-2)	Pgm1 Pgm2	1.00	0.93713	0.99999	glycolysis
Phosphoglycerate kinase 1 (EC 2.7.2.3)	Pgk1 Pgk-1	0.98	0.65422	0.9575	glycolysis
Phosphoglycerate kinase 1 (EC 2.7.2.3)	Pgk1 Pgk-1	0.92	0.12879	0.95655	glycolysis
Phosphoglycerate mutase 2 (EC 5.4.2.11) (EC 5.4.2.4) (BPG-dependent PGAM 2) (Muscle-specific phosphoglycerate mutase) (Phosphoglycerate mutase isozyme M) (PGAM-M)	Pgam2	0.96	0.5747	0.94932	glycolysis
Phosphoglycerate mutase 2 (EC 5.4.2.11) (EC 5.4.2.4) (BPG-dependent PGAM 2) (Muscle-specific phosphoglycerate mutase) (Phosphoglycerate mutase isozyme M) (PGAM-M)	Pgam2	1.08	0.25141	0.95655	glycolysis
Pyruvate kinase PKM (EC 2.7.1.40) (Pyruvate kinase muscle isozyme)	Pkm Pk3 Pkm2 Pykm	1.00	0.99014	0.99959	glycolysis
Pyruvate kinase PKM (EC 2.7.1.40) (Pyruvate kinase muscle isozyme)	Pkm Pk3 Pkm2 Pykm	0.96	0.35804	0.95655	glycolysis
Triosephosphate isomerase (TIM) (EC 5.3.1.1) (Triose-phosphate isomerase)	Tpi1 Tpi	0.95	0.22471	0.93301	glycolysis
Triosephosphate isomerase (TIM) (EC 5.3.1.1) (Triose-phosphate isomerase)	Tpi1 Tpi	0.99	0.68741	0.97634	glycolysis
ATP synthase F(0) complex subunit B1, mitochondrial (ATP synthase subunit b) (ATPase subunit b)	Atp5f1	0.93	0.36126	0.94327	OXPHOS
ATP synthase F(0) complex subunit B1, mitochondrial (ATP synthase subunit b) (ATPase subunit b)	Atp5f1	0.96	0.80294	0.99999	OXPHOS

ATP synthase F(0) complex subunit C2, mitochondrial (ATP synthase lipid-binding protein) (ATP synthase membrane subunit c locus 2) (ATP synthase proteolipid P2) (ATPase protein 9) (ATPase subunit c)	Atp5mc2 Atp5g2	1.11	0.37004	0.94327	OXPHOS
ATP synthase F(0) complex subunit C2, mitochondrial (ATP synthase lipid-binding protein) (ATP synthase membrane subunit c locus 2) (ATP synthase proteolipid P2) (ATPase protein 9) (ATPase subunit c)	Atp5mc2 Atp5g2	1.28	0.31711	0.95655	OXPHOS
ATP synthase subunit alpha, mitochondrial (ATP synthase F1 subunit alpha)	Atp5f1a Atp5a1	1.01	0.98506	0.99959	OXPHOS
ATP synthase subunit alpha, mitochondrial (ATP synthase F1 subunit alpha)	Atp5f1a Atp5a1	0.95	0.41962	0.95655	OXPHOS
ATP synthase subunit beta, mitochondrial (EC 3.6.3.14) (ATP synthase F1 subunit beta)	Atp5f1b Atp5b	0.95	0.64801	0.95629	OXPHOS
ATP synthase subunit beta, mitochondrial (EC 3.6.3.14) (ATP synthase F1 subunit beta)	Atp5f1b Atp5b	0.90	0.16308	0.95655	OXPHOS
ATP synthase subunit d, mitochondrial	Atp5pd	0.89	0.43693	0.94932	OXPHOS
ATP synthase subunit d, mitochondrial	Atp5pd	0.93	0.34577	0.95655	OXPHOS
ATP synthase subunit delta, mitochondrial (ATP synthase F1 subunit delta) (F-ATPase delta subunit)	Atp5f1d Atp5d	0.96	0.39344	0.94839	OXPHOS
ATP synthase subunit delta, mitochondrial (ATP synthase F1 subunit delta) (F-ATPase delta subunit)	Atp5f1d Atp5d	0.88	0.27865	0.95655	OXPHOS
ATP synthase subunit e, mitochondrial (ATPase subunit e) (ATP synthase membrane subunit e)	Atp5me Atp5i Atp5k Lfm-1 Lfm1	0.93	0.49294	0.94932	OXPHOS
ATP synthase subunit e, mitochondrial (ATPase subunit e) (ATP synthase membrane subunit e)	Atp5me Atp5i Atp5k Lfm-1 Lfm1	0.87	0.10131	0.95655	OXPHOS
ATP synthase subunit f, mitochondrial	Atp5j2	0.68	0.043335	0.93301	OXPHOS
ATP synthase subunit f, mitochondrial	Atp5j2	0.94	0.47673	0.95655	OXPHOS
ATP synthase subunit g, mitochondrial (ATPase subunit g)	Atp5l	0.86	0.20257	0.93301	OXPHOS
ATP synthase subunit g, mitochondrial (ATPase subunit g)	Atp5l	0.83	0.1348	0.95655	OXPHOS
ATP synthase subunit O, mitochondrial (Oligomycin sensitivity conferral protein) (OSCP)	Atp5o D12Wsu28e	0.86	0.22875	0.93301	OXPHOS
ATP synthase subunit O, mitochondrial (Oligomycin sensitivity conferral protein) (OSCP)	Atp5o D12Wsu28e	0.88	0.14575	0.95655	OXPHOS
ATP synthase-coupling factor 6, mitochondrial (ATPase subunit F6)	Atp5j	0.91	0.18229	0.93301	OXPHOS
ATP synthase-coupling factor 6, mitochondrial (ATPase subunit F6)	Atp5j	0.96	0.73642	0.99972	OXPHOS
Cytochrome c oxidase subunit 7A-related protein, mitochondrial (Cytochrome c oxidase subunit VIIa-related protein) (Silica-induced gene 81 protein) (SIG-81) (Supercomplex assembly factor I)	Cox7a2l Cox7rp Scaf1 Silg81	0.95	0.62075	0.95022	OXPHOS
Cytochrome c oxidase subunit 7A-related protein, mitochondrial (Cytochrome c oxidase subunit VIIa-related protein) (Silica-induced gene 81 protein) (SIG-81) (Supercomplex assembly factor I)	Cox7a2l Cox7rp Scaf1 Silg81	0.71	0.59343	0.95655	OXPHOS
Cytochrome c oxidase subunit 8B, mitochondrial (Cytochrome c oxidase polypeptide VIII-heart) (Cytochrome c	Cox8b Cox8h	0.87	0.42736	0.94932	OXPHOS

oxidase subunit 8-1) (Cytochrome c oxidase subunit 8H)					
Cytochrome c oxidase subunit 8B, mitochondrial (Cytochrome c oxidase polypeptide VIII-heart) (Cytochrome c oxidase subunit 8-1) (Cytochrome c oxidase subunit 8H)	Cox8b Cox8h	1.39	0.17505	0.95655	OXPHOS
NADH dehydrogenase (ubiquinone) complex I, assembly factor 6	Ndufaf6	0.89	0.95949	0.99959	OXPHOS
NADH dehydrogenase (ubiquinone) complex I, assembly factor 6	Ndufaf6	0.17	0.34659	0.95655	OXPHOS
NADH dehydrogenase [ubiquinone] 1 alpha subcomplex assembly factor 2 (Mimitin) (Myc-induced mitochondrial protein) (MMTN) (NDUFA12-like protein)	Ndufaf2 Ndufa12l	2.80	0.032032	0.89582	OXPHOS
NADH dehydrogenase [ubiquinone] 1 alpha subcomplex assembly factor 2 (Mimitin) (Myc-induced mitochondrial protein) (MMTN) (NDUFA12-like protein)	Ndufaf2 Ndufa12l	4.94	0.19739	0.95655	OXPHOS
NADH dehydrogenase [ubiquinone] 1 alpha subcomplex subunit 13 (Cell death regulatory protein GRIM-19) (Complex I-B16.6) (CI-B16.6) (Gene associated with retinoic and interferon-induced mortality 19 protein) (GRIM-19) (Gene associated with retinoic and IFN-induced mortality 19 protein) (NADH-ubiquinone oxidoreductase B16.6 subunit)	Ndufa13 Grim19	0.83	0.14633	0.93301	OXPHOS
NADH dehydrogenase [ubiquinone] 1 alpha subcomplex subunit 13 (Cell death regulatory protein GRIM-19) (Complex I-B16.6) (CI-B16.6) (Gene associated with retinoic and interferon-induced mortality 19 protein) (GRIM-19) (Gene associated with retinoic and IFN-induced mortality 19 protein) (NADH-ubiquinone oxidoreductase B16.6 subunit)	Ndufa13 Grim19	0.97	0.75923	0.99999	OXPHOS
NADH dehydrogenase [ubiquinone] 1 alpha subcomplex subunit 3 (Complex I-B9) (CI-B9) (NADH-ubiquinone oxidoreductase B9 subunit)	Ndufa3	0.60	0.029912	0.89582	OXPHOS
NADH dehydrogenase [ubiquinone] 1 alpha subcomplex subunit 3 (Complex I-B9) (CI-B9) (NADH-ubiquinone oxidoreductase B9 subunit)	Ndufa3	1.36	0.24418	0.95655	OXPHOS
NADH dehydrogenase [ubiquinone] 1 alpha subcomplex subunit 8 (Complex I-19kD) (CI-19kD) (Complex I-PGIV) (CI-PGIV) (NADH-ubiquinone oxi-doreductase 19 kDa subunit)	Ndufa8	0.84	0.053898	0.93301	OXPHOS
NADH dehydrogenase [ubiquinone] 1 alpha subcomplex subunit 8 (Complex I-19kD) (CI-19kD) (Complex I-PGIV) (CI-PGIV) (NADH-ubiquinone oxi-doreductase 19 kDa subunit)	Ndufa8	1.03	0.81742	0.99999	OXPHOS
NADH dehydrogenase [ubiquinone] 1 beta subcomplex subunit 1 (Complex I-MNLL) (CI-MNLL) (NADH-ubiquinone oxidoreductase MNLL subunit)	Ndufb1	0.71	0.011636	0.54511	OXPHOS
NADH dehydrogenase [ubiquinone] 1 beta subcomplex subunit 1 (Complex I-MNLL) (CI-MNLL) (NADH-ubiquinone oxidoreductase MNLL subunit)	Ndufb1	1.06	0.6539	0.96449	OXPHOS

NADH dehydrogenase [ubiquinone] 1 beta subcomplex subunit 8, mitochondrial (Complex I-ASHI) (CI-ASHI) (NADH-ubiquinone oxidoreductase ASHI subunit)	Ndufb8	0.85	0.14947	0.93301	OXPHOS
NADH dehydrogenase [ubiquinone] 1 beta subcomplex subunit 8, mitochondrial (Complex I-ASHI) (CI-ASHI) (NADH-ubiquinone oxidoreductase ASHI subunit)	Ndufb8	1.02	0.79882	0.99999	OXPHOS
NADH dehydrogenase [ubiquinone] 1 subunit C2 (Complex I-B14.5b) (CI-B14.5b) (NADH-ubiquinone oxidoreductase subunit B14.5b)	Ndufc2	0.95	0.62246	0.95027	OXPHOS
NADH dehydrogenase [ubiquinone] 1 subunit C2 (Complex I-B14.5b) (CI-B14.5b) (NADH-ubiquinone oxidoreductase subunit B14.5b)	Ndufc2	1.06	0.59667	0.95798	OXPHOS
NADH dehydrogenase [ubiquinone] flavoprotein 3, mitochondrial (Complex I-9kD) (CI-9kD) (NADH-ubiquinone oxidoreductase 9 kDa subunit)	Ndufv3	1.09	0.89706	0.99959	OXPHOS
NADH dehydrogenase [ubiquinone] flavoprotein 3, mitochondrial (Complex I-9kD) (CI-9kD) (NADH-ubiquinone oxidoreductase 9 kDa subunit)	Ndufv3	1.12	0.031707	0.95655	OXPHOS
NADH dehydrogenase [ubiquinone] iron-sulfur protein 2, mitochondrial (EC 1.6.5.3) (EC 1.6.99.3) (Complex I-49kD) (CI-49kD) (NADH-ubiquinone oxidoreductase 49 kDa subunit)	Ndufs2	0.91	0.42139	0.94932	OXPHOS
NADH dehydrogenase [ubiquinone] iron-sulfur protein 2, mitochondrial (EC 1.6.5.3) (EC 1.6.99.3) (Complex I-49kD) (CI-49kD) (NADH-ubiquinone oxidoreductase 49 kDa subunit)	Ndufs2	0.99	0.9317	0.99999	OXPHOS
NADH dehydrogenase [ubiquinone] iron-sulfur protein 5 (Complex I-15 kDa) (CI-15 kDa) (NADH-ubiquinone oxidoreductase 15 kDa subunit)	Ndufs5	0.95	0.5909	0.94932	OXPHOS
NADH dehydrogenase [ubiquinone] iron-sulfur protein 5 (Complex I-15 kDa) (CI-15 kDa) (NADH-ubiquinone oxidoreductase 15 kDa subunit)	Ndufs5	1.16	0.27845	0.95655	OXPHOS
Glycogen [starch] synthase, muscle (EC 2.4.1.11)	Gys1 Gys Gys3	0.84	0.030872	0.89582	starch
Glycogen [starch] synthase, muscle (EC 2.4.1.11)	Gys1 Gys Gys3	0.89	0.21493	0.95655	starch
Glycogen phosphorylase, muscle form (EC 2.4.1.1) (Myophosphorylase)	Pygm	1.04	0.23059	0.93301	starch
Glycogen phosphorylase, muscle form (EC 2.4.1.1) (Myophosphorylase)	Pygm	1.01	0.67451	0.9738	starch
UTP--glucose-1-phosphate uridylyltransferase (EC 2.7.7.9) (UDP-glucose pyrophosphorylase) (UDPGP) (UGPase)	Ugp2	0.84	0.0047343	0.3596	starch
UTP--glucose-1-phosphate uridylyltransferase (EC 2.7.7.9) (UDP-glucose pyrophosphorylase) (UDPGP) (UGPase)	Ugp2	0.81	0.00071701	0.62344	starch
2-oxoglutarate dehydrogenase, mitochondrial (EC 1.2.4.2) (2-oxoglutarate dehydrogenase complex component E1) (OGDC-E1) (Alpha-ketoglutarate dehydrogenase)	Ogdh Ki-aa4192	0.93	0.032818	0.89582	TCA
2-oxoglutarate dehydrogenase, mitochondrial (EC 1.2.4.2) (2-oxoglutarate dehydrogenase complex component E1) (OGDC-E1) (Alpha-ketoglutarate	Ogdh Ki-aa4192	0.95	0.46471	0.95655	TCA

dehydrogenase)					
Aconitate hydratase, mitochondrial (Aconitase) (EC 4.2.1.3) (Citrate hydro-lyase)	Aco2	0.93	0.33123	0.93301	TCA
Aconitate hydratase, mitochondrial (Aconitase) (EC 4.2.1.3) (Citrate hydro-lyase)	Aco2	0.97	0.48584	0.95655	TCA
Citrate synthase, mitochondrial (EC 2.3.3.1) (Citrate (Si)-synthase)	Cs	0.92	0.35427	0.93921	TCA
Citrate synthase, mitochondrial (EC 2.3.3.1) (Citrate (Si)-synthase)	Cs	1.01	0.88309	0.99999	TCA
Cytoplasmic aconitate hydratase (Aconitase) (EC 4.2.1.3) (Citrate hydro-lyase) (Iron regulatory protein 1) (IRP1) (Iron-responsive element-binding protein 1) (IRE-BP 1)	Aco1 Ireb1 Irebp	0.81	0.12331	0.93301	TCA
Cytoplasmic aconitate hydratase (Aconitase) (EC 4.2.1.3) (Citrate hydro-lyase) (Iron regulatory protein 1) (IRP1) (Iron-responsive element-binding protein 1) (IRE-BP 1)	Aco1 Ireb1 Irebp	1.26	0.21132	0.95655	TCA
Isocitrate dehydrogenase [NAD] subunit alpha, mitochondrial (EC 1.1.1.41) (Isocitric dehydrogenase subunit alpha) (NAD(+)-specific ICDH subunit alpha)	Idh3a	1.05	0.29978	0.93301	TCA
Isocitrate dehydrogenase [NAD] subunit alpha, mitochondrial (EC 1.1.1.41) (Isocitric dehydrogenase subunit alpha) (NAD(+)-specific ICDH subunit alpha)	Idh3a	1.02	0.88456	0.99999	TCA
Isocitrate dehydrogenase [NADP], mitochondrial (IDH) (EC 1.1.1.42) (ICD-M) (IDP) (NADP(+)-specific ICDH) (Oxalosuccinate decarboxylase)	Idh2	0.94	0.48439	0.94932	TCA
Isocitrate dehydrogenase [NADP], mitochondrial (IDH) (EC 1.1.1.42) (ICD-M) (IDP) (NADP(+)-specific ICDH) (Oxalosuccinate decarboxylase)	Idh2	1.00	0.90012	0.99999	TCA
Pyruvate carboxylase, mitochondrial (EC 6.4.1.1) (Pyruvic carboxylase) (PCB)	Pc Pcx	1.40	0.64128	0.95367	TCA
Pyruvate carboxylase, mitochondrial (EC 6.4.1.1) (Pyruvic carboxylase) (PCB)	Pc Pcx	0.94	0.65675	0.967	TCA

A/J and B6 mice were exposed to thermoneutral housing temperature (30°C) or to cold (6°C) for 7 days (*n*=4-6). Proteomic data were analyzed and assigned to KEGG metabolic pathways. Fold change (FC) between thermoneutral and cold-exposed mice was counted, transparent background corresponds to A/J mice, yellow to B6 mice.

STable 4.2.4 Selected proteins from proteomic analysis of gastrocnemius muscle in thermoneutral and cold exposed mice.

Protein name	Gene name	FC AJ/B6	p_raw	p_FDR	KEGG pathway
Beta-enolase (EC 4.2.1.11) (2-phospho-D-glycerate hydro-lyase) (Enolase 3) (Muscle-specific enolase) (MSE) (Skeletal muscle enolase)	Eno3 Eno-3	0.84	0.014676	0.17785	glycolysis
Beta-enolase (EC 4.2.1.11) (2-phospho-D-glycerate hydro-lyase) (Enolase 3) (Muscle-specific enolase) (MSE) (Skeletal muscle enolase)	Eno3 Eno-3	0.84	0.0013036	0.058396	glycolysis

Fructose-bisphosphate aldolase (EC 4.1.2.13)	Aldoart1	0.01	0.0054669	0.097345	glycolysis
Fructose-bisphosphate aldolase (EC 4.1.2.13)	Aldoart1	0.64	0.58608	0.86477	glycolysis
Fructose-bisphosphate aldolase A (EC 4.1.2.13) (Aldolase 1) (Muscle-type aldolase)	Aldoa Aldo1	0.79	0.0025481	0.066759	glycolysis
Fructose-bisphosphate aldolase A (EC 4.1.2.13) (Aldolase 1) (Muscle-type aldolase)	Aldoa Aldo1	0.80	0.0041188	0.10881	glycolysis
Glucose-6-phosphate isomerase (GPI) (EC 5.3.1.9) (Autocrine motility factor) (AMF) (Neuroleukin) (NLK) (Phosphoglucose isomerase) (PGI) (Phosphohexose isomerase) (PHI)	Gpi Gpi1	0.80	0.014215	0.17469	glycolysis
Glucose-6-phosphate isomerase (GPI) (EC 5.3.1.9) (Autocrine motility factor) (AMF) (Neuroleukin) (NLK) (Phosphoglucose isomerase) (PGI) (Phosphohexose isomerase) (PHI)	Gpi Gpi1	0.77	0.00052653	0.041637	glycolysis
Hexokinase-2 (EC 2.7.1.1) (Hexokinase type II) (HK II)	Hk2	0.88	0.034802	0.27248	glycolysis
Hexokinase-2 (EC 2.7.1.1) (Hexokinase type II) (HK II)	Hk2	0.95	0.22341	0.72954	glycolysis
Phosphoglucomutase-1 (PGM 1) (EC 5.4.2.2) (Glucose phosphomutase 1) (Phosphoglucomutase-2)	Pgm1 Pgm2	0.78	0.000022341	0.0055693	glycolysis
Phosphoglucomutase-1 (PGM 1) (EC 5.4.2.2) (Glucose phosphomutase 1) (Phosphoglucomutase-2)	Pgm1 Pgm2	0.82	0.0014252	0.060726	glycolysis
Phosphoglycerate kinase 1 (EC 2.7.2.3)	Pgk1 Pgk-1	0.83	0.00084975	0.040676	glycolysis
Phosphoglycerate kinase 1 (EC 2.7.2.3)	Pgk1 Pgk-1	0.78	0.0012819	0.058396	glycolysis
Phosphoglycerate mutase 2 (EC 5.4.2.11) (EC 5.4.2.4) (BPG-dependent PGAM 2) (Muscle-specific phosphoglycerate mutase) (Phosphoglycerate mutase isozyme M) (PGAM-M)	Pgam2	0.80	0.015294	0.1828	glycolysis
Phosphoglycerate mutase 2 (EC 5.4.2.11) (EC 5.4.2.4) (BPG-dependent PGAM 2) (Muscle-specific phosphoglycerate mutase) (Phosphoglycerate mutase isozyme M) (PGAM-M)	Pgam2	0.90	0.14765	0.63439	glycolysis
Pyruvate kinase PKM (EC 2.7.1.40) (Pyruvate kinase muscle isozyme)	Pkm Pk3 Pkm2 Pykm	0.84	0.0050441	0.092651	glycolysis
Pyruvate kinase PKM (EC 2.7.1.40) (Pyruvate kinase muscle isozyme)	Pkm Pk3 Pkm2 Pykm	0.81	0.0011296	0.054819	glycolysis
Triosephosphate isomerase (TIM) (EC 5.3.1.1) (Triosephosphate isomerase)	Tpi1 Tpi	0.82	0.000089614	0.01117	glycolysis
Triosephosphate isomerase (TIM) (EC 5.3.1.1) (Triosephosphate isomerase)	Tpi1 Tpi	0.85	0.0042249	0.10881	glycolysis
ATP synthase F(0) complex	Atp5f1	0.66	0.0021992	0.065998	OXPHOS

subunit B1, mitochondrial (ATP synthase subunit b) (ATPase subunit b)					
ATP synthase F(0) complex subunit B1, mitochondrial (ATP synthase subunit b) (ATPase subunit b)	Atp5f1	0.68	0.011615	0.21301	OXPHOS
ATP synthase F(0) complex subunit C2, mitochondrial (ATP synthase lipid-binding protein) (ATP synthase membrane subunit c locus 2) (ATP synthase proteolipid P2) (ATPase protein 9) (ATPase subunit c)	Atp5mc2 Atp5g2	0.38	0.0024227	0.066759	OXPHOS
ATP synthase F(0) complex subunit C2, mitochondrial (ATP synthase lipid-binding protein) (ATP synthase membrane subunit c locus 2) (ATP synthase proteolipid P2) (ATPase protein 9) (ATPase subunit c)	Atp5mc2 Atp5g2	0.44	0.13889	0.62911	OXPHOS
ATP synthase subunit alpha, mitochondrial (ATP synthase F1 subunit alpha)	Atp5f1a Atp5a1	0.78	0.017035	0.18963	OXPHOS
ATP synthase subunit alpha, mitochondrial (ATP synthase F1 subunit alpha)	Atp5f1a Atp5a1	0.73	0.00005939	0.011528	OXPHOS
ATP synthase subunit beta, mitochondrial (EC 3.6.3.14) (ATP synthase F1 subunit beta)	Atp5f1b Atp5b	0.76	0.016772	0.18963	OXPHOS
ATP synthase subunit beta, mitochondrial (EC 3.6.3.14) (ATP synthase F1 subunit beta)	Atp5f1b Atp5b	0.72	0.007594	0.15984	OXPHOS
ATP synthase subunit d, mitochondrial	Atp5pd	0.74	0.0060614	0.1017	OXPHOS
ATP synthase subunit d, mitochondrial	Atp5pd	0.77	0.046068	0.41272	OXPHOS
ATP synthase subunit delta, mitochondrial (ATP synthase F1 subunit delta) (F-ATPase delta subunit)	Atp5f1d Atp5d	0.76	0.07528	0.41836	OXPHOS
ATP synthase subunit delta, mitochondrial (ATP synthase F1 subunit delta) (F-ATPase delta subunit)	Atp5f1d Atp5d	0.69	0.00094093	0.051429	OXPHOS
ATP synthase subunit e, mitochondrial (ATPase subunit e) (ATP synthase membrane subunit e)	Atp5me Atp5i Atp5k Lfm-1 Lfm1	0.87	0.19956	0.59825	OXPHOS
ATP synthase subunit e, mitochondrial (ATPase subunit e) (ATP synthase membrane subunit e)	Atp5me Atp5i Atp5k Lfm-1 Lfm1	0.81	0.031481	0.35844	OXPHOS
ATP synthase subunit f, mitochondrial	Atp5j2	0.80	0.19661	0.59825	OXPHOS
ATP synthase subunit f, mitochondrial	Atp5j2	1.10	0.57938	0.86438	OXPHOS
ATP synthase subunit g, mitochondrial (ATPase subunit g)	Atp5l	0.76	0.093783	0.4636	OXPHOS
ATP synthase subunit g, mitochondrial (ATPase subunit g)	Atp5l	0.73	0.004594	0.11465	OXPHOS
ATP synthase subunit O, mitochondrial (Oligomycin	Atp5o D12Wsu28e	0.68	0.028343	0.24364	OXPHOS

sensitivity conferral protein) (OSCP)					
ATP synthase subunit O, mitochondrial (Oligomycin sensitivity conferral protein) (OSCP)	Atp5o D12Wsu28e	0.71	0.00045305	0.040532	OXPHOS
ATP synthase-coupling factor 6, mitochondrial (ATPase subunit F6)	Atp5j	0.71	0.0087363	0.12919	OXPHOS
ATP synthase-coupling factor 6, mitochondrial (ATPase subunit F6)	Atp5j	0.75	0.013799	0.24107	OXPHOS
Cytochrome c oxidase subunit 7A-related protein, mitochondrial (Cytochrome c oxidase subunit VIIa-related protein) (Silica-induced gene 81 protein) (SIG-81) (Supercomplex assembly factor I)	Cox7a2l Cox7rp Scaf1 Silg81	34.64	0.00021135	0.020625	OXPHOS
Cytochrome c oxidase subunit 7A-related protein, mitochondrial (Cytochrome c oxidase subunit VIIa-related protein) (Silica-induced gene 81 protein) (SIG-81) (Supercomplex assembly factor I)	Cox7a2l Cox7rp Scaf1 Silg81	25.60	0.00080474	0.05021	OXPHOS
Cytochrome c oxidase subunit 8B, mitochondrial (Cytochrome c oxidase polypeptide VIII-heart) (Cytochrome c oxidase subunit 8-1) (Cytochrome c oxidase subunit 8H)	Cox8b Cox8h	0.56	0.025793	0.23352	OXPHOS
Cytochrome c oxidase subunit 8B, mitochondrial (Cytochrome c oxidase polypeptide VIII-heart) (Cytochrome c oxidase subunit 8-1) (Cytochrome c oxidase subunit 8H)	Cox8b Cox8h	0.90	0.94193	0.99912	OXPHOS
NADH dehydrogenase (ubiquinone) complex I, assembly factor 6	Ndufaf6	18.00	0.040566	0.30123	OXPHOS
NADH dehydrogenase (ubiquinone) complex I, assembly factor 6	Ndufaf6	3.23	0.21995	0.72954	OXPHOS
NADH dehydrogenase [ubiquinone] 1 alpha subcomplex assembly factor 2 (Mimitin) (Myc-induced mitochondrial protein) (MMTN) (NDUFA12-like protein)	Ndufaf2 Ndufa12l	1.07	0.26431	0.64465	OXPHOS
NADH dehydrogenase [ubiquinone] 1 alpha subcomplex assembly factor 2 (Mimitin) (Myc-induced mitochondrial protein) (MMTN) (NDUFA12-like protein)	Ndufaf2 Ndufa12l	1.82	0.54512	0.8547	OXPHOS
NADH dehydrogenase [ubiquinone] 1 alpha subcomplex subunit 13 (Cell death regulatory protein GRIM-19) (Complex I-B16.6) (CI-B16.6) (Gene associated with retinoic and	Ndufa13 Grim19	0.79	0.048151	0.33211	OXPHOS

interferon-induced mortality 19 protein) (GRIM-19) (Gene associated with retinoic and IFN-induced mortality 19 protein) (NADH-ubiquinone oxidoreductase B16.6 subunit)					
NADH dehydrogenase [ubiquinone] 1 alpha subcomplex subunit 13 (Cell death regulatory protein GRIM-19) (Complex I-B16.6) (CI-B16.6) (Gene associated with retinoic and interferon-induced mortality 19 protein) (GRIM-19) (Gene associated with retinoic and IFN-induced mortality 19 protein) (NADH-ubiquinone oxidoreductase B16.6 subunit)	Ndufa13 Grim19	0.93	0.49257	0.84605	OXPHOS
NADH dehydrogenase [ubiquinone] 1 alpha subcomplex subunit 3 (Complex I-B9) (CI-B9) (NADH-ubiquinone oxidoreductase B9 subunit)	Ndufa3	0.55	0.0080922	0.12229	OXPHOS
NADH dehydrogenase [ubiquinone] 1 alpha subcomplex subunit 3 (Complex I-B9) (CI-B9) (NADH-ubiquinone oxidoreductase B9 subunit)	Ndufa3	1.25	0.33796	0.76742	OXPHOS
NADH dehydrogenase [ubiquinone] 1 alpha subcomplex subunit 8 (Complex I-19kD) (CI-19kD) (Complex I-PGIV) (CI-PGIV) (NADH-ubiquinone oxidoreductase 19 kDa subunit)	Ndufa8	0.76	0.017311	0.18963	OXPHOS
NADH dehydrogenase [ubiquinone] 1 alpha subcomplex subunit 8 (Complex I-19kD) (CI-19kD) (Complex I-PGIV) (CI-PGIV) (NADH-ubiquinone oxidoreductase 19 kDa subunit)	Ndufa8	0.93	0.35069	0.76885	OXPHOS
NADH dehydrogenase [ubiquinone] 1 beta subcomplex subunit 1 (Complex I-MNLL) (CI-MNLL) (NADH-ubiquinone oxidoreductase MNLL subunit)	Ndufb1	0.73	0.025331	0.23264	OXPHOS
NADH dehydrogenase [ubiquinone] 1 beta subcomplex subunit 1 (Complex I-MNLL) (CI-MNLL) (NADH-ubiquinone oxidoreductase MNLL subunit)	Ndufb1	1.09	0.41866	0.81776	OXPHOS
NADH dehydrogenase [ubiquinone] 1 beta subcomplex subunit 8, mitochondrial (Complex I-ASHI) (CI-ASHI) (NADH-ubiquinone oxidoreductase ASHI subunit)	Ndufb8	0.78	0.020689	0.21096	OXPHOS

NADH dehydrogenase [ubiquinone] 1 beta sub-complex subunit 8, mito-chondrial (Complex I-ASHI) (CI-ASHI) (NADH-ubiquinone oxidoreductase ASHI subunit)	Ndufb8	0.93	0.5315	0.85273	OXPHOS
NADH dehydrogenase [ubiquinone] 1 subunit C2 (Complex I-B14.5b) (CI-B14.5b) (NADH-ubiquinone oxidoreductase subunit B14.5b)	Ndufc2	0.74	0.039252	0.29719	OXPHOS
NADH dehydrogenase [ubiquinone] 1 subunit C2 (Complex I-B14.5b) (CI-B14.5b) (NADH-ubiquinone oxidoreductase subunit B14.5b)	Ndufc2	0.83	0.090321	0.57764	OXPHOS
NADH dehydrogenase [ubiquinone] flavoprotein 3, mitochondrial (Complex I-9kD) (CI-9kD) (NADH-ubiquinone oxidoreductase 9 kDa subunit)	Ndufv3	0.83	0.20245	0.59825	OXPHOS
NADH dehydrogenase [ubiquinone] flavoprotein 3, mitochondrial (Complex I-9kD) (CI-9kD) (NADH-ubiquinone oxidoreductase 9 kDa subunit)	Ndufv3	0.85	0.12572	0.6247	OXPHOS
NADH dehydrogenase [ubiquinone] iron-sulfur protein 2, mitochondrial (EC 1.6.5.3) (EC 1.6.99.3) (Complex I-49kD) (CI-49kD) (NADH-ubiquinone oxidoreductase 49 kDa subunit)	Ndufs2	0.81	0.040085	0.29975	OXPHOS
NADH dehydrogenase [ubiquinone] iron-sulfur protein 2, mitochondrial (EC 1.6.5.3) (EC 1.6.99.3) (Complex I-49kD) (CI-49kD) (NADH-ubiquinone oxidoreductase 49 kDa subunit)	Ndufs2	0.88	0.23909	0.7371	OXPHOS
NADH dehydrogenase [ubiquinone] iron-sulfur protein 5 (Complex I-15 kDa) (CI-15 kDa) (NADH-ubiquinone oxidoreductase 15 kDa subunit)	Ndufs5	0.73	0.042517	0.30532	OXPHOS
NADH dehydrogenase [ubiquinone] iron-sulfur protein 5 (Complex I-15 kDa) (CI-15 kDa) (NADH-ubiquinone oxidoreductase 15 kDa subunit)	Ndufs5	0.89	0.5317	0.85273	OXPHOS
Glycogen [starch] synthase, muscle (EC 2.4.1.11)	Gys1 Gys Gys3	0.87	0.10153	0.475	starch
Glycogen [starch] synthase, muscle (EC 2.4.1.11)	Gys1 Gys Gys3	0.93	0.36638	0.77853	starch
Glycogen phosphorylase, muscle form (EC 2.4.1.1) (Myophosphorylase)	Pygm	0.81	0.000071551	0.01117	starch
Glycogen phosphorylase, muscle form (EC 2.4.1.1) (Myophosphorylase)	Pygm	0.79	0.00012471	0.021788	starch

UTP--glucose-1-phosphate uridylyltransferase (EC 2.7.7.9) (UDP-glucose pyrophosphorylase) (UDPGP) (UGPase)	Ugp2	0.73	0.000041933	0.0081304	starch
UTP--glucose-1-phosphate uridylyltransferase (EC 2.7.7.9) (UDP-glucose pyrophosphorylase) (UDPGP) (UGPase)	Ugp2	0.70	0.000043867	0.0095795	starch
2-oxoglutarate dehydrogenase, mitochondrial (EC 1.2.4.2) (2-oxoglutarate dehydrogenase complex component E1) (OGDC-E1) (Alpha-ketoglutarate dehydrogenase)	Ogdh Kiaa4192	1.17	0.026808	0.23868	TCA
2-oxoglutarate dehydrogenase, mitochondrial (EC 1.2.4.2) (2-oxoglutarate dehydrogenase complex component E1) (OGDC-E1) (Alpha-ketoglutarate dehydrogenase)	Ogdh Kiaa4192	1.21	0.0016799	0.066117	TCA
Aconitate hydratase, mitochondrial (Aconitase) (EC 4.2.1.3) (Citrate hydrolyase)	Aco2	1.13	0.1551	0.53798	TCA
Aconitate hydratase, mitochondrial (Aconitase) (EC 4.2.1.3) (Citrate hydrolyase)	Aco2	1.16	0.014012	0.24188	TCA
Citrate synthase, mitochondrial (EC 2.3.3.1) (Citrate (Si)-synthase)	Cs	0.73	0.003641	0.082093	TCA
Citrate synthase, mitochondrial (EC 2.3.3.1) (Citrate (Si)-synthase)	Cs	0.79	0.004091	0.10881	TCA
Cytoplasmic aconitate hydratase (Aconitase) (EC 4.2.1.3) (Citrate hydrolyase) (Iron regulatory protein 1) (IRP1) (Iron-responsive element-binding protein 1) (IRE-BP 1)	Aco1 Ireb1 Irebp	0.94	0.80489	0.95514	TCA
Cytoplasmic aconitate hydratase (Aconitase) (EC 4.2.1.3) (Citrate hydrolyase) (Iron regulatory protein 1) (IRP1) (Iron-responsive element-binding protein 1) (IRE-BP 1)	Aco1 Ireb1 Irebp	1.46	0.0046704	0.11492	TCA
Isocitrate dehydrogenase [NAD] subunit alpha, mitochondrial (EC 1.1.1.41) (Isocitric dehydrogenase subunit alpha) (NAD(+)-specific ICDH subunit alpha)	Idh3a	0.91	0.20996	0.61065	TCA
Isocitrate dehydrogenase [NAD] subunit alpha, mitochondrial (EC 1.1.1.41) (Isocitric dehydrogenase subunit alpha) (NAD(+)-specific ICDH subunit alpha)	Idh3a	0.88	0.025717	0.31775	TCA
Isocitrate dehydrogenase [NADP], mitochondrial (IDH) (EC 1.1.1.42) (ICD-	Idh2	1.42	0.028305	0.24364	TCA

M) (IDP) (NADP(+)-specific ICDH) (Oxalosuccinate decarboxylase)					
Isocitrate dehydrogenase [NADP], mitochondrial (IDH) (EC 1.1.1.42) (ICD-M) (IDP) (NADP(+)-specific ICDH) (Oxalosuccinate decarboxylase)	Idh2	1.51	0.0032412	0.092825	TCA
Pyruvate carboxylase, mitochondrial (EC 6.4.1.1) (Pyruvic carboxylase) (PCB)	Pc Pcx	1.02	0.64372	0.85319	TCA
Pyruvate carboxylase, mitochondrial (EC 6.4.1.1) (Pyruvic carboxylase) (PCB)	Pc Pcx	0.69	0.017128	0.27203	TCA

A/J and B6 mice were exposed to thermoneutral housing temperature (30°C) or to cold (6°C) for 7 days (*n*=4-6). Proteomic data were analyzed and assigned to KEGG metabolic pathways. Fold change (FC) between A/J and B6 mice was counted, transparent background corresponds to thermoneutral, blue to cold-exposed mice.¨

Dataset 4.2.1 Acylcarnitines in BAT

Metabolite name (full)	AJ-TN	AJ-TN	AJ-TN	AJ-TN	AJ-TN	AJ-TN	AJ-CE	AJ-CE	AJ-CE	AJ-CE	AJ-CE	AJ-CE
ACar 2-M-4:0-OH (3-Hydroxyisovaleroylcarnitine)	30955	38294	25533	48216	24795	49453	469895	159782	193073	271427	586780	516952
ACar 22:0	595	812	1382	1301	802	1148	3370	1104	4331	6675	4290	1850
ACar 3:0-DC (Malonyl-carnitine)	82599	113244	51234	52641	87611	84358	372845	41716	119800	200915	375141	498922
ACar 15:2	84	84293	220722	9307	260587	298432	5233	364	90396	7876	32206	5583
ACar 5:1	6689	4799	13906	13744	5566	7373	25766	10580	13907	33661	24645	46411
ACar 5:0	74585	40866	93147	92997	36009	67275	108399	136271	85679	148217	103347	131596
ACar 2:0	4655272	2451691	10392454	8690860	3752633	6251243	11753141	11357987	9462024	9227179	12152665	15815248
ACar 20:0	9809	6422	59073	25535	23358	25435	59907	26202	94403	92378	58226	35025
ACar 4:0-OH (3-Hydroxybutyrylcarnitine)	122000	158269	466814	257159	133890	287036	578720	406706	494726	407619	685291	787220
ACar 18:1-OH (3-Hydroxyoleylcarnitine)	12654	10329	120665	55146	39139	21196	7059	26232	32106	20900	2844	12889
ACar 16:2 (2)	902	1250	16283	10653	6544	4340	904	4438	8350	3813	364	1693
ACar 3:0	379161	374033	612119	426284	294314	337872	504675	342991	292148	500478	596825	659982
ACar 16:0-OH (3-Hydroxyhexadecanoylcarnitine)	5089	4208	85483	30846	26302	17624	6718	14433	17295	12317	2918	9354
ACar 4:0	317257	238285	1465832	1023879	526430	888463	1051472	883985	868090	1206244	1081902	1355876
ACar 18:2 (2)	2782	2962	84499	36861	26217	13512	2454	14575	27777	15080	888	7234
ACar 20:5	196	98	293	1292	269	701	602	2676	2683	2154	208	881
ACar 12:1	2175	3094	25171	23861	9124	15179	6089	16460	23524	15529	5899	6646
ACar 16:1 (2)	1223	1400	39236	17310	16659	9848	2789	6994	10729	6483	1057	3674
ACar 8:1	216	332	2497	2646	1114	864	802	1964	3401	2206	1088	1813
ACar 14:1	26624	25254	220003	233380	55800	114288	23729	133207	229170	130645	14301	43620
ACar 6:0	25973	21560	166032	123379	43871	92627	49534	111569	143015	119062	47147	72503
ACar 15:1	180	278	2167	2279	587	1292	566	1760	2403	1793	459	937
ACar 20:2 (2)	83	92	24139	4671	7973	3601	1552	2032	3832	3175	718	799
ACar 22:1	6542	3672	47863	10188	10986	14108	16753	8029	18118	22064	12927	9400
ACar 17:1 (1)	1083	1374	5272	8390	1939	4963	919	4958	10000	7093	463	3346
ACar 22:2	1097	973	22703	5366	3459	4626	8249	6636	7465	10409	4800	7086
ACar 16:1 (1)	106333	142130	746904	797034	196562	544749	81230	430745	1007759	604112	37594	225715
ACar 20:1	16231	14170	437963	166347	115014	121478	53522	104942	195003	150117	23589	41107
ACar 13:0	213	942	2816	2021	3160	2752	1363	1805	15104	1990	5688	1122
ACar 10:1	2605	5059	29254	17487	20652	31771	11487	8762	21533	10700	10803	8472
ACar 20:3 (2)	500	636	9127	3754	1526	2137	708	3309	5847	4178	285	1084
ACar 18:3 (2)	203	314	10206	6614	3403	2531	1052	5212	8538	4742	399	2386
ACar 19:1 (2)	514	363	4391	2430	5217	3918	1162	61	1176	1576	875	719
ACar 19:1 (1)	429	321	2746	3419	1144	1915	397	2440	4110	2700	159	944
ACar 14:0	43655	48042	628363	442711	161535	265446	100714	274908	461082	335526	38737	123320
ACar 20:2 (1)	3922	5350	137603	69024	22997	39667	19407	76208	102808	108207	7782	25875
ACar 12:0	5769	6799	85106	66651	28425	52530	41245	59074	76842	63411	28533	25993
ACar 8:0	8321	7166	59972	50161	20036	34353	21614	48326	67169	47964	18014	26736
ACar 20:4	20238	22842	16921	35848	29089	27804	12606	32058	48531	51948	12141	41606
ACar 15:0	1299	953	5058	7257	2059	4307	1296	5864	11060	8542	518	2946
ACar 16:2 (1)	7104	8102	91440	94594	16835	47453	12345	97325	140440	110205	8192	35269
ACar 17:1 (2)	56	86	3310	1591	1466	1601	995	63	1180	1836	624	849
ACar 14:2	3593	2385	19597	39409	3651	20927	5619	48367	73593	44086	4590	12852
ACar 10:0	4902	4703	46240	42514	18954	30670	18161	48934	59068	38892	15561	15067
ACar 18:3 (1)	2014	3235	10479	23061	3148	15367	3801	21823	48734	42002	1497	10474
ACar 16:0	218428	233851	1921281	1753980	727089	1144974	315136	1139911	2630522	1596425	126607	685607
ACar 18:2 (1)	68309	102274	401364	781828	156013	497284	144723	651346	1544939	1233700	76089	529941
ACar 18:1	308339	353087	1893851	2667913	816091	1615589	271988	1456247	3317565	2458949	142361	1318930
ACar 17:0	1095	885	6442	6600	3192	3704	1481	5196	8979	6532	712	2762
ACar 20:3 (1)	1581	1511	7049	10355	4279	6371	3069	13131	21169	13461	952	6691
ACar 18:0	58871	53390	840404	441661	394293	343907	213709	266010	679115	452974	127197	256005

Metabolite name (full)	B6J-TN	B6J-TN	B6J-TN	B6J-TN	B6J-TN	B6J-TN	B6J-CE	B6J-CE	B6J-CE	B6J-CE	B6J-CE	B6J-CE
ACar 2-M-4:0-OH (3-Hydroxyisovaleroylcarnitine)	65604	27273	39282	26636	38438	32589	229665	133187	338845	183087	269474	255491
ACar 22:0	694	609	820	122	355	411	1324	2734	2026	2664	2031	1339
ACar 3:0-DC (Malonyl-carnitine)	29571	40292	31988	15342	46323	32858	236418	43495	378755	174619	452753	282759
ACar 15:2	611	442	149	225	181	58	252	280	753	148	2145	24
ACar 5:1	12192	14788	10060	10487	12463	6851	13056	19084	17916	45767	81726	64306
ACar 5:0	189151	94871	69250	165742	109511	79088	83074	165615	77826	198981	274617	287993
ACar 2:0	16270560	7239095	5356178	7969422	11578196	9162729	5500120	7730575	12552845	11258996	22485987	15361392
ACar 20:0	12660	40422	41729	4074	17290	3722	12007	50460	36265	49015	32168	14581
ACar 4:0-OH (3-Hydroxybutyrylcarnitine)	392860	414599	274804	195493	422666	206641	138282	163105	350104	566732	1003499	628761
ACar 18:1-OH (3-Hydroxyoleylcarnitine)	39756	158011	98007	14649	191409	30512	15920	34001	7258	23733	23737	29334
ACar 16:2 (2)	9644	24204	18578	3848	33619	4146	3091	8625	792	3236	1845	3457
ACar 3:0	1543712	640748	438221	1362938	902246	905952	424143	246266	644844	449619	2474906	1113638
ACar 16:0-OH (3-Hydroxyhexadecanoylcarnitine)	26175	98578	58753	9678	130652	14182	9024	20099	8660	25200	28523	14749
ACar 4:0	2521524	1424523	986271	970415	1343809	737008	624889	708568	1151781	1273313	2473681	1747378
ACar 18:2 (2)	28672	94676	60338	8508	137842	10338	6341	21606	2809	12362	4860	9520
ACar 20:5	1050	628	1115	300	726	480	1149	5327	512	1440	322	1015
ACar 12:1	38475	36235	23075	10526	49499	11735	15316	16439	8106	9398	8144	7781
ACar 16:1 (2)	15171	36754	24747	5624	57195	5605	3181	9922	3012	13343	7217	6111
ACar 8:1	2749	1948	1890	433	3004	1259	3451	3421	1318	2072	1878	2035
ACar 14:1	237575	415639	269841	55965	424787	72113	109106	191689	23700	77595	39481	61513
ACar 6:0	211384	196969	98836	67376	149793	64410	129287	159595	59505	96542	163046	90716
ACar 15:1	3231	4896	3124	551	4503	846	1293	2598	314	1173	583	1018
ACar 20:2 (2)	5388	26061	17623	1486	24097	1549	199	2696	987	4763	1287	1657
ACar 22:1	8919	53598	46349	2322	16542	1926	1308	10144	4436	11202	4470	3490
ACar 17:1 (1)	13136	17969	16468	1743	14737	2656	4258	9368	824	4261	2554	3622
ACar 22:2	7028	29903	23526	1479	10420	1542	823	8334	2536	4985	2155	2434
ACar 16:1 (1)	886334	1988256	1430048	172273	1636727	206333	414398	697495	72113	347471	188454	269470
ACar 20:1	159903	808244	671197	28974	406208	25457	23654	152917	36677	78177	41617	33435
ACar 13:0	2740	2418	2074	724	2888	652	1211	2573	978	1348	520	986
ACar 10:1	15190	6662	6288	2138	9829	6278	10509	12634	11450	6912	6933	7700
ACar 20:3 (2)	4286	11952	8421	741	9934	927	903	4271	584	2315	671	1098
ACar 18:3 (2)	5839	10420	9218	1723	20244	2437	3066	8746	972	3559	934	3048
ACar 19:1 (2)	1235	2912	2418	669	2732	360	501	456	1190	1717	3178	697
ACar 19:1 (1)	3909	6692	5614	636	4880	734	824	3785	329	1443	576	1103
ACar 14:0	507362	785097	555897	100926	974731	123168	202428	435859	120646	262291	151267	151290
ACar 20:2 (1)	89773	331124	242049	11068	164132	12556	20026	125650	13438	42081	14770	20916
ACar 12:0	85522	86670	51685	21154	94860	22699	51897	57560	47686	41932	51717	25998
ACar 8:0	69097	67802	35828	16472	42913	23907	45762	53500	20127	30283	39282	22390
ACar 20:4	31680	21998	23979	8087	22196	13209	21657	55026	14330	24137	18972	24840
ACar 15:0	9530	12161	11219	1512	11482	2201	4173	12365	949	5657	1303	3451
ACar 16:2 (1)	125613	155852	113885	15126	135617	25329	76297	170331	13092	50608	20748	33534
ACar 17:1 (2)	1892	2366	1859	768	2250	764	313	470	940	2683	3169	876
ACar 14:2	36128	25552	25797	4271	30728	13155	36849	64349	7581	21147	5235	11043
ACar 10:0	62682	44248	26122	12006	35366	17428	25546	32959	19275	22572	23076	14806
ACar 18:3 (1)	26784	31384	31627	3582	21886	6107	18943	38925	4196	19894	5095	8755
ACar 16:0	1560681	3974807	3343081	300422	3758113	321033	699915	1975296	273931	1083939	479064	517400
ACar 18:2 (1)	844540	923348	909375	100513	707545	196834	519666	1337696	123998	512932	284420	314884
ACar 18:1	2104421	4459309	3785561	360994	3768533	499161	969493	2479774	226910	985649	914804	979403
ACar 17:0	6990	11472	9465	1170	9114	1613	2400	8905	1297	4819	1548	2297
ACar 20:3 (1)	11900	17630	15190	2274	11610	2559	5152	26661	3280	7542	2635	5516
ACar 18:0	273675	934131	772927	75626	599950	72512	107061	416111	236915	370370	314053	146503

Dataset 4.2.2 Metabolites in BAT

Metabolite name (full)	AJ-TN	AJ-TN	AJ-TN	AJ-TN	AJ-TN	AJ-TN	AJ-CE	AJ-CE	AJ-CE	AJ-CE	AJ-CE	AJ-CE
Glycero-3-phosphocholine	8084035	6695226	8492851	4474279	6234651	4721598	1155541	616626	515243	574700	1364448	1364718
Ergothioneine	150092	145834	145259	90741	145118	124217	64534	74234	57029	71881	59389	75671
Urea	392624	329112	254125	402100	247083	333342	584202	916606	605457	844320	736287	717965
Trigonelline	117248	157376	121828	264537	104488	235427	385202	654327	388116	488564	496171	488479
Threonine	32602	37062	22427	36197	26217	32452	51281	41629	33662	55224	48839	53601
Citrulline	97375	169670	67383	139392	149354	132745	268363	223338	185329	297821	241285	290954
Glutathione (reduced)	293954	371547	180712	216791	255357	296195	607756	189344	318435	789998	716699	744979
N-Acetylornithine	5710	6853	4273	8207	4065	7718	10821	14210	12080	14110	11588	14168
Stachydrine (proline betaine)	85246	109188	95035	112682	113599	107306	308777	178991	142325	191833	419152	385601
1-Methylnicotinamide	45675	43341	34815	38958	22662	63937	42518	105592	42679	52490	54088	53537
Ornithine	2276	3476	1813	2752	2278	2530	4874	10969	3367	6610	4693	5802
Nepsilon-Methyllysine	2149	2876	2392	3048	2079	2491	5237	8422	4654	7499	5184	6087
Serine	14684	17754	9836	15536	10266	15751	23031	24566	18075	20015	19670	24615
N-Acetylhistamine	5148	7099	7149	11093	8692	7930	8018	9728	7381	11552	6149	13510
Betaine	7881713	13303668	6269210	10004482	10963568	6415133	34741800	10911281	12604920	17660446	42208359	41643542
Tryptophan	25753	25207	16869	26773	22017	20971	31559	44133	33958	33454	30637	35911
Phenylalanine	63557	60520	36151	60930	37471	51219	70587	113614	68480	79300	68791	85187
Isoleucine	53922	49617	29607	50209	33931	52348	63813	110114	62907	95471	59849	71234
Aspartic acid	15053	28183	9374	20096	17010	20084	38897	20424	33032	46857	39048	42921
Proline	197401	177331	106738	233678	119071	169223	264103	749473	355162	314655	184444	318674
Leucine	109809	99870	51016	99216	55232	100747	124068	209668	108114	171975	109452	139585
Methionine	22137	20086	12835	22518	15267	19260	21747	30833	20975	25184	22163	26760
N6,N6,N6-Trimethyllysine	32032	56348	35455	38333	32288	40921	75528	79267	56265	79389	81934	85144
N,N-Dimethylglycine	17455	30203	13643	28541	19095	25749	22819	52711	32609	32422	26587	31386
Glutamine	375886	590563	303837	812014	368201	758614	912441	1479111	1040635	1174601	690235	841702
Dihydroxyphenylalanine	97675	151339	66199	122657	126604	114200	179549	157017	146805	234566	177638	205344
Pantothenic acid	767010	733302	661085	556235	599228	646690	481172	328723	327910	570260	504233	558397
Glycerol-2-phosphate	6744	4742	1084	6783	2443	3252	8697	14642	8464	10255	8206	16877
TMAO	467441	624903	359681	372206	282039	414852	644354	682834	425008	598421	623670	576950
Glutamic acid	208733	473833	118489	182038	400759	216370	527122	221135	245298	472551	356907	460991
gamma-Butyrobetaine	429899	524423	459392	432877	404851	409070	1452653	506308	561034	804992	2056695	1781477
Histidine	84111	93162	49527	94137	34830	96252	127744	242099	170882	208251	106759	128988
5'-S-methyl-5'-thioadenosine	4964	10365	9653	11427	13907	12369	31273	16380	17369	24837	13064	20123
Arginine	59395	90594	78518	84743	55259	55136	83938	194454	75297	129074	72688	110166
S-Lactoylglutathione	4373	5483	9331	50211	2708	33134	13224	186356	46893	33986	9222	28740
Cytosine	46048	33113	17542	26184	16925	24922	25923	49999	37856	38217	32288	32989
Alanine	159395	210381	124317	335644	117050	270694	201820	512841	314655	365298	157901	234223
Uridine-5-diphosphoacetylglucosamine	4179	6966	5062	4481	4860	6287	4829	2358	2551	4510	4398	5615
Lysine	22093	38821	20360	39541	16832	34284	30182	110189	41175	69389	23054	38474
Thiamine	48405	44980	9809	13031	10834	12660	21646	19485	14864	18227	35574	26361
Histamine	503967	629601	652273	957308	654859	794585	748915	714136	705289	1132373	853328	980901
Guanosine 5'-monophosphate	18624	27558	10218	5204	21527	11845	9959	1731	309	5475	11101	10991
Tyrosine; [M+H]+	4679	4975	2267	9950	3309	5243	2489	16272	11785	9788	2303	8725
1-Methylhistidine	6243	9934	3331	10650	8261	8835	11438	16174	16482	10459	7551	9501
Acetylcholine	12344	31490	6853	14483	25893	17687	22807	6262	10649	16774	11270	15608
Val-Arg	1231	1791	2947	107	1295	2809	4503	312	1135	2140	9375	9630
Guanosine	35921	31477	6028	7633	9610	14138	7390	6705	5900	8529	7217	5871
Adenosine	42005	50529	10958	10515	33432	22627	90952	4543	4738	25956	131738	39498
Cytidine; [M+H]+	19142	21116	7938	9484	9066	10339	21632	6653	7705	10606	17328	20364
Guanine	5597	3155	5550	1405	1669	1756	2288	1924	1047	1290	4029	3485
Nicotinamide	2906363	3308542	1118673	958032	1111927	1309464	1339615	1192389	1043808	1588949	2473918	2293451
Carnosine	11874	28791	8110	44155	2174	37089	7731	201432	92394	90654	6400	20132
Anserine	26310	48535	17781	138500	2029	108780	20460	699176	291741	286947	5998	41656
Asparagine	10457	12209	7785	12421	8598	11525	5395	11663	9772	10238	5537	6840
beta-Nicotinamide adenine dinucleotide	9004	7430	43998	25050	48977	20659	71734	25815	24555	17630	65025	68502
beta-Nicotinamide adenine dinucleotide, reduced	534	280	576	6407	3837	13593	12388	2070	2586	25554	4427	11937
Glutathione (oxidized)	4487	7344	9527	6277	7205	7193	25189	3009	3549	8041	12868	16400
Adenosine 5'-diphosphoribose	20646	39286	5833	6411	9856	8904	6807	3488	2119	7712	14471	12514
Creatine	10676765	14829885	8351078	25675093	6512951	20396856	10957057	40827273	25851921	28181267	9052867	13420147
Inosine	486126	653986	262213	342767	237751	402624	409697	394353	301999	377878	363675	346935
Creatine phosphate	246	4036	720	998	1118	1420	481	76286	31663	5196	339	819
Glycine	10427	10415	6173	14731	6329	12632	9989	28817	17296	10480	7163	8623
Adenosine 5'-monophosphate	11528	19653	21441	2251	26871	5653	23986	285	276	4797	23096	20012
Dimethylarginine	8676	11187	8101	8368	6794	9992	9619	14618	8450	8959	8871	9582
Inosine 5'-monophosphate	95475	143585	31499	56072	26610	77909	30866	46042	36712	55989	23511	38922
Carnitine; [M+H]+	30766229	40180067	19999288	21397319	27255904	25387780	51987510	14181062	18789258	30596887	54973846	54988607
Creatinine	356501	339427	208066	688297	164178	473347	216612	1707787	1020235	527224	228883	263301
Ile-Gln	1668	1985	4819	566	1487	2302	3844	145	391	1652	7712	6661
Choline	22857155	25241515	5417365	10806493	15797413	13997256	18829793	5897844	6666534	12964059	21239392	17512380
Hypoxanthine	747479	798103	253338	177436	212200	231943	412462	150939	153689	314521	492695	464171
Hexose X-phosphate	802	953	2979	3108	181	1228	527	8186	4280	1681	203	890
1-Methyladenosine	9443	10047	7554	7708	6358	8960	6866	11360	7828	6906	5982	6512

Metabolite name (full)	B6J-TN	B6J-TN	B6J-TN	B6J-TN	B6J-TN	B6J-TN	B6J-CE	B6J-CE	B6J-CE	B6J-CE	B6J-CE	B6J-CE
Glycero-3-phosphocholine	18451341	12620653	8200677	8779515	13776411	10015496	1181194	1046495	1476175	909354	2704655	2002762
Ergothioneine	150131	129746	109678	121001	146781	133251	67069	55172	76542	53883	74781	71998
Urea	503733	331334	390275	296745	354918	357192	839590	765962	682903	796719	652214	835234
Trigonelline	234357	89723	159994	96691	120942	120642	540456	428111	422825	446749	412030	511813
Threonine	29778	21586	27088	16216	21673	21098	46805	48053	38339	39949	53525	56588
Citrulline	142064	64925	129844	53442	70853	81239	271050	274556	260194	200423	191670	276286
Glutathione (reduced)	146295	67947	109700	70222	148178	125387	573634	470114	641945	273041	632391	442579
N-Acetylornithine	14443	6043	8971	5633	6433	7081	18931	19089	12101	16776	13749	18239
Stachydrine (proline betaine)	114399	56078	65889	67357	71217	75053	159570	94798	199465	151854	207584	197990
1-Methylnicotinamide	142489	115050	96331	91369	108363	108057	123699	127575	119038	116085	103067	334536
Ornithine	3560	1547	2989	3270	3435	3035	9750	22823	5253	9229	7155	10851
Nepsilon-Methyllysine	8274	2914	6521	2575	4748	2806	22253	26035	7280	11668	7202	8123
Serine	14708	4999	12963	6652	7688	8555	23885	23139	14705	18749	19971	27524
N-Acetylhistamine	7166	1620	2529	1529	2899	1428	5857	5322	6286	7001	9796	10075
Betaine	6617301	4163321	4132866	4191771	4648015	5141867	13735155	6434438	19883618	7991880	20043441	14468912
Tryptophan	25370	16143	17978	12202	17460	17973	29149	39455	19885	33020	32684	40752
Phenylalanine	67103	37920	44051	33945	44785	43271	89212	106695	63398	76514	81390	103195
Isoleucine	51026	39925	41605	22758	46615	35508	81723	88220	55115	80834	76069	97446
Aspartic acid	22464	10268	18269	6972	13805	13215	37639	26652	51715	23735	43327	35644
Proline	223044	126157	179597	124970	123836	159527	330806	644453	230820	359513	521769	589445
Leucine	123111	78926	83308	53653	95656	76434	197488	207160	113506	148956	181965	187218
Methionine	21352	14264	17564	12045	17561	15791	27565	37977	21852	23508	29405	30584
N6,N6,N6-Trimethyllysine	79203	23711	54087	25450	36402	30430	100064	132897	74068	53783	79752	57440
N,N-Dimethylglycine	22319	12304	13220	7335	14398	12468	24684	22906	16395	21943	19090	25435
Glutamine	714354	365998	707865	251003	468129	434493	1234212	1502748	643817	975230	1009963	1341327
Dihydroxyphenylalanine	133360	78684	134251	61648	77667	81416	235247	213825	158983	136351	118874	167836
Pantothenic acid	791464	527329	342304	326672	637791	457624	324973	235797	310946	389839	292672	377562
Glycerol-2-phosphate	2132	85	3444	231	1574	2723	8241	5635	6010	3254	24022	11507
TMAO	1116054	684925	448137	465506	740157	391612	902572	520592	1233412	1070016	1358547	1066235
Glutamic acid	296036	131429	205939	93717	158291	144841	496262	412126	628175	367674	334317	806424
gamma-Butyrobetaine	681776	291747	310934	287882	368395	363495	623714	408587	1198278	506938	908143	800025
Histidine	123656	34874	111254	28569	63059	60601	207206	223536	94894	126865	62649	136143
5'-S-methyl-5'-thioadenosine	21401	6062	15733	8481	10391	9429	17501	16941	10591	24242	21185	29135
Arginine	203861	58696	172701	75320	82215	75805	230729	329994	87312	290873	131488	137264
S-Lactoylglutathione	14177	1496	8437	1002	5941	7597	16316	29526	7987	16344	45794	22996
Cytosine	28676	17551	22430	15475	17698	24521	30615	51200	21370	34041	21328	35338
Alanine	253751	121610	240334	90490	127671	155160	344791	414054	163782	256341	310630	306824
Uridine-5-diphosphoacetylglucosamine	10207	5111	4008	4887	7959	5925	5968	5428	5776	4442	8184	10787
Lysine	79661	13680	79717	19031	26702	24382	132878	315514	29506	128325	38859	51948
Thiamine	18324	11991	9601	7349	12348	11948	51021	19482	22824	16920	20131	23366
Histamine	862168	521948	575717	607425	715765	630299	1004807	1010776	678821	1547604	524916	1359669
Guanosine 5'-monophosphate	3767	16582	6660	14320	25696	15510	17112	11210	15170	6949	12953	12561
Tyrosine; [M+H]+	4936	3692	4620	1969	2079	3292	5728	15539	2707	9443	6935	16841
1-Methylhistidine	15972	3464	10721	3188	5078	6927	17156	25387	8132	10322	5697	14790
Acetylcholine	21929	6258	16423	5957	8982	11013	12964	6845	10619	7277	5010	9122
Val-Arg	1128	2380	195	2866	2022	2244	3672	1137	6922	7200	45676	3678
Guanosine	15751	6173	6377	9255	13553	11343	25897	16753	6293	7988	7430	19747
Adenosine	11938	11524	10725	16997	16367	21056	136986	16379	104359	21006	65575	46631
Cytidine; [M+H]+	12498	7107	6865	8359	8625	8578	16623	15911	10566	9892	11854	19442
Guanine	1880	4186	5362	8085	3344	4957	2495	1114	5557	1358	4082	1460
Nicotinamide	1418283	1178972	1026608	769097	1508469	1332471	3491014	1981064	1592099	1179543	2350984	1951619
Carnosine	45457	2788	37302	1873	7525	15601	98200	313209	7752	103029	10467	50119
Anserine	63714	1389	80687	879	2705	24713	121960	418482	6420	139751	4397	61349
Asparagine	10658	6923	10373	5452	7063	6347	9647	16853	5213	11615	7800	14649
beta-Nicotinamide adenine dinucleotide	71956	62860	30473	47638	64625	38630	6857	1687	81805	21519	78352	31005
beta-Nicotinamide adenine dinucleotide, reduced	9679	219	7498	895	1903	3776	3362	1365	4941	5581	7121	8948
Glutathione (oxidized)	6814	6126	10998	8715	7564	5652	8419	6282	13322	12761	22291	17937
Adenosine 5'-diphosphoribose	6887	10552	5477	7668	14100	10637	20283	17139	9262	5244	15910	12385
Creatine	20223172	7033381	19483818	5450486	7681500	10328167	26352049	30070805	8507804	17595546	10360859	15322539
Inosine	446604	305144	225407	289169	336829	283284	733812	673673	286389	351373	295329	468542
Creatine phosphate	4075	2981	3565	1457	1402	658	795	1568	2932	1387	375	309
Glycine	20271	6569	16277	5142	7001	9070	18299	26245	8412	12869	8786	22669
Adenosine 5'-monophosphate	2729	26758	5036	22519	23974	19750	9724	3472	22413	11605	17866	20422
Dimethylarginine	17473	4784	11996	4782	8382	6923	16245	18050	9212	9179	6584	12062
Inosine 5'-monophosphate	43486	51442	50980	18322	58204	33402	232657	250544	23975	56100	18599	47932
Carnitine; [M+H]+	38064339	19250584	16646693	19228831	27699394	25129618	42378629	14553636	51049371	21458305	49024950	34209841
Creatinine	554154	220473	451455	146569	206421	279822	784800	697741	198132	352764	174904	294392
Ile-Gln	2323	3549	1146	2303	7625	5637	2896	279	4976	5175	30660	5096
Choline	15109262	10084446	10730955	4774406	10867618	9372507	14222452	7781828	17757379	6683179	6616289	17180021
Hypoxanthine	487074	251053	221618	305894	517686	313067	872025	896778	265573	319147	272096	457549
Hexose X-phosphate	2672	1465	393	3465	928	1241	2216	3344	318	3708	2379	942
1-Methyladenosine	17167	7427	6116	4855	7826	7245	9853	9610	6944	5562	8903	6912

Dataset 4.2.3 Metabolites in gastrocnemius muscle

Metabolite name (full)	AJ-TN	AJ-TN	AJ-TN	AJ-TN	AJ-TN	AJ-TN	AJ-TN	AJ-CE	AJ-CE	AJ-CE	AJ-CE	AJ-CE	AJ-CE
Nepsilon-Methyllysine	4960	3829	3969	4181	3893	4084	3402	2954	2817	3522	4027	4337	3635
Glycine	74342	69159	88557	66772	74121	57725	36573	19402	19918	20484	19289	15920	16588
Serine	41549	37496	41557	39526	37177	39208	23980	19114	21235	19968	18772	19700	19383
1-Methylhistidine	12407	20608	15818	12976	18807	20668	10577	6514	9885	7182	9165	9424	8800
Pantothenic acid	205265	208694	187087	227724	287487	222043	123638	108647	106204	97935	131830	124015	141394
Dimethylarginine	20650	23005	25693	24131	20384	15559	16719	4825	10157	10144	9385	11745	9804
Lysine	128052	99043	121214	113471	83517	105202	63474	62640	43966	51511	51709	62317	41320
Arginine	114920	72832	98576	93559	81141	93619	42796	40019	48066	44224	46732	73726	58752
Asparagine	17848	16904	19639	17245	17871	23124	11751	8743	9410	10690	9035	10541	11790
N-Acetylhistamine	17151	11443	12958	16174	21886	17948	10307	8153	9288	6866	9466	7156	11543
Trigonelline	394873	350427	331147	398107	372066	339053	243514	482124	602108	440483	544979	553663	587020
Choline	3304616	2970592	2381478	3320360	3382083	3458955	1815017	3594192	3559878	2946593	3287791	3295833	4262634
Threonine	77879	68028	75332	66674	61820	69000	39979	37817	34057	37463	46082	38990	39697
Citrulline	298897	250322	240122	235856	251530	324205	212776	156932	200419	160417	212874	215787	189544
N-Acetylornithine	18726	15815	17014	15287	16512	14139	10649	14479	12174	15243	14420	15804	14922
TMAO	423101	362912	343992	428218	329221	454907	184823	542837	702567	470645	431956	467094	630540
N6,N6,N6-Trimethyllysine	177548	154980	168895	150426	105506	116153	99033	74328	73843	97533	88231	111643	75525
Proline	1335673	1395723	1455151	1344383	1543862	1311223	833859	1282306	1231899	969465	1345353	1497308	1173816
Ornithine	7426	7590	8455	5075	6283	4883	4164	11143	8046	5682	7137	8147	4065
N,N-Dimethylglycine	45140	51128	52311	43547	47600	52904	33524	47930	49241	38073	45435	41974	44571
Urea	969729	897894	843746	765124	824255	782644	530838	1072494	1105533	782472	1367214	1217406	1242660
Dihydroxyphenylalanine	256559	201299	209512	188212	163345	189485	160041	88951	135385	147205	157392	178875	145385
Glutamine	1233739	1312636	1232849	1227106	1387838	1443462	974160	988282	838971	1002695	968960	877028	1060806
Leucine	149169	171680	166911	128885	157188	134521	102317	184489	191706	134063	235700	197526	197980
Methionine	55586	54464	52017	50229	55234	51296	30025	39975	33076	28327	47557	38317	45656
1-Methylnicotinamide	63213	52434	44338	52627	54232	48834	40330	63803	56766	39768	68501	63978	53737
Betaine	6183508	5531132	6640411	7293267	4935774	6002086	3823104	6831483	6476008	4610128	4052950	4385490	5280827
Carnosine	3059112	2094671	1960228	1534620	1108179	1957666	1806526	2311860	1875335	1678785	2120406	2226419	1071607
Creatinine	3398061	3746101	3359292	2955779	3714635	2687802	1895017	2341173	2643526	1981656	2464634	3157173	2932149
Ergothioneine	18423	23155	12689	20527	11653	19971	12531	23775	27165	23835	23457	24526	43135
3-Methylhistidine	24141	17159	14595	15433	12482	15907	15004	14776	13903	12424	11335	14635	8693
Stachydrine (proline betaine)	130014	116811	116305	134709	113806	136612	80879	116344	131795	95451	109596	110401	116669
Carnitine	18891379	18576818	14748074	18265269	13124555	18656047	11384309	13490186	12864944	12659897	13242843	12543669	16230337
Histamine	768614	366949	409196	250352	210321	248261	170658	741158	523173	288025	288948	345490	263801
Glutamic acid	357096	302379	261247	261838	251229	387758	244683	239216	231706	235493	292092	248859	244569
Valine	122485	123939	125361	111069	129260	127109	80682	156323	140200	126054	185946	139739	154291
Ala-Gln	8163	10905	6733	9039	8088	9829	14387	7111	12795	7387	11798	16386	10801
Glutathione (reduced)	472470	225057	341737	268699	475111	388647	186966	269831	113770	267455	297132	260978	210247
gamma-Butyrobetaine	691318	626834	600351	667301	561200	684288	437836	558904	616178	614758	595525	598305	635823
Isoleucine	86377	96381	88141	75399	107975	86361	60552	102478	108034	81770	153867	106399	113341
beta-Nicotinamide adenine dinucleotide	30734	31905	27045	18099	13164	20263	12577	20964	17700	22187	17284	16911	15508
Creatine	49168882	42728722	44357621	43720937	37921726	47153104	34113946	45119293	36602378	45892575	43677199	47469029	45116409
1-Methyladenosine	13481	14823	13718	16064	11512	12430	10786	12815	14169	12128	8637	12044	9705
Histidine	198199	187603	194586	195917	171062	156699	124369	105017	143050	162129	135753	133436	122182
Glycerophosphate(2)	13687	13591	13664	15155	16207	21574	13502	14521	14652	19645	16450	19753	18899
Nicotinamide	698847	1039640	822577	1464602	2230373	2039598	1452552	1010911	1499834	1215149	2039675	2060583	2495868
Phenylalanine	101451	122795	117032	94456	109463	108487	59036	118000	113587	95134	128350	121706	125800
Alanine	567110	512747	537230	539148	472221	588270	392775	492955	441356	488008	486017	518341	507037
Thiamine	15325	12512	11273	13155	15639	11624	9324	14563	14511	11289	14261	12548	13501
5'-S-methyl-5'-thioadenosine	44315	31235	30130	32422	30618	31173	19942	25246	26970	34344	20084	20219	20156
Adenosine	43596	36411	32654	81836	6785	33336	5099	108287	97278	99250	16521	17368	15396
Glycero-3-phosphocholine	164624	189182	148573	248503	211094	227668	134918	188404	324171	184429	175464	216227	291457
Tryptophan	29046	35691	36214	25734	28941	31653	13958	31332	30265	30238	31890	29467	32359
Guanine	2652	2074	2509	4921	563	1007	1491	5961	16588	5012	829	1260	1120
Glutathione (oxidized)	9516	5542	4890	4912	1870	1785	2145	4024	2406	7805	1244	962	298
Hexose X-phoshate (2)	15402	7700	18682	12047	7186	9960	11057	28142	10708	34464	10869	9435	4621
1-Methylhistamine	16083	12504	12939	19284	29017	24837	13473	23419	18910	10598	23688	36503	26586
Disaccharide	864	513	745	1809	297	436	1058	304	471	1172	2133	1100	249
Creatine phosphate	1458358	993011	847675	558051	251025	544939	214859	917195	624017	575614	382814	241533	236475
Inosine 5'-monophosphate	10156	7215	17714	22517	236661	270948	185251	23019	51784	56694	247566	359877	287100
S-Lactoylglutathione	17214	149106	67660	107075	88871	83245	144950	48715	225203	28749	90649	155620	127055
Hexose X-phoshate (1)	15178	9097	12952	12994	4466	6667	7362	21809	13362	22594	8901	5562	3900
Anserine	4790438	3354138	2984849	3175205	2331359	3300343	3007453	3845626	3147047	2936014	3006073	3142926	1969825
Acetylcholine	10125	12245	11160	11739	7093	8804	2331	8766	11736	15156	4346	7132	10043
Tyrosine	22452	26866	23623	24707	26584	29340	12824	18743	23735	20157	31089	27052	28935
beta-Nicotinamide adenine dinucleotide, reduced	12441	2614	7735	13480	331	1328	6914	12136	6226	12459	1554	1599	544

Metabolite name (full)	B6J-TN	B6J-TN	B6J-TN	B6J-TN	B6J-TN	B6J-TN	B6J-TN	B6J-CE	B6J-CE	B6J-CE	B6J-CE	B6J-CE	B6J-CE	B6J-CE
Nepsilon-Methyllysine	13146	16226	11263	10085	8551	13733	6940	9223	10648	9274	8209	8182	10446	6018
Glycine	103643	85147	100195	87157	54627	87924	61171	41548	29496	51744	33418	29321	29229	22468
Serine	30259	31848	33506	34206	23122	33478	23832	17025	17345	20174	19160	17471	19575	14763
1-Methylhistidine	36528	26237	21233	36159	29828	33731	31658	16126	20939	11568	16782	14975	14000	11317
Pantothenic acid	102212	93304	96940	161120	97762	121545	108348	57250	74091	61642	67496	81893	53921	88768
Dimethylarginine	41847	37002	33637	30891	26962	45811	22586	16250	23504	14477	12193	11851	19425	9859
Lysine	211159	355415	278630	233818	136767	232332	109580	109997	134761	118466	107479	115530	108441	56775
Arginine	116744	273184	248860	178516	143937	209332	119168	119925	140828	103522	94969	115605	122557	78598
Asparagine	12465	19072	16018	19259	12274	18259	14533	8370	10746	9744	10050	12242	12137	9565
N-Acetylhistamine	11233	2391	3978	1850	3861	1842	1327	6285	6878	6148	5310	6978	5041	7651
Trigonelline	456991	267556	257733	335588	295607	384369	258081	440398	487260	464440	451237	502607	430466	456691
Choline	5627740	6118515	4730166	4814519	5038805	6376644	4691688	4698590	3850857	3267899	3204818	3108496	2982050	3030017
Threonine	56048	69846	64246	67569	46881	75159	47455	37943	43312	46133	47360	43569	39984	34235
Citrulline	258258	295680	230214	334922	221668	302286	269982	163206	191872	164848	219941	198856	151422	141564
N-Acetylornithine	32205	25230	23105	28150	16840	26866	19600	20319	23841	23124	22235	23716	17870	17064
TMAO	276597	289923	224208	297240	229380	311427	230384	299669	350191	309722	362468	383754	322248	380126
N6,N6,N6-Trimethyllysine	178525	247194	194304	194756	163246	250298	108984	133229	151842	155187	131272	115026	233498	95786
Proline	2004165	1737345	1667696	1775481	1827521	2245192	1593531	1884085	1594507	2523273	1731228	1763322	1691296	1367128
Ornithine	33253	15298	12636	12752	7607	15966	8907	12919	8977	12401	11987	13683	15112	10133
N,N-Dimethylglycine	56496	30503	26762	35371	34298	41769	31503	33854	28494	32214	33286	33098	27617	25771
Urea	863764	965455	910489	1114072	871053	1017165	963288	1130879	1184158	1012844	1364680	1338923	1193587	1057263
Dihydroxyphenylalanine	185153	219351	180043	237342	177136	222115	170255	141642	161698	145884	172515	125134	122765	117678
Glutamine	1116056	1142832	1318128	1385360	951693	1303869	949777	991680	1128920	1036693	989146	836894	693795	701143
Leucine	183091	211953	153399	176098	183138	211922	169537	177607	216390	213222	192880	219829	204389	189510
Methionine	45625	65457	53258	75127	58649	69075	55572	39298	46209	49380	53077	52294	45658	44578
1-Methylnicotinamide	66812	62731	55220	48580	103453	100405	46268	95260	66592	81415	74302	93741	79561	81383
Betaine	9984589	4207115	4197711	4356045	4391081	5599413	4892807	3746874	3150312	4215615	3842019	3411673	3569246	3486043
Carnosine	2547569	3032397	2979964	3462373	2011572	2387044	1789502	2642411	2789857	4114719	2609548	2788378	2984567	2121695
Creatinine	3950591	2783886	2650784	3236329	3385820	3940110	3677422	2209953	2410018	2593533	2387726	2935413	2749255	2137715
Ergothioneine	36674	15495	10843	14016	16072	17046	19739	20339	28328	21558	50234	18336	20065	38816
3-Methylhistidine	17297	20500	19337	25770	14104	17461	14021	12659	14941	18772	15010	14485	12921	10865
Stachydrine (proline betaine)	147016	82848	92473	113553	89752	115050	97899	87610	90255	91039	91327	101187	82955	90618
Carnitine	13507695	12361141	11245465	15433786	13258798	14145004	11698006	12237879	10435201	13164989	16692351	10525084	12225238	11920932
Histamine	156148	365809	291119	152792	97438	218207	213858	152038	173381	204585	180988	153009	282792	343110
Glutamic acid	204018	262434	235015	348182	212547	206570	329626	192381	227805	189901	308850	234965	175521	172296
Valine	188834	137547	112598	138787	124167	142654	112386	125300	136992	143971	128150	169427	132317	143612
Ala-Gln	12258	9621	8659	15750	10250	9529	10593	10857	15627	17021	11893	14511	17178	11222
Glutathione (reduced)	363640	354281	385011	521344	387202	298830	302033	273931	226300	503355	315674	234052	245438	214577
gamma-Butyrobetaine	480759	449414	453541	604968	550311	519301	571154	465147	533860	569803	708186	484881	507443	541431
Isoleucine	93223	118381	78306	100732	93641	116202	96644	85236	119810	104065	92208	121331	93721	100382
beta-Nicotinamide adenine dinucleotide	21493	9326	14976	15740	13972	16456	12006	23304	26085	37023	20537	18390	19224	12782
Creatine	34901846	42346336	43343528	49411323	40898412	47342470	37145786	37826758	37866648	40626603	33648710	38668250	37189543	39227258
1-Methyladenosine	13451	12614	10727	11218	8553	13646	11590	11020	10600	12643	9852	10654	10005	10232
Histidine	296353	240235	238874	261810	121273	180155	104707	146065	216959	191707	179098	144121	119325	94200
Glycerophosphate(2)	11691	14196	13159	20041	13263	10620	13160	16641	19761	15598	16349	16104	13076	12697
Nicotinamide	2022351	1470935	1505084	1863954	2430143	2620718	2797219	976291	1610617	1390337	2300748	2129004	2154982	2165885
Phenylalanine	111726	119880	110053	140051	111036	150354	114257	88839	118024	121345	117746	122434	118046	118333
Alanine	504791	537944	576972	622065	520793	622798	459270	467874	489621	566354	471018	504178	464090	427801
Thiamine	30395	12303	10704	10281	15106	16826	12875	9962	11925	10098	12862	9772	10914	12597
5'-S-methyl-5'-thioadenosine	34732	33662	30664	34926	22368	23092	20350	28788	24945	31389	27942	26369	18904	16462
Adenosine	12488	41148	21039	23209	3039	7133	27523	29136	50842	19567	17839	12506	18848	19845
Glycero-3-phosphocholine	260758	249723	189617	153368	160613	320541	258017	202823	344460	213414	218302	211737	255051	265537
Tryptophan	24488	25593	26696	23602	20473	30125	24331	19625	37236	28981	18636	29185	23666	28618
Guanine	1708	14220	11230	1795	1347	3337	7105	1429	1793	638	2346	5257	2802	2406
Glutathione (oxidized)	9129	7375	4633	4835	697	1308	1358	3493	3531	5919	4197	1499	1142	1708
Hexose X-phoshate (2)	7331	11646	15171	15068	4419	12099	3145	18889	11316	12672	7268	9489	7194	4396
1-Methylhistamine	16494	15014	14670	17099	27384	43373	33208	9440	12625	13886	15938	21436	25784	35061
Disaccharide	453	18106	1472	424	218	2569	546	982	256	588	297	611	780	1084
Creatine phosphate	715651	799193	698970	801761	172357	162467	90433	521620	727993	1030684	719645	483120	214132	154858
Inosine 5'-monophosphate	25835	8539	19226	32573	311295	376926	338903	14613	46422	20863	30515	120747	255220	258761
S-Lactoylglutathione	67451	52900	71536	87443	40631	113002	99235	71952	174252	46913	61300	162221	155431	104780
Hexose X-phoshate (1)	10022	9181	16252	15602	2774	11874	3281	14121	12914	11566	8677	9431	5970	3739
Anserine	3021417	3983875	3929461	4842823	2184458	2663760	2429585	2933175	3422975	4371168	3169428	3047127	2986674	2462919
Acetylcholine	7573	8889	6455	9063	5113	8061	6733	25533	19513	12104	7419	5114	2453	4837
Tyrosine	18435	22369	24494	30239	21444	27905	25511	15517	26613	23761	26344	26166	27622	30166
beta-Nicotinamide adenine dinucleotide, reduced	596	25816	14330	20967	223	1703	1212	13591	6676	2725	4885	2532	1322	1645

B. Publications enclosed in full
(Publication A, Publication C)